

Functional characterization of BAR
domain proteins in actomyosin
network organization during
Drosophila embryogenesis

Submitted in partial fulfilment of the
requirements of the degree of

DOCTOR OF PHILOSOPHY

By

Swati Sharma

20132007



INDIAN INSTITUTE OF SCIENCE EDUCATION AND
RESEARCH PUNE

CERTIFICATE

It is certified that the thesis entitled "**Functional characterization of BAR domain proteins in actomyosin network organization during *Drosophila* embryogenesis**" submitted by **Ms. Swati Sharma** represents her original work which was carried out by the candidate at IISER, Pune, under my guidance and supervision during the period from August 2015 to August 2021.

The work presented here or any part of it has not been included in any other thesis submitted previously for the award of any degree or diploma from any other University or institution. I further certify that the above statements made by her in regard to her thesis are correct to the best of my knowledge.

Date: 07-09-2021

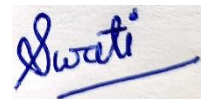
A handwritten signature in black ink, appearing to read 'Richa Rikhy', with a stylized flourish at the end.

Dr. Richa Rikhy
(Supervisor)

DECLARATION

I declare that this written submission represents my idea in my own words and where others' ideas have been included; I have adequately cited and referenced the original sources. I also declare that I have adhered to all principles of academic honesty and integrity and have not misrepresented or fabricated or falsified any idea/data/fact/source in my submission. I understand that violation of the above will be cause for disciplinary action by the Institute and can also evoke penal action from the sources which have, thus, not been properly cited or from whom proper permission has not been taken when needed. The work reported in this thesis is the original work done by me under the guidance of Dr. Richa Rikhy.

Date: 07-09-2021



Swati Sharma

Reg. no. 20132007

Acknowledgements

I got the opportunity to meet, learn, evolve and collaborate with a whole bunch of people during the last 8 years of my Integrated PhD program. I would like to thank every individual who became a part of this journey and contributed to my overall progress till now. Firstly, I would like to express my deepest gratitude towards my mentor, Dr. Richa Rikhy for giving me the opportunity to work in her lab when I was genuinely in need. I was able to create my little scientific footsteps as she always gave me the freedom in terms of choosing the projects, designing the experiments and following the leads. She mentored me in building scientific aptitude by giving scientific training which includes critical thinking in designing experiments, data analysis, troubleshooting, data interpretations, scientific writing and presentation skills. She is always curious about unsuccessful or failed experiments which helped me in overall learning to get deeper insights about the process of research. Initially, I was strong-headed in taking decisions related to experiments but gradually I learned to process her scientific ideas and inputs. The great landmark in the project was getting a CRISPR mutant which won't be possible without her idea of doing sterility assay screening. She has always put trust and confidence in me which helped me to become a better version of myself. Most importantly for tolerating my laughter in lab meetings. I thoroughly enjoyed working with her and at times it was full of adventure. Lastly, I genuinely inculcated deeper respect for her as she provided her incredible support which helped me sail through pandemic times with ease.

Next, I would like to thank IISER Pune, the Biology department and the common lab system which provides opportunities to interact and collaborate to carry out sharing of reagents and instrumentation facilities with other labs. I would like to thank Girish lab members for inputs in common lab meetings and for helping me in cloning for generating reagents. Big thanks to the academic office at IISER, Pune for guiding me through administrative procedures concerning PhD, fellowship, contingency and travel grants. Thanks to IISER and CSIR funding for monthly fellowships which provided financial support, funding towards various conferences and EMBO for providing travel grants for international conferences. As my entire PhD work heavily relies on microscopy, I want to

thank IISER, Pune Imaging facility and the Leica Imaging center especially Vijay, Santosh, Aditi and Rahul for the microscopy training and guiding me from time to time. I would also like to thank the Bloomington stock center for providing a variety of fly stocks and DSHB for antibodies that were used in the majority of experiments. The fly stock center of IISER, Pune- Snehal and Ashwini for maintaining backup stocks is of great help whenever we require stocks for experiments. Special thanks to Yashwant for managing the fly media center and housekeeping staff for autoclaving and washing plastic wares. I realized that they carry out huge amounts of work for fly maintenance during pandemic days.

I would like to thank NCBS fly facility for generating GRAF transgenics used in the project and Rajeshwari from Bioklone for generating GRAF antibodies. I am very grateful to *elife* reviewers for their suggestions which helped us to improve the manuscript.

I would like to deeply thank RR lab members for creating a friendly and comfortable environment. All the lab members contributed via useful suggestions, ideas and discussions in lab meetings. Initially, I carried out projects along with Aparna to understand the basic skills and techniques required for the project. Darshika, patiently helped me whenever I get into trouble with experiments and had a lot of fun working with her. I had a lot of entertainment because of Dnyanesh and he definitely helped me in thinking through scientific ideas. Sayali helped me in data analysis and interpretation related to the *Drosophila* cellularization system. Bhavin for being there to coordinate and manage the lab during pandemic times. The young members of the lab, Debasmita, Somya, Sanjana, Rahul, Harsh and Shashwat for maintaining an equally friendly and fun environment in the lab. I would especially like to thank Divya, for her contributions in domain deletion analysis which helped me to quickly reach the final output and also patiently sitting with me for the entire thesis proofreading. In addition, I would thank Praveena di and Ankita for proofreading.

I especially want to thank both Sameer and Bipasha for providing immense support and spend the maximum time with both of them during my PhD. Both of them always

showed their humility and respect towards me irrespective of any situation. Sameer is a very understanding and compassionate person who helped me in building confidence and gave me hope in the toughest times during my PhD. I admire and adore Bipasha for her discipline, persistence and calmness. She was the one to whom I told all my mischiefs without any hesitation. I was fortunate that I got my best buddies and great scientific peers in the lab.

I am extremely grateful to my Integrated PhD batchmates (Deepak, Kashyap, Divya, Amar, Akhila, Adarsh, Harpreet, Aditi, Ron, Sandeep, Shivani, Charu, Neeladri, Mehak, Dhriti, Anish, Anshul, Bharat). I got friends for life in this batch with whom I had parties, dinner, joy, adventures and lots of trips. Special thanks to Ron, Sandeep, Neeladri and Anish for creating a space where I could be myself, free from worries and judgements. After a long day of work the only thing, you look forward to is spend quality time with friends.

A special thanks to Dhriti, Mehak and Prajna for their joyful company to relieve any emotional stress during lockdown times.

I want to thank my entire family who provided their unconditional support and patience throughout my PhD. I would like to thank my parents who gave me the freedom to chase my dreams.

Last but not the least, I am eternally grateful to “Brahma Kumaris Meditation Center”. They provided me with the knowledge that immensely helped me to explore my inner world to bring out the best in me. At last, I would like to “Thank GOD-infinite times” for everything.

Table of contents

CERTIFICATE.....	ii
DECLARATION.....	iii
Acknowledgements.....	iv
Table of Contents.....	1
List of Figures.....	7
List of Tables.....	10
List of Abbreviations.....	11
Abstract.....	14
Synopsis.....	15
CHAPTER 1	
Introduction.....	28
1.1 Cytokinesis in multicellular tissues.....	28
1.2 BAR domain proteins in membrane curvature induction or sensation.....	29
1.3 Mechanism by which BAR domain proteins induce membrane curvature.....	35
1.4 Role of BAR domain proteins in cytokinesis.....	37
1.5 Steps of cytokinesis.....	39
1.5.1 Initiation of cytokinesis: Central spindle complex.....	39
1.5.2 Cleavage furrow assembly to regulate contractile ring formation and constriction.....	41
1.5.2.1 Specification of active RhoA zone.....	41

1.5.2.2 Regulation of Myosin II.....	43
1.5.2.3 Actin assembly and its regulators.....	47
1.5.3 Cleavage furrow ingression and abscission: Membrane trafficking.....	50
1.6 Variations in cytokinesis during <i>Drosophila</i> development.....	52
1.7 Aims and objectives.....	58
CHAPTER 2	
Material and Methods.....	60
2.1 <i>Drosophila</i> stocks and genetics.....	60
2.2 Generation of GRAF null mutant using the Crispr-Cas9 method.....	64
2.3 Generation of GRAF-GFP, domain deletions and point mutations transgenics.....	65
2.4 Generation of anti-GRAF antibody.....	70
2.5 Immunostaining.....	71
2.5 Live imaging of <i>Drosophila</i> embryos.....	73
2.6 Laser ablations.....	74
2.7 Microscopy.....	74
2.8 Image quantification and analysis.....	74
2.8.1 Quantification of mean fluorescence intensity from immunostainings.....	74
2.8.2 Quantification of mean fluorescence intensity from live-imaging.....	75
2.8.3 Quantification of the contractile ring area.....	77
2.8.4 Quantification of furrow membrane length.....	77

2.8.5 Quantification of displacement and initial recoil velocity after laser ablation.....	78
2.9 Statistical analysis.....	78
CHAPTER 3	
GRAF is essential for actomyosin contractility during <i>Drosophila</i> Cellularization.....	
	79
3.1 Introduction.....	79
3.2 Material and methods.....	81
3.3 Results.....	83
3.3.1 <i>Drosophila</i> GRAF multi-domain organization is conserved across multicellular organisms.....	83
3.3.2 GRAF depletion using shRNA knockdown and generation of GRAF knockout using CRISPR-Cas9 strategy.....	84
3.3.3 GRAF depletion leads to hyper constriction of contractile ring in cellularization.....	87
3.3.4 GRAF protein recruits at the contractile ring during early and mid cellularization stages.....	92
3.4 Conclusion and discussion.....	94
CHAPTER 4	
GRAF regulates the recruitment of key contractile proteins at the cleavage furrow during cellularization.....	
	96
4.1 Introduction.....	96
4.2 Material and methods.....	99
4.3 Results.....	104

4.3.1 GRAF protein modulates Rho-GTP and Myosin II for the regulation of contractility during <i>Drosophila</i> cellularization.....	104
4.3.2 GRAF depletion leads to enhanced contractility of the basal actomyosin network.....	107
4.3.3 GRAF RhoGAP domain is essential for contractility during cellularization.....	109
4.3.4 GRAF overexpression leads to loss of contractility during cellularization.....	113
4.3.5 GRAF depletion and overexpression results in perturbation of Myosin II distribution at the contractile ring during cellularization.....	115
4.3.6 Diaphanous recruitment to the contractile ring is severely reduced on GRAF depletion.....	119
4.3.7 Anillin, Peanut and PatJ distributions at the furrow tip are perturbed in <i>Graf</i> depletion.....	121
4.4 Conclusion and discussion.....	122

CHAPTER 5

GRAF functions as a Rho-GAP in Rho-dependent pathway to regulate constriction during cellularization.....	125
5.1 Introduction.....	125
5.2 Material and methods.....	127
5.3 Results.....	131
5.3.1 GRAF overexpression driven loss of contractility is suppressed by an additional increase of RhoGEF2.....	131
5.3.2 GRAF depletion induced hypercontractility in cellularization is suppressed by additional depletion of RhoGEF2.....	134
5.3.3 RhoGEF2 overexpressed and depleted embryos retain GRAF protein at the contractile ring during cellularization.....	137

5.3.4 Hyper constriction defects in MBS depleted embryos are suppressed by GRAF overexpression.....	139
5.3.5 GRAF depletion induced hypercontractility in cellularization is lost by additional depletion of ROK.....	140
5.3.6 GRAF is a bonafide Rho-GAP protein that acts as a negative regulator for constriction during cellularization.....	142
5.4 Conclusion and discussion.....	143

CHAPTER 6

GRAF domain function in contractility and recruitment of protein at the contractile ring during cellularization.....	146
6.1 Introduction.....	146
6.2 Material and methods.....	148
6.3 Result.....	151
6.3.1 GRAF BAR, PH, RhoGAP and SH3 domains are necessary for regulation of ring constriction during cellularization.....	151
6.3.2 GRAF BAR, PH, RhoGAP and SH3 domain deletions lead to altered distribution of Myosin II in cellularization.....	152
6.3.3 The BAR and SH3 domains are necessary for the enrichment of GRAF on the ring.....	154
6.3.4 The PH and RhoGAP domains are important for the dissociation of GRAF from the ring.....	156
6.4 Conclusion and discussion.....	158

Chapter 7

Thesis summary and future perspectives.....	163
7.1 Recruitment of GRAF: association and dissociation dynamics at the contractile ring.....	164
7.2 GRAF function in regulating actin network during cellularization.....	165

7.3 GRAF interaction with cadherin and associated proteins involved in membrane trafficking regulation during cellularization.....	166
7.4 GRAF role in conventional cytokinesis.....	167
Appendix.....	171
A.1 Screening based on RNAi mediated knockdown of BAR domain proteins and its assessment using embryonic lethality, phenotype and localization.....	171
A.2 RhoGAP domain proteins screening based on RNAi mediated knockdown to check for embryonic lethality.....	174
Bibliography.....	179

List of Figures

Chapter 1

- 1.1 Characterization of F-BAR, N-BAR and I-BAR family domain architecture and its membrane curvature model
- 1.2 Central spindle complex formation, positioning and signalling
- 1.3 Schematic diagram showing RhoA signalling pathway activating actin and Myosin II
- 1.4 Variations in cytokinesis: Incomplete cytokinesis, pseudocleavage and cellularization during *Drosophila* embryogenesis

Chapter 3

- 3.1 Phylogenetic tree of GRAF protein across various species
- 3.2 *Graf* depletion using shRNA knockdown and generation of GRAF knockout using CRISPR-Cas9 strategy.
- 3.3 *Graf* depletion leads to hyper constriction of contractile rings during cellularization
- 3.4 *Graf* depletion phenotypes using *Graf²ⁱ* and *Graf^{grna}*.
- 3.5 GRAF protein is enriched at the furrow in mid cellularization.
- 3.6 GRAF spatio-temporal recruitment regulates contractility during the *Drosophila* cellularization.

Chapter 4

- 4.1 GRAF-GFP, Sqh-mCherry and AnillinRBD-GFP levels are enriched at the furrow tip in mid cellularization
- 4.2 *Graf* mutant embryos show hypercontractility during early and mid cellularization
- 4.3 RhoGAP domain of GRAF is essential for ring constriction in cellularization
- 4.4 *Graf^{CR57}*; GRAF-GFP and *Graf^{CR57}*; GRAF Δ RhoGAP-GFP recruitment dynamics
- 4.5 GRAF overexpression shows inhibition of ring constriction in cellularization

- 4.6 *Graf* depleted embryos show increased Myosin II in cellularization
- 4.7 GRAF depletion and overexpression lead to perturb Myosin II distribution
- 4.8 Diaphanous recruitment to the contractile ring is severely reduced in *Graf* depletion
- 4.9 Anillin, Peanut and PatJ mislocalization at the furrow tip in *Graf* depletion
- 4.10 GRAF is required for the recruitment of key contractile proteins during the *Drosophila* cellularization

Chapter 5

- 5.1 GRAF overexpression driven loss of ring constriction is suppressed by RhoGEF2 overexpression in cellularization.
- 5.2 *Graf*^{CR57} hyper constriction phenotype is suppressed by RhoGEF2 depletion.
- 5.3 RhoGEF2 depletion and overexpression retain GRAF recruitment.
- 5.4 GRAF overexpression suppresses the hyper constriction phenotype in MBS depleted embryos.
- 5.5 The hyper constriction phenotype of *Graf*^{CR57} embryos is suppressed by additional depletion of Rok.
- 5.6 GRAF is a bonafide Rho-GAP protein that requires Myosin II activity for constriction during cellularization

Chapter 6

- 6.1 GRAF BAR, PH, RhoGAP and SH3 domains are necessary for ring constriction regulation via Myosin II recruitment during cellularization.
- 6.2 The BAR and SH3 domains are necessary for the GRAF on the ring.
- 6.3 The PH and RhoGAP domains are important for the dissociation of GRAF from the ring.
- 6.4 GRAF domains are necessary for Myosin II dependent ring constriction

Chapter 7

- 7.1 Summary models

Appendix

1. Knockdown of BAR domain proteins MIM, sorting nexin16 and RhoGAP92B show disorganized actin architecture.
2. Centaurin beta 1A knockdown embryos show actin clumps during mid and late cellularization.
3. Tumbleweed knockdown in the ovary shows nurse membrane collapse and actin aggregation in developing oocyte in RhoGAP15B depletion.

List of Tables

Chapter 2

- 2.1 *Drosophila* stocks and their source
- 2.2 *Drosophila* crosses
- 2.3 Primers for sequencing and cloning GRAF
- 2.4 Antibodies and Dyes

Chapter 3

- 3.1 *Drosophila* stocks and their source

Chapter 4

- 4.1 *Drosophila* stocks and their source

Chapter 5

- 5.1 *Drosophila* stocks and their source

Chapter 6

- 6.1 *Drosophila* stocks and their source

Appendix

- A. BAR domain protein screening based on embryonic lethality, phenotype and localization during *Drosophila* syncytial and cellularization stage.
- B. RhoGAP domain protein screening based on embryonic lethality from 5 days and 2 weeks old flies at 29°C temperature.
- C. *Drosophila* stocks used for BAR domain and RhoGAP proteins screening

List of Abbreviations

ABBA	Actin-bundling protein with BAIAP2 homology
AH	Amphipathic helices
AML	Acute myeloid leukaemia
ANOVA	Analysis of variance
AP-2	Adaptor protein complex-2
ArfGAP	Arf GTPase activating protein
ArfGEF	Arf-Guanine nucleotide exchange factor
Arp2/3	Actin-related protein 2/3
ASAP	ArfGAP with SH3 domain, ankyrin repeat and PH domain
ATP	Adenosine triphosphatase
BAR	Bin/Amphiphysin/Rvs
Bnk	Bottleneck
CenB1A	Centaurin beta1A
Cip4	Cdc42 interacting protein 4
CLICs	Clathrin-independent carriers
CPC	Chromosomal passenger complex
CRIB	CDC42-Rac interactive binding
CRISPR	Clustered regularly interspaced short palindromic repeat
Dia	Diaphanous
DRFs	Diaphanous-related formins
DROK	<i>Drosophila</i> Rho-kinase
E-cad	E-cadherin
EMT	Epithelial-mesenchymal transition
FAK	Focal adhesion kinase
F-BAR	Fes/CIP4 homology-BAR
FBP17	Formin-binding protein 17
FCHO	FCH only
FCHSD	FCH and double SH3 domain proteins

FER	FES related
FIP	Family of interacting proteins
FX	F-BAR extension
GAS7	Growth arrest-specific 7
GEEC	Glycosylphosphatidylinositol- anchored protein enriched compartments
GFP	Green fluorescent protein
GRAF	GTPase regulator associated focal adhesion kinase
GTP	Guanosine-5'-triphosphate
HR1	Protein kinase C-related kinase homology region 1
I-BAR	Inverse BAR
ICA-69	Islet cell autoantigen-69
IRSp53	Insulin receptor tyrosine kinase substrate p53
IRTKS	Insulin receptor tyrosine kinase substrate
KIF4	Kinesin-4
MBS	Myosin binding subunit of myosin phosphatase
MDS	Myelodysplastic syndrome
MEFs	Mouse embryonic fibroblasts
MICAL1	Microtubule associated monooxygenase, calponin and LIM domain containing 1
MIM	Missing-in-metastasis
Myosin II	Non-muscle Myosin II
N-BAR	N-terminal amphipathic helix BAR
NOSTRIN	Nitric oxide synthase traffic inducer
NPF	Asparagine proline phenylalanine
N-WASP	Neural wiskott-aldrich syndrome protein
OD	Optical density
PACSIN	Protein kinase C and casein kinase 2 substrates in neurons
Pav	Pavarotti
PCR	Polymerase chain reaction
PFA	Paraformaldehyde
PH	Pleckstrin homology
PI(3,4,5)P2	Phosphatidylinositol 3,4,5-bisphosphate

PI(4,5)P3	Phosphatidylinositol 4,5-trisphosphate
PI3K	Phosphatidylinositol 3-kinase
Pnut	Peanut
PS	Phosphatidylserine
PX	Phox homology
Pxl1	Paxillin-related protein 1
RBD	RhoGTP Binding Domain
RhoGAP	Rho GTPase activating protein
RhoGEF	Rho GTP exchange factor
RMIc	Regulatory myosin light chain
ROI	Region of interest
Rok	Rho-kinase
SD	Standard deviation
Sep1	Septin1
Sep2	Septin2
Sep4	Septin4
Sep5	Septin5
SH2	Src homology-2
SH3	Src homology-3
Sqh	Squash
srGAP	Slit-Robo GTPase-activating protein
Tyr-kinase	Tyrosine kinase
WDR44	WD repeat domain 44
WH2	WASP homology 2
μHD	μ-homology domain

Abstract

Membrane remodelling is coupled to cytoskeletal dynamics in cell migration and cleavage furrow formation during cytokinesis. Metazoan embryogenesis serves as an interesting context to study the function of membrane remodelling proteins containing a BAR domain on the actomyosin network during cell formation and division. We used *Drosophila* embryogenesis to perform a screen for elucidating the role of the BAR domain containing proteins in plasma membrane associated actin remodelling in the blastoderm embryo. Depletion of several BAR domains containing proteins gave defects in actin remodelling during early morphogenesis and cell division. We further characterized the role of a multi-domain protein GRAF in regulating cytokinetic furrow formation in *Drosophila* cellularization. GRAF contains a BAR, PH, RhoGAP and SH3 domain and is present in multicellular organisms. RhoGTPase exchange factors (RhoGEF) and RhoGTPase activating proteins (RhoGAP) together regulate the levels of Rho-GTP to drive actomyosin ring constriction in cleavage furrow formation. We found that a CRISPR-Cas9 induced null mutant of GRAF showed ring hyper constriction due to increased Rho-GTP and Myosin II levels in cleavage furrow formation in a RhoGAP domain dependent manner. RhoGEF2 depletion and Myosin II inactivation in Rho Kinase suppressed the hyper constriction defect in *Graf* mutants. GRAF was enriched at the cleavage furrow during the early stages of cleavage furrow formation. BAR and SH3 domains were required for cleavage furrow recruitment whereas PH and RhoGAP domains played a role in its dissociation from the furrow. In addition to Myosin II, GRAF also regulated the distribution of key actin regulatory proteins at the cleavage furrow. In summary, we found that the spatiotemporal recruitment of GRAF to the cleavage furrow fine-tuned Rho-GTP levels and regulated actomyosin ring constriction during cleavage furrow formation in *Drosophila* cellularization

Synopsis

Name of the Student: Swati Sharma

Registration number: 20132007

Name of Thesis advisor: Dr. Richa Rikhy

Date of Registration: 1st August 2015

Place: Indian Institute of Science Education and Research, Pune

Title: **Functional characterization of BAR domain proteins in actomyosin network organization during *Drosophila* embryogenesis**

1. Introduction

Cytokinesis is the fundamental process to ensure the successful separation of daughter cells. Cytokinesis initiation requires precise membrane curvature induction forming a cleavage furrow. After membrane curvature induction, the cleavage furrow ingresses towards the cell interior. The force required for cleavage furrow ingression is provided by the contractile ring beneath the membrane. The contractile ring consists of an actomyosin network that recruits at the equatorial plane. Thus, actin and non-muscle Myosin II (Myosin II) are the central molecules involved in executing the contraction of contractile rings (Mangione & Gould, 2019). It is responsible to generate tension to carry out the contraction process either by Myosin II motors or actin depolymerization (Conrad & Rappaport, 1981; Fededa & Gerlich, 2012; Glotzer, 2005; Green et al., 2012; Guertin et al., 2002; Mangione & Gould, 2019; Pollard & O'Shaughnessy, 2019). Contractile ring positioning is dependent on anaphase spindle complex positioning. The recruitment of key molecules at the contractile ring is directed by local regulation of Rho activity (Basant & Glotzer, 2018). The contractile ring constriction is executed when the motor activity of Myosin II translocates actin filaments (Hiramoto, 1975; Stachowiak et al., 2014; Yoneda & Dan, 1972). Contractile ring constriction further leads to cleavage furrow ingression to the point where the cell finally pinches off to generate daughter cells (Barr & Gruneberg, 2007; Schiel & Prekeris, 2010).

Cytokinesis requires the proper coordination of membrane ingression dynamics as well as the actomyosin driven constriction process. There is a class of proteins called BAR domain proteins that consist of domains that bind to the membrane as well as actin regulators. BAR domain proteins that sense or induce curvature act as bridges between the membrane and cytoskeletal function in the cytokinesis. In *Drosophila*, the F-BAR protein Syndapin is involved in the cytokinesis in S2 cell lines. Syndapin interacts with phosphatidylinositol 4,5-bisphosphate PI(4,5)P2 lipids in *in vitro* assays and with the contractile ring protein Anillin (Takeda et al., 2013). In addition, Syndapin is required for pseudocleavage furrow ingression in *Drosophila* syncytial stages (Sherlekar & Rikhy, 2016). Another N-BAR domain protein called Amphiphysin involved in endocytosis visualized in the form of tubules occurring at the ingressing furrow tip during syncytial stages (Sokac & Wieschaus, 2008). Amphiphysin null embryos show the absence of tubules and show faster cleavage furrow ingression (Su et al., 2013). In addition, approximately 35% of all BAR domain proteins consists of ArfGAP, RhoGAP, or RhoGEF domains which regulate various GTPases or in turn regulated by Rho-GTPases (Aspenström, 2019; de Kreuk & Hordijk, 2012). Rho-GTPases signalling regulate the actin cytoskeleton remodelling in cytokinesis. Thus, BAR domain proteins become potential candidates to dissect their function in cytokinesis via the regulation of Rho-GTPases signalling.

Ring constriction in cytokinesis involves the actomyosin network containing actin regulatory proteins comprising crosslinker, stabilizer and nucleators (Adam et al., 2000; Afshar et al., 2000; Field et al., 2005; Grosshans et al., 2005; Krueger et al., 2019; Mavrakis et al., 2014a). Actin crosslinkers such as *fimbrin* mutant show retention of polygonal shape during late cellularization whereas *bottleneck* and *cheerio* mutants show hyper constriction defects during early stage (Krueger et al., 2019). Mutants in F-actin stabilising proteins Anillin and the septin Peanut show defects in a ring shape (Field et al., 2005; Mavrakis et al., 2014b). Mutants of actin nucleators such as Diaphanous cause decreased constriction and ingression defects during cellularization (Afshar et al., 2000; Grosshans et al., 2005). In addition to the actin network, Myosin II activation occurs by

the spatiotemporal generation of Rho-GTP and recruitment of kinases to the site of actomyosin assembly. During cellularization, temporal Myosin II recruitment gradually increases in the assembly phase, reaching a plateau in the ring formation and finally declining in the constricted stage during the cellularization process. Phospho-deficient mutants of the light chain of Myosin II, Squash, show contractility inhibition during cellularization (Xue & Sokac, 2016). Further, Rok and Drak mutant embryos and treatment of embryos with a pharmacological inhibitor of Rok, Y-27632, show an impairment of actomyosin contractility due to reduced Myosin II phosphorylation (Chougule et al., 2016; Krajcovic & Minden, 2012; Xue & Sokac, 2016).

Spatial and temporal recruitment and regulation of molecules associated with actomyosin networks also become crucial for the assembly and contractility process. The conventional cytokinesis process is mechanistically similar to cellularization (Kotadia et al., 2010). *Drosophila* cellularization provides a great opportunity to study plasma membrane ingression with actomyosin contraction. Cellularization begins during the interphase of cycle 14. At this stage, the invagination of the plasma membrane initiates followed by membrane expansion till it reaches 40µm depth. This process is divided into three phases: early, mid and late. The early phase shows plasma membrane invagination and cleavage furrow assembly. During this phase, the hexagonal network of the actomyosin array at the leading edge is established. During mid stage, the accumulation of Myosin II drives the transition from hexagonal network to ring formation at the base of nuclei. During late stages, actomyosin contraction is seen in the contractile ring and results in closure of the cell (Kiehart, 1990; Krueger et al., 2019; Royou et al., 2004; Schejter & Wieschaus, 1993; Xue & Sokac, 2016; Young et al., 1993).

Drosophila embryogenesis cellularization stages provide a good system to study BAR domain proteins involved in contractile ring constriction *in vivo*. Thus, BAR domain proteins may act as a bridge between actin dynamics and membrane remodelling during contractile ring formation. In an initial partial screen for the function of the BAR domain containing proteins in the plasma membrane and actomyosin remodelling during embryogenesis, we found that depletion of GRAF led to hypercontractility during

cellularization. We have identified the GRAF molecule which is a promising candidate in regulating the actomyosin network during cellularization. GRAF is a multidomain consisting of BAR, PH, RhoGAP and SH3 domains. This molecule was originally identified as a binding partner of the C-terminal domain of focal adhesion kinase. Previous studies have shown that GRAF colocalized to both focal adhesions paxillin and FAK, cortical actin and stress fibers in mammalian cells MEFs and in chick embryonic cells (Hildebrand et al., 1996; Luo et al., 2017). In addition, GRAF recruitment leads to stabilized cortical actin and cell spreading (Barrios & Wieder, 2009). In *Xenopus* GRAF1 depleted embryos result in progressive muscle degeneration causing defective myofibrillogenesis, defective motility and embryonic lethality due to elevated RhoA activity (Doherty et al., 2011). GRAF1 variant containing a GAP domain having R412Q point mutation (GAPm) (Taylor et al., 1999) that blocks enzymatic activity transfected in cultured L6 cells shows a reduction in RhoA activity (Doherty et al., 2011). GRAF3 deficient mice showing hypertensive phenotype to angiotensin II abrogated when treated with a ROCK inhibitor, Y-27632. *Graf* deficient mice show increased contractility due to elevated Rho-GTP levels, enhanced Myosin II foci and myosin light chain phosphorylation in isolated blood vessels (Bai et al., 2013). *Graf* depletion leads to cellular blebbing marked by increased Myosin II foci (Holst et al., 2017). We identified the GRAF function and pathway associated with the regulation of ring constriction.

2. Results

2.1 GRAF function is essential for actomyosin organization and contractility

We assessed the GRAF function in contractile ring formation and constriction in *Drosophila* cellularization. This study will focus on dissecting the steps of constriction and GRAF role in affecting ring architecture during cellularization. Initially we establish the conservation of GRAF protein across multicellular organisms. We found that *Drosophila* GRAF protein with the domain organization is conserved across the other multicellular organisms *C.elegans*, *Drosophila*, *Xenopus*, *Chicken*, *Zebrafish* and *Humans*. The evolution in GRAF multi-domain nature is likely to be associated with multicellular complexity arising due to regulation of cell adhesion and contractility. We generated a

GRAF CRISPR mutant (*Graf*^{CR57}) having a premature stop codon with an absence of any functional domain. The *Graf* mutant is confirmed using sequencing and embryonic lethality.

We used the maternal knockdown strategy in *Graf*^f embryos which shows enhanced constriction throughout cellularization. These embryos stained with F-actin show loose polygonal networks where edges become wavy and detached from each other in early cellularization, premature constriction during mid stages and hyper constriction of rings in late stages when compared to control. *Graf* mutant shows more severe defects when compared to knockdown embryos by showing premature constriction during early stages and hyper constriction during mid and late stages. In addition, ring constriction is executed once it reaches the bottom of the nuclei in control embryos. *Graf*^f and *Graf*^{CR57} embryos show squeezed nuclei having bottleneck shaped similar to *Bottleneck* mutants due to premature ring constriction in mid cellularization.

These defects are correlated with GRAF recruitment dynamics. GRAF antibody staining and GRAF-GFP show differential recruitment across the cellularization stages. GRAF shows the increased localization at the contractile ring formed at the furrow tip from early to mid stages and becomes cytoplasmic during late stages. GRAF is spatially enriched at edges at the furrow tip where the contractile ring forms and is occasionally absent at vertices during an early stage. During mid stage, GRAF becomes enriched in regions where rings are contacting each other and occasionally absent from curved regions. Lastly, GRAF staining reduces from the ring and become cytoplasmic in late cellularization.

Taken together, the GRAF depleted phenotype of premature and hyper constriction of rings in cellularization signifies untimely constriction of the actomyosin network. The dynamics of recruitment of GRAF also correlate with the dynamic organization of actomyosin networks.

2.2 GRAF is essential for the regulation of Rho-GTP and Myosin II recruitment during cellularization

We assessed how GRAF regulates the downstream molecules Rho-GTP and Myosin II in contractile ring formation in *Drosophila* cellularization. GRAF-GFP specifically colocalizes along with a transgenic construct containing a RhoGTP binding domain of Anillin (AnillinRBD). AnillinRBD marks Rho-GTP and Sqh-mCherry marks Myosin II during early and mid stages. Rho-GTP is present at the furrow tip along with Myosin II during early, mid and late, even when GRAF-GFP become reduced at the ring during late cellularization. *Graf* depletion leads to increased Myosin II distribution at the contractile ring during cellularization. Laser ablations experiment shows the increased contractility in *Graf* mutants in the early and mid stages suggesting that GRAF plays a crucial role in resisting Myosin II-dependent contractility during the early and mid stages of cellularization. In addition, GRAF regulates the recruitment of key contractile ring proteins such as Diaphanous, Anillin, and PatJ. We found that the GRAF RhoGAP domain depletion causes hypercontractility phenotype which phenocopy *Graf* mutant during cellularization.

2.3 GRAF protein function in Rho-dependent pathway for regulating constriction during cellularization

We dissected the mechanism by which GRAF regulates contractile ring constriction in the Rho dependent pathway. GRAF overexpression leads to an expanded ring, which implies further that ring constriction is inhibited during cellularization stages. In contrast, maternally overexpressed RhoGEF2 gave rise to hyper constriction during cellularization. The combinations of GRAF overexpression in the background of RhoGEF2 overexpression suppressed the expanded ring in GRAF overexpression embryos and rescued the ring constriction similar to control. Overexpression of GRAF and RhoGEF2 have opposite effects on Rho-GTP levels, its combination is likely to lead to appropriate Rho-GTP levels thereby restoring the rate of constriction similar to controls. RhoGEF2 depletion shows inhibition of constriction of rings whereas the *Graf* mutant

shows an antagonistic effect of hyper constriction. There is a reduction in Myosin II intensity in RhoGEF2 whereas enhanced Myosin II intensity in *Graf* mutant. *Graf*^{CR57}; *RhoGEF2*ⁱ combination suppressed enhanced constriction and showed ring constriction similar to control embryos in early and mid cellularization. This combination shows the balance of Rho-GTP levels and retention of Myosin II recruitment resulting in ring constriction similar to control embryos in early and mid cellularization.

We further dissected the role of Myosin II constriction in mediating hyper constriction in *Graf* mutant embryos. Rho-Kinase (Drok) is known to activate Myosin II by phosphorylation in a Rho-GTP dependent manner whereas Myosin II phosphatase inactivates Myosin II by dephosphorylation (M. Glotzer, 2005). Rho kinase depletion leads to expanded rings due to loss of ring constriction with the diffused signal of Myosin II when compared to control. The combination of *Graf*^{CR57}; *rok*ⁱ results in the suppression of the hyper constriction phenotype seen in *Graf*^{CR57} embryos. ROK acts downstream of Rho-GTP which is unlikely to affect Rho-GTP in *rok*ⁱ mutant embryos. It is interesting to note that the ring area in the *Graf*^{CR57}; *rok*ⁱ combination mutant embryos were significantly higher as compared to controls due to the absence of active Myosin II. In addition, we achieved maternal knockdown of the Myosin II binding subunit (MBS) of Myosin II phosphatase which leads to Myosin II activation resulting in a severe reduction in constriction ring at the furrow tip. The suppression of hyper constriction phenotype is seen in maternally expressed *mbs*ⁱ; GRAF-OE embryos. Taken together, GRAF protein regulates the rate of constriction by maintaining Rho-GTP levels which is crucial for timely Myosin II activation driving the constriction process.

2.4 GRAF domain function in contractility and recruitment of actin regulatory protein at the contractile ring during cellularization

We assessed the role of GRAF domains in contractile ring formation in cellularization. We expressed transgenes containing domain deletions maternally in the background of *Graf*^{CR57}. Deletions of individuals domains in the following combinations *Graf*^{CR57}; GRAF Δ BAR-GFP, *Graf*^{CR57}; GRAF Δ PH-GFP, *Graf*^{CR57}; GRAF Δ RhoGAP-GFP

and *Graf*^{CR57}; GRAF Δ SH3-GFP which showed hyper constriction during cellularization. There was an increase in Myosin II at the ring in these combinations as compared to *Graf*^{CR57}; GRAF-GFP. GRAF is specifically recruited at the furrow tip cellularization and involved in the restriction of the transition from the polygonal network to the ring formation stage. GRAF is lost from the furrow tip during late cellularization. In order to assess the change in GRAF recruitment dynamics during cellularization, we quantified the relative distribution of the fluorescently tagged domain deleted proteins as compared to GRAF-GFP in mid and late cellularization. *Graf*^{CR57}; GRAF Δ BAR-GFP and *Graf*^{CR57}; GRAF Δ SH3-GFP shows significantly reduced GRAF intensity at the contractile ring during mid cellularization when compared to control. In contrast, *Graf*^{CR57}; GRAF Δ RhoGAP-GFP and *Graf*^{CR57}; GRAF Δ PH-GFP shows enriched signal with intense puncta at the furrow tip when compared to *Graf*^{CR57}; GRAF-GFP during late cellularization. In summary, GRAF BAR and SH3 domains are needed for protein recruitment at the contractile ring during mid cellularization whereas GRAF PH and Rho-GAP domains are required for the dissociation of the protein at the contractile ring during late cellularization.

The spatial pattern of GRAF recruitment varies with the dynamics of the actomyosin network. GRAF localizes precisely to the furrow tip in early cellularization, increases in mid cellularization and finally becomes cytoplasmic at late stages. *Graf* depletion showing pre-mature and hyper constriction defects are caused by inhibition of Rho-GTPase hydrolysis resulting in increased Rho-GTP levels. This increased Rho-GTP levels, in turn, activate Myosin II which is essential for ring constriction. In contrast, ROK depletion, which inactivates Myosin II, in *Graf* depletion background shows expanded rings due to inhibition of constriction (Sharma & Rikhy, 2021). This suggests that the constriction process is dependent on Myosin II activity. In summary, our findings show that the RhoGEF activity of RhoGEF2 and the RhoGAP activity of *Graf* is required to maintain appropriate levels of Rho-GTP for activation of Myosin II for ring constriction during cellularization. All domains of GRAF are required for restricting Myosin II dependent contractility. SH3 and BAR domains of GRAF regulate its recruitment at the

furrow tip during mid cellularization whereas RhoGAP and PH domains regulate the protein dissociation during late cellularization.

Taken together, multidomain proteins like GRAF containing membrane binding and RhoGAP domains are poised to regulate Rho-GTP levels in a highly regulated manner spatially and temporally during actomyosin contractility in different systems during cell migration and morphogenesis. Their presence in multicellular organisms and localization at focal adhesions and polarized epithelia suggests that they will regulate morphogenetic transitions occurring due to a change in adhesion and contractility.

3. References

- Adam, J. C., Pringle, J. R., & Peifer, M. (2000). Evidence for functional differentiation among *Drosophila* septins in cytokinesis and cellularization. *Molecular Biology of the Cell*, 11(9), 3123–3135.
- Afshar, K., Stuart, B., & Wasserman, S. A. (2000). Functional analysis of the *Drosophila* diaphanous FH protein in early embryonic development. *Development*, 127(9), 1887–1897.
- Aspenström, P. (2019). BAR Domain Proteins Regulate Rho GTPase Signaling. *Advances in Experimental Medicine and Biology*, 1111, 33–53.
- Bai, X., Lenhart, K. C., Bird, K. E., Suen, A. A., Rojas, M., Kakoki, M., Li, F., Smithies, O., Mack, C. P., & Taylor, J. M. (2013). The smooth muscle-selective RhoGAP GRAF3 is a critical regulator of vascular tone and hypertension. *Nature Communications*, 4, 2910.
- Barr, F. A., & Gruneberg, U. (2007). Cytokinesis: Placing and Making the Final Cut. In *Cell* (Vol. 131, Issue 5, pp. 847–860). <https://doi.org/10.1016/j.cell.2007.11.011>
- Barrios, J., & Wieder, R. (2009). Dual FGF-2 and Intergrin $\alpha 5\beta 1$ Signaling Mediate GRAF-Induced RhoA Inactivation in a Model of Breast Cancer Dormancy. In *Cancer Microenvironment* (Vol. 2, Issue 1, pp. 33–47). <https://doi.org/10.1007/s12307-009-0019-6>
- Basant, A., & Glotzer, M. (2018). Spatiotemporal Regulation of RhoA during Cytokinesis. *Current Biology: CB*, 28(9), R570–R580.

- Chougule, A. B., Hastert, M. C., & Thomas, J. H. (2016). Drak Is Required for Actomyosin Organization During *Drosophila* Cellularization. *G3*, 6(4), 819–828.
- Conrad, G. W., & Rappaport, R. (1981). Mechanisms of Cytokinesis in Animal Cells. In *Mitosis/Cytokinesis* (pp. 365–396). <https://doi.org/10.1016/b978-0-12-781240-3.50020-2>
- de Kreuk, B.-J., & Hordijk, P. L. (2012). Control of Rho GTPase function by BAR-domains [Review of *Control of Rho GTPase function by BAR-domains*]. *Small GTPases*, 3(1), 45–52.
- Doherty, J. T., Lenhart, K. C., Cameron, M. V., Mack, C. P., Conlon, F. L., & Taylor, J. M. (2011). Skeletal muscle differentiation and fusion are regulated by the BAR-containing Rho-GTPase-activating protein (Rho-GAP), GRAF1. *The Journal of Biological Chemistry*, 286(29), 25903–25921.
- Fededa, J. P., & Gerlich, D. W. (2012). Molecular control of animal cell cytokinesis. In *Nature Cell Biology* (Vol. 14, Issue 5, pp. 440–447). <https://doi.org/10.1038/ncb2482>
- Field, C. M., Coughlin, M., Doberstein, S., Marty, T., & Sullivan, W. (2005). Characterization of anillin mutants reveals essential roles in septin localization and plasma membrane integrity. *Development*, 132(12), 2849–2860.
- Glotzer, M. (2005). The Molecular Requirements for Cytokinesis. In *Science* (Vol. 307, Issue 5716, pp. 1735–1739). <https://doi.org/10.1126/science.1096896>
- Green, R. A., Paluch, E., & Oegema, K. (2012). Cytokinesis in Animal Cells. In *Annual Review of Cell and Developmental Biology* (Vol. 28, Issue 1, pp. 29–58). <https://doi.org/10.1146/annurev-cellbio-101011-155718>
- Grosshans, J., Wenzl, C., Herz, H.-M., Bartoszewski, S., Schnorrer, F., Vogt, N., Schwarz, H., & Müller, H.-A. (2005). RhoGEF2 and the formin Dia control the formation of the furrow canal by directed actin assembly during *Drosophila* cellularisation. *Development*, 132(5), 1009–1020.
- Guertin, D. A., Trautmann, S., & McCollum, D. (2002). Cytokinesis in eukaryotes. *Microbiology and Molecular Biology Reviews: MMBR*, 66(2), 155–178.
- Hildebrand, J. D., Taylor, J. M., & Parsons, J. T. (1996). An SH3 domain-containing GTPase-activating protein for Rho and Cdc42 associates with focal adhesion kinase. *Molecular and Cellular Biology*, 16(6), 3169–3178.

- Hiramoto, Y. (1975). FORCE EXERTED BY THE CLEAVAGE FURROW OF SEA URCHIN EGGS. In *Development, Growth and Differentiation* (Vol. 17, Issue 1, pp. 27–38). <https://doi.org/10.1111/j.1440-169x.1975.00027.x>
- Holst, M. R., Vidal-Quadras, M., Larsson, E., Song, J., Hubert, M., Blomberg, J., Lundborg, M., Landström, M., & Lundmark, R. (2017). Clathrin-Independent Endocytosis Suppresses Cancer Cell Blebbing and Invasion. *Cell Reports*, *20*(8), 1893–1905.
- Kiehart, D. P. (1990). The actin membrane skeleton in *Drosophila* development. *Seminars in Cell Biology*, *1*(5), 325–339.
- Kotadia, S., Crest, J., Tram, U., Riggs, B., & Sullivan, W. (2010). Blastoderm Formation and Cellularisation in *Drosophila melanogaster*. In *Encyclopedia of Life Sciences*. <https://doi.org/10.1002/9780470015902.a0001071.pub2>
- Krajcovic, M. M., & Minden, J. S. (2012). Assessing the critical period for Rho kinase activity during *Drosophila* ventral furrow formation. *Developmental Dynamics: An Official Publication of the American Association of Anatomists*, *241*(11), 1729–1743.
- Krueger, D., Quinkler, T., Mortensen, S. A., Sachse, C., & De Renzis, S. (2019). Cross-linker-mediated regulation of actin network organization controls tissue morphogenesis. *The Journal of Cell Biology*, *218*(8), 2743–2761.
- Luo, W., Janoštiak, R., Tolde, O., Ryzhova, L. M., Koudelková, L., Dibus, M., Brábek, J., Hanks, S. K., & Rosel, D. (2017). ARHGAP42 is activated by Src-mediated tyrosine phosphorylation to promote cell motility. *Journal of Cell Science*, *130*(14), 2382–2393.
- Mangione, M. C., & Gould, K. L. (2019a). Molecular form and function of the cytokinetic ring. *Journal of Cell Science*, *132*(12). <https://doi.org/10.1242/jcs.226928>
- Mavrikis, M., Azou-Gros, Y., Tsai, F.-C., Alvarado, J., Bertin, A., Iv, F., Kress, A., Brasselet, S., Koenderink, G. H., & Lecuit, T. (2014a). Septins promote F-actin ring formation by crosslinking actin filaments into curved bundles. *Nature Cell Biology*, *16*(4), 322–334.
- Mavrikis, M., Azou-Gros, Y., Tsai, F.-C., Alvarado, J., Bertin, A., Iv, F., Kress, A., Brasselet, S., Koenderink, G. H., & Lecuit, T. (2014b). Septins promote F-actin ring formation by crosslinking actin filaments into curved bundles. *Nature Cell Biology*,

16(4), 322–334.

- Pollard, T. D., & O’Shaughnessy, B. (2019). Molecular Mechanism of Cytokinesis. In *Annual Review of Biochemistry* (Vol. 88, Issue 1, pp. 661–689). <https://doi.org/10.1146/annurev-biochem-062917-012530>
- Royou, A., Field, C., Sisson, J. C., Sullivan, W., & Karess, R. (2004). Reassessing the role and dynamics of nonmuscle myosin II during furrow formation in early *Drosophila* embryos. *Molecular Biology of the Cell*, 15(2), 838–850.
- Schejter, E. D., & Wieschaus, E. (1993). Functional elements of the cytoskeleton in the early *Drosophila* embryo. *Annual Review of Cell Biology*, 9, 67–99.
- Schiel, J. A., & Prekeris, R. (2010). Making the Final Cut — Mechanisms Mediating the Abscission Step of Cytokinesis. In *The Scientific World JOURNAL* (Vol. 10, pp. 1424–1434). <https://doi.org/10.1100/tsw.2010.129>
- Sherlekar, A., & Rikhy, R. (2016). Syndapin promotes pseudocleavage furrow formation by actin organization in the syncytial *Drosophila* embryo. *Molecular Biology of the Cell*, 27(13), 2064–2079.
- Sokac, A. M., & Wieschaus, E. (2008). Local actin-dependent endocytosis is zygotically controlled to initiate *Drosophila* cellularization. *Developmental Cell*, 14(5), 775–786.
- Stachowiak, M. R., Laplante, C., Chin, H. F., Guirao, B., Karatekin, E., Pollard, T. D., & O’Shaughnessy, B. (2014). Mechanism of cytokinetic contractile ring constriction in fission yeast. *Developmental Cell*, 29(5), 547–561.
- Su, J., Chow, B., Boulianne, G. L., & Wilde, A. (2013). The BAR domain of amphiphysin is required for cleavage furrow tip–tubule formation during cellularization in *Drosophila* embryos. In *Molecular Biology of the Cell* (Vol. 24, Issue 9, pp. 1444–1453). <https://doi.org/10.1091/mbc.e12-12-0878>
- Takeda, T., Robinson, I. M., Savoian, M. M., Griffiths, J. R., Whetton, A. D., McMahon, H. T., & Glover, D. M. (2013). *Drosophila* F-BAR protein Syndapin contributes to coupling the plasma membrane and contractile ring in cytokinesis. *Open Biology*, 3(8), 130081.
- Taylor, J. M., Macklem, M. M., & Parsons, J. T. (1999). Cytoskeletal changes induced by GRAF, the GTPase regulator associated with focal adhesion kinase, are mediated by Rho. In *Journal of Cell Science* (Vol. 112, Issue 2, pp. 231–242).

<https://doi.org/10.1242/jcs.112.2.231>

Xue, Z., & Sokac, A. M. (2016). Back-to-back mechanisms drive actomyosin ring closure during *Drosophila* embryo cleavage. In *Journal of Cell Biology* (Vol. 215, Issue 3, pp. 335–344). <https://doi.org/10.1083/jcb.201608025>

Yoneda, M., & Dan, K. (1972). Tension at the Surface of the Dividing Sea-Urchin Egg. In *Journal of Experimental Biology* (Vol. 57, Issue 3, pp. 575–587). <https://doi.org/10.1242/jeb.57.3.575>

Young, P. E., Richman, A. M., Ketchum, A. S., & Kiehart, D. P. (1993). Morphogenesis in *Drosophila* requires nonmuscle myosin heavy chain function. *Genes & Development*, 7(1), 29–41.

CHAPTER 1

Introduction

1.1 Cytokinesis in multicellular tissues

Cell division is a fundamental cellular process that gives rise to multicellularity. It starts from cell growth, genome duplication, chromosome segregation and finally cell division (M. Glotzer, 2005). The final step of cell division which leads to the physical separation of a cell is called cytokinesis. Successful cytokinesis is necessary for proper genome segregation and the appropriate division of cytoplasmic contents among the daughter cells. Any failure or perturbation during cytokinesis results in cell death and the production of multinucleate and aneuploid cells; these cells can further function as oncogenic precursors (D'Avino et al., 2015; Li, 2007; Mangione & Gould, 2019; Normand & King, 2010; Storchova & Pellman, 2004)

The cytokinesis machinery uses approximately 20 proteins that are conserved across most animals, i.e., vertebrates, insects and nematodes (Echard et al., 2004; Eggert et al., 2004; Sönnichsen et al., 2005). These proteins are components of the central spindle, contractile ring, and vesicles. The central spindle functions as a hub of molecules required for the initiation of the cleavage furrow (Dechant & Glotzer, 2003; Jantsch-Plunger et al., 2000; Mishima et al., 2002, 2004; Mollinari et al., 2002). Most of the molecules involved in the formation and constriction of the contractile ring are activated by the RhoA pathway (Somers et al., 2003). During cleavage furrow ingression, vesicle fusion provides the molecules needed for membrane addition. These vesicles are acquired through the vesicular trafficking pathway (Low et al., 2003; M. Murthy & Schwarz, 2004; A. R. Skop, 2004).

The driving force to execute cytokinesis comes from the constriction of the contractile ring. The force acting on cleavage furrow partitions the cell into two through a contractile ring that is attached to the plasma membrane. The contractile ring is a dense network of actin bundles and Myosin II filaments (Mangione & Gould, 2019). The positioning of the contractile ring is guided by the spindle complex in the anaphase. The recruitment of key molecules at the contractile ring is directed by the local regulation of Rho activity (Basant & Glotzer, 2018). The constriction of the contractile ring can be attributed to the motor activity of Myosin II, which results in the translocation of the actin filaments (Hiramoto, 1975; Stachowiak et al., 2014; Yoneda & Dan, 1972). This ring constriction further leads to cleavage furrow ingression to the point where the cell finally separates to generate daughter cells (Green et al., 2012). Cytokinesis is highly dependent on the regulation of membrane and actin dynamics which is guided by the class of proteins called BAR domain proteins.

1.2 BAR domain proteins in membrane curvature induction or sensation

Cells contain different classes of membrane deforming proteins that give rise to membrane curvature during cytokinesis. As a function of their concentration and spatiotemporal localization, these proteins modulate membrane shape in form of membrane curvature, tubulation and generation of vesicles i.e., precisely bend and cut the membranes in a highly orchestrated fashion. In order to verify the same, BAR domain proteins, such as Amphiphysin, Endophilin, Cip4 and FES related proteins (FES) that modulate tubule formation have been purified and their function investigated using synthetic lipid vesicles in *in vitro* assays (Farsad et al., 2001; Itoh et al., 2005; Takei et al., 1999). The results showed that BAR domain proteins do not simply function as adaptors for membrane and cytoskeleton effectors; rather they are likely the direct modulators of membrane shape.

BAR domain proteins are named after Bin1 from mammals (Sakamuro et al., 1996), Amphiphysin (Lichte et al., 1992) and Rvs167 from yeast (Sivadon et al., 1997) that are characterized independently and found to exhibit sequence similarity in terms of the membrane-binding domain. In recent years, the BAR domain has emerged as an

adaptor that links the membrane to the cytoskeleton- a phenomenon that is especially evident during endocytosis (Qualmann et al., 2011; M. J. Taylor et al., 2011; Tsujita et al., 2006). These domains are present in numerous proteins that are known to be involved in mediating membrane dynamics and are highly conserved across evolution (David et al., 1994; Sakamuro et al., 1996). The precise sensing of highly curved membranes is achieved by a banana-shaped α -helical dimer of these domains as revealed by the crystal structure of the BAR domains of Amphiphysin (Peter et al., 2004) and Endophilin (Gallop et al., 2006; Masuda et al., 2006; Mim et al., 2012; Weissenhorn, 2005). The banana-shaped BAR module is a concave surface that forms a lipid-binding surface (Qualmann et al., 2011). Apart from sensing curvature, the BAR domain can also induce membrane lipids to form tubules *in vitro* and *in vivo* (Frost et al., 2008; Henne et al., 2007; Itoh et al., 2005; Mim et al., 2012; Shimada et al., 2007). For further stabilization of these tubules, BAR domain proteins form higher-order structures and polymerize into long filamentous structures around the tubules (Dawson et al., 2006; Itoh et al., 2005). In addition to the BAR domain, these proteins harbour auxiliary domains that are involved in membrane binding (e.g., PH and PX domains, which are known to bind the specific phospholipids in the membrane (Lemmon, 2008)) and mediating protein-protein interactions (e.g., SH3 domain). The interactions mediated by the BAR domain enable three types of cellular processes—membrane deformation, vesicle formation and actin assembly— which are directly or indirectly also dependent on the interactions mediated by the SH3 domain. The SH3 domain of BAR domain proteins is known to interact with cytoskeletal assembly factors and the vesicle scission protein, Dynamin (Gallop et al., 2006; Icking et al., 2005, 2006; Itoh et al., 2005; Kessels & Qualmann, 2004; Kovacs et al., 2006; Masuda et al., 2006; Peter et al., 2004; Rao et al., 2010; Salazar et al., 2003; Tsujita et al., 2006). This domain can also recruit Rho family GTPases, which are known as master regulators of the actin assembly (Hall, 2012; Ridley, 2015).

Under *in vivo* conditions, highly curved tubules at the membrane are formed in response to external forces that arise as a result of endocytic coat protein activity, actin polymerization, and molecular motor activity. In most cases, BAR domain proteins are recruited at these tubular structures to enable their stabilization. *In vitro* assays measuring

the fluorescence intensity of BAR proteins recruited to the membrane tubules connected to a giant vesicle revealed that these proteins can sense the membrane curvature (Sorre et al., 2012). This experiment revealed that the density of BAR protein on a membrane tubule was 10 to 100 fold higher than the density on the quasi-flat surface of a vesicle (Baumgart et al., 2011); at low densities, as those observed on the vesicle surface, BAR proteins do not induce membrane tubulation (Shi & Baumgart, 2015). This curvature sorting property of proteins is dependent on the extent of BAR protein enrichment. All tested BAR proteins are specifically sorted on the membrane tubules, including β 2 Centaurin (Sorre et al., 2012), Syndapin 1 (Ramesh et al., 2013) (F-BAR); Amphiphysin (Heinrich et al., 2010; Sorre et al., 2012), Endophilin (Simunovic et al., 2016; Chen Zhu et al., 2012), BIN1 (T. Wu et al., 2014), and ArfGAP1 (Ambroggio et al., 2010) (N-BARs); and IRSp53 (Prévost et al., 2015) (I-BAR).

1.2.1 BAR domain proteins: Structural characteristics and classification of BAR domain proteins

The BAR domain proteins are broadly classified into three different classes based on the presence of characteristic domains such as classical BAR/ N-BAR, F-BAR and I-BAR. BAR/N-BAR and F-BAR proteins have concave surfaces and induce negative membrane curvature (e.g., invaginations) whereas I-BAR proteins have convex surfaces and induce positive membrane curvature (e.g., protrusions).

1.2.1.1 F-BAR

F-BAR proteins are characterized by the presence of an F-BAR domain, wherein an FES-CIP4 homology (FCH) domain (Aspenström, 1997) is next to a coiled-coil domain, giving rise to a single functional unit, i.e., F-BAR (Frost et al., 2007; Henne et al., 2007; Itoh et al., 2005; Shimada et al., 2007) (Figure 1.1D). The mammalian F-BAR family is further subcategorized into nine subfamilies, i.e., CIP4, FCHO, SrGAP, PACSIN, PSTPIP, FCHSD, FES/FER, NOSTRIN and GAS7 subfamilies (Ahmed et al., 2010; Aspenström, 2009; Roberts-Galbraith & Gould, 2010; Suetsugu et al., 2010; Takenawa, 2010) (Figure 1.1A). *In vitro* experiments have shown that F-BAR proteins such as FBP17 and CIP4 induce liposome tubulation. These proteins dimerize by means of α -helical structures,

which bind to phosphatidylserine (PS) and phosphatidylinositol 4,5-bisphosphate (PI(4,5)P₂) (Heath & Insall, 2008). In addition to the F-BAR domain, BAR domain proteins harbour various auxiliary domains, i.e., the SH2 domain, SH3 domain, RhoGAP domain, tyrosine kinase domain, WW domain, protein kinase C-related kinase homology region 1 (HR1) domain and μ -homology domain. Some F-BAR proteins—involved in vesicle recycling and endocytosis—harbour an SH3 domain that interacts with synaptojanin, N-WASP and Dynamin (Rao et al., 2010).

1.2.1.2 N-BAR

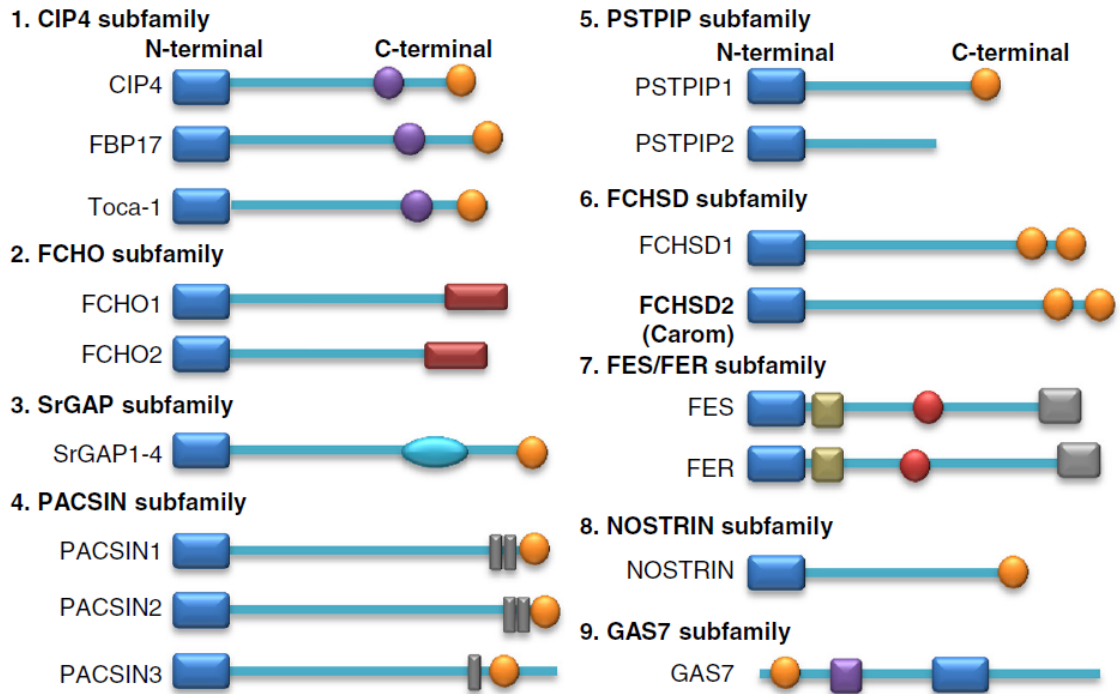
Proteins containing only the BAR domain are classified as classical BAR domain proteins (e.g. Bin 1). Co-occurrence of BAR domains with membrane binding domains, such as amphipathic α -helix, PX domain (Phox homology domain), and PH domain (Pleckstrin homology domain) further increases the efficiency of membrane binding (Rao & Haucke, 2011) (Figure 1.1B). N-BAR domain proteins are characterized by the presence of an amphipathic helix at the N-terminal of the BAR domain fold (Casal et al., 2006; Peter et al., 2004) (Figure 1.1D), wherein the helix senses the membrane. The N-BAR domain proteins exhibit enhanced membrane binding ability owing to the insertion of the amphipathic helix into the membrane resulting in the stabilization of membrane curvature (Daum et al., 2016; Yoon et al., 2012). In the presence of N-BAR proteins such as Amphiphysin1 and Endophilin1, liposomes generate tubule-like structures. N-BAR domain proteins such as Amphiphysin, Endophilin, Sorting nexin9 harbour an SH3 domain that binds to the proline-rich domain of Dynamin, thereby aiding endocytosis by binding to the curvature of the vesicle neck (Gallop et al., 2006; Masuda et al., 2006; Mim et al., 2012; Weissenhorn, 2005; Peter et al., 2004; Tarricone et al., 2001)

1.2.1.3 I-BAR

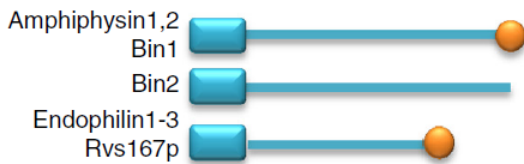
I-BAR (inverse BAR) domain proteins, such as IRSp53, IRTKS, and MIM bind to phosphoinositide-rich membranes, especially PI(4,5) P₂ and generate tubular structures (Mattila et al., 2007; Saarikangas et al., 2009) (Figure 1.1C). In addition to detecting PI(4,5)P₂-enriched regions, they modulate membrane shape by inducing PI(4,5)P₂

clustering (Saarikangas et al., 2009). Proteins belonging to this family such as IRSp53 and MIM I-BAR domains are composed of α -helical antiparallel dimers (S. H. Lee et al., 2007; Millard et al., 2005). In contrast to BAR and F-BAR domains, I-BAR domains display convex geometry and bind to the inner leaflet of membrane tubules, thereby inducing negative membrane curvature (Figure 1.1D). Thus, these proteins are involved in generating protrusions rather than invaginations (Mattila et al., 2007; Saarikangas et al., 2009; Suetsugu et al., 2006). I-BAR proteins induce the generation of protrusions in filopodia and lamellipodia by virtue of the SH3 domain that is known to enable actin bundling and exhibits inverted geometry that enables membrane binding (Scita et al., 2008; Yamagishi et al., 2004). The CRIB domain of IRSp53 interacts with a small GTPase Cdc42 and its SH3 domain interacts with the proline-rich sequence of actin regulators, such as WAVE-2, Mena, and Eps8 (Funato et al., 2004; Krugmann et al., 2001; Miki et al., 2000). The proline-rich regions of MIM interact with the actin regulator cortactin (Lin et al., 2005). The Pink BAR protein is the only BAR protein that is expressed in epithelial cells and induces the formation of planar membrane sheets instead of membrane tubulations (Pykäläinen et al., 2011).

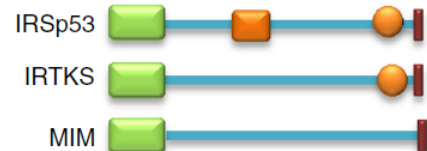
A F-BAR family



B N-BAR family



C I-BAR family



D Membrane curvature forms caused by BAR domain proteins

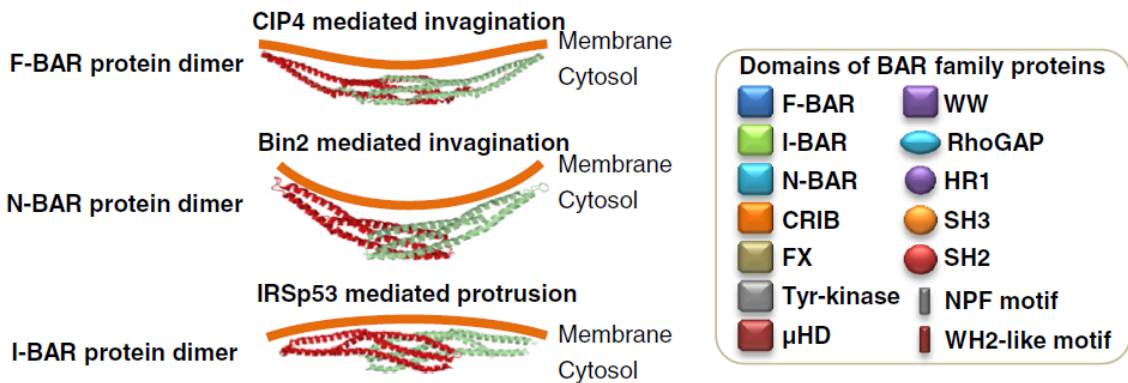


Figure 1.1: Characterization of F-BAR, N-BAR and I-BAR family domain architecture and its membrane curvature model. BAR domain superfamily classification is based on the presence of distinct

domain structures of F-BAR, N-BAR, and I-BAR. BAR domain proteins are known to form homodimers that interact and bind to membranes resulting in membrane curvature. (A) F-BAR domain family. The F-BAR family is divided into nine subfamilies based on specific domain combinations. (B) N-BAR domain family. (C) I-BAR domain family. (D) Membrane curvature is caused by specific BAR domain proteins. F-BAR, N-BAR, and I-BAR bind differently to membranes and generate different forms of membrane curvature. Abbreviations: BAR, Bin/Amphiphysin/Rvs; F-BAR, Fes/CIP4 homology-BAR; FX, F-BAR extension; I-BAR, Inverse BAR; N-BAR, N-terminal amphipathic helix BAR; CRIB, CDC42-Rac interactive binding; HR1, Protein kinase C-related kinase homology region 1; NPF, Asparagine proline phenylalanine; RhoGAP, Rho GTPase-activating protein; SH2, Src homology-2; SH3, Src homology-3; WH2, WASP homology 2; Tyr-kinase, Tyrosine kinase; μ HD, μ -homology domain. Adapted from (S. Liu et al., 2015)

1.3 Mechanism by which BAR domain proteins induce membrane curvature

Different classes of BAR domain proteins are responsible for generating different scales of curvature.

1.3.1 BAR domain proteins induce local membrane curvature

1.3.1.1 Curvature induction in the membrane in response to interaction with the BAR domain.

Induction of spontaneous membrane curvature is mediated by the electrostatic interaction between molecules—such as proteins, ions, or solid particles—and one side of the leaflet (Lipowsky, 2013). These molecules do not require to be intrinsically curved in order to induce spontaneous curvature, but the banana-curved shape of the BAR domain proteins makes them more effective in inducing membrane curvature. The positively charged amino acids in the banana-shaped α -helical dimer use electrostatic forces to bind negatively charged lipids such as PS or PI(4,5)P₂. These electrostatic forces create a strong adhesive interface crucial for generating curvature (Blood & Voth, 2006).

1.3.1.2 Insertion of amphipathic helices to induce membrane curvature

Several studies have reported the presence of one or more amphipathic helices (AH) in BAR domain proteins (Peter et al., 2004; Qualmann et al., 2011). These AHs insert their helices into the lipid bilayer in a shallow manner, thereby pushing the lipids apart and inducing local curvature. A striking example is the short amphipathic moiety of the pleckstrin homology (PH) domain of β 1 centaurin, which can wedge into the bilayer, thereby inducing curvature in one leaflet of the bilayer (Pang et al., 2014). According to theoretical studies, spontaneous curvature is highly dependent on the protein insertion depth (Campelo et al., 2008; Zemel et al., 2008).

1.3.1.3 Low density crowding of BAR domain proteins promotes membrane curvature sensing

Crowding occurs when protein oligomerizes in high enough local concentration on the membrane surface resulting in induction of membrane curvature (Guigas & Weiss, 2016). Crowding induced membrane curvature can be attributed to the disordered subregions in BAR domain proteins (Busch et al., 2015). Much more surface coverage is required to achieve the same curvature than what is required by the N-BAR domain of Endophilin. *In silico* molecular simulations of the binding of N-BAR proteins to large lipid vesicles and planar bilayer also reveal that the proteins assemble into string-like aggregates (Bickel et al., 2001; Breidenich et al., 2000). Thus, the *in vivo* association of BAR proteins (at low densities) with membranes will depend on the composition of the membrane and tension modulators such as actin and actin regulatory proteins.

1.3.2 Mechanism by which BAR domain proteins induce large-scale membrane curvature

1.3.2.1 Tubulation or Scaffolding: Curvature generation

The high density of BAR domain proteins with higher-order organization induces morphological alterations in the membrane, e.g., tubulation (Chou et al., 2001; Dommersnes & Fournier, 1999; Park & Lubensky, 1996; Y. Schweitzer & Kozlov, 2015).

Endophilin, an N-BAR containing protein at a density >5% results in the onset of tubulation from the quasi-flat surface of giant vesicles (Simunovic et al., 2015).

Another consequence of the high density of BAR domain proteins is that the self-assembly of these proteins results in the establishment of a scaffold, which affects the membrane surface tension and shapes the membrane into stable tubules. The direct evidence of scaffold is observed in N-BAR proteins such as Endophilin (Renard et al., 2015) and Amphiphysin (Sorre et al., 2012) whereas indirect evidence of scaffolding in the case of the F-BAR protein Syndapin (F-BAR) (Ramesh et al., 2013). Scaffold formation is observed when the underlying flat membrane is exposed to Amphiphysin (N-BAR; density >5%) (Sorre et al., 2012). In a biological context, the scaffold is involved in processes, such as the constriction of the neck of the endocytic vesicles, which is required to elongate the neck and fission of the membrane during the last step of endocytosis.

1.4 Role of BAR domain proteins in cytokinesis

F-BAR domain proteins act as bridges between the membrane and cytoskeletal function during processes, such as endocytosis, cell motility and cytokinesis (S. Liu et al., 2015; Roberts-Galbraith & Gould, 2010). Membrane dynamics and cytoskeletal remodelling are a crucial part of cytokinesis, right from yeast to humans. A plethora of studies have dissected the mechanism by which F-BAR domain proteins play a role in cytokinesis. The yeast F-BAR domain protein Cdc15p is known to interact with formin (cdc12p) and myosin (myo1) to influence medial actin dynamics (Carnahan & Gould, 2003; Graziano et al., 2014; Laporte et al., 2011; S. Liu et al., 2015; Roberts-Galbraith et al., 2010; Wachtler et al., 2006; Willet et al., 2015; Yan et al., 2013). Another F-BAR domain protein Imp2 recruits other proteins in order to stabilize the contractile ring. The SH3 domain of Cdc15p and Imp2 recruits Fic1 (C2 domain-containing protein) and Pxl1 (paxillin-related protein 1), which are required for the anchoring, stability and constriction of the contractile ring (Ge & Balasubramanian, 2008; Pinar et al., 2008; Pollard & Wu, 2010; Roberts-Galbraith et al., 2009; Wachtler et al., 2006). The *Saccharomyces cerevisiae* F-BAR protein Hof1 localizes to the bud neck and interacts with Cdc10 (septin) via its N-terminal domain. The SH3 domain of this protein interacts with Myo1 (Myosin II

heavy chain) and maintains its symmetry during ring constriction (Meitingner et al., 2013; Oh et al., 2013). In *Drosophila* embryo, formin Diaphanous (Dia) plays an essential role in membrane stabilization via F-actin bundling during cellularization. During this process, an F-BAR protein Cip4 has been shown to physically and functionally interact with Dia. Cip4 overexpression phenocopies *dia* mutant defects and has been established as an antagonist for Dia (Yan et al., 2013). Another *Drosophila* F-BAR protein Syndapin has been shown to be involved in cytokinesis in the S2 cell line. Syndapin has been shown to interact with PI(4,5)P2 and with a contractile ring protein Anillin (Takeda et al., 2013). Further, Syndapin is required for the ingression of the pseudocleavage furrow during the syncytial stages of *Drosophila* (Sherlekar & Rikhy, 2016). Another interesting N-BAR domain, Amphiphysin—involved in endocytosis—was visualized as tubules occurring at the ingressing furrow tip in the *Drosophila* syncytial blastoderm embryo (Sokac & Wieschaus, 2008a). These tubules are absent in *amphiphysin* null embryos, which exhibit faster cleavage furrow ingression (Su et al., 2013)

Approximately 35% of all BAR domain proteins harbour ArfGAP, RhoGAP, or RhoGEF domains, all of which regulate various GTPases or are in turn regulated by Rho-GTPases (Aspenström, 2019; de Kreuk & Hordijk, 2012). This is especially important in light of the fact that the Rho-GTPase pathway is involved in regulating actin cytoskeleton remodelling during cytokinesis. Several reports show the direct regulation of BAR domain proteins by Rho-GTPases, including the F-BAR family-members—Toca1 (Bu et al., 2010; Ho et al., 2004; Watson et al., 2016), CIP4 (Aspenström, 1997; Pichot et al., 2010), and Syndapin 2 (PACSIN2) (de Kreuk et al., 2011), BAR domain protein Arfaptin (D'Souza-Schorey et al., 1997; Van Aelst et al., 1996) and all members of I-BAR superfamily IRSp53 (Abou-Kheir et al., 2008; Disanza et al., 2013; Kast et al., 2014; Krugmann et al., 2001; Lim et al., 2008; Miki et al., 2000), MIM (Bompard et al., 2005; Drummond et al., 2018), ABBA (Saarikangas et al., 2008; Zeng et al., 2013; Zheng et al., 2010), IRTKS (Sudhakaran et al., 2016) and Pinkbar (Sudhakaran et al., 2016). Thus, BAR domain proteins have emerged as potential candidates involved in cytokinesis that function via the regulation of Rho-GTPase signalling.

1.5 Steps of cytokinesis

1.5.1 Initiation of cytokinesis: Central spindle complex

Anti-parallel bundles consist of 10-30 microtubules that begin to organize in early anaphase in PtK₁ cells, as revealed by serial electron micrographs (Mastronarde et al., 1993). During anaphase progression, antiparallel microtubule bundles known as the spindle midzone (overlap zone) are recruited between the separating chromosomes (Michael Glotzer, 2009). These bundled microtubules specify the division plane. The average length of the spindle midzone occupied by microtubule bundles was ~5 μm in the early and middle anaphase and restricted to ~1 μm in late anaphase in mammalian cell line PtK1 (Mastronarde et al., 1993) (Figure 1.2A). At the end of anaphase, the proteolytic destruction of cyclins leads to the inactivation of mitotic kinases that promote the activation of several proteins, which trigger the assembly of the central spindle (Echard & O'Farrell, 2003; Michael Glotzer, 2009). The central spindle is formed by the specific recruitment and enrichment of the key regulators of cytokinesis in the restricted region of microtubule bundles. Central spindle assembly requires CPC, Centralspindlin, PRC1, and two kinesins MLKP1 and KIF4. CPC is known to phosphorylate MLKP1 and recruits Centralspindlin to the midzone which is essential for central spindle assembly (Douglas et al., 2010; Giet & Glover, 2001; Guse et al., 2005; Hauf et al., 2003; Hu et al., 2008; Kaitna et al., 2000; Severson et al., 2000; Verbrugghe & White, 2004; Changjun Zhu et al., 2005) (Figure 1.2A). Centralspindlin is a heterotetrameric complex composed of Kinesin-6, MLKP1, and CYK4 (Pavicic-Kaltenbrunner et al., 2007). CYK4 contains a GAP domain and is predicted to exhibit GTPase activity towards Rho family molecules. PRC1 selectively binds and crosslinks microtubule bundles in antiparallel orientation (Bieling et al., 2010; Gaillard et al., 2008; Janson et al., 2007; Loiodice et al., 2005) (Figure 1.2B). PRC1 facilitates the recruitment of KIF4 to the microtubule overlap zone (Hu et al., 2011; Kurasawa et al., 2004; Changjun Zhu & Jiang, 2005). *In vitro* analysis shows that PRC1 cooperates with KIF4 to enable microtubule growth, thereby increasing the length of the overlap zones. In contrast to PRC1, KIF4 uses its motor activity to reach the plus end of the microtubule and suppresses their dynamics to maintain the overlap zone (Bieling et al., 2010) KIF4 depletion in cells results in increased length of the spindle

midzone (twice the normal length) (Hu et al., 2011; Kurasawa et al., 2004; Changjun Zhu & Jiang, 2005). This extended overlap zone exhibits wider distribution of RhoA and Anillin during ingression as motor proteins are required for the transport of key Rho regulators (Hu et al., 2011).

1.5.1.1 Central spindle complex in metazoan embryos

MLKP1 and its orthologs—ZEN-4 in *C. elegans* and Pavarotti (Pav) in *Drosophila*—are crucial for central spindle assembly during cytokinesis. ZEN-4 embryonic mutants were generated in *C. elegans* using three independent methods, i.e., RNAi, mosaic analysis, and use of temperature-sensitive mutants. Embryos lacking ZEN-4 were unable to form the central spindle and were characterized by cleavage furrow ingression defects near completion (Powers et al., 1998; Raich et al., 1998; Severson et al., 2000). *C. elegans* embryos with defective CYK-4 and ZEN-4 exhibit phenocopy and show similar spindle assembly defects. CYK-4 and ZEN-4 are localized to the central spindle and characterized as CYK-4/ZEN-4 complexes in *C. elegans* embryo extract (Jantsch-Plunger et al., 2000).

Drosophila, *pav* mutant embryos exhibit disrupted cleavage furrow ingression and central spindle assembly; these are different from those observed in *C. elegans* and can be attributed to significant differences in the Pavarotti localization in *Drosophila* cells compared to that of the ZEN-4 ortholog in *C. elegans*. Initially, in metaphase, Pav-KLP is associated with the centrosomes and cell cortex and is later recruited to the contractile ring associated with the central spindle (Adams et al., 1998), whereas in *C. elegans*, ZEN-4 specifically localized on the central spindle (Nislow et al., 1990; Powers et al., 1998; Raich et al., 1998). In *Drosophila*, *pav* and other mutants that are defective in central spindle assembly enable us to conclude that contractile ring assembly is dependent on the central spindle assembly (M. G. Giansanti et al., 1998).

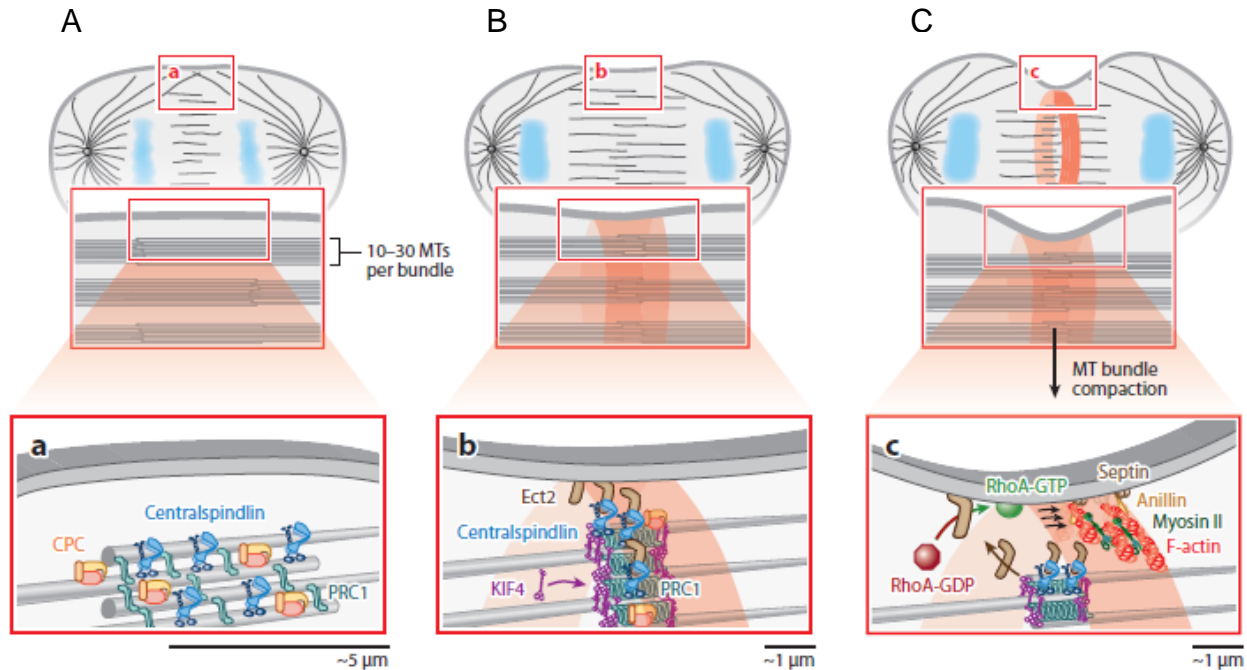


Figure 1.2: Central spindle complex formation, positioning and signalling. (A) In early anaphase, PRC1 is required to bundle antiparallel microtubules. After this, centralspindlin, and the chromosomal passenger complex (CPC) is observed at the overlap spindle zone, which further bundled overlapping microtubules of opposite polarity. (B) In mid anaphase, PRC1 recruits KIF4 to the overlap zone. KIF4 moves to the plus end of the microtubule and limits its growth to the narrow overlap zone. This is followed by Ect2 binding to centralspindlin where it is loaded onto the equatorial membrane region. (C) At the equatorial membrane, Ect2 triggers RhoA-GDP conversion into Rho-GTP in order to promote contractile ring assembly. Adapted from (Green et al., 2012)

1.5.2 Cleavage furrow assembly to regulate contractile ring formation and constriction

1.5.2.1 Specification of active RhoA zone

Contractile ring assembly occurs between cortex and anaphase spindle in animal cells. The spindle guides the formation of a confined equatorial zone of active RhoA (Bement et al., 2006; A. Piekny et al., 2005; Wadsworth, 2005). Active RhoA causes the recruitment and activation of key effector contractile ring proteins including Rho-kinase resulting in Myosin II activation, and formin which trigger assembly of unbranched actin filaments (Bement et al., 2006; Goode & Eck, 2007; Matsumura et al., 2011; A. Piekny et al., 2005) (Figure 1.2C).

In classical micromanipulation experiments in *Echinarachnius parma* eggs, the relocation of spindle apparatus causes previous furrow regression and promotes the development of new furrows above the new spindle midplane (Rappaport, 1985). The spindle directly contributes towards the formation of a defined equatorial zone of active RhoA (Bement et al., 2006; A. Piekny et al., 2005). Active RhoA concentrates in a narrow zone that precedes the furrow and later coincides with the furrow. This zone is conserved across four different echinoderms and vertebrate *Xenopus laevis*. RhoA zone forms despite the disruption of actin and Myosin II (Straight et al., 2003), which established this as an upstream molecule in controlling cytokinesis. RhoA zone formation is controlled by the spindle microtubules as shown by micromanipulation of the spindle and pharmacological manipulation of the microtubule. In sea urchin embryos, the micromanipulation experiment shows that repositioning of the spindle causes RhoA activity zone translocation followed by new furrow formation (Bement et al., 2005). In *Drosophila* embryos, ectopic Rho1 activation induced ectopic furrow formation. The establishment and positioning of these ectopic furrows are dependent on the overlap of antiparallel microtubules as shown by the pharmacological disruption experiment. This ectopic furrow consists of core components actin, Myosin II and membrane which is similar to conventional cytokinetic furrows (Crest et al., 2012).

The mechanisms by which the spindle promotes a narrow zone of active RhoA are not well characterized. There are ideas suggesting a bipartite mechanism in which signals from the spindle midzone activate RhoA at the cell equator whereas its suppression is mediated by dynamic microtubules nucleated by the centrosomal asters (D'Avino et al., 2005; von Dassow, 2009). In addition to spindle-based activation, there is a RhoA flux model which implicates the differential spatial activity of RhoGEF and RhoGAP as crucial in specifying the RhoA active zone. RhoA is activated by the GTPase exchange factor (RhoGFF) which converts GDP to GTP and is inactivated by GTPase activating proteins (RhoGAP), which enhance the hydrolysis rate of GTP. In the RhoA flux model, localized RhoGFF (Ect2) activity mediated RhoA activation is balanced by global RhoGAP (MgcRacGAP) mediated RhoA inactivation (Hirose et al., 2001; Issei Mabuchi et al., 1993;

Prokopenko et al., 1999; Tatsumoto et al., 1999). It also predicts that the equatorial active RhoA zone will diffuse through the membrane as the rate of GAP mediated RhoA turnover decreases, resulting in a broadening RhoA zone (Bement et al., 2006). There are studies that identified Ect2 as the critical RhoGFF during cytokinesis. It has been proposed that spindle-based mechanisms that lead to the activation and recruitment of Ect2 at the cell equator are correlated with RhoA zone formation. However, GAP mediated RhoA inactivation contributing towards RhoA zone dimensions and dynamics is still unclear. In addition, studies are required to identify the relevant candidate RhoGAP which acts opposite to Ect2.

Ect2 (an orthologue of *Drosophila* Pebble) is known to bind centralspindlin and preferentially recruit at the equatorial membrane to initiate cytokinesis (Prokopenko et al., 1999; Tatsumoto et al., 1999) (Figure 1.2B). The localization of Ect2 (RhoGEF) at the membrane is crucial for proper cytokinesis as shown in human cells (Su et al., 2011) and this is further established in *C.elegans* as well (Gómez-Cavazos et al., 2020). It causes RhoA activation that further strengthens and sharpens the RhoA zone (Bement et al., 2015; D. Zhang & Glotzer, 2015). Rho-GTPase-activating protein (RacGAP50C) part of the centralspindlin complex is required to recruit Pbl/Ect2 at contractile rings (Hirose et al., 2001; Somers et al., 2003; Wadsworth, 2005). The RhoGEF, RhoGEF2 which recruits to pseudo cleavage furrow in syncytial and furrow canal in cellularization stages. It activates Rho1 to initiate furrow ingression and contractile ring assembly in the syncytial stage and cellularization respectively. The position of activated Rho1 cortical stripe with core cytokinetic machinery resembles conventional cytokinesis (Crest et al., 2012).

1.5.2.2 Regulation of Myosin II

After the establishment of the active RhoA zone, RhoA-GTP activates downstream molecules in pathways that result in actin polymerization and Myosin II activation (Basant & Glotzer, 2018; Schwayer et al., 2016) (Figure 1.3). Among all myosins, non-muscle Myosin II (Myosin II) is established as one of the conserved and central molecules in cytokinesis. Initially, Myosin II recruits as foci to the division plane and then reorganizes into a ring (Maupin & Pollard, 1986; Manos Mavrakakis et al., 2014; Noguchi & Mabuchi,

2001; Vavylonis et al., 2008; J.-Q. Wu et al., 2003; Zhou & Wang, 2008). Any perturbation in Myosin II function results in cytokinesis failure as seen in starfish blastomeres (I. Mabuchi & Okuno, 1977), *Dictyostelium discoideum* (De Lozanne & Spudich, 1987; Knecht & Loomis, 1987), budding yeast (Bi et al., 1998; Lippincott & Li, 1998), and fission yeast (Bezanilla et al., 1997; Goff et al., 2000; Kitayama et al., 1997; May et al., 1997; Motegi et al., 1997; Naqvi et al., 2000), *Drosophila* (Karess et al., 1991; Young et al., 1993), *C.elegans* (Guo & Kemphues, 1996; Shelton et al., 1999) and most animal cell types (Matsumura et al., 2011).

Myosin II motor is made up of a parallel dimer of heavy chains, each connected to a regulatory light chain (rMlc) and essential light chain (DeBiasio et al., 1996). These structures assemble into filaments that form a complex with actin filaments. This molecule shows directional movement results in translocating actin filaments by regulating actin turnover and disassembly providing predominant force to drive contractile ring constriction (Guha et al., 2005; Haviv et al., 2008; Kondo et al., 2011; I. Mabuchi & Okuno, 1977; Mangione & Gould, 2019; K. Murthy & Wadsworth, 2005; Pollard & O’Shaughnessy, 2019; Reymann et al., 2016; Schwyer et al., 2016). There are different pathways that are required for Myosin II activation, recruitment and its ATPase activity at the cleavage furrow site, as shown by live imaging and RNAi (Echard et al., 2004; Eggert et al., 2004; Gönczy et al., 2000; Sönnichsen et al., 2005). Activation of Myosin II is achieved by phosphorylation by Rho-Kinase (Dean et al., 2005; Ishizaki et al., 1996; T. Mizuno et al., 1999) (Figure 1.3). In animal cells, phosphorylation of the rMlc—which is present between the motor domain and the coiled-coil—regulates Myosin II activation (Matsumura et al., 2011). Phosphorylation of rMlc activates Myosin II by releasing it from an auto-inhibited state followed by its assembly into the filaments and activating its ATPase (actin-stimulated adenosine triphosphatase) activity (Amano et al., 1996; Kunda & Baum, 2009; Totsukawa et al., 2000). The function of phosphorylation of Myosin II was dissected in cytokinesis using the non-phosphorylatable Myosin II allele and phosphomimetic allele. In absence of phosphorylation, severe cytokinesis defects were observed in a non-phosphorylatable Myosin II allele. In contrast, phosphomimetic allele substitutes for Myosin II function in *Drosophila* embryogenesis (Jordan & Karess, 1997).

RhoA is known to activate Rho kinase (ROCK) and citron kinases that are localized at the cleavage furrow (Amano et al., 1996; Cunto et al., 1998; Eda et al., 2001; Kimura et al., 1996; Kosako et al., 1999; Madaule et al., 1998; Matsumura et al., 2011; Nakagawa et al., 1996), which in turn activates Myosin II via phosphorylation (Amano et al., 1996) and regulates cytokinesis (Echard et al., 2004; Hickson et al., 2006; A. J. Piekny & Mains, 2002). In contrast, ROCK phosphorylates and inhibits the Myosin II phosphatase subunit (Kimura et al., 1996) (Figure 1.3) which indirectly further promotes Myosin II activation (Matsumura, 2005; Yamashiro et al., 2003). Myosin II activation is observed at the furrow during anaphase followed by its assembly into the ring and Myosin II heavy chain is needed to regulate its dynamic behaviour at the furrow (Matsumura et al., 1998; Yumura, 2001). Genetic interaction reveals Myosin II as the most important substrate target by ROCK (Winter et al., 2001). In addition, there are several additional kinases such as citron kinase which phosphorylate Myosin II (Yamashiro et al., 2003). Depletion of citron kinase in cells is able to progress to later stages of cytokinesis in contrast to ROCK. Hence, ROCK is established as the major rMlc kinase (Matsumura, 2005; Naim et al., 2004; Shandala et al., 2004; Yamashiro et al., 2003).

Biochemical studies related to contractile rings are mainly focused on actin and Myosin II. *In vitro* study shows that contractile ring forms a stable biochemical entity that can be isolated and can be induced to contract (I. Mabuchi et al., 1988). *In vivo* studies show that these rings are highly dynamic in nature with a high turnover of actin and Myosin II (K. Murthy & Wadsworth, 2005; Yumura, 2001). The alignment of actomyosin filaments in contractile rings and its implications in force generation is still not clear. The actin and Myosin II orientation in the contractile ring clues provided by electron micrographs in sea urchin embryos resulted in the proposal of a purse-string model (Henson et al., 2017; Schroeder, 1972). In this model, contraction is executed when myosin movement causing actin filament sliding resulting in shortening of the ring. Thus, actin filament sliding generates an ingression force that is directed inward. Another model is observed from mammalian cells in which fluorescently labelled actin filament is organized parallel to an axis of the chromosome segregation. Actomyosin contraction in this orientation is in such a way that inwardly directed force is absent (DeBiasio et al.,

1996; Fishkind & Wang, 1993; Oegema et al., 2000). A comprehensive study analysed Myosin II movement during cytokinesis in live 3T3 cells (DeBiasio et al., 1996). In this study, Myosin II—in the form of fibers—was shown to flow toward the equator and form a meshwork. This meshwork consisted of fibers that are oriented both parallel and perpendicular to the cleavage plane. A similar cortical flow of Myosin II has been observed in *Xenopus* eggs (Noguchi & Mabuchi, 2001). Myosin II localization even in the absence of motor activity suggests that there could be more mechanisms contributing to Myosin II localization apart from cortical flows.

Myosin II is highly dynamic in nature and established as an essential cytokinetic protein. There are contrary studies under some conditions in *Dictyostelium* cells and highly adherent mammalian cells that are able to execute cytokinesis in absence of Myosin II and reduction in its activity (De Lozanne & Spudich, 1987; Gerisch & Weber, 2000; Kanada et al., 2005; Neujahr et al., 1997; Yumura, 2001). In *Drosophila* cellularization, Myosin II activity promotes slow constriction during phase I but are largely dispensable for fast constriction during phase-2 (Xue, 2017).

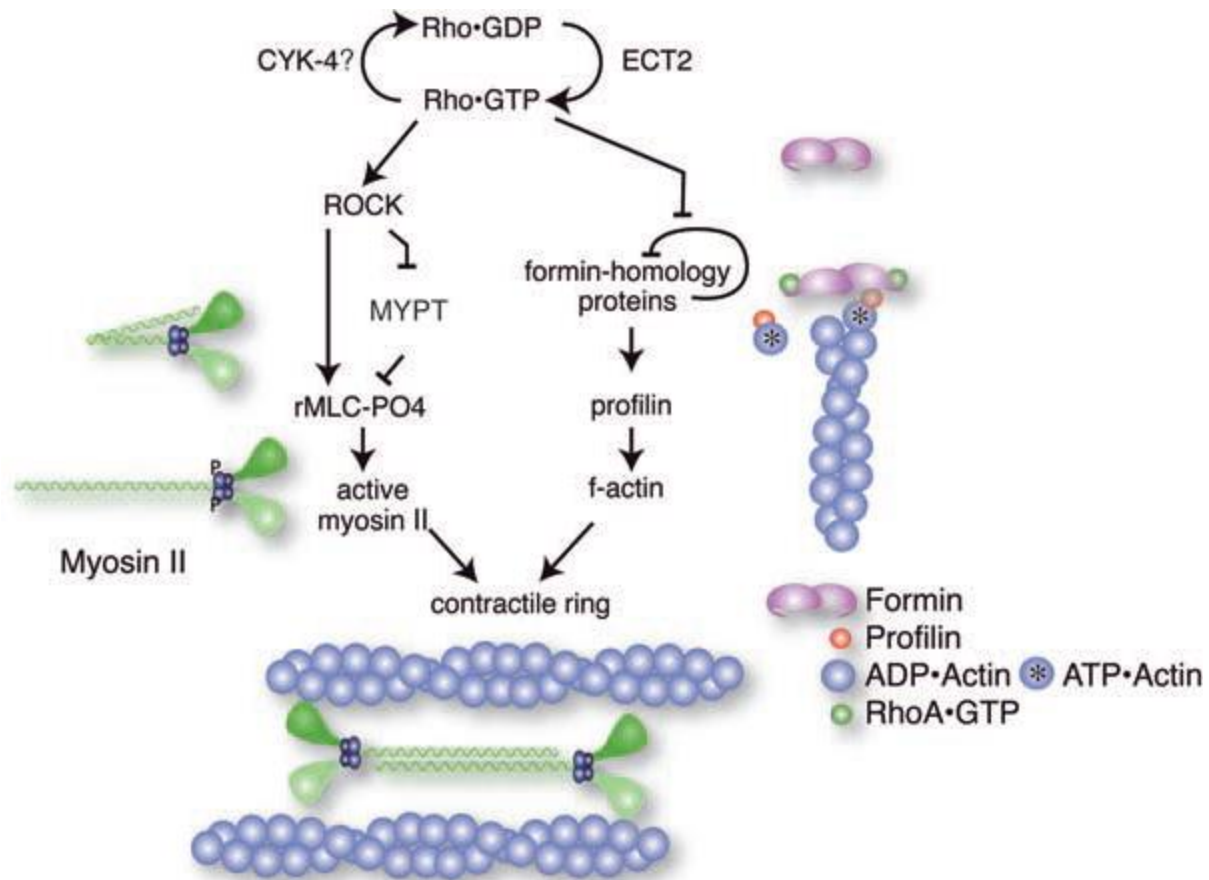


Figure 1.3: Schematic diagram showing RhoA signalling pathway activating actin and Myosin II. RhoA pathway which activates actin filament assembly and Myosin II motor to form a contractile ring. RhoA triggers phosphorylation regulatory light chain myosin (green) causes its activation. Rho-GTP is required to relieve the formin autoinhibition and promote the actin filaments assembly at the barbed end. Adapted from (M. Glotzer, 2005)

1.5.2.3 Actin assembly and its regulators

Actin assembly and dynamics is required in cleavage furrow positioning, contractile ring formation and constriction during cytokinesis (Basant & Glotzer, 2018; Eggert et al., 2006; Fededa & Gerlich, 2012; M. Glotzer, 2005; Green et al., 2012; Mangione & Gould, 2019; Pollard & O’Shaughnessy, 2019). Defects in actin assembly can also affect the organization of the central spindle apparatus. The consequences of improper actin organization at the contractile ring show enlarged and polyploid spermatids with disorganized spindles (Maria Grazia Giansanti et al., 2004; M. G. Giansanti et al., 1998).

The contraction activity of Myosin II is dormant until it is bound with actin filaments. Actin filaments form the second major component of the contractile ring, often organized in anti-parallel bundles. The organization of actin filaments is dependent on different nucleating complexes. Branched filaments generated by the ARP2/3 complex are involved in the leading edge of migrating cells (Svitkina & Borisy, 1999), whereas arp2/3 are only weakly involved in forming contractile ring apparatus (Severson et al., 2002; Withee et al., 2004). Formin binds to the barbed end of actin and allows actin filament growth (Kovar et al., 2003; Pruyne, 2002; Sagot et al., 2002). The formins are composed of conserved domains called FH1, that binds to Profilin, and FH2, that binds to actin region (Xu et al., 2004). Formin interacts with Profilin facilitating ATP hydrolysis, resulting in the release of free energy to favour progressive growth of actin filaments (Pring et al., 2003; Romero et al., 2004; Zigmond, 2004) (Figure 1.3). Formin remains in autoinhibited form because of intramolecular interaction of the N and C terminal when unbound from actin filaments (Takeya et al., 2008). When N-terminal binds to active RhoA, autoinhibition gets relieved (Alberts, 2001) (Figure 1.3). Spatially restricted active RhoA causes local activation of both actin filament assembly and Myosin II. Apart from formin, another actin-binding protein is Cofilin/ADF which functions as an actin severing protein required to regulate actin dynamics during cytokinesis (Gunsalus et al., 1995; Ono et al., 2003). *In vitro* Cofilin plays a dual role in affecting filament growth by severing and destabilizing actin filaments as well as increasing the elongation competent barbed ends number to promote growth. In order to regulate the actin dynamics, the net effect of Cofilin depends on the factors that regulate filament ends and actin monomer concentration (Andrianantoandro & Pollard, 2006; Ennomani et al., 2016; McCullough et al., 2008; Mendes Pinto et al., 2012, 2013). *Cofilin* mutants contain an abundance of actin filaments in the contractile ring especially during the late stages of cytokinesis (Xue & Sokac, 2016). *Twinstar* (Cofilin) mutants in *Drosophila* spermatocytes show abnormal furrows with actin accumulation, resulting in cleavage inhibition (Gunsalus et al., 1995). Thus, the primary function of cofilin *in vivo* is to destabilize actin filaments. Like Cofilin, Anillin which is another actin-binding protein is shown to be implicated in late stages of cytokinesis using genetic experiments but its biochemical function is not fully understood in the context of

cytokinesis (Makoto Kinoshita et al., 2002; Ono et al., 2003). Anillin is a multidomain protein that localizes to the membrane furrow via its pleckstrin homology domain and binds with both Myosin II and septin complexes (Christine M. Field et al., 2005; Makoto Kinoshita et al., 2002; Maddox et al., 2005; Oegema et al., 2000; Ono et al., 2003; Straight et al., 2005). *Anillin* depletion in animal cells gives rise to late cytokinetic defects, required for completion (Echard et al., 2004; Somma et al., 2002; Straight et al., 2005) and plays a non-essential role during contractile ring formation and ingression (Echard et al., 2004; Christine M. Field et al., 2005; Makoto Kinoshita et al., 2002; Somma et al., 2002; Straight et al., 2005). In *Drosophila* cellularization, *anillin* mutants show perturbed F-actin localization making a hexagonal network at furrow tips instead of the rings. In addition, Myosin II localization is reduced and Peanut localization is altered at the cellularization front which results in failure in forming a contractile ring (Christine M. Field et al., 2005). Anillin with its partner septin remains associated with a mature intercellular bridge (late cytokinesis stage) even after Myosin II and F-actin dissociation (Echard et al., 2004; Christine M. Field et al., 2005; C. M. Field & Alberts, 1995; Oegema et al., 2000; A. J. Piekny & Maddox, 2010) as shown in incomplete cytokinesis in *Drosophila* spermatocytes (M. G. Giansanti et al., 1999; Goldbach et al., 2010; Hickson & O'Farrell, 2008; Robinson & Cooley, 1996; Straight et al., 2003).

Septin forms heteromeric complexes which self-assemble into high order structures (Saarikangas & Barral, 2011). It acts as an actin crosslinker that concentrates at the cytokinetic site (Fares et al., 1995; Haarer & Pringle, 1987; G. R. Hime et al., 1996; M. Kinoshita et al., 1997; Longtine et al., 1996; Neufeld & Rubin, 1994; Xie et al., 1999) where it binds to the membrane (Bertin et al., 2010; J. Zhang et al., 1999) and Anillin (Christine M. Field et al., 2005; Makoto Kinoshita et al., 2002; Oegema et al., 2000). Pnut, Sep1, Sep2, Sep4, and Sep5 are five septins identified and studied in *Drosophila* (Adam et al., 2000; Fares et al., 1995; C. M. Field et al., 1996; M. Mavrakakis, 2016; Neufeld & Rubin, 1994). Peanut is shown by *in vivo* functional studies to convert linear actin filaments into curved networks during *Drosophila* cellularization. *In vitro* reconstitution assay shows that bundle actin filaments are converted into rings when incubated with purified septins proteins. In *peanut* mutants, there is inhibition of constriction at the

contractile ring due to aberrant organization of F-actin and Myosin II (Manos Mavrakis et al., 2014). It was observed that in cellularization, Cofilin, Anillin and Peanut control spatial F-actin organization which results in switching from phase1 (slow constriction) to phase2 (fast constriction). During phase-2, F-actin disassembly is necessary to execute fast constriction (Xue, 2017; Xue & Sokac, 2016).

Anillin acts as a scaffold and maintains both septin and Myosin II association at the contractile ring (A. J. Piekny & Maddox, 2010; Straight et al., 2005). Depletion of both Anillin/septin and Rho-kinase cause cytokinesis failure when compared to *C.elegans* embryos where only Rho-kinase is depleted (Maddox et al., 2007). Along with Anillin, formins assemble contractile rings and regulate actin dynamics during cleavage furrow ingression. Furrow ingression depends on anti-capping proteins (like Ena/VASP and Diaphanous-related formins (DRFs) and Profilin regulated actin polymerization (Grevengoed et al., 2003). Rho positively regulates the nucleation activity of Dia which induces actomyosin ring formation and constriction (Watanabe et al., 1997).

In *Drosophila* cellularization, actin cross-linkers such as Bottleneck (bnk), Cheerio and Fimbrin regulate actin organization during contractile ring formation. *Cheerio* and *Bnk* knockdowns show pre-mature rounding and constriction due to failure of actin network assembly (Krueger et al., 2019; Reversi et al., 2014; Schejter & Wieschaus, 1993b). On the contrary, *Fimbrin* knockdown results in a stable actin network assembly which shows a significant delay in a contractile ring formation. Thus, these actin crosslinkers perform opposite roles where *Cheerio* facilitate hexagonal patterning whereas *Fimbrin* is required for remodelling of a hexagonal network into the contractile ring (Krueger et al., 2019).

In cytokinesis, local concentration and turnover of actin (K. Murthy & Wadsworth, 2005; Yumura, 2001) influences the dynamic balance of polymerization and depolymerization. Cytochalasin treatment promotes membrane ingression, but jasplakinolide stabilizes actin which inhibits furrow ingression (Guha et al., 2005; O'Connell et al., 2001). Thus, these experiments suggest that selective actin depolymerization is crucial for cytokinesis to regulate furrow dynamics. In addition to the

actin dynamics, successful cytokinesis requires extensive membrane trafficking (McKay & Burgess, 2011; Neto et al., 2011; Strickland, 2004; Tang, 2012).

1.5.3 Cleavage furrow ingression and abscission: Membrane trafficking

Membrane trafficking affects cleavage furrow ingression and abscission of the cytokinesis (Barr & Gruneberg, 2007; Conrad & Rappaport, 1981; Prekeris & Gould, 2008). Vesicle trafficking ensures the recycling of regulatory proteins and remodelling factors during the ingression and abscission processes (Neto & Gould, 2011). The recycling vesicular trafficking involves small GTPases – Rab35, Rab11 and Arf6, which is crucial for successful cytokinesis (Montagnac et al., 2008; Schiel & Prekeris, 2013). Rab35 knockdown and its dominant negative form show an increase in a number of binucleated cells. Thus, Rab35 is essential for the bridge stability and abscission during terminal steps of cytokinesis in *Drosophila* S2 cells and HeLa cells (Kouranti et al., 2006). Rab11 was shown to be required for furrow ingression in *C.elegans*, as shown by regulating vesicle recycling to the plasma membrane (Ahna R. Skop et al., 2001). Rab11 mutants display cytokinesis failure by affecting furrow ingression and actomyosin ring constriction in *Drosophila* S2 cells, spermatocytes (Maria Grazia Giansanti et al., 2007; Pelissier et al., 2003) and cellularization stages (Pelissier et al., 2003; Riggs et al., 2003). Rab11 is required for the recruitment of its effector molecule Nuclear fallout (Nuf) to the cleavage furrow (Maria Grazia Giansanti et al., 2007; Hickson et al., 2003; Pelissier et al., 2003; Riggs et al., 2003). Nuf recruits RhoGEF2 to the cleavage furrow (Cao et al., 2010) for Rho1 activation resulting in local Dia-induced actin polymerization and Myo-II activation. Similarly in mammalian cells, FIP3/Arfophilin (Nuf ortholog) and Rab11 both accumulate at the cleavage furrow and either protein depletion results in cytokinesis failures (Wilson et al., 2005). Rab11 effector FIP3 and FIP4 (both orthologous to Nuf) forms a complex with Arf6 and its targeting to the central spindle depends on Arf6 (Fielding et al., 2005; Wilson et al., 2005) where it interacts with the exocyst complex and finally results in vesicle fusion to the plasma membrane (Fielding et al., 2005; Prigent et al., 2003). In addition, Arf6 is essential for furrow ingression and acts downstream of recycling endosomes in *Drosophila* spermatocytes (Dyer et al., 2007).

RalA is a small GTPase needed for exocyst complex assembly that controls secretory vesicle delivery to the plasma membrane in *Drosophila* S2 cells (Moskalenko et al., 2002). RalA depleted embryos show missing pseudo-cleavage furrows with F-actin localized in punctae, suggesting its function in initiating furrow formation. RalA recruitment precedes F-actin localization during furrow formation suggesting that membrane trafficking is likely to function upstream of cytoskeletal remodelling (Holly et al., 2015).

Endocytic mutants such as *Clathrin* and *Dynamin* show defects in cytokinesis in *Dictyostelium*, *C. elegans*, *zebra fish* and mammalian cell lines (Gerald et al., 2001; Niswonger & O'Halloran, 1997; J. K. Schweitzer et al., 2005; Thompson et al., 2002; Wienke et al., 1999). Dynamin inhibition shows slower cleavage furrow ingression rates. in *Drosophila* syncytial embryos (Oegema et al., 2000; Rikhy et al., 2015; Sokac & Wieschaus, 2008a; Su et al., 2013) and cellularization (Pelissier et al., 2003; Swanson & Poodry, 1980)

Steppke, a cytohesin Arf-guanine nucleotide exchange factor (GEF) (Gillingham & Munro, 2007), promotes local endocytic events to control plasma membrane furrow ingression both during the syncytial stages I and cellularization of the *Drosophila* embryo. At the ingressing furrow tip, Steppke shows ArfGEF activity and its interaction with the AP-2 clathrin adaptor complex is required to regulate endocytic events. Steppke activities restrain actomyosin networks at the furrow tip by reducing local Rho1 protein levels. *Steppke* mutants lead to increased actin polymerization and Myosin II activation through Rho1 pathway resulting in abnormal constriction forming taut sheets which spread out perpendicularly, invading space occupied by nuclei (D. M. Lee & Harris, 2013). Steppke interacting protein called Stepping stone (Sstn) mutant and RNAi embryos mimic *steppke* loss of function embryos by showing Rho1 dependent abnormal cytoskeletal expansion at the pseudo cleavage and cellularization furrows base. Sstn, cytohesin adaptor, acts upstream of Steppke to regulate Arf-GEF activity at the furrow tip. The direct interaction between Steppke and Sstn occur through their coiled coil domain, which is necessary for stabilize localization at the furrow tip in the syncytial embryo (J. Liu et al., 2015).

1.6 Variations in cytokinesis during *Drosophila* development

Conventional cytokinesis occurs at the cell equator and results in the physical separation of a mother cell into two equal daughters. *Drosophila* embryogenesis as a model system that shows modified traditional cytokinesis during the course of development. The contractile assembly of this modified cytokinesis varies temporally and spatially when compared to conventional cytokinesis, but the machinery involved in this process is similar to the cytokinetic ring (Michael Glotzer, 2001; Guertin et al., 2002; Kumar et al., 2015). The *Drosophila* embryo is transparent and membrane dynamics can be observed by live imaging and any distortion can be easily detected. During embryogenesis, specialized membrane structures of negative and positive curvatures such as furrows and microvilli-like structures are present within the same system. This system will provide insights into how membrane curvature related proteins influence cleavage furrow ingression and contractile ring constriction.

Drosophila embryos show variations in cytokinesis such as: incomplete cytokinesis, pseudo cleavage furrow formation and cellularization

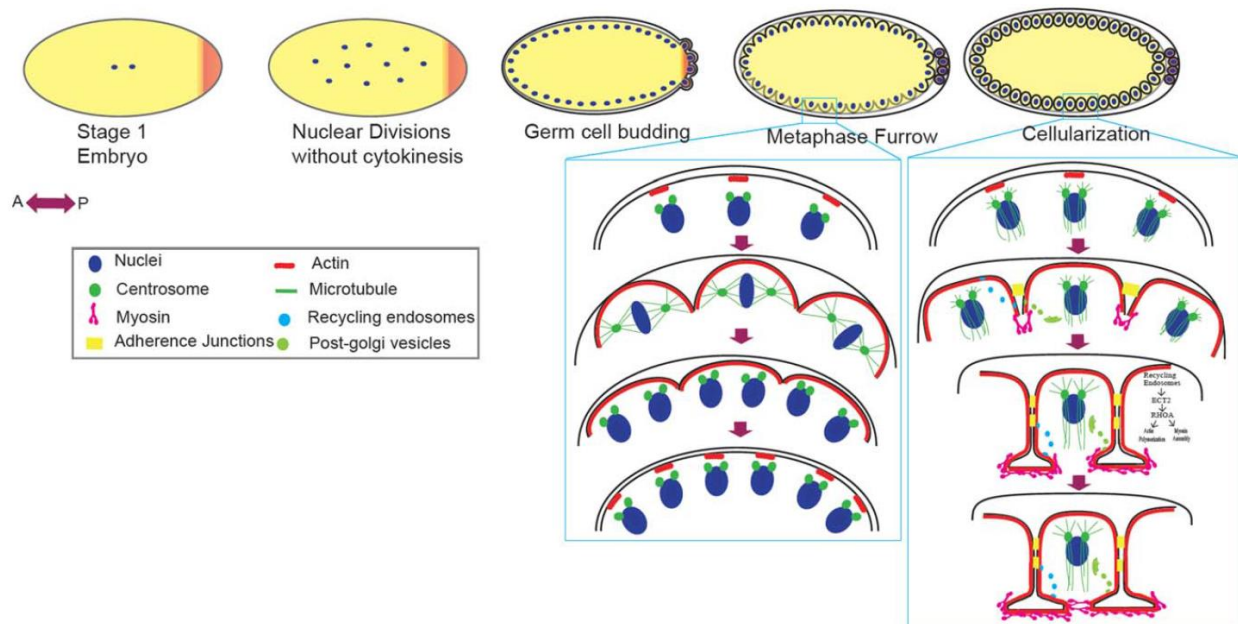


Figure 1.4: Variations in cytokinesis: Incomplete cytokinesis, pseudocleavage and cellularization during *Drosophila* embryogenesis. Nuclear cycles 1-13 show division of nuclei in the absence of cytokinesis. Nuclear cycles 1-8 occur deep within the interior of the embryo. At the 9th nuclear division, nuclei migrate to the surface and further continue to divide without cytoplasmic division. During these cortical divisions, pseudocleavage/partial furrows form during cycles 10-13 in the syncytial blastoderm. During the interphase of the 14th nuclear division, the plasma membrane extends to form around individual nuclei to form individual epithelial cells. The actomyosin machinery assembles at the base of the extending plasma membrane and is similar to conventional cytokinesis. Adapted from (Kumar et al., 2015)

1.6.1 Incomplete Cytokinesis

In the case of incomplete cytokinesis, karyokinesis occurs but is not followed by cytokinesis. During *Drosophila* early embryogenesis, after fertilization, multiple cycles of rapid nuclear division occur in the interior of the embryo without the formation of the cleavage furrow. During this stage, nine rapid synchronous nuclear divisions give rise to 300-400 nuclei. Thus, nuclei replication and division occur without completing cytokinesis, forming a syncytium stage (Gwatkin, 1995; Kumar et al., 2015) (Figure 1.4).

1.6.2 Pseudocleavage furrows

The nuclei which are formed in the embryo interior migrate outwards in nuclear cycle 9 to the periphery of the embryo where four synchronous nuclear divisions occur i.e. cycle 10 to cycle 13. All nuclei share a common plasma membrane and cytoplasm during their first 13 nuclear divisions called the syncytial blastoderm stage where mitosis occurs in the absence of cytokinesis (Mazumdar & Mazumdar, 2002). During the syncytial stage, these nuclei are surrounded by actin which is organized between plasma membrane and centrosomes during interphase and mitosis. The actin forming microvilli structures remodel from caps (Afshar et al., 2000; Foe & Alberts, 1983; Karr & Alberts, 1986; Manos Mavrakis et al., 2009; Stevenson et al., 2002; Turner et al., 1977; Warn et al., 1980, 1984; Young et al., 1991) into the structure called the pseudocleavage furrow that ingresses towards the interior during metaphase, persists until late anaphase and then regress during telophase. Pseudocleavage furrows formed in between adjacent nuclei and spindles are partial furrows during cycles 10-13 of syncytial stages (D. M. Lee

& Harris, 2014) (Figure 1.4). These pseudocleavage furrows ensure proper chromosome segregation by aligning adjacent spindles that interact with chromosomes (Foe & Alberts, 1983; Frescas et al., 2006; Manos Mavrakis et al., 2009). The pseudocleavage furrow actin dynamics are tightly connected to the nuclear cycles, making this an interactive model to be able to study the coordination between cytoskeletal dynamics and nuclear cycles (Cao et al., 2010; Guertin et al., 2002). Cortical actin is spread throughout embryos in *centrosomin* mutants lacking astral microtubules which suggest that asters are required for proper actin dynamics (Kao & Megraw, 2009). Mutants that perturb pseudocleavage furrow formation show the presence of fused spindles and abnormal nuclear division (W. Sullivan et al., 1993). The conservation of components involved in traditional cleavage furrows such as Myosin II, Anillin, septins, spectrins, formins and actin are also found in the pseudocleavage furrow (Afshar et al., 2000; Cao et al., 2008; Fares et al., 1995; C. M. Field & Alberts, 1995; Manos Mavrakis et al., 2009; Miller & Kiehart, 1995; Rikhy et al., 2015; Sherlekar & Rikhy, 2016; Stevenson et al., 2002).

There are important similarities and differences between syncytial metaphase furrows and conventional cytokinesis. In conventional cytokinesis, cleavage furrow occurs after the separation of sister centrosomes and the formation of a bipolar spindle. This determines furrow positioning at a midway point and perpendicular to the spindle axis. These furrows form during anaphase and telophase. In contrast, syncytium metaphase furrows occur before the separation of sister centrosomes. Metaphase furrows are established from early prophase to anaphase. They form around monopolar microtubular arrays. However, in both systems, processes are highly regulated by the cell cycle and require invagination of the plasma membrane. Also, an association of cortical actin with plasma membrane and actin cytoskeleton rearrangements are required for plasma membrane invagination (Kotadia et al., 2010).

There are some parallels between cytokinesis of complete cells during cleavage furrow assembly and syncytial division cycles during pseudocleavage furrow formation in *Drosophila* embryos. Central spindle proteins generate localized stable strips of activated RhoA during anaphase in conventional cytokinesis (A. Piekny et al., 2005; Wagner &

Glotzer, 2016; Yüce et al., 2005). Similarly in syncytial embryos, Rho1 is initially localized at the apical ring and further extends basally at the pseudocleavage furrow during ingression. Thus, Rho1 cortical stripe positioning is equivalent to the conventional cytokinesis, but the timing is different and coincides with pseudocleavage furrow formation (Crest et al., 2012). In addition, similar to cytokinesis, furrow invagination in the syncytium is dependent on the fusion of vesicles that originate from golgi and centrosome-associated recycling endosome (Lecuit & Wieschaus, 2000; Riggs et al., 2003)

1.6.3 Cellularization

Cellularization of the early *Drosophila* embryo provides a great opportunity to study the molecular mechanisms regulating actomyosin-driven contraction in a spatiotemporal manner. Transition from the syncytial to cellular blastoderm occurs at the embryo cortex in the interphase of cycle 14 by cleavage to separate each nucleus by plasma membrane boundaries in a process called cellularization (Mazumdar & Mazumdar, 2002; Schejter & Wieschaus, 1993a; William Sullivan & Theurkauf, 1995). The leading edge of the invaginating plasma membrane between adjacent nuclei occurs as an infolding termed as furrow canal. The actomyosin network assembles at the base of the furrow canal and forms a polygonal network in early cellularization. This transforms into a contractile ring in mid cellularization. Finally, ring constriction partially closes the base of the cell during late cellularization (Kiehart, 1990; Krueger et al., 2019; Royou et al., 2004; Schejter & Wieschaus, 1993a; Xue & Sokac, 2016; Young et al., 1993) (Figure 1.4). The actomyosin ring organization and constriction in cellularization are similar to conventional cytokinesis in somatic cells (Kotadia et al., 2010).

What could be the relationship between mechanisms involving various molecular components that mediate cellularization and cytokinesis? Certain features and molecular components are shared both in cytokinesis and cellularization. For instance, there are many molecular components that are shared by cellularization and cytokinesis including actin, Myosin II, and formin (Kotadia et al., 2010). However, there is segregation of

molecules that differ in cytokinesis and cellularization in *Drosophila* but they are fundamentally similar to higher systems (Eggert et al., 2006). For instance, both RhoGEF2 and pebble are homologues of human ECT2, RhoGEF2 is involved in cellularization whereas Pebble, is involved in normal cytokinesis (G. Hime & Saint, 1992; Lehner, 1992). There are specific zygotic genes (*nullo*, *sry-fi* and *bottleneck*), that are functional in the cellularization stage, but are no longer expressed after cellularization and hence are no longer functional during normal cytokinesis (Schejter et al., 1992; Schweisguth et al., 1990, 1991; Sokac & Wieschaus, 2008a, 2008b)

Both the processes depend on membrane ingression and actomyosin ring contraction. During normal cytokinesis, the two processes occur in parallel, also in the case of cellularization: membrane invagination of the cleavage furrow occur along with systematic transition of actomyosin network at the base of the cell (Keaton, 2007). Cellularization shows systematic transition of actomyosin network that can be exploited for scoring ring architectural defects that remain for approximately 45 minutes. In addition, the most significant challenge in understanding cytokinesis is to study the proteins involved both in mitosis and cytokinesis. Mutation in these genes causes mitotic arrest, which makes it difficult to score for a cytokinetic defect. For example, Polo kinase plays a dual role in mitosis and cytokinesis but does not score in the genetic screening of cytokinesis (Eggert et al., 2006). This system can be exploited to study the role of proteins involved in both mitosis and cytokinesis. It might provide the mechanistic details about this protein by studying them in syncytial (metaphase stage) and cellularization (contractile ring formation stage) processes (Kotadia et al., 2010).

The division state of nuclei in cellularization is mechanistically similar to that in conventional cytokinesis. Cellularization occurs whilst nuclei remain in cycle 14th interphase stage, and nuclei division does not occur throughout cellularization. Astral microtubules present at the top of the nuclei are required to direct actin remodelling and furrow ingression through RhoA- dependent pathway, forming an actomyosin network similar to cytokinesis (Foe et al., 2000). During furrow ingression, post-Golgi and recycling endosomes vesicles contribute towards membrane addition, which plays a crucial role in

driving furrow elongation (Figard et al., 2013; Figard & Sokac, 2014; Lecuit & Wieschaus, 2000; D. M. Lee & Harris, 2014; Riggs et al., 2003; Sisson et al., 2000).

Several BAR domain proteins are known to bind to the membrane *in vitro* but mechanistic details about their function *in vivo* are still unknown. Also, BAR domain containing proteins have been shown to be important for several actin remodelling processes. *Drosophila* embryogenesis shows profound plasma membrane as well as cytoskeletal remodelling, thus this system can be exploited to study BAR domain proteins which could yield steps of morphogenesis dependent upon their function. Thus, specific localization and dynamics of BAR domain proteins on the membrane become an integral part to morphogenesis during *Drosophila* embryogenesis. Their possible defects can be easily scored at the level of syncytial cycles, and cellularization which will further provide insights into their precise functions. This system will help us to understand the function of BAR domain proteins involved in coordinating and regulating specific membrane remodelling processes. We devised the following aims and objectives towards studying the BAR domain function in regulating cleavage furrow formation in *Drosophila* embryogenesis

1.7 Aims and objectives

1.7.1 Screening for BAR domain protein distribution and estimating their requirement in embryogenesis by scoring lethality

- Checking the effect of RNAi mediated knockdown of BAR domain proteins on the survival of the embryo
- Screening for defects in actin organization in BAR domain proteins knockdown embryos

1.7.2 Characterization of GRAF-BAR domain protein depletion on cleavage furrow formation during *Drosophila* embryogenesis

- Generation of GRAF knockout using CRISPR-Cas9 strategy
- Checking the effect of *Graf* knockdown and mutant defects on the contractile ring architecture

1.7.3 Localization and loss of function effects of GRAF on cleavage furrow formation during *Drosophila* embryogenesis

- Checking the distribution of GRAF protein at the cleavage furrow
- Checking the effect of perturbations in key contractile ring proteins in *Graf* depleted embryos

1.7.4 Assessing the molecular mechanism of GRAF on cleavage furrow formation

- Dissecting the role of GRAF in Rho-dependent pathway in regulating constriction using genetic analysis

1.7.5 Characterizing GRAF domain specific function during *Drosophila* embryogenesis

- Generation of domain specific fluorescently tagged GRAF transgenes in *Drosophila*
- Assessing the role of GRAF domains' recruitment to the contractile ring and in constriction of the contractile ring

CHAPTER 2

Material and Methods

2.1 *Drosophila* stocks and genetics

Fly stocks and crosses were maintained in regular cornmeal agar. The detailed genotypes, stock numbers, source of stocks and temperature of crosses are a part of Table 2.1 and 2.2.

Stock	Genotype	Source/Reference
1	Canton-S	Lab stock originally obtained Bloomington <i>Drosophila</i> Stock Center
2	<i>nanos</i> -Gal4	Lab stock
3	w; <i>mat67</i> -Gal4; <i>mat15</i> -Gal4	Girish Ratnaparkhi, IISER, Pune, India
4	w; P{Sqh-mCherry.M}3	Bloomington <i>Drosophila</i> Stock Center (BDSC), Indiana, USA
5	y[1] v[1]; P{TRiP.HMC03427}attP40 (GRAF shRNA1, <i>Graf</i>)	BDSC, #51853
6	y[1] v[1]; P{TRiP.GL01207}attP40 (Myosin II binding subunit, MBS shRNA)	BDSC, #41625
7	y[1] sc[*] v[1] sev[21]; P{TRiP.HMS01118}attP2 (RhoGEF2 shRNA)	BDSC, #34643

8	y[1] w[*]; P{UASpT7.RhoGEF2}5 (RhoGEF2 overexpression)	BDSC, #9386
9	ubi-GFP::AnillinRBD/TM3	(Munjal et al., 2015) Thomas Lecuit, France
10	w-FM7a/w-FM7a(white eye)	Girish Ratnaparkhi, IISER, Pune, India
11	UASp-rok-shRNA (<i>rok</i>)	(Yixie Zhang et al., 2018)
12	y[1] w[67]c[23] P{EPgy2}Graf[EY09461] (GRAF overexpression)	BDSC, #17571
13	w; <i>mat67</i> Spider-GFP-Sqh-mcherry/TM3ser	(Martin et al., 2009)
14	y[1] sc[*] v[1] Graf[CR57]/FM7a (<i>Graf</i> ^{CR57})	This study
15	y[1] sc[*] v[1] sev[21]; P{TKO.GS00762}attP40	BDSC, #76993
16	P{KK102763}VIE-260B (GRAF shRNA2, <i>Graf</i> ²ⁱ)	Vienna <i>Drosophila</i> Stock Center, #v110812
17	y[1] sc[*] v[1] sev[21]; P{y[+t7.7] v[+t1.8]=nos-Cas9.R}attP40	<i>Drosophila</i> facility, NCBS
18	[w]*;p[UASp-GRAF-EGFPG1] attp40/cyo	This study
19	[w]*;p[UASp-GRAFΔRhoGAP-GFP] attp40/cyo	This study
20	y[1] w[67]c[23] P{EPgy2}Graf[EY09461]/FM7a; P{UASpT7.RhoGEF2}5/Tb (GRAF-OE;RhoGEF2-OE)	This study
21	y[1] sc[*] v[1] sev[21];	This study

	P{TRiP.HMC03427}attP40/cyo;P{TRiP.HMS01118}attP2/Tb (<i>Graf^f;RhoGEF2ⁱ</i>)	
22	mat67-Sqh-mCherry; <i>ubi</i> -AnillinRBD-GFP-NG4/Tb	This study
23	y[1] sc[*] v[1] GRAF[CR57]/FM7a; P{TRiP.HMS01118}attP2/Tb (<i>Graf^{CR57};RhoGEF2ⁱ</i>)	This study
24	y[1] sc[*] v[1] GRAF[CR57]/FM7a; UASp-rok-shRNA/Tb (<i>Graf^{CR57};rokⁱ</i>)	This study
25	y[1] w[67]c[23] P{EPgy2}Graf[EY09461]/FM7a; P{TRiP.GL01207}attP40/cyo (GRAF-OE; <i>mbsⁱ</i>)	This study
26	y[1] sc[*] v[1] GRAF[CR57]/FM7a;mat67Sqh-mCherry/cyo	This study
27	y[1] sc[*] v[1] GRAF[CR57]/FM7a; p[pUASp GRAF EGFP G1] attp40/cyo	This study
28	y[1] sc[*] v[1] GRAF[CR57]/FM7a; p[pUASp GRAF ΔRhoGAP-EGFP] attp40/cyo	This study
29	[w]*;p[UASp-GRAFΔBAR-GFP] attp40/cyo	This study
30	[w]*;p[UASp-GRAFΔPH-GFP P1] attp40/cyo	This study
31	[w]*;p[UASp-GRAFΔSH3-GFP] attp40/cyo	This study
32	y[1] sc[*] v[1] GRAF[CR57]/FM7a; p[UASp-GRAFΔBAR- GFP] attp40/cyo	This study
33	y[1] sc[*] v[1] GRAF[CR57]/FM7a; p[UASp-GRAFΔPH-GFP P1] attp40/cyo	This study
34	y[1] sc[*] v[1] GRAF[CR57]/FM7a; p[UASp-	This study

	GRAF Δ SH3- GFP] attp40/cyo	
35	[w]*;p[UASp-GRAF BARPtmt-GFP] attp40/cyo	This study
36	[w]*;p[UASp-GRAF RhoGAPtmt-GFP] attp40/cyo	This study
37	[w]*;p[UASp-GRAF Y381FPtmt-GFP] attp40/cyo	This study

Table 2.1: *Drosophila* stocks and their source

F2 embryos were imaged from these crosses, using above stock numbers/genotypes. Non-balancer females were used for cages. Stocks # (Virgins x males)	Temperature (°C)
2 x 1 control	28
2 x 5 <i>Graf^f</i> using <i>nanos</i> -Gal4	28
3 x 16 <i>Graf²ⁱ</i> using <i>mat</i> -Gal4	28
17X15 <i>Graf^{gRNA}</i> using <i>nanos</i> -Cas9	28
14x14 <i>Graf^{CR57}</i>	25
26X27 <i>Graf^{CR57}</i> ;GRAF-GFP/ <i>mat67</i> -Gal4, Sqh-mCherry	18, 25
22X1 <i>mat67</i> Sqh-mCherry/+; <i>ubi</i> -AnillinRBD-GFP NG4/+	25
13x1 <i>mat67</i> -Gal4 Spider-GFP-Sqh-mcherry/+	25
26X26 <i>Graf^{CR57}</i> ; <i>mat67</i> -Gal4, Sqh-mCherry	25
26x28 <i>Graf^{CR57}</i> ;GRAF Δ RhoGAP-GFP/ <i>mat67</i> -Gal4, Sqh- mCherry	18, 25
3x12 GRAF-OE using <i>mat</i> -Gal4	28
13X12 GRAF-OE; <i>mat67</i> Spider-GFP-Sqh-mCherry	25

3X8 RhoGEF2-OE using <i>mat-Gal4</i>	25
13X8 RhoGEF2-OE; <i>mat67</i> Spider-GFP-Sqh-mCherry	25
2X7 <i>RhoGEF2ⁱ</i> using <i>nanos-Gal4</i>	28
3X7 <i>RhoGEF2ⁱ</i> using <i>mat-Gal4</i>	25
13X7 <i>RhoGEF2ⁱ</i> ; <i>mat67-Gal4</i> Spider-GFP-Sqh-mCherry	25
13X20 GRAF-OE;RhoGEF2-OE/ <i>mat67-Gal4</i> Spider-GFP, Sqh-mCherry	25
3X20 GRAF-OE;RhoGEF2-OE using <i>mat-Gal4</i>	28
2X21 <i>Grafⁱ</i> ; <i>RhoGEF2ⁱ</i> using <i>nanos-Gal4</i>	28
3X6 <i>mbsⁱ</i> using <i>mat-Gal4</i>	25
3X25 GRAF-OE; <i>mbsⁱ</i> using <i>mat-Gal4</i>	25
13x11 <i>rokⁱ</i> / <i>mat67-Gal4</i> Spider-GFP-Sqh-mCherry	25
13X24 <i>Graf^{CR57}</i> ; <i>rokⁱ</i> / <i>mat67-Gal4</i> Spider-GFP-Sqh-mCherry	25
26X32 <i>Graf^{CR57}</i> ;GRAFΔBAR-GFP/ <i>mat67-Gal4</i> , Sqh- mCherry	18
26X33 <i>Graf^{CR57}</i> ;GRAFΔPH-GFP/ <i>mat67-Gal4</i> , Sqh- mCherry	18
26X34 <i>Graf^{CR57}</i> ;GRAFΔSH3-GFP/ <i>mat67-Gal4</i> , Sqh- mCherry	18

Table 2.2: *Drosophila* crosses

2.2 Generation of GRAF null mutant using the Crispr-Cas9 method

Flies containing *nos-Cas9* were crossed to ubiquitous expressing gRNA against the first exon of GRAF to obtain F1 males containing *nos-Cas9*/GRAF gRNA (X. Ren et al., 2013; Zirin et al., 2020). In the germline of F1 males, the Cas9 enzyme cleaved the first exon of GRAF leading to NHEJ repair and the occurrence of different mutations.

These males were crossed with FM7a virgin females. 155 F2 female progeny containing the mutant chromosome and the FM7a balancer were crossed individually to FM7a males. The crosses were checked for male lethality and non-lethal stocks were tested for reduced progeny. 1 line was male lethal, several lines contained reduced progeny and several lines did not carry any remarkable phenotype. Genomic DNA was extracted from homozygous flies in lines having optimum progeny and those containing reduced progeny compared to control. The exon1 of *Graf* was amplified from genomic DNA using primers 23 and 24 (Table 2.3). The PCR product was detected by agarose gel electrophoresis and purified before sending it for sequencing to assess the presence of mutations in exon1. Homozygous flies from 21 lines were sequenced, of these 18 lines contained reduced progeny and 3 lines did not show any phenotype. 100% of the lines sequenced gave mutations in exon 1 of the *Graf* gene. Homozygous flies from lines with reduced progeny showed mutations in the *Graf* gene that led to a premature stop codon. Homozygous flies from lines that did not give any phenotype also gave mutations in exons which did not alter the reading frame of the gene and were presumably not crucial for GRAF function.

2.3 Generation of GRAF-GFP, domain deletions and point mutations transgene

The *Graf* cDNA sequence was extracted from the LD28528 pOT2 vector (BDGP, USA) using primers 1,3 (Table 2.3). The cDNA in LD28528 contained 3 mutations causing premature stop codon when compared to the gene sequence available at Flybase: FBgn0030685. These mutations were rectified by site-directed mutagenesis as follows C212T, A420G and deletion of T468 residue using primers 25-30 (Table 2.3). The modified residues were confirmed using sequencing. This intact *Graf* cDNA sequence was used to generate a fluorescently tagged GRAF-GFP construct with GFP at the C-terminus. PCR amplification was performed on the GRAF and GFP gene using primers 1,3 and 2,4 respectively (Table 2.3). Overlap PCR was performed to give rise to GRAF with a serine linker followed by GFP tagged at the C-terminal of the *Graf* cDNA amplified products using primer 1,4 (Table 2.3). The PCR product at the end has a sequence homologous to BamH1 digested pUASp vector ends. The purified product from the overlap PCR was digested with BamH1. The pUASp vector was used in a 10:1 ratio for

transformation in DH10B derived E.coli strain PPY (Yongwei Zhang et al., 2012, 2014). This strain recombines the pUASp vector and inserts using the *in-bacto* homologous recombination strategy. PCR was performed to confirm the gene in the vector and further, the DNA sequence was confirmed by sequencing using primers 1,4 (Table 2.3).

BAR deletion: PCR amplification was performed on pUASp GRAF-GFP vector using primers 5,4 to achieve BAR domain deletion of GRAF that spans the residues 79 to 648bp in the ORF.

PH deletion: The PH domain deletion of GRAF that spans the residues 811 to 1143bp in the ORF was achieved using overlap PCR. PCR amplification was performed on pUASp GRAF-GFP vectors using primers 1,7 and 8,4.

RhoGAP deletion: The deletion of the RhoGAP domain of GRAF that spans the residues 1177 to 1764bp in the ORF was achieved using overlap PCR. PCR amplification was performed on pUASp GRAF-GFP vectors using primers 1,9 and 10,4.

SH3 deletion: The deletion of the RhoGAP domain of GRAF that spans the residues 2860 to 3048bp in the ORF was achieved using overlap PCR. PCR amplification was performed on pUASp GRAF-GFP vectors using primers 1,11 and 12,4.

BAR point mutation: The BAR point mutation of K129,139,140E was achieved using overlap PCR. PCR amplification was performed on pUASp GRAF-GFP vectors using primers 1,13 and 14,4.

RhoGAP point mutation: The RhoGAP point mutation of R422Q was achieved using overlap PCR. PCR amplification was performed on pUASp GRAF-GFP vectors using primers 1,15 and 16,4.

GRAF phospho-mutant: The GRAF phospho-mutant Y381F was achieved using overlap PCR. PCR amplification was performed on pUASp GRAF-GFP vectors using primers 1,17 and 18,4.

The overlap PCR was performed to give rise to the desired deletion and point mutation with a serine linker followed by GFP tagged at the C-terminal region of *Graf* cDNA amplified products using primer 1,4 (Table 2.3). This purified product had an end homologous region to BamH1 and both the PCR product and the pUASp vector were individually digested with BamH1. The purified product and vector was used in a 10:1

ratio to transform in E.coli strain PPY. Finally, primer 1,4 (Table 2.3) was used for confirming the product with PCR and the DNA sequence was confirmed by sequencing. The final product GRAF-GFP, domain deletion and point mutations plasmids were purified using a midiprep kit. The purified plasmids were used to inject in embryos to generate transgenics

S.No.	Primer Name	Primer sequence(5'->3')	Amplification
1	GRAF_pUASp_Homo_Kpn1_GRAF(start)_FP	CCGCATAGGCCACTAGTGGATCT GGTACCATGGGCGGCGGCAAAA ATGTACG	GRAF-GFP cloned in pUASp vector
2	GRAF(end)_serine linker_GFP(start)_FP	ACTATGTGGAACATTTGAAGCCG CACCATTCTCGAGCTCCAGCAT GGTGAGCAAGGGCGAGGAGCT	
3	GRAF(end)_serine linker_GFP(start)_RP	AGCTCCTCGCCCTTGCTCACCAT GCTGGAGCTCGAGGAATGGTGC GGCTTCAAATGTTCCACATAGT	
4	GFP_pUASp_Homo_RP	AACGTTTCGAGGTCTGACTCTAGAG GATCCTTACTTGTACAGCTCGTC CATGCCGAGAGTGAT	
5	BAR_del_FP	CCGCATAGGCCACTAGTGGATCT GGTACCATGACTCGGGAAAATTT CGAGGAGGCACG	GRAF Δ BAR-GFP cloned in pUASp vector
7	PH_del_RP	GCTGACTTTGATTTTGCCGGGAG CCAGTTCCTCGGGCTTTGTGCGT TTTTCC	GRAF Δ PH-GFP cloned in pUASp vector

8	PH_del_FP	GGAAAACGCACAAAGCCCGAG GAACTGGCTCCCGGCAAATCAA AGTCAGC	
9	RhoGAP_del_RP	CCTTCGTGGCGTCCGGCAACTTT GCCTCGCTGACTTTGATTTTGCC G	GRAF Δ RhoG AP-GFP cloned in pUASp vector
10	RhoGAP_del_FP	CGGCAAATCAAAGTCAGCGAGG CAAAGTTGCCGGACGCCACGAAG G	
11	SH3_del_RP	AGCTCCTCGCCCTTGCTCACCAT GCTGGAGCTCGAGGATGACAAAT CACGTTTTATTTGGTTGACGTCAC GATT	GRAF Δ SH3- GFP cloned in pUASp vector
12	SH3_del_FP	AATCGTGACGTCAACCAAATAAAA CGTGATTTGTCATCCTCGAGCTC CAGCATGGTGAGCAAGGGCGAG GAGCT	
13	BAR_Ptmt(K129,139, 140E)_RP	TTTTTATCAAATTTCTCCTCGTTTT CTTTGACGCCACCGATTTGCTTCT CTCGAAAATCCTC	GRAF BAR Ptmt-GFP cloned in pUASp vector
14	BAR_Ptmt(K129,139, 140E)_FP	GAGGATTTTCGAGAGAAGCAAAT CGGTGGCGTCAAAGAAAACGAG GAGAAATTTGATAAAAA	
15	RhoGAP(R422Q)_Pt mt_RP	GGTTCCAACACCGCTCTTCTGGT ATATGCCCTCATCCTC	GRAF RhoGAP Ptmt-GFP cloned in
16	RhoGAP(R422Q)_Pt	GAGGATGAGGGCATATAACCAGAA	

	mt_FP	GAGCGGTGTTGGAACC	pUASp vector
17	GRAF Y381F Ptmt RP	TTGCCGGGAGCCAGGAATGTCG GCTCCGTG	GRAF Y381F Ptmt-GFP cloned in pUASp vector
18	GRAF Y381F Ptmt FP	CACGGAGCCGACATTCCTGGCTC CCGGCAA	
19	GRAF FL AB vecOH FP	ACGAAAATCTGTATTTCCAAGGCA TGGGCGGCGGCACAAAATGT	6XHis-GRAF FL-Strep tag cloned in pet15b vector
20	Vect GRAF FL ABOH RP	ACATTTTTGCCGCCGCCATGCC TTGGAAATACAGATTTTCGT	
21	Vect GRAF FL ABOH FP	AACATTTGAAGCCGCACCATTGG TCTCATCCTCAGTTCTGA	
22	GRAF FL AB vecOH RP	TCGAACTGAGGATGAGACCAATG GTGCGGCTTCAAATGTTCCAC	
23	GRAF mutant scr1 FP	GTAAATGTTGCAAACACCGCAGT TTTCTCGAAACTCAACC	GRAF mutant screening
24	GRAF mutant scr RP	TACTACTTACTCTTTGCCGCACTC ATAAGATCTTTGACCT	
25	Pot2 212 CtoT FP	CAATTGGCCATTTTACTTAACGAT TTT	GRAF gene modification
26	Pot2 212 CtoT RP	AAAATCGTTAAGTAAAATGGCCAA TTG	
27	Pot2 420 AtoG FP	AAGAAAACAAAAGAAATTTGATA AAA	

28	Pot2 420 AtoG RP	TTTTATCAAATTTCTTTTTGTTTTC TT	
29	Pot2 468 delT FP	GCAGGAGCGTTTCCTCAATATGT C	
30	Pot2 468 delT RP	GACATATTGAGGAAACGCTCCTG C	

Table 2.3: Primers for sequencing and cloning GRAF

2.4 Generation of anti-GRAF antibody

The pUASP GRAF-GFP vector was used to amplify GRAF full length sequence using primers 19 and 22 (Table 2.3) and pET-15b expression vector amplification was carried out by primers 20 and 21 (Table 2.3). The GRAF full length amplified product and vector was transformed into E.coli strain PPY in a 10:1 ratio. PCR and sequencing were performed to confirm the presence of the GRAF insert using primers 19 and 22 (Table 2.3). The N-terminal region of the GRAF gene had a 6X His tag which was used for protein purification.

Polyclonal antibodies were developed against full-length GRAF protein in New Zealand White rabbit at Bioklone, India by the following procedure. Immunizations were given subcutaneously. After primary immunization of the rabbit with 200g of GRAF in Freund's adjuvant (Sigma), boosters were administered with 150g of GRAF at 21-day intervals. Production bleeds were collected from the immunized rabbit on the 14th day after each booster. The antibody titres in rabbit sera were measured in indirect ELISA. A hundred microliters of purified GRAF protein was coated in the wells of microtiter plates or strips (Nunc maxisorp) at a concentration of 3 g/ml, overnight at 4 °C. After blocking with 5% skimmed milk in PBS for 1 h at 37 °C, the wells were washed twice with PBS. Varying dilutions of rabbit sera were added to the wells and incubated overnight at 4 °C. After washes with PBS-Tween 20 (PBST) followed by PBS, the wells were incubated with

goat anti-rabbit IgG-HRP (Merck, India), 1:2000, for 45 min at room temperature. Following washes with PBST and PBS, wells were incubated with TMB (Invitrosense ultra-blue) at room temperature for 20 min in dark. After the addition of the stop solution (2N H₂SO₄), optical density (OD) values were measured at 450 nm using an 800™ TS absorbance reader (BioTek, Winooski, VT 05404, USA). Antibodies from the sixth bleed were purified on Protein A agarose beads (Sigma).

GRAF antibody staining on *Drosophila* embryos was standardized using various fixation protocols involving paraformaldehyde and heptane fixation along with methanol devitellinization and heat fixation. It was found that GRAF antibody staining gets preserved the best on heat fixation and all experiments for GRAF staining were therefore performed with heat fixation.

2.5 Immunostaining

0-3.5 hrs embryos were collected on sucrose-agar plates, washed, dechorionated with 100% bleach and washed again. To visualize GRAF, Zipper and Dlg immunostained embryos, dechorionated embryos were heat fixed with boiled 1X Triton salt solution (10x-0.5% Triton X-100 and 7% NaCl in water) for 1 min and instantly adding ice-cold 1X washing buffer. After cooling on ice, embryos were devitellinized in a 1:1 mix of MeOH and heptane followed by three washes in 1X PBST (1X PBS with 0.3% Triton X-100) for 5 min each. After washing, embryos were blocked in 2% BSA in 1X PBST for 1 hr and then incubated in primary antibody (Table 2.4) overnight at 4 °C. This was followed by three 1X PBST washes and incubated in fluorescently coupled secondary antibodies (Molecular probes) at 1:1000 dilution for 1 hr at room temperature. Embryos were washed three times in 1X PBST for 5 min each. DNA was labelled with Hoechst 33258 (1:1000, Molecular Probes) for 5 min in the second 1X PBST wash. Finally, embryos were mounted in Slow fade Gold antifade (Molecular Probes). For Anillin, Peanut and PatJ immunostainings, dechorionated embryos were fixed using 1:1 mixture of 4% paraformaldehyde (PFA) and heptane for 20 min, followed by MeOH devitellinization

To visualize F-actin, embryos were fixed using a 1:1 mix of 8%PFA in 1XPBS: heptane for 20 min and followed by hand devitellinization. Fluorescently coupled phalloidin (Molecular Probes) was used to label F-actin in embryos in cellularization for 1 hour at room temperature followed by washes and DNA labelling.

REAGENT	SOURCE	IDENTIFIER	DILUTION
Antibodies			
Rabbit anti-GRAF	Bioklone	This Study	1:500; Pre- absorbed using <i>Gra</i> ^{CR57} null mutant embryos
Mouse anti-Dlg	DSHB	4F3, RRID: AB_528203	1:100
Rabbit anti-Zipper	Thomas Jeffrey, Texas Tech University, TX, USA	(Chougule et al., 2016)	1:200
Rabbit anti-Dia	S V Wasserman, University of California, San Diego, USA	(Afshar et al., 2000)	1:1000
Rabbit anti-Anillin	Julie A Brill, The Hospital for Sick Children, Toronto, Canada	(Goldbach et al., 2010)	1:1000
Mouse anti-Peanut	DSHB	4C9H4,RRID: AB_528429	1:5

Rabbit anti-PatJ	Hugo Bellen lab	-	1:1000
Alexa 488 coupled Goat anti Mouse	Molecular Probes	A-1100, RRID: AB_2534069	1:1000
Alexa 488 coupled Goat anti Rabbit	Molecular Probes	A-11008, RRID: AB_143165	1:1000
Alexa 568 coupled Goat anti Mouse	Molecular Probes	A-11004, RRID: AB_141371	1:1000
Alexa 568 coupled Goat anti Rabbit	Molecular Probes	A-1101, RRID: AB_143157	1:1000
Hoechst 33258	Molecular Probes	H-3569	1:1000
Slow Fade Gold	Molecular Probes	S-36937	-
Alexa 488 coupled Phalloidin	Molecular Probes	A-12379, RRID: AB_2315147	1:100
Alexa 568 coupled Phalloidin	Molecular Probes	A-12380, RRID: AB_2759224	1:100
Alexa 647 coupled Phalloidin	Molecular Probes	A-22287, RRID:AB_2620155	1:100

Table 2.4: Antibodies and Dyes

2.5 Live imaging of *Drosophila* embryos

For live imaging, 2-2.5 hr embryos were collected on sucrose agar plates and dechorionated with 100% bleach for 1 min and mounted on 2 well coverslip bottom Labtek chambers. Mounted embryos were filled with 1X PBS (Manos Mavrakis et al., 2008) and imaged using 40X/1.4NA oil objective on Zeiss or Leica SP8 microscope with a frame rate of 1.74s/frame and 2s/frame respectively.

2.6 Laser ablations

Control and *Graf*^{CR57} embryos expressing Sqh-mCherry were used for visualizing contractile rings for laser ablation experiments using the Zeiss LSM780 microscope. Laser ablation was achieved by using an 800 nm multiphoton femtosecond pulsed Mai Tai laser. The region of interest used for ablations was set to a line of 510-pixel length (42.51 μm) and captured with a speed of 1.58 μs per pixel and 20 iterations. The Sqh-mCherry was imaged using a 561 nm laser excitation with a time interval of 1.27 s. A sagittal section was taken before ablations to estimate furrow length for early (less than 6 μm) and mid stages (6–16 μm) of cellularization. Three sections were taken before the ablations in approximately 3 s, the time taken for ablations is approximately 3.22 s and imaging was carried out for approximately 70 s after ablations.

2.7 Microscopy

Zeiss laser scanning confocal microscope LSM710, LSM780 and Leica laser scanning microscope SP8 containing laser lines at 488, 561, 633 nm were used to image immunostained fixed or live embryos. The 40X objective having NA 1.4 of these microscopes was used for imaging. The laser power, scan speed and gain were adjusted with the range indicator mode such that 8-bit image acquisition was in 0-255 range. For both fixed or live imaging, an averaging 2 was used during image acquisition. Optical sectioning of 1.08 μm and 0.68 μm was used to acquire images at Zeiss and Leica confocal microscopes respectively.

2.8 Image quantification and analysis

2.8.1 Quantification of mean fluorescence intensity from immunostainings

The imaging of fixed control and mutant embryos immunostained with antibodies against GRAF along with Dlg and Zipper along with Dlg was carried out on the Leica SP8 confocal microscope at the same laser power and gain settings. To estimate the mean fluorescence intensity of GRAF and Zipper from immunostaining, a single optical section from the Z-stack containing the brightest intensity at the furrow tip was chosen.

Fluorescence intensity was obtained in this section by drawing ROIs using the segmented line tool around the ring to get the average intensity using Fiji software (<http://fiji.sc/wiki/index.php/Fiji>) (Rueden et al., 2017). The ring intensity obtained was divided by the cytosol intensity obtained from a large square ROI in the apical most region above the nuclei from the same image. This membrane to cytosol ratio for GRAF antibody fluorescence in control embryos, *Graf*^{CR57}, GRAF-OE and Zipper antibody fluorescence in control and *Graf*^{CR57} was plotted for different stages of cellularization.

2.8.2 Quantification of mean fluorescence intensity from live-imaging

Live imaging of embryos containing different genotypes (AnillinRBD-GFP, GRAF-GFP and GRAFΔRhoGAP-GFP, Sqh-mCherry in GRAF-OE and *Graf*^{CR57}) were used to quantify the fluorescence intensity change with respect to time. Images with Z projection of sum intensity were obtained from two stacks above and two stacks below of the brightest section at the furrow tip covering a depth of 4 μm. ROIs across the furrow tip from 5 or 10 rings were drawn in these images for each time point to obtain the mean signal intensity. The mean intensity obtained at each time point was represented as a ratio to the maximum mean fluorescence value obtained across cellularization within each embryo and finally plotted as a 'normalized intensity versus time'.

Live imaging of Sqh-mCherry expressing embryos in various genotypes was used to quantify fluorescence intensity change during the last five time points in late cellularization. To estimate these changes quantitatively across all genotypes, images were obtained with sum intensity per pixel across the Z-axis from a total of five stacks: two stacks above and two stacks below of the brightest section at the furrow tip covering a depth of 4 μm in late cellularization. The mean ring intensity per pixel was extracted by drawing a segmented ROI on the ring. The inter-ring intensity per pixel was extracted by drawing an ROI in between adjacent rings that had reduced Sqh-mCherry intensity. The ring intensity per pixel was expressed as a ratio to interring intensity per pixel. Finally, the normalized intensity of the ring was shown as a scatter plot.

Live imaging of embryos containing different genotypes (*Graf*^{CR57}, *Graf*^{CR57};GRAF-GFP, *Graf*^{CR57};GRAFΔBAR-GFP, *Graf*^{CR57};GRAFΔPH-GFP, *Graf*^{CR57};GRAFΔRhoGAP-GFP and *Graf*^{CR57};GRAFΔSH3-GFP) were used to quantify the Sqh-mCherry intensity in interring region during mid stages (13μm). To estimate these changes quantitatively across all genotypes, images were obtained with sum intensity per pixel across the Z-axis from a total of five stacks: two stacks above and two stacks below of the brightest section at the furrow tip covering a depth of 4 μm by taking five time points during the mid cellularization. The mean ring intensity per pixel was extracted by drawing a segmented ROI on the ring. The inter-ring intensity per pixel was extracted by drawing an ROI in between adjacent rings that had increased Sqh-mCherry intensity. The inter-ring intensity per pixel was expressed as a ratio to ring intensity per pixel (mean ring intensity subtracted cytosol intensity). Finally, the normalized intensity of the ring was shown as a scatter plot.

Live imaging of embryos containing different genotypes (*Graf*^{CR57};GRAF-GFP, *Graf*^{CR57};GRAFΔBAR-GFP, *Graf*^{CR57};GRAFΔPH-GFP, *Graf*^{CR57};GRAFΔRhoGAP-GFP and *Graf*^{CR57};GRAFΔSH3-GFP) were used to quantify the GFP fluorescence intensity change during mid (13μm) and late stages (30μm). Images with Z projection of sum intensity were obtained from two stacks above and two stacks below of the brightest section at the furrow tip covering a depth of 4 μm. ROIs across the furrow tip from 5 or 10 rings were drawn in these images for each time point to obtain the mean signal intensity. The mean intensity obtained at each time point was represented as a ratio to the cytosolic mean fluorescence value obtained across cellularization within each embryo and finally plotted as a 'normalized intensity vs stages'.

A line ROI passing through the ring for a single optical plane was used to obtain an intensity profile of Sqh-mCherry, GRAF-GFP and AnillinRBD-GFP in embryos across different stages of cellularization. The intensity at the documented time points was represented as a ratio to the maximum intensity usually across cellularization for each of these embryos.

2.8.3 Quantification of the contractile ring area

The area of the contractile ring was quantified using fixed embryos stained with fluorescently labelled phalloidin and movies obtained with Sqh-mCherry in different genotypes.

Phalloidin stained embryos marking contractile rings at the basal most region were extracted for quantification of contractile ring area from control, *Graf^f* and *Graf^{CR57}*. These images were converted to 8-bit and transformed into binary images. The binary images were inverted and segmented to identify individual rings and the area was quantified for different stages of cellularization. The area was plotted in groups of early (furrow length less than 6 μm), mid (furrow length 6-16 μm) and late (furrow length more than 16 μm) stages of cellularization based on furrow length to compare between control and mutant embryos.

Live movies from embryos expressing Sqh-mCherry of different genotypes were used to quantify contractile ring area. Sqh-mCherry fluorescence images containing sum intensity were obtained across 5 optical sections at the base of the furrow with the brightest section in the middle. 5-10 rings were marked manually using a polygon tool in these images and the area was computed in ImageJ. The mean \pm s.d. for the area was computed and plotted with time using Graphpad Prism 5.0.

2.8.4 Quantification of furrow membrane length

Sqh-mCherry fluorescence was used to identify furrow tips during cellularization. Membrane length was measured using the ImageJ line tool every 2 mins in (5 furrow lengths per time point were recorded in each embryo). These lengths were plotted against time as a scatter plot using Graphpad Prism 5.0.

2.8.5 Quantification of displacement and initial recoil velocity after laser ablation

The manual tracking plugin of Fiji software was used to extract xy coordinates from control and ablated regions. These xy coordinates were used to get distance between the two points with the following formula:

$$D = \sqrt{(y_2 - y_1)^2 + (x_2 - x_1)^2}$$

where (x1,y1) and (x2,y2) are the coordinates of the contractile ring edge seen below and above the ablation region respectively.

The ring displacement was estimated for each time point after ablations. The displacement of edges measured before ablations was subtracted from all the time points after ablations. The displacement was calculated from five independent embryos. The mean displacement and standard deviation with respect to time were plotted for control and *Grac^{CR57}* mutant embryos across the early and mid stages. The displacement at the last time point at approximately 70 s was used to plot maximum displacement. The initial recoil velocity was calculated by fitting a linear function on points between 0 and 23 s on the plot of displacement versus time in each embryo.

2.9 Statistical analysis

The mean±s.d. was computed from a total of 15 rings obtained as 5 rings each from 3 living embryos and 5 rings each from more than 3 fixed embryos (the n value for each experiment is a part of each legend) for intensity and area quantification. The statistical significance was determined using a non-parametric Mann-Whitney test, two tailed student's t-test to compare two means. One-way ANOVA, repeated measures with Dunnett's multiple comparison test was used to compare 3 or more means together by comparing all points to a control point. Graphs for area versus time and Sqh-mCherry, AnillinRBD-GFP and GRAF-GFP intensity were represented with smoothing using the 2nd order, seven-neighbors 'Savitsky-Golay' smoothing algorithm.

CHAPTER 3

GRAF is essential for actomyosin contractility during *Drosophila* cellularization

3.1 Introduction

Cytokinesis is the fundamental process to ensure the successful separation of daughter cells. During the initial step of cytokinesis, precise membrane curvature induction will lead to the formation of the cleavage furrow. After membrane curvature induction, cleavage furrow ingresses towards the cell interior. The force required for cleavage furrow ingression is provided by the contractile ring beneath the membrane. The contractile ring consists of an actomyosin network that is assembled at the equatorial plane. The contractile ring is responsible for generating the tension required to carry out the contraction process either by Myosin II motors or actin depolymerization. Thus, actin and Myosin II are the central molecules involved in executing the contraction of contractile rings. Spatial and temporal regulation of molecules associated with actomyosin networks also becomes crucial for the assembly and contractility process.

Cytokinesis initiates with the positioning of contractile ring which guides cleavage furrow ingression. The regulation of furrow ingression process is executed by a class of membrane deforming proteins called BAR domain proteins. There are studies dissecting the role of BAR domain proteins in *Drosophila* such as Cip4 overexpression which phenocopy Diaphanous depletion causing cytokinetic defects (Yan et al., 2013). Another BAR domain protein, Amphiphysin is required for cleavage furrow tip tubules formation. Cleavage furrow tip tubules are absent in *amphiphysin* null embryos and correlate with a faster ingression rate of the cleavage furrow (Su et al., 2013). Previous work in our lab has shown depletion of *syndapin* mutant results in shorter pseudocleavage furrows in *Drosophila* syncytial embryos. *Syndapin* mutant also shows disorganized actin, possibly

via aberrant recruitment of Diaphanous and Peanut (Sherlekar & Rikhy, 2016). Hence a systematic analysis of BAR domain protein function in *Drosophila* embryogenesis is required to dissect their role in coordinating actin and membrane remodelling activities.

We identified GRAF protein from BAR domain protein screening performed during *Drosophila* embryogenesis. GRAF is a multidomain protein consisting of BAR, PH, RhoGAP and SH3 domains (Lundmark et al., 2008). This molecule was originally identified as a binding partner of the C-terminal domain of focal adhesion kinase (Hildebrand et al., 1996; J. M. Taylor et al., 1998). Previous studies have shown that GRAF colocalizes to cortical actin, stress fibers, focal adhesions paxillin and FAK in mammalian cells (MEFs) and chick embryonic cells (Hildebrand et al., 1996; Luo et al., 2017). In addition, GRAF recruitment leads to stabilized cortical actin and cell spreading (Barrios & Wieder, 2009). GRAF loss leads to depletion of epithelial markers resulting in the acquisition of mesenchymal markers. This causes an enhanced migratory ability due to an increase in actin stress fibers, focal adhesions and elevated mesenchymal markers (Regev et al., 2017).

There are several reports on human *GRAF1* genes having abnormally methylated promoters, mutations and deletions associated with acute myeloid leukaemia (AML) or myelodysplastic syndrome (MDS) (Bojesen et al., 2006; Borkhardt et al., 2000; J. Qian et al., 2011; Z. Qian et al., 2010). GRAF has also been previously shown to regulate EGFR signalling through the clathrin-independent pathway of the *Drosophila* hematopoietic system (Kim et al., 2017). Thus, GRAF1 protein is specifically involved in the internalization of cargoes in CLIC/GEEC pathway (G. J. Doherty & Lundmark, 2009; J. T. Doherty et al., 2011; Lundmark et al., 2008). This pathway leads to a reduction in cell volume due to membrane internalization in hypotonic conditions. The reduction in cell volume triggers GRAF recruitment via BAR and PH domains which result in reduced membrane tension. In the absence of GRAF, cellular blebbing is marked by increased Myosin II foci (Holst et al., 2017)

GRAF studies provide evidence regarding its role in stabilizing actin fibers and regulating Myosin II levels. Actin and Myosin II are required in contractile ring formation and constriction. Therefore, we assessed the role of GRAF in contractile ring formation in *Drosophila* cellularization. This study will focus on dissecting the effect of GRAF on ring architecture and its recruitment during cellularization to regulate constriction.

3.2 Material and methods

3.2.1 *Drosophila* stocks

Fly stocks and crosses were maintained in regular cornmeal agar. The detailed genotypes, stock numbers and source of stocks are a part of Table 3.1.

Stock	Genotype	Source/Reference
1	Canton-S	Lab stock originally obtained Bloomington <i>Drosophila</i> Stock Center
2	<i>nanos</i> -Gal4	Lab stock
3	w; <i>mat67</i> -Gal4; <i>mat15</i> -Gal4	Girish Ratnaparkhi, IISER, Pune, India
4	y[1] v[1]; P{TRiP.HMC03427}attP40 (GRAF shRNA1, <i>Graf^f</i>)	BDSC, #51853
5	y[1] sc[*] v[1] <i>Graf</i> [CR57]/FM7a (<i>Graf^{CR57}</i>)	This study
6	y[1] sc[*] v[1] <i>sev</i> [21]; P{TKO.GS00762}attP40	BDSC, #76993
7	P{KK102763}VIE-260B (GRAF shRNA2, <i>Graf²ⁱ</i>)	Vienna <i>Drosophila</i> Stock Center, #v110812
8	y[1] sc[*] v[1] <i>sev</i> [21]; P{y[+t7.7] v[+t1.8]=nos-Cas9.R}attP40	<i>Drosophila</i> facility, NCBS

Table 3.1: *Drosophila* stocks and their source

3.2.2 Immunostaining

0-3.5 hr embryos were collected on sucrose-agar plates, washed, dechorionated with 100% bleach and washed again. To visualize GRAF and Dlg immunostained embryos, dechorionated embryos were heat fixed with boiled 1X Triton salt solution (10x-0.5%Triton X-100 and 7%NaCl in water) for 1 min and instantly adding ice-cold 1X washing buffer. After cooling on ice, embryos were devitellinized in a 1:1 mix of MeOH and heptane followed by three washes in 1X PBST (1X PBS with 0.3% Triton X-100) for 5 min each. After washing, embryos were blocked in 2% BSA in 1X PBST for 1 hr and then incubated in primary antibody (Table 2.4) overnight at 4 °C. This was followed by three 1X PBST washes and incubated in fluorescently coupled secondary antibodies (Molecular probes) at 1:1000 dilution for 1 hr at room temperature. Embryos were washed three times in 1X PBST for 5 min each. DNA was labelled with Hoechst 33258 (1:1000, Molecular Probes) for 5 min in the second 1X PBST wash. Finally, embryos were mounted in Slow fade Gold antifade (Molecular Probes).

To visualize F-actin, embryos were fixed using a 1:1 mix of 8%PFA in 1XPBS: heptane for 20 min and followed by hand devitellinization. Fluorescently coupled phalloidin (Molecular Probes) was used to label F-actin in embryos in cellularization for 1 hour at room temperature followed by washes and DNA labelling.

3.2.3 Analysis

3.2.3.1 Quantification of mean fluorescence intensity from immunostainings

The imaging of fixed control and mutant embryos immunostained with antibodies against GRAF along with Dlg was carried out on the Leica SP8 confocal microscope at the same laser power and gain settings. To estimate the mean fluorescence intensity of GRAF from immunostaining, a single optical section from the Z-stack containing the brightest intensity at the furrow tip was chosen. Fluorescence intensity was obtained in this section by drawing ROIs using the segmented line tool around the ring to get the average intensity using Fiji software (<http://fiji.sc/wiki/index.php/Fiji>) (Rueden et al., 2017). The ring intensity obtained was divided by the cytosol intensity obtained from a large square ROI in the apical most region above the nuclei from the same image. This

membrane to cytosol ratio for GRAF antibody fluorescence in control embryos, *Graf*^{CR57} and *Graf*^Δ was plotted for different stages of cellularization.

3.2.3.2 Quantification of the contractile ring area

Phalloidin stained embryos marking contractile rings at the basal most region were extracted for quantification of contractile ring area from control, *Graf*^Δ and *Graf*^{CR57}. These images were converted to 8-bit and transformed into binary images. The binary images were inverted and segmented to identify individual rings and the area was quantified for different stages of cellularization. The area was plotted in groups of early (furrow length less than 6 μm), mid (furrow length 6-16 μm) and late (furrow length more than 16 μm) stages of cellularization based on furrow length to compare between control and mutant embryos.

3.3 Results

3.3.1 *Drosophila* GRAF multi-domain organization is conserved across multicellular organisms

We performed BAR domain proteins screening and estimated their requirement in embryogenesis by scoring lethality (Table A, details are mentioned in Appendix). We identified GRAF from this screen which shows the second highest embryonic lethality after Nostrin. The *Drosophila* GRAF protein is a multi-domain protein consisting of BAR, PH, RhoGAP and SH3 from N to the C terminus. The closest homologue from *Saccharomyces cerevisiae* is RGA2 protein which contains only a RhoGAP domain. *Saccharomyces pombe* contains a similar protein *rga2* containing a PH and SH3 domain whereas the *gacJJ* protein in *Dictyostelium* contains a PH, RhoGAP and SH3 domain. The complexity arises in *Drosophila* having multi-domain architecture consisting of BAR, PH, RhoGAP and SH3. We found that *Drosophila* GRAF protein with the domain organization is conserved across the other multicellular organisms *C.elegans*, *Drosophila*, *Xenopus*, *Chicken*, *Zebrafish* and *Humans* (Figure 3.1A, B). The evolution in GRAF multi-domain nature is likely to be associated with multicellular complexity across

metazoans. It might be relevant for the regulation of cell-cell adhesion to generate multicellularity.

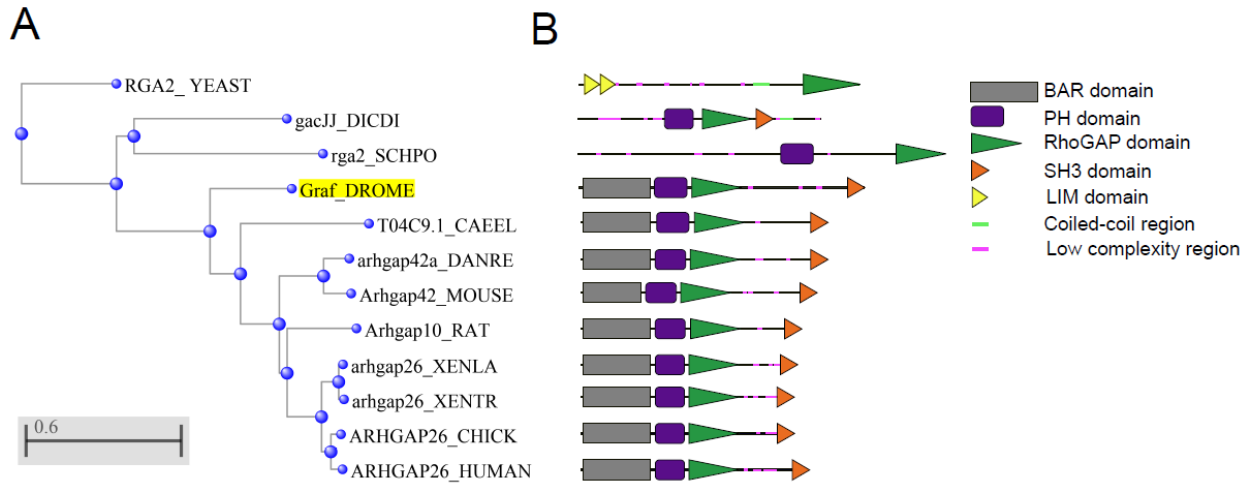


Figure 3.1: Phylogenetic tree of GRAF protein across various species.

(A) The amino acid sequences for *Drosophila melanogaster* GRAF and its orthologs from *Schizosaccharomyces cerevisiae* (RGA2), *Dictyostelium discoideum* (gacJJ), *Saccharomyces pombe* (RGA2), *Caenorhabditis elegans* (T04C9.1), *Danio rerio* (Arhgap42a), mouse (Arhgap42), rat (Arhgap10), *Xenopus laevis* (Arhgap26), *Xenopus tropicalis* (Arhgap26), gallus gallus (ARHGAP26) and humans (ARHGAP26) amino-acid sequence were obtained from UniPort software. These 12 protein sequences were aligned in the NCBI multiple protein blast using the neighbour-joining method. The *Drosophila* GRAF protein is highlighted in yellow. The domains present in each species are marked in each of the 12 proteins.

(B) Multicellular organisms from *C.elegans* to humans in the list contain a conserved BAR, PH, RhoGAP and SH3 domain from the N terminus to the C terminus. Bar represents the number of substitution events per site.

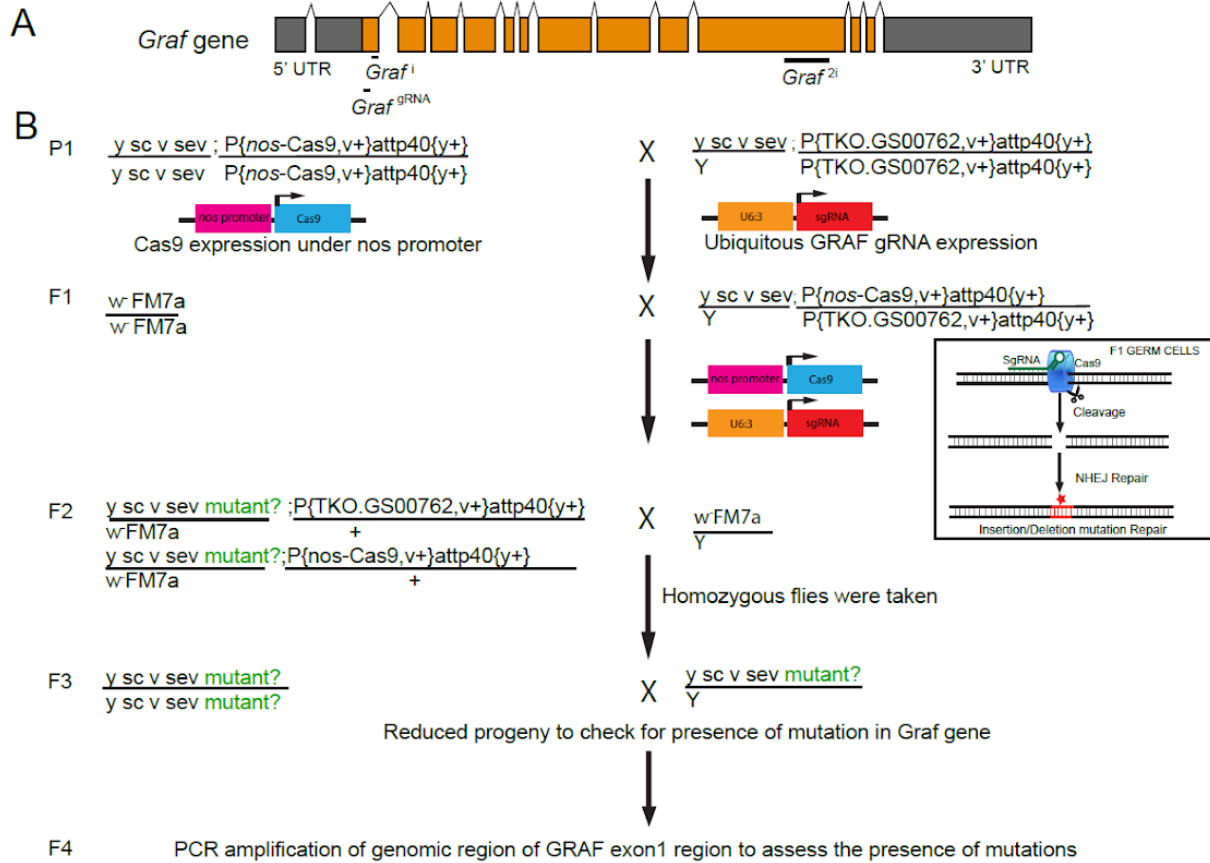
3.3.2 GRAF depletion using shRNA knockdown and generation of GRAF knockout using CRISPR-Cas9 strategy

To study the function of the GRAF protein, shRNA and CRISPR Cas-9 strategy were used to generate *Graf* loss of function embryos. In order to lower GRAF protein levels, *Graf* shRNA1 (*Graf^{f1}*) and *Graf* shRNA2 (*Graf^{f2}*) were used. The transgenic lines consist of *Graf* shRNA1 against exon1 whereas *Graf* shRNA2 (*Graf^{f2}*) against exon 10 region of *Graf* gene locus (Figure 3.2A). These shRNAs are downstream of UAS enhancer elements. Using the UAS-Gal4 strategy, these shRNAs were crossed with

maternal *nanos*-Gal4 and *mat67*-Gal4;*mat16*-Gal4 respectively to achieve maternal knockdown during oogenesis and embryogenesis. F1 females containing the Gal4 and shRNA gave embryos that were lethal at 24 hours (94%, n=532 embryos containing *Graf*^f and 98%, n=540 embryos containing *Graf*^{f2}).

Graf knockout mutants were generated by the CRISPR Cas9 strategy. A transgenic fly stock containing a guide RNA (gRNA) against exon1 (at 2751 residue from transcription start site) of the *Graf* gene was crossed to flies expressing Cas9 maternally under *nanos* promoter during oogenesis (X. Ren et al., 2013; Zirin et al., 2020). *Graf*^{gRNA} embryos obtained from F1 females expressing the gRNA and Cas9 consist of transient knockout of GRAF protein. The efficiency of gRNA was observed either by embryonic lethality or scoring for embryonic defects.

Parental(P1) cross consisted of virgin female flies, expressing Cas9 under *nanos* promoter, crossed to male, expressing GRAF gRNA express under ubiquitous U6:3 promoter. 155 independent males having *nanos* Cas9 and gRNA were selected and crossed with FM7a balancer virgin flies. The progenies from this cross were propagated for 2-3 generations to yield homozygous flies. These homozygous flies were scored for sterility assay to identify putative homozygous mutant flies with reduced progeny (see materials and methods for details and Figure 3.2B). PCR amplification of exon1 was carried out from these homozygous flies from 18 lines which gave reduced progeny and 3 lines that were similar to controls. PCR amplified products were purified and confirmed by sequencing for insertions and deletions. The 18 lines with a reduced progeny phenotype showed small insertions or deletions leading to a frameshift which results in a premature stop codon in exon1 of the *Graf* gene. The 3 fly lines that served as fertile controls also showed small insertions or deletions but the coding frame was intact (Figure 3.2C). The fly line CR57, named *Graf*^{CR57} henceforth, containing a possible stop codon at the 27th amino acid compared to the full-length GRAF protein with 1025 amino acids. This mutant generates a premature stop codon with the absence of any functional domain and was chosen for further analysis (Figure 3.2D). *Graf*^{CR57}/*Graf*^{CR57} homozygous adult females gave null mutant embryos that showed 71% lethality (n=336).



C

CRISPR Mutant scored	Exon1 DNA bp modification	Effect on translation
35	8bp deleted after 64bp	Pre-mature stop codon at 27 th position
46,49,57,69,70,88,92,95,112,154	7bp deleted after 63bp	Pre-mature stop codon at 28 th position
138	Addition of AAA after 65bp & proceed with 10bp deletion	Pre-mature stop codon at 28 th position
144	4bp deleted after 66bp	Pre-mature stop codon at 29 th position
68	4bp deleted after 64bp	Pre-mature stop codon at 29 th position
116	Replacement of AG to TT bp after 66bp	Pre-mature stop codon at 30 th position
44	1bp deleted after 66bp	Pre-mature stop codon at 30 th position
19	8bp deleted after 64bp	Pre-mature stop codon at 31 st position
101	Insertion of [TCGTC]bp after 67bp	Pre-mature stop codon at 32 th position
74C (no phenotype)	12bp deleted after 61bp	Intact coding frame after 25aa
78C (no phenotype)	Insertion 15bp after 67bp	Intact coding frame after 23aa
51C (no phenotype)	Insertion 4bp & proceed with deletion [TTTC-] after 66bp	Intact coding frame after 24aa

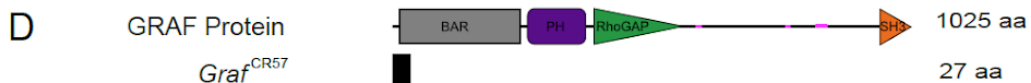


Figure 3.2: *Graf* depletion using shRNA knockdown and generation of GRAF knockout using CRISPR-Cas9 strategy

(A) GRAF genomic locus is shown with UTR, introns and exons. *Graf*, *Graf^{RNA}* target the exon 1 region, and *Graf²ⁱ* target the exon 10 region. *Graf* null mutant generation using the Crispr-Cas9 strategy. **(B)** Females containing the *nanos*-Cas9 transgene were crossed to males containing a transgene that ubiquitously expresses *Graf^{RNA}* against exon1. The F1 generation males containing the *nanos*-Cas9 and *Graf^{RNA}* were crossed with homozygous FM7a virgin females. The exon1 of the *Graf* gene will get cleaved by Cas9 during spermatogenesis and be subjected to DNA repair by the non-homologous end joining (NHEJ) pathway. The F2 generation virgin females containing the putative mutant X chromosome and FM7a balancer were crossed individually to FM7a males. Several lines containing homozygous flies which gave reduced progeny were obtained. 18 lines that gave reduced progeny and 3 lines that served as healthy controls were used for confirmation of mutations in the exon1 of *Graf*. PCR was carried out for exon1 from the genomic DNA of these flies and sent for sequencing. **(C)** The table shows mutations obtained in exon1 from DNA sequencing. The 18 lines showing reduced progeny gave small insertions and deletions that led to a frameshift and a stop codon. The 3 lines that served as healthy controls also gave small insertions and deletions and the frame of the *Graf* gene was intact in these lines. **(D)** GRAF protein (1025aa) contains a BAR, PH, RhoGAP and SH3 domain. *Graf^{CR57}* has a stop codon at amino acid 28 and is predicted to form a 27aa peptide

3.3.3 GRAF depletion leads to hyper constriction of contractile ring in cellularization

Drosophila cellularization occurs in cycle 14 interphase where the membrane extends around approximately 6000 nuclei to form individual cells. During this stage, the furrow membrane extends between adjacent nuclei from 3 μm to 40 μm in approximately 45 min at 25 °C. The nuclei are spherical in the early stages and elongate during mid cellularization. Embryos at cellularization stage were stained with fluorescently coupled phalloidin which marks cortical F-actin at the furrow tip. At the furrow tip, the process is divided broadly into 3 stages such as early, mid and late depending on the furrow length. During the early stages of cellularization (furrow length 3-6 μm) in control embryos, the actomyosin network assembles and forms a tight polygonal network at the furrow tip (white arrowheads, Figure 3.3A) (He et al., 2016; Xue & Sokac, 2016). This polygonal architecture is remodelled to a circular shape forming a contractile ring at the furrow tip in mid cellularization (furrow length 6-16 μm). This contractile ring constricts further during

late cellularization at the base of elongated nuclei (furrow length 16-40 μm) (Xue & Sokac, 2016) (Figure 3.3A).

Graf^f expressing embryos showed enhanced constriction throughout cellularization (Figure 3.3B, 3.4A). In *Graf*^f embryos, F-actin shows loose polygonal networks where edges become wavy and detached from each other in early cellularization. The distorted polygonal network leads to premature constriction during mid stages and hyper constriction of rings in late stages when compared to control. Quantification of the F-actin network area at the furrow tip from *Graf*^f fixed embryos showed a significant decrease as compared to controls in early, mid and late cellularization (Figure 3.3D).

In contrast to *Graf*^f embryos, *Graf*^{CR57} embryos show severe defects by showing premature ring formation during early cellularization and hyper constriction in mid and late cellularization (Figure 3.3B). Quantification of ring area of *Graf*^{CR57} embryos in cellularization showed a significant decrease in early, mid and late stages when compared to controls and *Graf*^f (Figure 3.3D). Thus, *Graf* depletion causes pre-mature and hyper constriction of the rings during cellularization when compared to controls (Figure 3.3E).

To achieve proper cell shape, contractility is executed once the furrow tip reaches the bottom of the nuclei. In the case of both *Graf*^f and *Graf*^{CR57} embryos, the nuclei become squeezed, possibly due to premature ring constriction in mid cellularization. This defect gives rise to bottleneck shaped nuclei similar to *bnk* mutants (Figure 3.3C). Loss of polygonal F-actin organization and premature ring constriction at the furrow tip are also seen in embryos depleted of Bottleneck or Cheerio, actin crosslinker proteins in cellularization (Krueger et al., 2019; Reversi et al., 2014; Schejter & Wieschaus, 1993b).

Figure 3.3: *Graf* depletion leads to hyper constriction of contractile rings during cellularization

(A) Schematic depiction of cellularization in the *Drosophila* embryo with the plasma membrane (black), nuclei (grey) and contractile ring (red) organization at the base of the furrow. The base of the furrow where the contractile ring assembles is hexagonal at the early stage, circular at the mid stage and constricted at the late stage. **(B)** *Graf* depletion leads to hyper constricted contractile rings in cellularization. Phalloidin (grey)-labelled furrow tip sections show polygonal organization (white arrowhead) in control embryos, *nanos-Gal4*; *Grafⁱ* shows circular organization, and *Graf^{CR57}* shows ring constriction (white arrowhead) in the early cellularization. Control embryos show circular rings, and *Grafⁱ* and *Graf^{CR57}* embryos show constricted rings in mid cellularization. Control embryos show constricted rings, and *Grafⁱ* and *Graf^{CR57}* embryos show hyper constricted rings in late cellularization. *Grafⁱ*, 95.7% (n = 70 embryos), and *Graf^{CR57}*, 96.8% (n = 31 embryos), show enhanced constriction as compared to controls (n = 54 embryos) in different stages of cellularization. **(C)** DNA labelled by Hoechst shows the bottleneck appearance during mid cellularization in *Grafⁱ* (48.1% show bottleneck nuclei, n = 27 embryos in different stages of cellularization) and *Graf^{CR57}* (52.94% show bottleneck nuclei, n = 34 embryos in different stages of cellularization) (yellow line marks nuclei morphology). **(D)** Scatter plot shows the area of the ring in the control, *Grafⁱ* and *Graf^{CR57}* during early (3–6 μm furrow length), mid (6–16 μm) and late (16–40 μm) stages of cellularization (n = 60 rings, 10 per embryo, 6 embryos each). **(E)** *Graf^{CR57}* mutant embryos show premature ring formation in the early stage and hyper constriction in mid and late stages with nuclei getting squeezed to show a bottleneck phenotype. Data is represented as mean \pm s.d. **p<0.01, ***p<0.001, two-tailed Mann–Whitney test. Scale bars: 5 μm .

Graf²ⁱ and *Graf^{gRNA}* expressing embryos show enhanced ring constriction (Figure 3.4A) similar to *Grafⁱ* and *Graf^{CR57}* embryos. Taken together, *Graf* depleted embryos show premature and untimely constriction of the F-actin network at the furrow tip in cellularization, thereby giving rise to bottle-neck shaped nuclei. GRAF function is therefore likely to be involved in inhibiting ring constriction in cellularization.

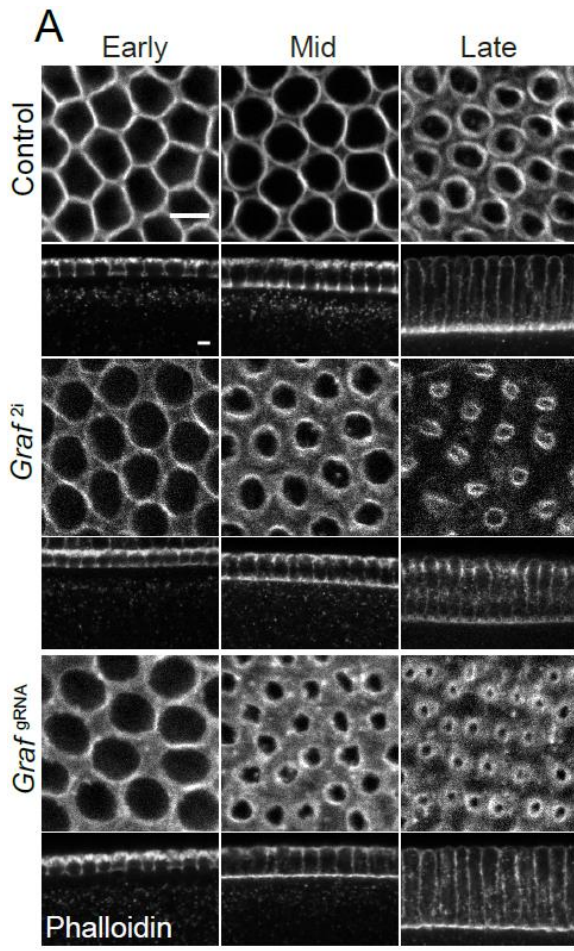


Figure 3.4: *Graf* depletion phenotypes using *Graf*²ⁱ and *Graf*^{grna}

*Graf*²ⁱ and *Graf*^{grna} expressing embryos show enhanced ring constriction. Phalloidin (grey)-stained control embryos in early cellularization show polygonal organization of the furrow tip, whereas *Graf*²ⁱ and *Graf*^{grna}; *nanos*-Cas9 show rings. In mid cellularization, control embryos show circular rings and *Graf*²ⁱ and *Graf*^{grna}; *nanos*-Cas9 expressing embryos show constricted rings. In late cellularization, control embryos (n = 54 embryos) show constricted rings, and *Graf*²ⁱ (95.23% showed enhanced constriction in cellularization, n = 21 embryos) and *Graf*^{grna}; *nanos*-Cas9 (89.18% showed enhanced constriction in cellularization, n = 37 embryos) embryos hyper constricted rings.

3.3.4 GRAF protein recruits at the contractile ring during early and mid cellularization

In order to visualize the distribution of GRAF during *Drosophila* cellularization, we generated a polyclonal antibody against full-length GRAF protein (see Materials and methods). Control embryos were co-stained with GRAF and Dlg, which marks the lateral membranes. The grazing plane across the furrow tip showed enriched GRAF recruitment at edges (white arrows, Figure 3.5A) which was occasionally absent at the vertices in early cellularization. GRAF antibody staining increased at regions where rings are contacting each other during mid cellularization and was occasionally absent from curved regions (yellow arrowhead, Figure 3.5A). Finally, GRAF staining became cytoplasmic in late cellularization. The sagittal plane shows GRAF enrichment at the furrow tip during early and mid cellularization (Figure 3.5A). Quantification of GRAF intensity using staining shows increased intensity from early to mid which gets reduced in late stages (Figure 3.5B).

The GRAF staining was drastically reduced in *Graf*^{CR57} and *Graf*^f mutant embryos as compared to controls (Figure 3.5A, D). GRAF antibody signal was quantified as a ratio of the cortex to the cytosol. *Graf*^{CR57} showed a greater reduction in fluorescence intensity as compared to *Graf*^f in comparison with corresponding controls (Figure 3.5C, E). This also correlates with the more severe defects in ring constriction seen in *Graf*^{CR57} as compared to *Graf*^f. Thus, *Graf*^{CR57} shows a complete loss of function whereas *Graf*^f shows a partial loss-of-function phenotype for GRAF protein.

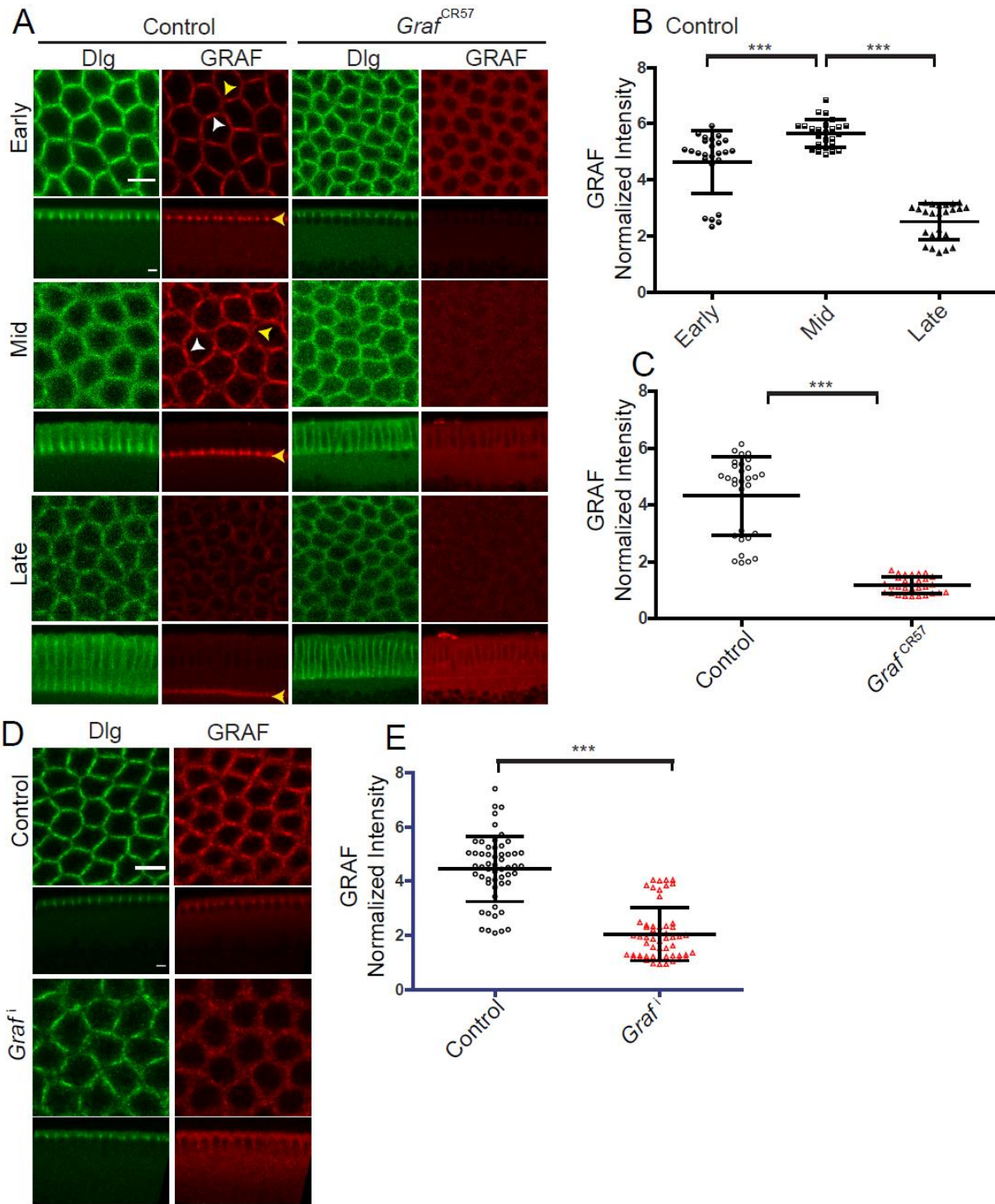


Figure 3.5: GRAF protein is enriched at the furrow in mid cellularization.

GRAF localizes at the furrow tips in cellularization. Control embryos ($n = 36$ embryos) immunostained with GRAF (red) and Dlg (green) show GRAF enrichment at the furrow tip in early and mid cellularization (white arrowhead shows edge enrichment, whereas yellow arrowhead shows a curved region with weaker signal). GRAF is decreased from the furrow tip in late cellularization. *Graf*^{CR57} (100%, $n = 11$) embryos show depletion of GRAF antibody in cellularization. (B) Quantification of GRAF antibody fluorescence intensity

as a cortex to cytosol ratio shows increased staining in mid cellularization as compared to early and late cellularization (n = 25 rings, 5 per embryo, 5 embryos per stage, 25 embryos) (furrow length used for early = 4–6 μm , mid = 7–11 μm , late = 17–31 μm). (C) *Graf*^{CR57} (furrow length range: 3–24 μm) shows loss of GRAF antibody staining intensity compared to controls (furrow length range: 5–25 μm) (n = 30 rings, 5 per embryo, 6 embryos). (D) *Graf* shows a decrease in GRAF antibody staining compared to control embryos (64%, n = 14 embryos). (E) Quantification of GRAF antibody fluorescence intensity as a cortex to cytosol ratio shows reduction of intensity in *Graf* (furrow length range: 3–20 μm) compared to controls (furrow length range: 3–14 μm) (n = 55 rings, 5 per embryo, 11 embryos each). Data are represented as mean \pm s.d. ***p<0.001 (two-tailed Mann–Whitney test). Scale bars: 5 μm .

3.4 Conclusion and discussion

The increased presence of GRAF in early and mid cellularization is likely to influence actomyosin assembly. Later, it becomes cytoplasmic in the late stages which influences the timing of contractility. *Graf* depletion shows accelerated ring constriction throughout cellularization (Figure 3.6) (Sharma & Rikhy, 2021). GRAF acts as a negative regulator which is likely involved in regulating the precise timing of the actomyosin contraction process.

In summary, the recruitment changes in GRAF is likely to correlate with the dynamic restructuring of the actomyosin network in cellularization.

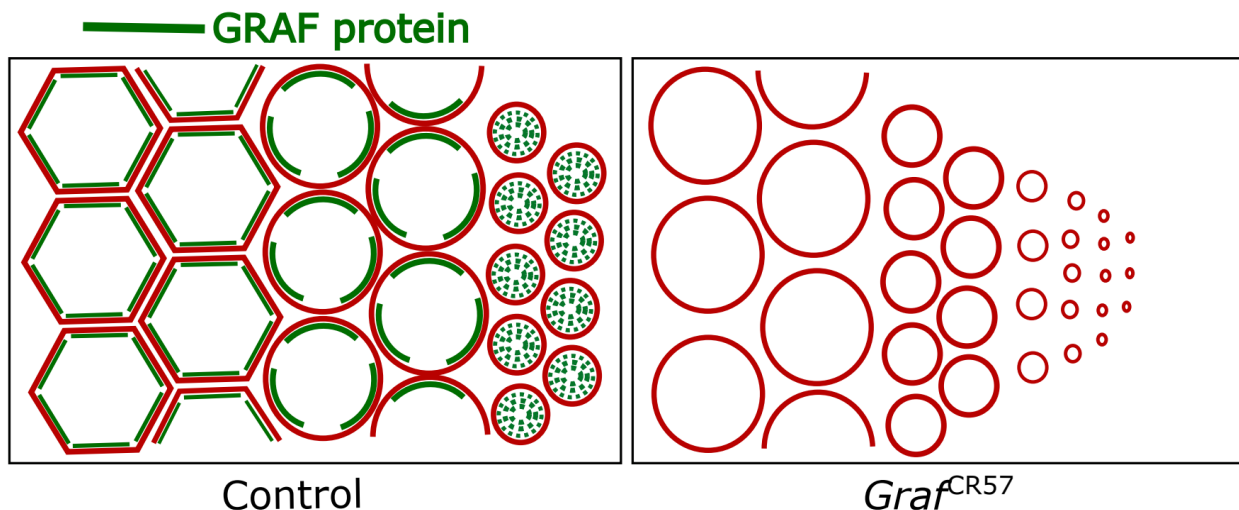


Figure 3.6: GRAF spatio-temporal recruitment regulates contractility during the *Drosophila* cellularization. GRAF(green) specific recruitment at the contractile ring(red) during early and mid stages. During late stages, the protein becomes cytoplasmic resulting in systematic constriction. *Graf*^{CR57} depletion causes premature and hyper constriction defects. Thus, GRAF shows enrichment at the furrow tip till mid

cellularization which could be directly involved in regulating the precise timings of actomyosin contraction process.

Bottleneck and *Cheerio* mutants give rise to bottleneck nuclei defects which phenocopy the *Graf*^{CR57} mutant defects. Bottleneck recruitment pattern is similar to GRAF where it gets enriched till mid cellularization and is reduced from the constricted ring during late stages. Bottleneck and *Cheerio* are actin crosslinkers involved in actin bundling to form a tight polygonal network during cellularization (Krueger et al., 2019; Reversi et al., 2014; Schejter & Wieschaus, 1993b; Thomas & Wieschaus, 2004). Future studies on the recruitment of Bottleneck and *Cheerio* in *Graf* mutant embryos will reveal their interaction during polygonal actomyosin network stabilization in cellularization.

Phosphatidylinositol 3,4,5 phosphate (PI(3,4,5)P3) and PI(4,5)P2 are enriched at contractile rings (Reversi et al., 2014). PI(3,4,5)P3 presence is important for limiting actomyosin contractility during the slow phase of cellularization, whereas PI(4,5)P2 is important for promoting actomyosin contractility during the fast phase of cellularization. Decrease in PI(3,4,5)P3 and an increase in PI(4,5)P2 leads to a hyper constriction phenotype (Reversi et al., 2014) similar to *Graf* mutant embryos. The ratio of PI(4,5)P2/PI(3,4,5)P3 is important to orchestrate the actomyosin contractility during cellularization. Future studies of any imbalance in phospholipid composition of the furrow in *Graf* mutant embryos will reveal their interaction with each other during actomyosin ring constriction in cellularization. *In vitro* studies reveal that PH and BAR domains of GRAF protein interact with PI(4,5)P2-containing liposomes (Lundmark et al., 2008) whereas *bnk* interact preferentially with PI(3,4,5)P3 (Reversi et al., 2014). It is further possible that *Graf* depletion leads to an imbalance of PI(4,5)P2/PI(3,4,5)P3 levels which indirectly influences the loss of Bottleneck from the furrow.

CHAPTER 4

GRAF regulates the recruitment of key contractile proteins at the cleavage furrow during cellularization

4.1 Introduction

The cortical actomyosin activity generates force and leads to plasma membrane remodelling (Heer & Martin, 2017; Jodoin et al., 2015; Martin et al., 2009; Mason et al., 2013; Munjal et al., 2015; Murrell et al., 2015). This force generation is highly dependent on the spatiotemporal regulation of the activity of the molecular motor Myosin II (Heisenberg & Bellaïche, 2013; Rauzi et al., 2010). Myosin II activity is controlled by its phosphorylation which is executed by Rho Kinase (Amano et al., 2010; Kasza et al., 2014; Levayer & Lecuit, 2012; Vasquez et al., 2014). Rho Kinase is activated by Rho-GTP, which is small GTPases belonging to the Ras superfamily (Prudnikova et al., 2015). These molecular switches undergo cycling between GTP bound active and GDP bound inactive states (Agarwal & Zaidel-Bar, 2019). Guanine nucleotide exchange factor (GEFs) and GTPases-activating proteins (GAPs) catalyze Rho-GDP and Rho-GTP cycling (Bos et al., 2007; Van Aelst & D'Souza-Schorey, 1997). Rho-GTP exchange factors (Rho-GEF) lead to the generation of Rho-GTP from Rho-GDP whereas Rho-GTPase activating proteins (Rho-GAP) promote hydrolysis of the GTP to generate Rho-GDP (Jacobs & Hall, 2005). The spatiotemporal distribution of Rho-GEFs and Rho-GAPs is critical in fine-tuning the levels of Rho-GTP for Myosin II activation and inhibition in different cell processes (Agarwal & Zaidel-Bar, 2019; Chircop, 2014; Mulinari & Häcker, 2010; S. K. Wu & Priya, 2019).

As expected, microinjection of Rho1 inhibitor, C3 exoenzyme, and human dominant negative N19Rho disrupts the cleavage furrow by altering the actin cytoskeleton during cellularization. This defect results in cellularization halts and finally blocked gastrulation (Crawford et al., 1998). Dominant negative DRhoA expression showing gastrulation defects phenocopies DRhoGEF2 mutant (Barrett et al., 1997; Crawford et

al., 1998; Halsell et al., 2000; Padash Barmchi et al., 2005). Rho-GTP is known to activate the downstream kinases Drok and Drak which in turn activate Myosin II via phosphorylation. Diaphanous (Dia) is another downstream target of Rho-GTP (Alberts, 2001) and a major regulator of the actin cytoskeleton during cellularization (Afshar et al., 2000)

Myosin II activation occurs by the spatiotemporal generation of Rho-GTP and recruitment of kinases to the site of actomyosin assembly. During cellularization, temporal Myosin II recruitment gradually increases in the assembly phase, reaching a plateau in the ring stage and finally declining in the constricted stage. Phospho-deficient mutants of the light chain of Myosin II, Squash (Sqh), show contractility inhibition during cellularization (Xue & Sokac, 2016). In addition, zipper staining which marks Myosin II heavy chain in *sqh*¹ mutant (*sqh* germline mutant) embryos shows irregular aggregates compared to uniform staining on contractile rings in wild type embryos (Royou et al., 2004). Further, Rok and Drak mutant embryos and treatment of embryos with a pharmacological inhibitor of Rok, Y-27632, show an impairment of actomyosin contractility due to reduced Myosin II phosphorylation (Chougule et al., 2016; Krajcovic & Minden, 2012; Xue & Sokac, 2016). In addition, PatJ is shown to indirectly activate Myosin II by reducing Myosin II dephosphorylation (Sen et al., 2012).

In addition to Myosin II, the presence of scaffold protein such as Anillin and septin, Peanut maintain contractile ring architecture. Anillin is recruited at the furrow tip and regulate contractile ring formation. Perturbation in contractile ring formation is observed in *anillin* mutants due to reduced localization in Myosin II and altered localization of Peanut (Christine M. Field et al., 2005). In *peanut* mutants, there are defective actin rings at the furrow tip, showing inhibition of constriction due to aberrant organization of F-actin and Myosin II. Thus, Peanut is crucial for the conversion of linear actin filaments into curved structures necessary for ring formation (Manos Mavrikis et al., 2014).

The GRAF RhoGAP domain influences the GTPase activity of RhoA specifically. RhoA activity was measured using G-LISA luminescence-based RhoA-specific activation

assay. RhoA activity was significantly increased in GRAF1-depleted C2C12 cells in comparison with control siRNA-treated cells (J. T. Doherty et al., 2011). During the onset of skeletal muscle differentiation, GRAF1 morpholino-injected *Xenopus* embryos exhibit significantly higher levels of RhoA activity when compared to control MO-injected embryos at stages 22 and 25. In *Xenopus*, GRAF1 depleted embryos result in progressive muscle degeneration causing defective myofibrillogenesis, defective motility and embryonic lethality due to elevated RhoA activity (J. T. Doherty et al., 2011). GRAF1 variant containing a GAP domain having R412Q point mutation (GAPm) (J. M. Taylor et al., 1999) that blocks enzymatic activity transfected in cultured L6 cells shows a reduction in RhoA activity. In addition, GAPm transfection in C2C12 cells inhibits skeletal muscle differentiation (J. T. Doherty et al., 2011). Microinjection of rho inhibitor (C3 exoenzyme) phenocopies GRAF overexpression, showing reduced Rho activity, giving rise to filopodia-like extensions in growing cells (J. M. Taylor et al., 1999). The hypertensive phenotype in response to angiotensin II in GRAF3 deficient mice is abrogated when treated with a ROCK inhibitor, Y-27632. GRAF deficient mice show increased contractility due to elevated Rho-GTP levels, enhanced Myosin II foci and Myosin II light chain phosphorylation in isolated blood vessels (Bai et al., 2013). GRAF depletion leads to cellular blebbing marked by increased Myosin II foci (Holst et al., 2017).

We assessed the interaction of GRAF with Rho-GTP, Myosin II, Dia, Peanut and PatJ in regulating contractile ring constriction in *Drosophila* cellularization. GRAF specifically localised along with Myosin II to the furrow in the early stages of cellularization and was lost from the furrow in the late stages. We found that the RhoGAP activity of GRAF is relevant in regulating constriction during cellularization. *Graf* depletion results in increased Myosin II recruitment at the contractile ring.

4.2 Material and methods

4.2.1 *Drosophila* stocks

Fly stocks and crosses were maintained in regular cornmeal agar. The detailed genotypes, stock numbers and source of stocks are a part of Table 4.1.

Stock	Genotype	Source/Reference
1	Canton-S	Lab stock originally obtained Bloomington <i>Drosophila</i> Stock Center
2	<i>nanos</i> -Gal4	Lab stock
3	w; <i>mat67</i> -Gal4; <i>mat15</i> -Gal4	Girish Ratnaparkhi, IISER, Pune, India
4	y[1] v[1]; P{TRiP.HMC03427}attP40 (GRAF shRNA1, <i>Graf</i> [#])	BDSC, #51853
5	y[1] v[1]; P{TRiP.GL01207}attP40 (Myosin II binding subunit, MBS shRNA)	BDSC, #41625
6	y[1] w[67]c[23] P{EPgy2}Graf[EY09461] (GRAF overexpression)	BDSC, #17571
7	w; <i>mat67</i> Spider-GFP-Sqh-mCherry/TM3ser	(Martin et al., 2009)
8	<i>mat67</i> -Sqh-mCherry; <i>ubi</i> -AnillinRBD-GFP-NG4/Tb	This study
9	y[1] sc[*] v[1] GRAF[CR57]/FM7a; <i>mat67</i> Sqh-mCherry/ <i>cyo</i>	This study
10	y[1] sc[*] v[1] GRAF[CR57]/FM7a; p[pUASp GRAF EGFP G1] attp40/ <i>cyo</i>	This study
11	y[1] sc[*] v[1] GRAF[CR57]/FM7a; p[pUASp GRAF	This study

	Δ RhoGAP-EGFP] attp40/cyo	
--	----------------------------------	--

Table 4.1: *Drosophila* stocks and their source

4.2.2 Live imaging of *Drosophila* embryos

For live imaging, 2-2.5 hrs. embryos were collected on sucrose agar plates and dechorionated with 100% bleach for 1 min and mounted on 2 well coverslip bottom Labtek chambers. Mounted embryos were filled with 1X PBS (Manos Mavrakis et al., 2008) and imaged using 40X/1.4NA oil objective on Zeiss or Leica SP8 microscope with a frame rate of 1.74s/frame and 2s/frame respectively.

4.2.3 Immunostaining

0-3.5 hrs embryos were collected on sucrose-agar plates, washed, dechorionated with 100% bleach and washed again. To visualize GRAF, Zipper and Dlg immunostained embryos, dechorionated embryos were heat fixed with boiled 1X Triton salt solution (10x-0.5%Triton X-100 and 7%NaCl in water) for 1 min and instantly adding ice-cold 1X washing buffer. After cooling on ice, embryos were devitellinized in a 1:1 mix of MeOH and heptane followed by three washes in 1X PBST (1X PBS with 0.3% Triton X-100) for 5 min each. After washing, embryos were blocked in 2% BSA in 1X PBST for 1 hr and then incubated in primary antibody (Table 2.4) overnight at 4 °C. This was followed by three 1X PBST washes and incubated in fluorescently coupled secondary antibodies (Molecular probes) at 1:1000 dilution for 1 hr at room temperature. Embryos were washed three times in 1X PBST for 5 min each. DNA was labelled with Hoechst 33258 (1:1000, Molecular Probes) for 5 min in the second 1X PBST wash. Finally, embryos were mounted in Slow fade Gold antifade (Molecular Probes). For Anillin, Peanut and PatJ immunostainings, dechorionated embryos were fixed using 1:1 mixture of 4% paraformaldehyde (PFA) and heptane for 20 min, followed by MeOH devitellinization

To visualize F-actin and Diaphanous, embryos were fixed using a 1:1 mix of 8%PFA in 1XPBS: heptane for 20 min and followed by hand devitellinization. Devitellinized embryos were washed and followed the same procedure as mentioned above. Fluorescently coupled phalloidin (Molecular Probes) was used alongwith

secondary antibody to label F-actin in embryos in cellularization for 1 hour at room temperature followed by washes and DNA labelling.

4.2.3 Laser ablations

Control and *Graf*^{CR57} embryos expressing Sqh-mCherry were used for visualizing contractile rings for laser ablation experiments using the Zeiss LSM780 microscope. Laser ablation was achieved by using an 800 nm multiphoton femtosecond pulsed Mai Tai laser. The region of interest used for ablations was set to a line of 510-pixel length (42.51 μm) and captured with a speed of 1.58 μs per pixel and 20 iterations. The Sqh-mCherry was imaged using a 561 nm laser excitation with a time interval of 1.27 s. A sagittal section was taken before ablations to estimate furrow length for early (less than 6 μm) and mid stages (6–16 μm) of cellularization. Three sections were taken before the ablations in approximately 3 s, the time taken for ablations is approximately 3.22 s and imaging was carried out for approximately 70 s after ablations.

4.2.4 Analysis

4.2.4.1 Quantification of mean fluorescence intensity from immunostaining

The imaging of fixed control and mutant embryos immunostained with antibodies against GRAF along with Dlg and Zipper along with Dlg was carried out on the Leica SP8 confocal microscope at the same laser power and gain settings. To estimate the mean fluorescence intensity of GRAF and Zipper from immunostaining, a single optical section from the Z-stack containing the brightest intensity at the furrow tip was chosen. Fluorescence intensity was obtained in this section by drawing ROIs using the segmented line tool around the ring to get the average intensity using Fiji software (<http://fiji.sc/wiki/index.php/Fiji>) (Rueden et al., 2017). The ring intensity obtained was divided by the cytosol intensity obtained from a large square ROI in the apical most region above the nuclei from the same image. This membrane to cytosol ratio for GRAF antibody fluorescence intensity in control embryos and GRAF-OE was plotted for cellularization stages. Similarly, the membrane to cytosol ratio for Zipper antibody fluorescence intensity in control and *Graf*^{CR57} was plotted for cellularization stages. In addition, the membrane

to cytosol ratio for Anillin antibody fluorescence intensity in control and *Graf*^f was plotted for cellularization stages.

4.2.4.2 Quantification of mean fluorescence intensity from live-imaging

Live imaging of embryos containing different genotypes (AnillinRBD-GFP, GRAF-GFP and GRAF Δ RhoGAP-GFP, Sqh-mCherry in GRAF-OE and *Graf*^{CR57}) were used to quantify the fluorescence intensity change with respect to time. Images with Z projection of sum intensity were obtained from two stacks above and two stacks below of the brightest section at the furrow tip covering a depth of 4 μ m. ROIs across the furrow tip from 5 or 10 rings were drawn in these images for each time point to obtain the mean signal intensity. The mean intensity obtained at each time point was represented as a ratio to the maximum mean fluorescence value obtained across cellularization within each embryo and finally plotted as a 'normalized intensity versus time'.

Live imaging of Sqh-mCherry expressing embryos in various genotypes was used to quantify fluorescence intensity change during the last five time points in late cellularization. To estimate these changes quantitatively across all genotypes, images were obtained with sum intensity per pixel across the Z-axis from a total of five stacks: two stacks above and two stacks below of the brightest section at the furrow tip covering a depth of 4 μ m in late cellularization. The mean ring intensity per pixel was extracted by drawing a segmented ROI on the ring. The inter-ring intensity per pixel was extracted by drawing an ROI in between adjacent rings that had reduced Sqh-mCherry intensity. The ring intensity per pixel was expressed as a ratio to interring intensity per pixel. Finally, the normalized intensity of the ring was shown as a scatter plot.

4.2.4.3 Quantification of the contractile ring area

Live movies from embryos expressing Sqh-mCherry of different genotypes were used to quantify contractile ring area. Sqh-mCherry fluorescence images containing sum intensity were obtained across 5 optical sections at the base of the furrow with the brightest section in the middle. 5-10 rings were marked manually using a polygon tool in

these images and the area was computed in ImageJ. The mean \pm s.d. for the area was computed and plotted with time using Graphpad Prism 5.0.

4.2.4.4 Quantification of furrow membrane length

Sqh-mCherry fluorescence was used to identify furrow tips during cellularization. Membrane length was measured using the ImageJ line tool every 2 mins in (5 furrow lengths per time point were recorded in each embryo). These lengths were plotted against time as a scatter plot using Graphpad Prism 5.0.

4.2.4.5 Quantification of displacement and initial recoil velocity after laser ablation

The manual tracking plugin of Fiji software was used to extract xy coordinates from control and ablated regions. These xy coordinates were used to get distance between the two points with the following formula:

$$D = \sqrt{(y_2 - y_1)^2 + (x_2 - x_1)^2}$$

where (x1,y1) and (x2,y2) are the coordinates of the contractile ring edge seen below and above the ablation region respectively.

The ring displacement was estimated for each time point after ablations. The displacement of edges measured before ablations was subtracted from all the time points after ablations. The displacement was calculated from five independent embryos. The mean displacement and standard deviation with respect to time were plotted for control and *Grac*^{CR57} mutant embryos across the early and mid stages. The displacement at the last time point at approximately 70 s was used to plot maximum displacement. The initial recoil velocity was calculated by fitting a linear function on points between 0 and 23 s on the plot of displacement versus time in each embryo.

4.3 Results

4.3.1 GRAF modulates Rho-GTP and Myosin II for the regulation of contractility during *Drosophila* cellularization

To visualize the recruitment of GRAF to the furrow in live embryos during cellularization, we generated the UASp-GRAF-GFP transgene. GRAF-GFP was expressed using maternal gal4 along with fluorescently labelled Myosin II light chain, Sqh-mCherry in the *Graf*^{CR57} mutant background. We found that GRAF-GFP was already present at the furrow enriched at edges whereas Sqh-mCherry was seen in foci in early cellularization (Figure 4.1A). The GRAF-GFP and Sqh-mCherry relative fluorescence intensity across a single optical plane were quantified across a line segment passing through edges across adjacent furrow tips. The fluorescence intensity peak of GRAF-GFP is higher than Sqh-mCherry during early cellularization (Figure 4.1A). This suggests that GRAF-GFP partially colocalized with Sqh-mCherry at the furrow tip. GRAF-GFP and Sqh-mCherry were recruited at the contractile ring and their signal completely coincides at the furrow tip during mid stages of cellularization. Their fluorescence peaks were entirely colocalized during mid cellularization. Gradually, the GRAF-GFP fluorescence signal peak reduced relative to Sqh-mCherry but remains colocalized during mid cellularization as it progresses towards the constricted ring. GRAF-GFP was lost from the furrow tip in late cellularization when weak Sqh-mCherry fluorescence was still visible (Figure 4.1A).

We further compared Sqh-mCherry recruitment dynamics to that of Rho-GTP at the furrow. Rho-GTP was visualized by maternally expressing the transgene containing GFP tagged Anillin Rho-GTP binding domain (Anillin-RBD-GFP) under the control of *ubiquitin* promoter (Mason et al., 2016; Munjal et al., 2015). AnillinRBD-GFP was present as foci at the vertex which colocalized with Sqh-mCherry in early cellularization during the assembly of the actomyosin network at the furrow tip. AnillinRBD-GFP was present along with Sqh-mCherry at the contractile ring in mid and late cellularization as shown in images (Figure 4.1B). The fluorescence of AnillinRBD-GFP colocalized completely with Sqh-mCherry in early, mid and late stages as seen in the line scans. Even though the

AnillinRBD-GFP fluorescence was reduced in late stages, it was present at the furrow tip along with Sqh-mCherry when GRAF-GFP was lost in late cellularization (Figure 4.1B).

The GRAF-GFP, Sqh-mCherry and AnillinRBD-GFP fluorescence levels were also quantified relative to their maximum intensity during cellularization. The relative fluorescence of GRAF-GFP, Sqh-mCherry and Rho-GTP increased from early to mid cellularization with a peak between 25-30 min and decreased in late cellularization (Figure 4.1C-H). Taken together, we find that Myosin II begins to assemble at the furrow tip in early cellularization when GRAF-GFP and Rho-GTP are already present and enriches at the furrow during mid cellularization. Thus, the recruitment profile reveals that GRAF localizes to the furrow tip and colocalizes with Myosin II and Rho-GTP. GRAF together with Myosin II and Rho-GTP might regulate the precise constriction timings during cellularization.

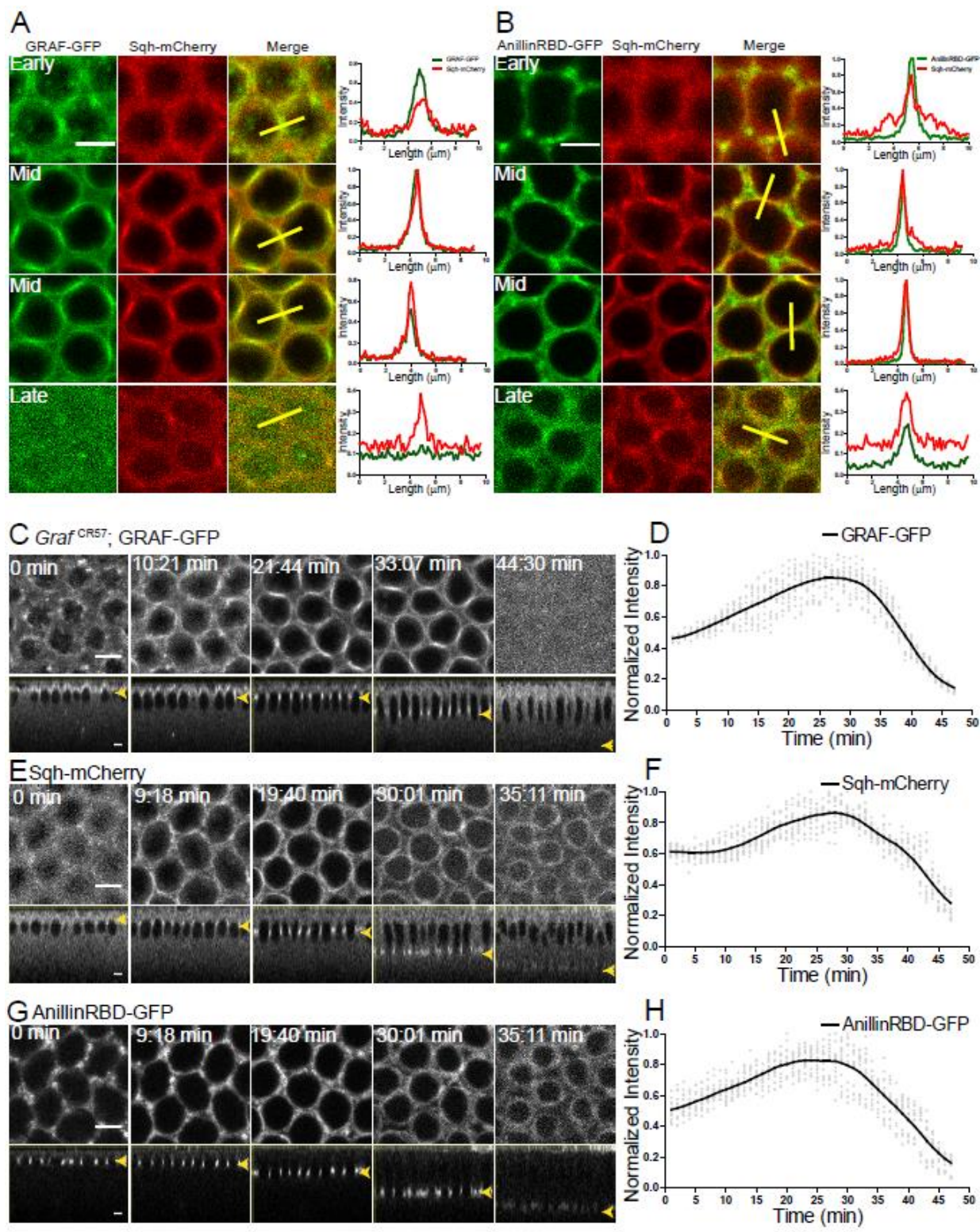


Figure 4.1: GRAF-GFP, Sqh-mCherry and AnillinRBD-GFP levels are enriched at the furrow tip in mid cellularization

(A) GRAF-GFP (green) colocalizes with Sqh-mCherry (red) in early and mid cellularization whereas GRAF-GFP is cytosolic in late cellularization. (B) AnillinRBD-GFP (green) colocalizes with Sqh-mCherry (red) in early, mid and late cellularization. A yellow bar depicted in the merged image is used for quantification shown in the neighbouring plots. (C-H) GRAF-GFP furrow tip dynamics is similar to Sqh-mCherry and AnillinRBD-GFP. Time lapse imaging of (C) *Graf*^{CR57}; GRAF-GFP, (E) Sqh-mCherry and (G) AnillinRBD-GFP shows a similar peak in mid cellularization (yellow arrowhead marks furrow tip). Quantification of normalized intensity of (D) GRAF-GFP, (F) Sqh-mCherry and (H) AnillinRBD-GFP plotted against time (n=15 rings, 5 rings per embryo, 3 embryos). Scale bars: 5 μ m.

4.3.2 GRAF depletion leads to enhanced contractility of the basal actomyosin network.

We used laser ablations to assess the contractility of the basal actomyosin network in early and mid stages of cellularization. Sqh-mCherry in controls and *Graf*^{CR57} was used to mark the furrow tip for laser ablations. Laser ablations were performed in a line cutting across approximately 4-5 contractile rings at the furrow tip during early and mid cellularization (yellow dashed line, Figure 4.2A,E). The ablation across the rings caused a break in the actomyosin network and led to a movement of the ablated edges. The ablated edges movement and final displacement are dependent on the tension in the actomyosin network. The final displacement and rate of movement of the ablated edges at approximately 70s were calculated for controls and *Graf*^{CR57}. We found a significant increase in the rate of displacement of the edges of the contractile rings in *Graf*^{CR57} embryos as compared to controls in early and late stages (Figure 4.2B,F). *Graf*^{CR57} embryos showed an approximately fourfold increase in maximum displacement at 70s as compared to controls in both early and mid cellularization (Figure 4.2C,G). Similarly, initial recoil velocities of the edges after ablations were increased by approximately twofold in *Graf*^{CR57} embryos in early and mid stages of cellularization as compared to controls (Figure 4.2D,H). This increased displacement and a recoil velocity of the ring edges suggests that the actomyosin network in *Graf*^{CR57} has increased contractility. The increased contractility in *Graf* mutants in the early and mid stages shows that GRAF plays

a crucial role in resisting Myosin II-dependent contractility during the early and mid stages of cellularization.

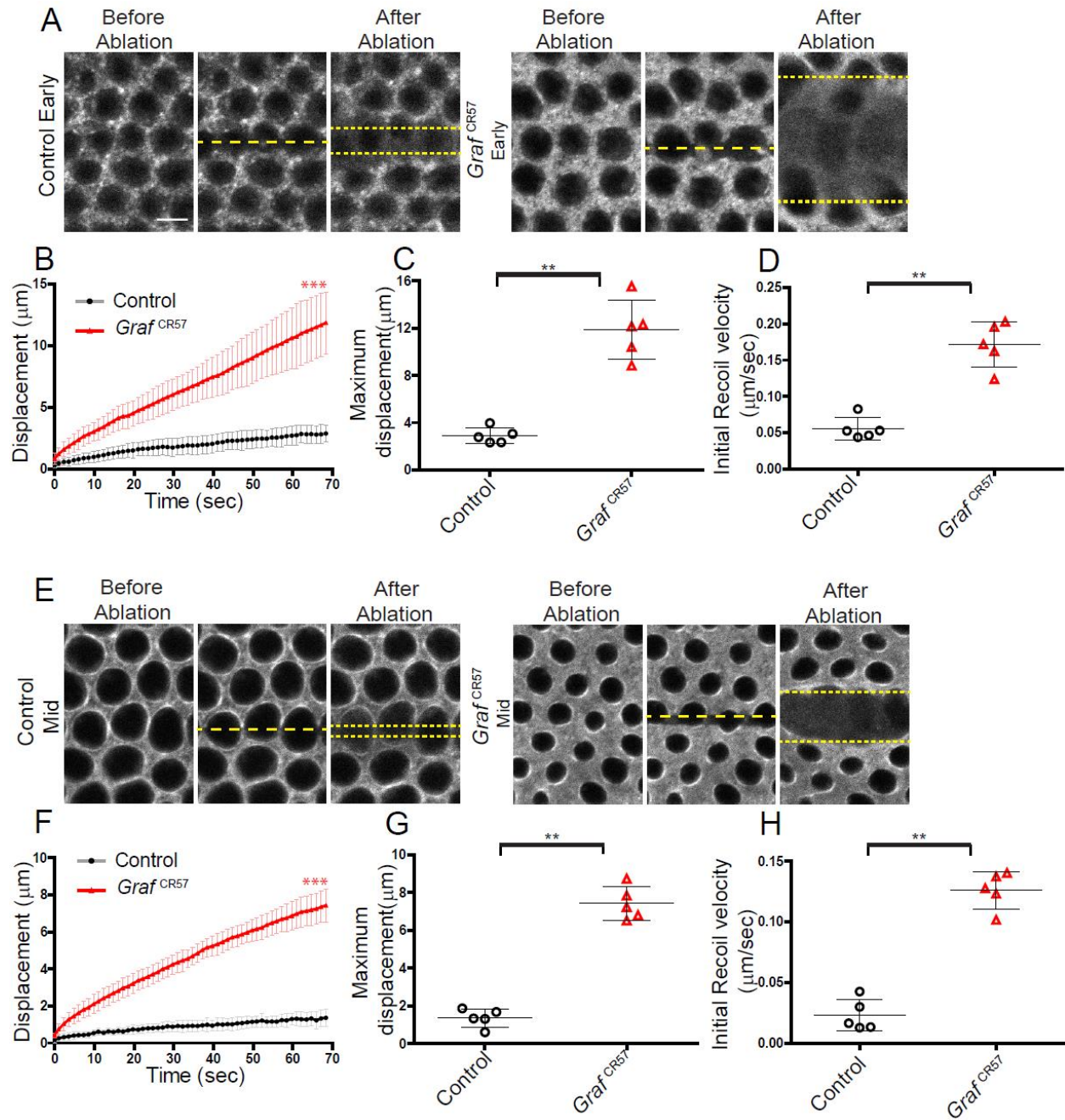


Figure 4.2: Graf mutant embryos show hypercontractility during early and mid cellularization. Laser ablation was performed using a single line at the furrow tip during early and mid cellularization. (A, E) Representative images show control and *Graf^{CR57}* mutant embryos with the region before, at 0 s (marked with yellow dotted line) and 70 s after ablations (recoil region marked with yellow dotted line) in early and mid cellularization, respectively. (B, F) Quantifications of ring displacement after laser ablation during early and mid phase (control: black line, n = 5 embryos; *Graf^{CR57}* mutant: red line, n = 5 embryos each). Scatter

plot showing (C, G) maximum displacement of the ring and (D, H) initial recoil velocity after laser ablation during early and mid-phase (n = 5 embryos each). Data are represented as mean \pm s.d. **p<0.01, ***p<0.001, two-tailed Mann–Whitney test.

4.3.3 GRAF RhoGAP domain is essential for contractility during cellularization

Previous studies have shown that in the hexagonal phase Myosin II inhibition occurs due to fine-tuning of RhoGAP activity (Mason et al., 2016). In addition, optogenetic activation of RhoGEF2 during priming and late stage leads to increased Myosin II levels which perturb actomyosin network configuration. In contrast, the polygonal network is resilient to Myosin II activation due to predicted RhoGAP presence which acts as an important step in restricting ring constriction (Krueger et al., 2019). Loss of GRAF possibly leads to an increase in Rho-GTP levels thereby causing constriction in early and mid cellularization and hyper constriction in late cellularization.

Since GRAF has a RhoGAP domain, this domain might influence the Rho-GTP levels along with recruitment dynamics of Rho-GTP at the contractile rings in the furrow tip in *Graf*^{CR57}. In order to visualize Rho-GTP recruitment *in vivo*, we used GFP tagged Rho-GTP binding domain (RBD) of Anillin (AnillinRBD-GFP) expressed under the control of *ubiquitin* promoter (Mason et al., 2016; Munjal et al., 2015) along with Sqh-mCherry. AnillinRBD-GFP was seen as foci that colocalized with Sqh-mCherry in early cellularization during the actomyosin assembly phase at the furrow tip. During mid and late cellularization, AnillinRBD-GFP was uniformly present along with Sqh-mCherry at the contractile ring in images (Figure 4.3A). The co-localization of AnillinRBD-GFP and Sqh-mCherry was quantified using line scans across the edges of adjacent rings in furrow tips were used from single optical planes which estimate the fluorescence intensity relative to the maximum seen in cellularization (yellow line, Figure 4.3B). AnillinRBD fluorescence peaks colocalized with Sqh-mCherry from early to mid stages and decreased in late stages of cellularization in control embryos (Figure 4.3B). Both AnillinRBD-GFP and Sqh-mCherry signal were more spread with non-overlapping fluorescence peaks during early and mid stages of cellularization in *Graf*^{CR57} embryos compared to sharp colocalization peaks in control. (Figure 4.3C,D). This increase in Rho-GTP and Sqh-mCherry spread in

the early and mid stages of cellularization correlated with hypercontractility in *Graf*^{CR57} embryos. The perturbed RhoGTP level possibly influences the Myosin II activity to disrupt basal contractility. In this context, we perturbed the RhoGAP domain in GRAF which might function to hydrolyze active RhoGTP to convert inactive RhoGDP form.

We analysed the role of the RhoGAP domain in the GRAF protein in regulating ring constriction during cellularization. For this, we generated a transgene having fluorescently tagged GRAF with the Rho-GAP domain deleted, UASp-GRAF Δ RhoGAP-GFP (Figure 4.3E). We expressed GRAF Δ RhoGAP-GFP and GRAF-GFP maternally in the *Graf*^{CR57} mutant background to score the effect of the Rho-GAP deletion on actomyosin ring constriction in cellularization. Live imaging of embryos of the *Graf*^{CR57}, *Graf*^{CR57}; GRAF-GFP and *Graf*^{CR57}; GRAF Δ RhoGAP-GFP genotypes was carried out along with Sqh-mCherry. Qualitatively, the *Graf*^{CR57}, and *Graf*^{CR57}; GRAF Δ RhoGAP-GFP showed hyper constriction when compared to control and *Graf*^{CR57}; GRAF-GFP (Figure 4.3F). The ring area in *Graf*^{CR57} embryos was significantly lower than controls during cellularization (Figure 4.3F,G). The ring area in *Graf*^{CR57} embryos was significantly reduced as compared to controls with time during cellularization (Figure 4.3F,G). This hyper constriction phenotype in *Graf*^{CR57} was suppressed in *Graf*^{CR57}; GRAF-GFP embryos. *Graf*^{CR57}; GRAF Δ RhoGAP -GFP embryos on the other hand showed hyper constriction of rings similar to *Graf*^{CR57} (Figure 4.3F,G). Thus, the full-length GRAF-GFP suppressed the constriction defect of *Graf*^{CR57}.

GRAF Δ RhoGAP-GFP was recruited to the furrow in early and mid cellularization and was lost from the furrow in late cellularization similar to GRAF-GFP (Figure 4.4A,B). Also, GRAF Δ RhoGAP-GFP appeared in punctae in early cellularization, leading to relatively higher levels as compared to GRAF-GFP (Figure 4.4A,B). Even though GRAF Δ RhoGAP-GFP was recruited to the furrow, its levels were significantly reduced on the furrow membrane as compared to GRAF-GFP in mid cellularization (Figure 4.4A,B). In summary, the RhoGAP domain in GRAF protein is necessary for its recruitment to the furrow and for restricting ring constriction during cellularization.

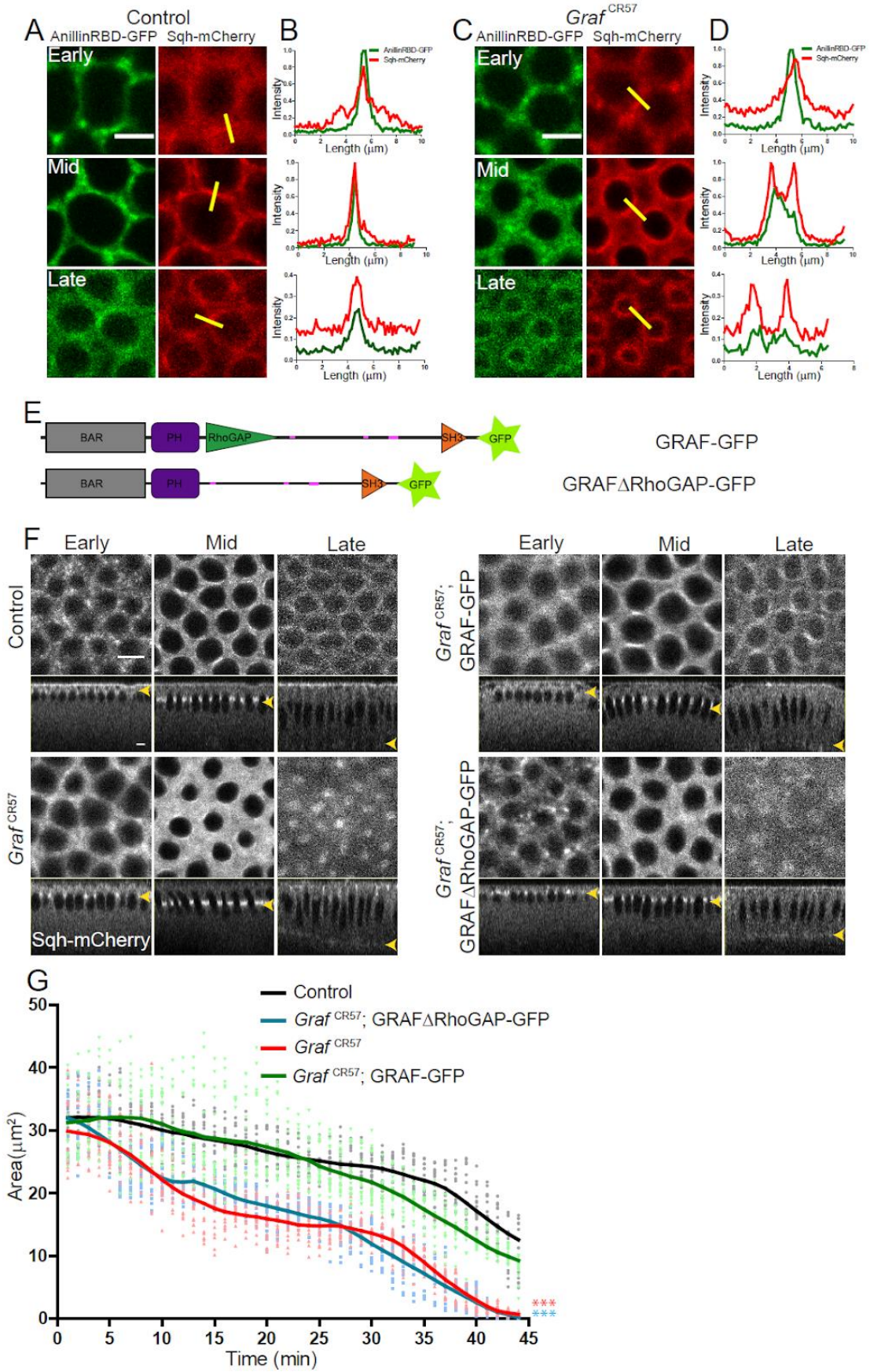


Figure 4.3: RhoGAP domain of GRAF is essential for ring constriction in cellularization

(A,C) AnillinRBD-GFP (green) colocalises with Sqh-mCherry (red) in early, mid and late cellularization in controls. In *Graf^{CR57}*; AnillinRBD-GFP and Sqh-mCherry both signals are more spread in as compared in between adjacent rings. One representative image chosen from n=3 embryos of controls and *Graf^{CR57}* are shown. (B,D) A yellow bar is depicted in the Sqh-mCherry image which is used for the estimation of the intensity line profile. (E) Schematic showing full-length GRAF protein with GFP and GRAF Δ RhoGAP-GFP proteins. (F) *Graf^{CR57}* and *Graf^{CR57}*;GRAF Δ RhoGAP-GFP embryos expressing Sqh-mCherry show hyper-contractility compared to controls and *Graf^{CR57}*; GRAF-GFP (yellow arrowhead highlights furrow tip at all stages). (G) Quantification shows a significantly higher ring area for controls and *Graf^{CR57}*; GRAF-GFP as compared to *Graf^{CR57}*, *Graf^{CR57}*;GRAF Δ RhoGAP-GFP expressing Sqh-mCherry. (n=15 rings, 5 rings per embryo, 3 embryos). Data is represented as mean \pm s.d. ***P<0.001 One way ANOVA, Repeated Measure with Dunnett's multiple comparison test, each point of the mutant compared to the control. Scale bars: 5 μ m.

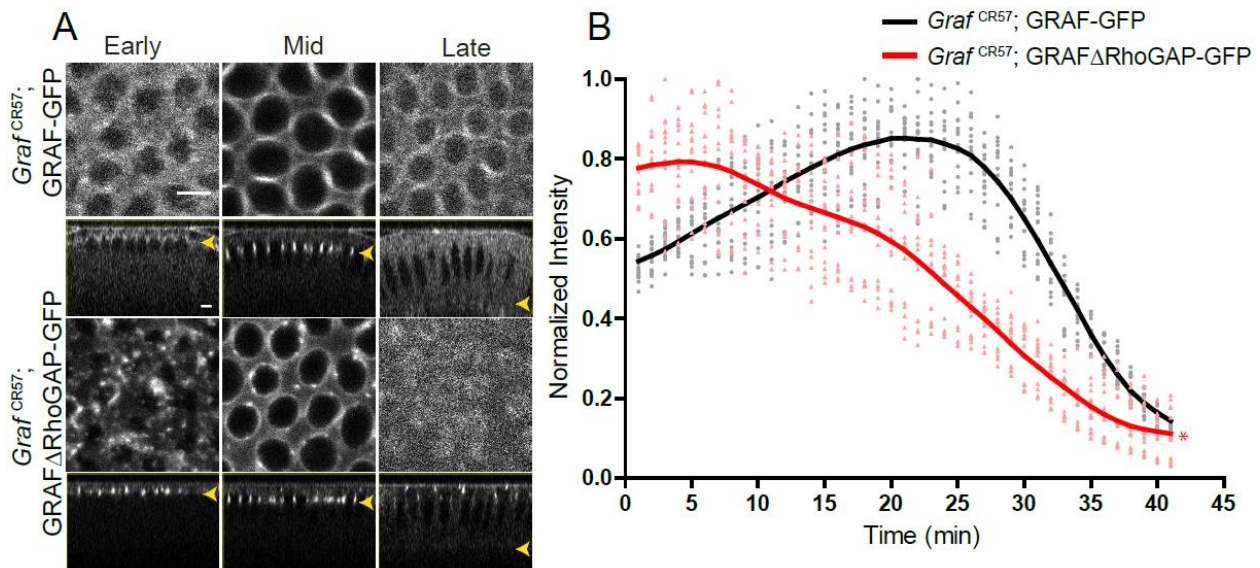


Figure 4.4: *Graf^{CR57}*; GRAF-GFP and *Graf^{CR57}*; GRAF Δ RhoGAP-GFP recruitment dynamics

(A) Snapshots from live imaging of *Graf^{CR57}*; GRAF-GFP and *Graf^{CR57}*; GRAF Δ RhoGAP-GFP shows that *Graf^{CR57}*; GRAF Δ RhoGAP-GFP in aggregates in early cellularization followed by a furrow tip recruitment (seen in the form of rings) in mid cellularization and loss at the furrow in late cellularization (yellow arrowhead denotes furrow tip). (B) Quantification of fluorescence intensity relative to the maximum shows higher intensity for *Graf^{CR57}*; GRAF Δ RhoGAP-GFP at early stages as compared to *Graf^{CR57}*; GRAF Δ RhoGAP-GFP (n=15 rings, 5 rings per embryo, 3 embryos). Data is represented as mean \pm s.d. *P<0.05, two-tailed Mann-Whitney test.

4.3.4 GRAF overexpression leads to loss of contractility during cellularization

Graf^{EP09461} contains a gypsy transposon tagged line containing a UASp element inserted in the 5'UTR region of GRAF in the same orientation of the native gene (Figure 4.5A). GRAF protein overexpression during cellularization was achieved by crossing *Graf*^{EP09461} to *mat67-Gal4*, called GRAF-OE. Control and GRAF-OE embryos were co-stained with GRAF and Dlg antibodies. GRAF-OE embryos showed an increase in GRAF staining as compared to controls (Figure 4.5B). Quantification of GRAF fluorescence intensity during these stages showed a significant increase in GRAF-OE as compared to controls (Figure 4.5C).

Graf depletion led to the hyper constriction of rings in cellularization. In contrast to *Graf* depletion, we analysed whether GRAF-OE could inhibit ring constriction in cellularization. GRAF-OE embryos in the cellularization stage were imaged live with Sqh-mCherry. GRAF-OE showed expanded rings during the mid and late stages of cellularization (Figure 4.5D). We found that the ring area was significantly higher in GRAF-OE as compared to controls throughout cellularization (Figure 4.5E). GRAF overexpression, therefore, led to inhibition of ring constriction during cellularization.

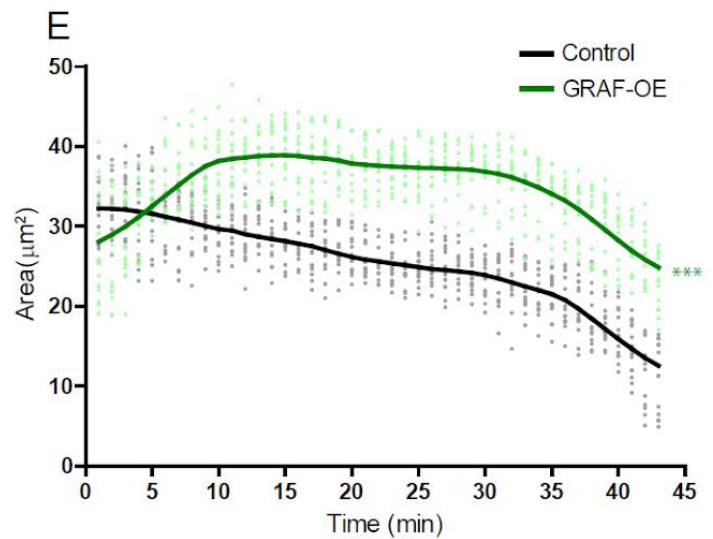
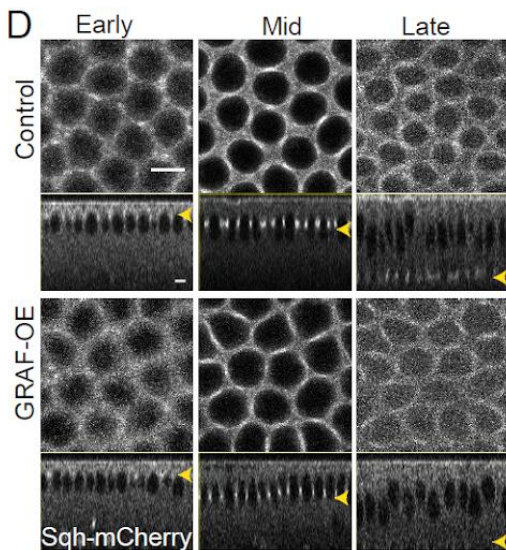
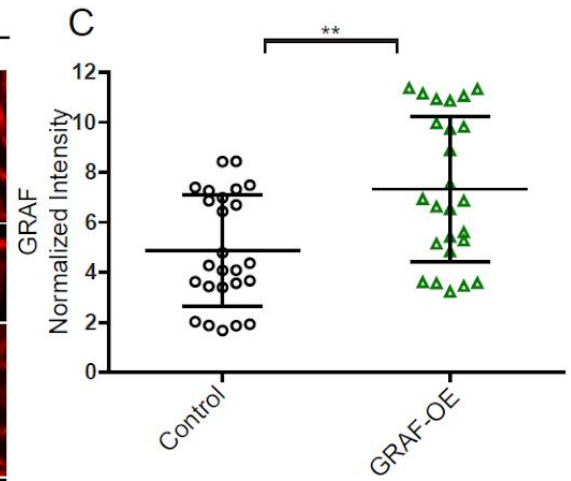
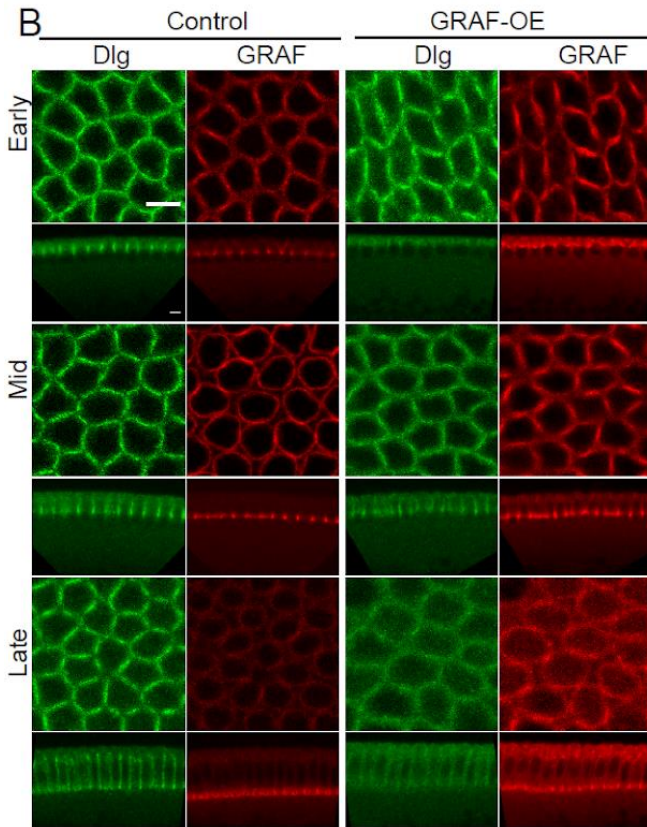
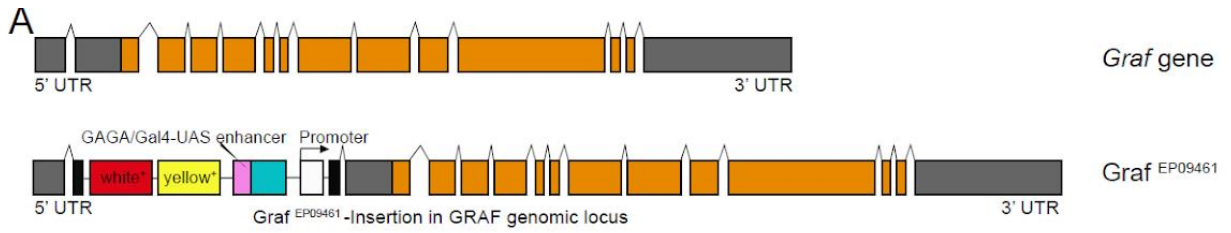


Figure 4.5: GRAF overexpression shows inhibition of ring constriction in *cellularization*. Schematic shows Graf gene and the GRAF overexpression line, $\text{Graf}^{\text{EP09461}}$ containing a P-element (with a UAS site) insertion in 5'UTR in an orientation to drive the downstream Graf gene. **(B)** GRAF-OE crossed to mat-Gal4 shows an increase in GRAF (100%, $n = 19$) when stained with GRAF (red) and Dlg (green) (control $n = 24$ embryos). **(C)** Quantification shows an increased GRAF antibody fluorescence in GRAF-OE (furrow length range: 7–19 μm) embryos compared to controls (furrow length range: 7–20 μm) ($n = 25$ rings, 5 per embryo, 5 embryos each). **(D)** Sqh-mCherry images and **(E)** area quantification show a significantly higher ring area in GRAF-OE as compared to controls (yellow arrowhead marks the furrow tip) ($n = 15$ rings, 5 per embryo, 3 embryos)(control values were repeated from Figure 4.3 for comparison). Data are represented as mean \pm s.d. ** $p < 0.01$, *** $p < 0.001$, two-tailed Mann–Whitney test. Scale bars: 5 μm .

4.3.5 GRAF depletion and overexpression results in perturbation of Myosin II distribution at the contractile ring during cellularization

We assessed the distribution of Myosin II heavy chain, Zipper in control and $\text{Graf}^{\text{CR57}}$ fixed embryos using immunostaining. Zipper patches in $\text{Graf}^{\text{CR57}}$ appeared larger than controls in early cellularization and Zipper was also enriched in between adjacent rings in mid cellularization (white arrowheads, Figure 4.6A). Quantitative analysis of zipper fluorescence at the furrow tip relative to the cytoplasm shows significantly increased intensity in $\text{Graf}^{\text{CR57}}$ throughout cellularization as compared to control embryos (Figure 4.6B).

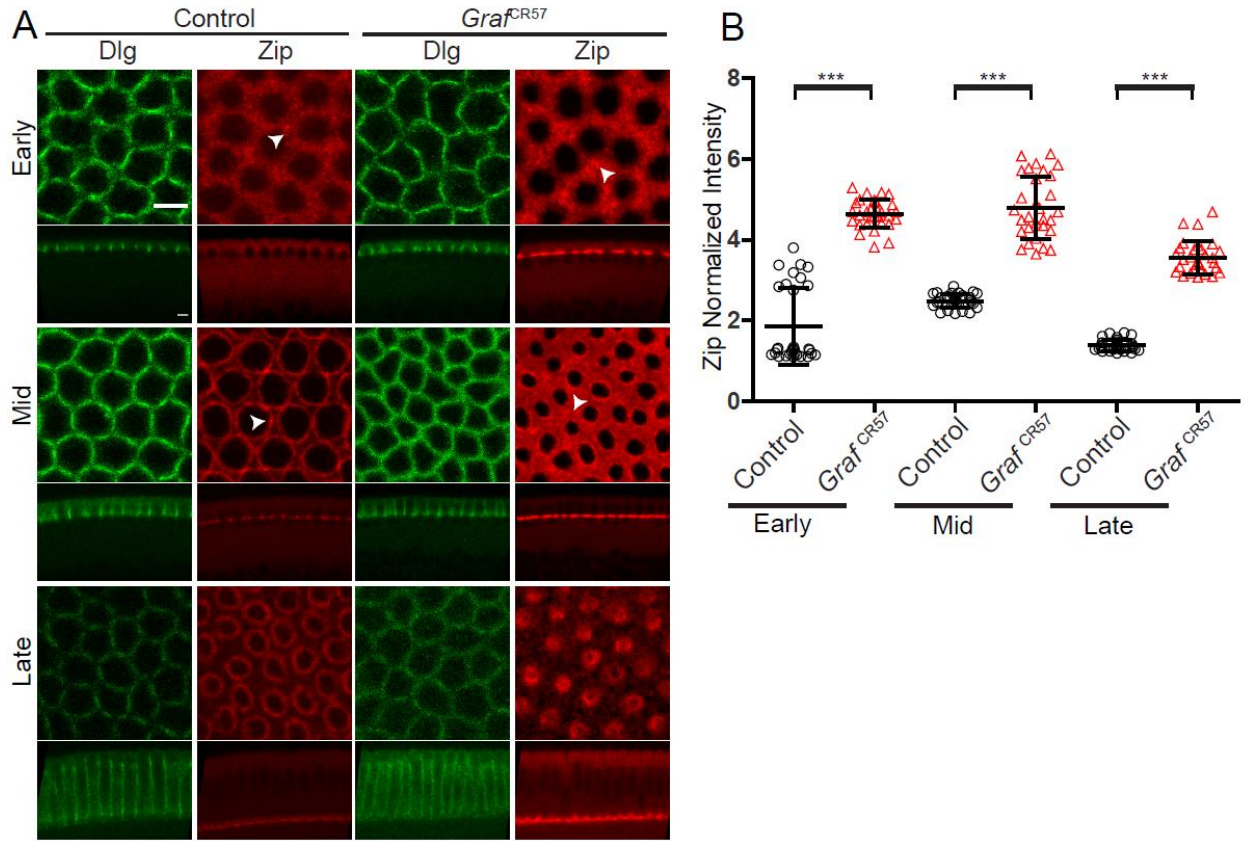


Figure 4.6: *Graf* depleted embryos show increased Myosin II in cellularization

(A) Fixed images of control and *Graf^{CR57}* embryos (100%, n=31 embryos) stained with Dlg (green) and Zipper (red) showing higher Zipper intensity in early (white arrowhead shows Zipper foci), mid (white arrowhead shows Zipper ring enrichment in control and spreading in *Graf^{CR57}* mutant) and late cellularization (control n=16 embryos). **(B)** Cortex to cytosol ratio of Zipper antibody fluorescence shows a significant increase in *Graf^{CR57}* as compared to controls (n=30 rings, 10 per embryo, 3 embryos each). Data are represented as mean \pm s.d. *** $p < 0.001$, two-tailed Mann–Whitney test. Scale bars: 5 μ m.

Live imaging embryos containing *Graf* depletion and overexpression were used to analyse Myosin II distribution at the furrow tip and furrow extension dynamics. The fluorescence intensity of Sqh-mCherry initially increased from early to mid cellularization and then decreased during late cellularization in controls. We found that GRAF-OE embryos showed a delay in Sqh-mCherry enrichment at the furrow as compared to controls. *Graf^{CR57}* on the other hand showed a sustained Sqh-mCherry signal at the furrow throughout cellularization and it remained significantly higher at later stages of cellularization (Figure 4.7A,B). The delay in Sqh-mCherry recruitment at the furrow on

Graf overexpression and sustained Sqh-mCherry at the furrow on *Graf* depletion imply that the recruitment of Myosin II at the furrow is regulated by GRAF in cellularization. Sqh-mCherry recruitment to the furrow tip was used to estimate furrow lengths with respect to time in cellularization. The furrow ingression dynamics, which is divided into slow and fast phases, in GRAF-OE were similar to controls during cellularization (Figure 4.7C) (Figard et al., 2013; He et al., 2016; Lecuit & Wieschaus, 2000; Merrill et al., 1988; Royou et al., 2004; Warn & Magrath, 1983). In contrast, the furrow ingression dynamics of *Graf*^{CR57} mutant shows an extended slow phase and the fast phase started at a later time point. The fast phase in *Graf*^{CR57} mutant embryos occurred at a slower rate compared to control embryos (Figure 4.7C). Eventually, the final membrane length achieved was similar to control.

Graf^{CR57} embryos contained sustained Sqh-mCherry recruitment on rings in late cellularization marked by the yellow region in the graph in Figure 4.7B. This yellow region represents the last 5 time points from late cellularization stages which are used to quantify Sqh-mCherry intensity per pixel from rings relative to the inter ring region (Figure 4.7B). This intensity is estimated in GRAF-OE, *Graf*^{CR57}, *Graf*^{CR57}; GRAFΔRhoGAP- GFP and *Graf*^{CR57}; GRAF-GFP as a readout of the change in Myosin II recruitment (Figure 4.7D). The Sqh-mCherry intensity was indeed reduced in GRAF-OE whereas it is increased in *Graf*^{CR57} and *Graf*^{CR57}; GRAFΔRhoGAP-GFP compared to controls (Figure 4.7D). The increased Sqh-mCherry recruitment phenotype in *Graf*^{CR57} embryos was suppressed in *Graf*^{CR57}; GRAF-GFP (Figure 4.7D). Increased Sqh-mCherry and Zipper levels at the furrow on *Graf* depletion during cellularization implies that the Myosin II recruitment at the furrow tip is inhibited by GRAF. This inhibition is dependent specifically upon its RhoGAP domain. Thus, Myosin II acts as a downstream target that provides mechanistic insights into the enhanced constriction in *Graf* depleted embryos.

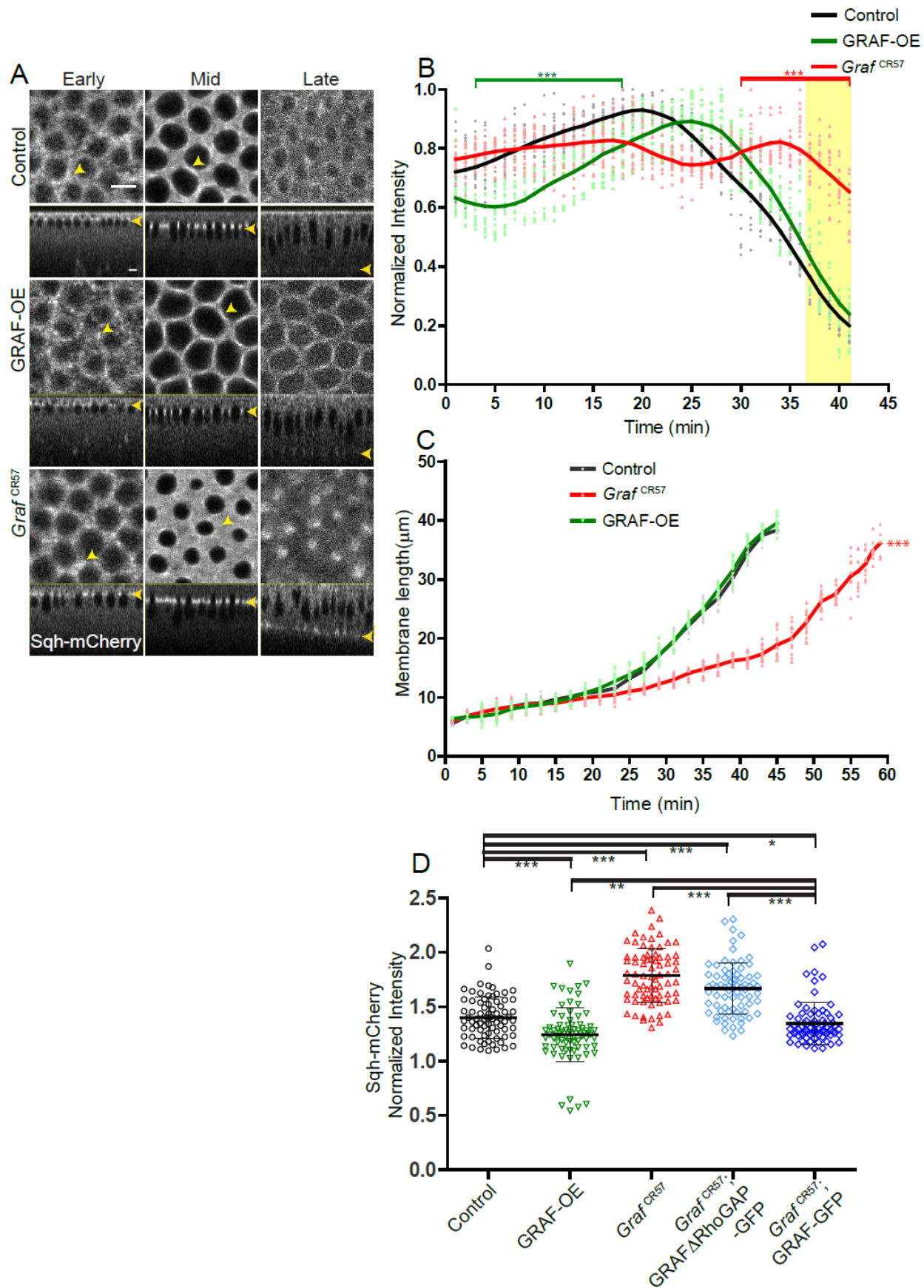


Figure 4.7: GRAF depletion and overexpression lead to perturb Myosin II distribution

(A) Control, GRAF-OE and *Graf*^{CR57} embryos expressing Sqh-mCherry (grey) are shown in early (yellow arrowhead marks Sqh-mCherry foci), mid (yellow arrowhead marks Sqh-mCherry enrichment) and late cellularization (yellow arrowhead in sagittal sections marks the furrow tip). **(B)** Quantification of Sqh-mCherry fluorescence in GRAF-OE embryos (each time point between 3 to 18 min is significantly different from controls and *Graf*^{CR57}) shows a delay in Sqh-mCherry enrichment at the furrow as compared to controls. *Graf*^{CR57} embryos (each time point between 30 to 41 min is significantly different from controls) show sustained Sqh-mCherry in late-cellularization as compared to controls (n=15 rings, 5 per embryo, 3 embryos). Data is represented as mean±s.d. (**P<0.001. Two-way ANOVA, Bonferroni post-tests where each genotype compared to control, time points 3 to 18 in GRAF-OE are statistically different from controls and *Graf*^{CR57}, times points in the 30 to 41 min in *Graf*^{CR57} are statistically different from controls and GRAF-OE). The last 5 time points are highlighted in the yellow shaded region. **(C)** Furrow length quantified from live imaging with Sqh-mCherry for controls, *Graf*^{CR57} and GRAF-OE show a similar trend of the slow and fast phase of ingression in GRAF-OE as compared to controls. The slow phase is extended in *Graf*^{CR57} and the final length is achieved at a later time in the fast phase (n=15 furrow lengths, 5 furrows per embryo, 3 embryos). Data is represented as mean±s.d. ***P<0.001; One way ANOVA, Repeated Measure with Dunnett's multiple comparison test, the *Graf*^{CR57} is statistically different from control and GRAF-OE. **(D)** Quantification of Sqh-mCherry in late cellularization (The last 5 time points in the yellow shaded region are used to estimate the ring intensity as a ratio to interring regions in different genotypes in Figure 7B) in GRAF-OE shows a reduction in intensity whereas *Graf*^{CR57} and *Graf*^{CR57}; GRAFΔRhoGAP-GFP shows higher intensity as compared to controls. *Graf*^{CR57}; GRAF-GFP shows a rescue in Sqh-mCherry as compared to *Graf*^{CR57} (n=75 rings, 5 rings per time point, 5 time points, 3 embryos each). Data is represented as mean±s.d. *P<0.05, **P<0.01, ***P<0.001, two-tailed Mann-Whitney test. Scale bars: 5 μm.

4.3.6 Diaphanous recruitment to the contractile ring is severely reduced on GRAF depletion.

Apart from Myosin II perturbation, disorganized actin networks could contribute towards premature and accelerated contractility of the actomyosin network. To investigate GRAF function in regulating actin regulators, we analysed Diaphanous (known as formin) recruitment in *Graf* depletion. To analyse its distribution in control and *Graf*^f embryos, fixed embryos were stained with anti-Dia antibodies. In control embryos, Diaphanous is enriched at the contractile ring formed at the furrow base during cellularization (Figure 4.8A). In contrast, Diaphanous recruitment is severely reduced and becomes cytoplasmic in *Graf*^f embryos throughout all stages of cellularization (Figure 4.8B). Hence, the

Diaphanous recruitment defect is correlated with actin remodelling defect which might depend on increased Rho-GTP.

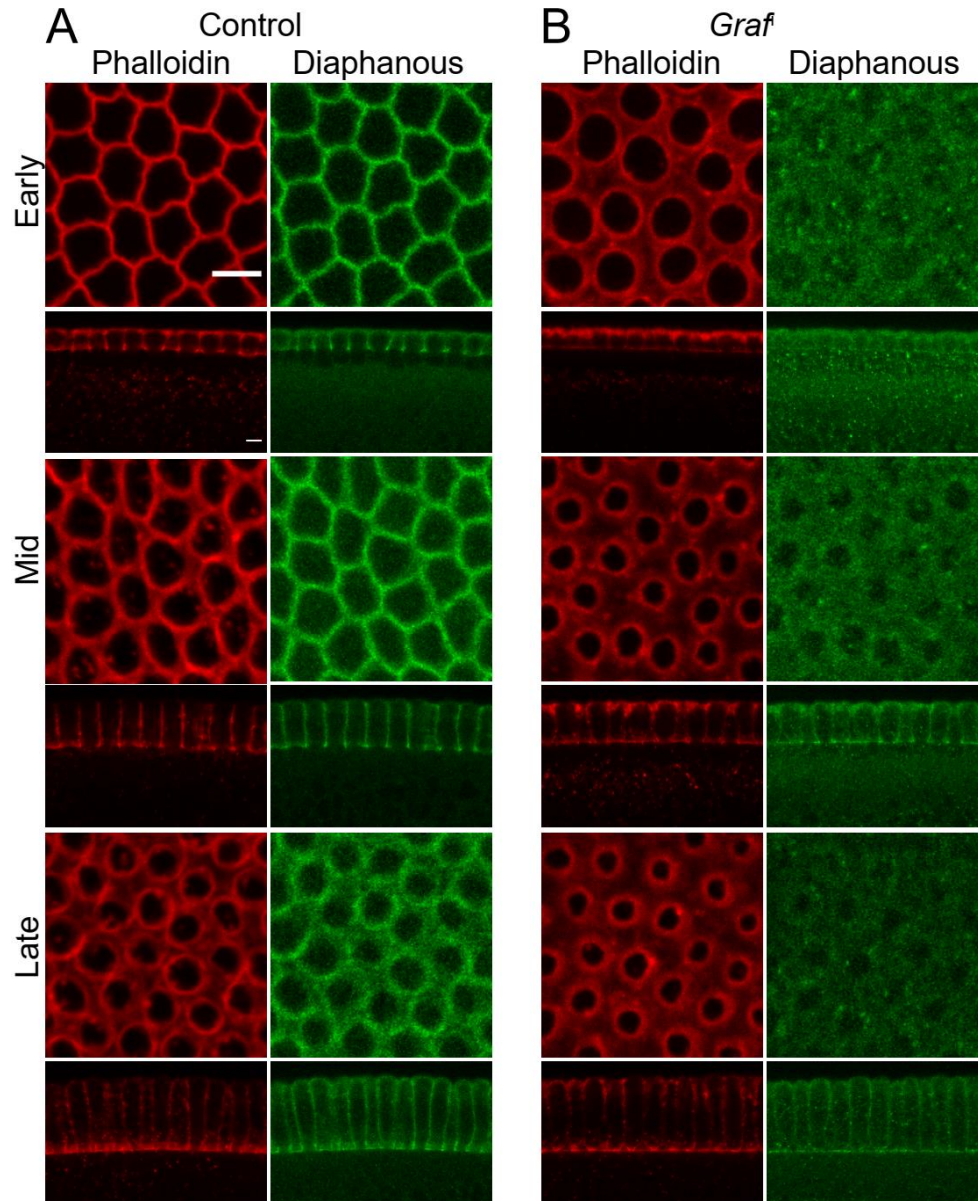


Figure 4.8: Diaphanous recruitment to the contractile ring is severely reduced in *Graf* depletion.

(A) Embryos stained with phalloidin (red) marking F-actin and Diaphanous (green) using an anti-Dia antibody during early, mid and late cellularization. The localization of Diaphanous is enriched at furrow tip during early, mid and late cellularization in control embryos. (B) In *Graf* knockdown embryos, Diaphanous protein is reduced from contractile rings and becomes cytoplasmic during cellularization (100%, n=43 embryos). Scale bar: 5 μ m.

4.3.7 Anillin, Peanut and PatJ distributions at the furrow tip are perturbed in *Graf* depletion.

Contractile ring consists of an actomyosin network which is organized by key regulator proteins such as Anillin, Peanut and PatJ. Anillin and Peanut act as scaffolds which is important in contractile ring organization during cellularization (Christine M. Field et al., 2005; Manos Mavrakis et al., 2014). PatJ is shown to directly interact with MBS and reduce Myosin II dephosphorylation resulting in Myosin II activation (Sen et al., 2012). To analyse these protein distributions in control and *Graf* knockdown embryos, embryos were stained with Anillin and Peanut antibodies. The localization of Anillin protein was analysed in the early, mid and late stages of cellularization. In the control, Anillin was selectively enriched on the rings at the furrow tip throughout cellularization (Figure 4.9A). In *Graf* knockdown embryos, the Anillin recruitment shows a diffuse pattern with visible enrichment in the inter-ring space during early and mid cellularization when compared to the control. During late cellularization, Anillin is selectively more enriched at the hypercontractile rings when compared to controls (Figure 4.9A). The quantitative analysis of Anillin intensity shows a significantly increased signal in *Graf* knockdown when compared to control (Figure 4.9B). The perturbed Anillin distribution is similar to Myosin II distribution in *Graf* depletion. In addition, Peanut and PatJ qualitatively show diffuse localization at the contractile ring and in inter-ring space during mid cellularization (Figure 4.9C). In summary, Anillin, Peanut and PatJ mislocalization in *Graf* depletion are likely to contribute towards ring architecture.

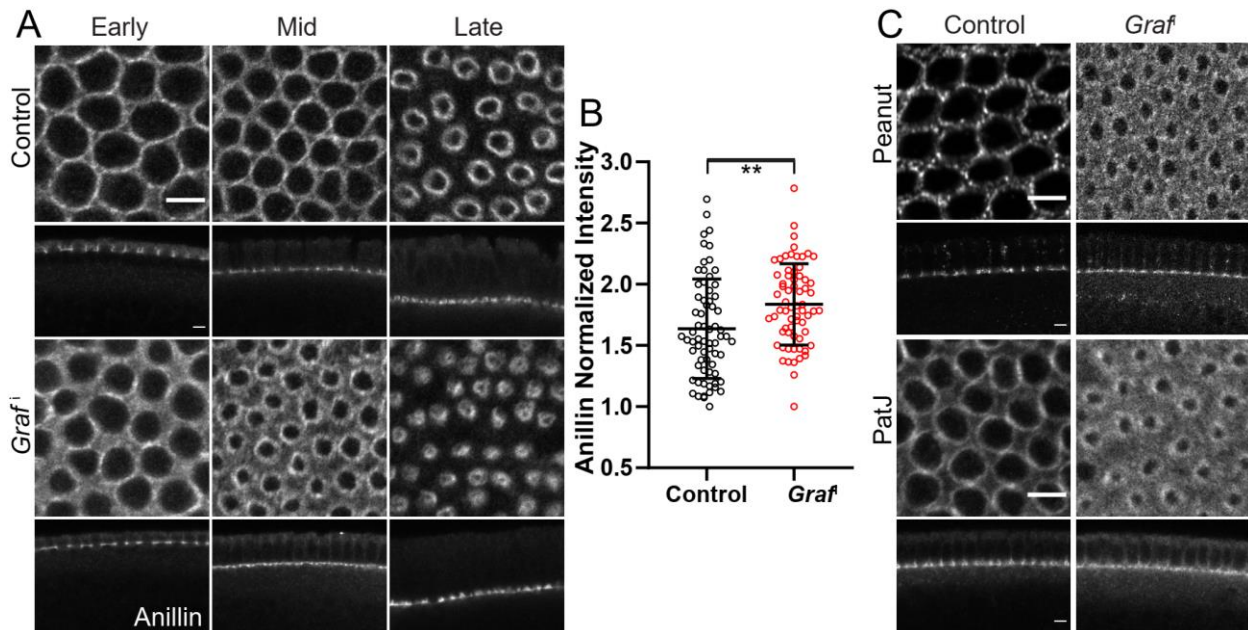


Figure 4.9: Anillin, Peanut and PatJ mislocalization at the furrow tip in *Graf* depletion. (A) Embryos were stained with Anillin, Peanut and PatJ in control and *Graf* depletion during cellularization. In control embryos, Anillin is recruited at the furrow tip during early, mid and late stages. In *Graf* depletion embryos, Anillin is more diffused and enriched at inter-ring space during early and mid stages whereas it becomes enriched at the hypercontractile ring during late stages (86.6%, n= 15 embryos). (B) The Anillin normalized intensity shows a significant increase in signal in *Graf*^Δ embryos (*Graf*^Δ n=66 rings, 3 embryos) when compared to control (Control n=68 rings, 4 embryos). (C) The Peanut (90%, n=11 embryos) and PatJ (85.7%, n=14 embryos) also show spread signal in between rings in *Graf* knockdown embryos when compared to control during mid stages. Data is represented as mean±s.d. **P<0.01, two-tailed Mann-Whitney test. Scale bar: 5µm.

4.4 Conclusion and discussion

Rho-GTP is therefore likely to regulate the transition of Myosin II from the polygonal to the circular architecture. It is possible that Rho-GTP levels directly influence Myosin II activity to regulate the ring contractility. Laser ablation of the actomyosin network reveals enhanced contractility due to increased tension in the network. For the first time, we have shown that Rho-GTP marked by AnillinRBD-GFP shows a complete overlap with Myosin II throughout cellularization. Nevertheless, Myosin II assembles in patches and forms a polygonal network in early cellularization and drives ring constriction in mid cellularization (Krueger et al., 2019; Xue & Sokac, 2016). Our data show that GRAF shows a partial overlap with Myosin II assembly during early cellularization and a

complete overlap during mid cellularization. Myosin II activity is crucial for the constriction of the ring formed during mid cellularization. GRAF is lost from the furrow canal at late stages of cellularization, whereas AnillinRBD and Myosin II are still present. *Graf* depletion causes increased Rho-GTP levels and Myosin II recruitment in cellularization. Actomyosin network with sustained Rho-GTP levels in *Graf* mutant embryos correlates with increased Myosin II that likely leads to enhanced ring constriction throughout cellularization. The enhanced ring constriction in the absence of the RhoGAP domain of GRAF could be due to reduced Rho-GTP hydrolysis. GRAF directly or indirectly regulates the key contractile proteins such as Anillin, Peanut, PatJ and Diaphanous which are crucial in maintaining the integrity of contractile ring architecture during *Drosophila* cellularization (Figure 4.10). It is likely that depletion of Anillin and Peanut could suppress the constriction defect seen in *Graf* mutant embryos.

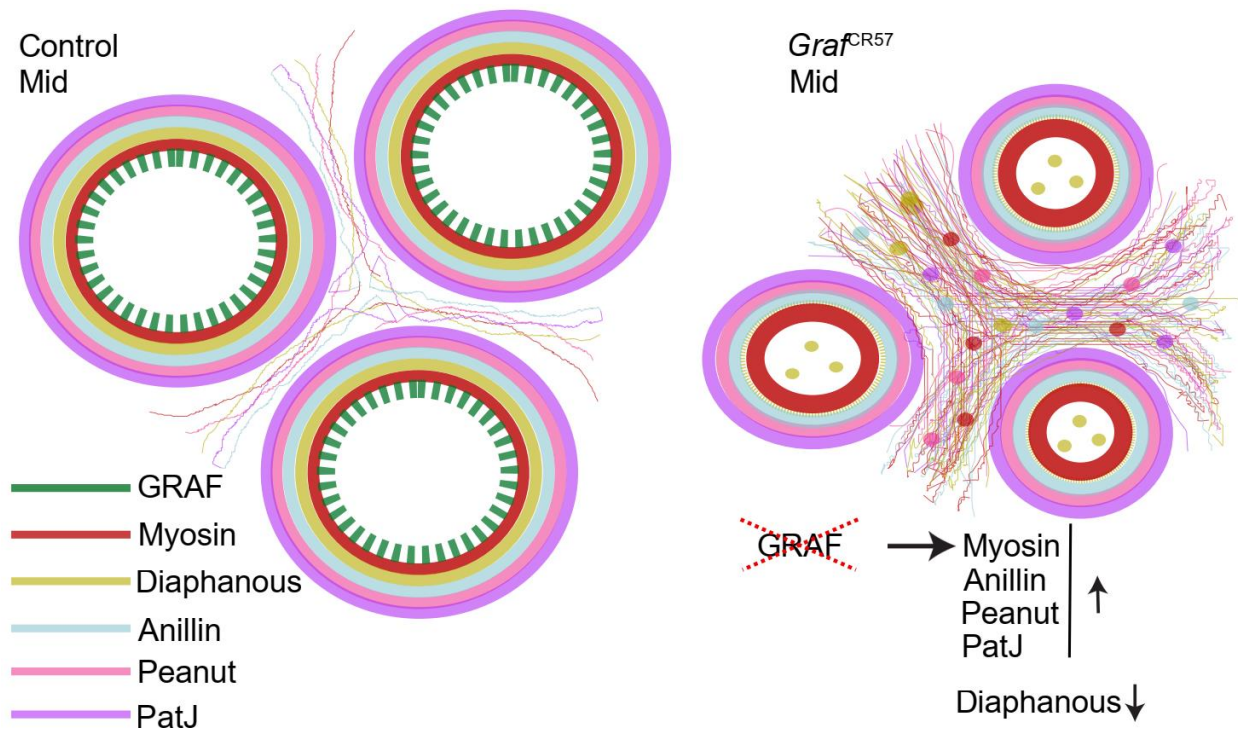


Figure 4.10: GRAF is required for the recruitment of key contractile proteins during the *Drosophila* cellularization. GRAF (green) modulates the levels of contractile ring proteins such as Myosin II (red), Anillin (blue), Peanut (pink), PatJ (purple) and Diaphanous (yellow) in control embryos. *Graf* depletion shows sustained Myosin II, Anillin, Peanut and PatJ recruitment during late cellularization correlating with increased contraction in the ring. In contrast, Diaphanous get reduced in *Graf* mutants

In this study, we have shown that the RhoGAP domain-containing protein GRAF inhibits ring constriction by regulating Myosin II levels at the furrow during cellularization. The RhoGAP domain deletion phenocopies the hypercontractility seen in *Graf* null mutant embryos. GRAF has been shown previously to bind RhoA with greater affinity as compared to other Rho family proteins (G. J. Doherty & Lundmark, 2009; J. T. Doherty et al., 2011; Hildebrand et al., 1996; Luo et al., 2017). This is consistent with previous studies showing increased RhoA-GTP levels seen in *Xenopus* embryo extracts obtained from GRAF1 morpholino injected embryos. This implies that the RhoGAP domain of GRAF is involved in Rho-GTP hydrolysis thereby decreasing Rho activity in constriction during cellularization. GRAF1 GAP domain having point mutation(R412Q) lead to attenuated RhoA activity in cultured L6 cells and failed to induce skeletal muscle differentiation in C2C12 cells (J. T. Doherty et al., 2011). This residue can be mutated in *Drosophila* GRAF protein to check for conservation of GAP activity across the metazoans. *Graf* mutants also show sustained Rho-GTP levels during late cellularization correlating with increased ring constriction. This suggests that the absence of Rho-GTPase activity of GRAF might trigger increased Rho-GTP levels, leading to uncontrolled and untimely constriction events.

Another RhoGAP containing protein, CGAP, is required for RhoA-GTP cycling to produce Myosin II pulses for apical constriction during gastrulation in *Drosophila*. C-GAP mutant embryos show premature and hyper constriction which phenocopies *Graf* depletion during cellularization (Mason et al., 2016). It is likely that C-GAP depletion in *Graf* mutant embryos would enhance the hyper constriction phenotype seen in cellularization. In addition, *Bottleneck* mutants show hyper constriction and sustained Myosin II recruitment at the furrow in cellularization (Krueger et al., 2019; Reversi et al., 2014; Schejter & Wieschaus, 1993b) similar to *Graf* mutant embryos.

CHAPTER 5

GRAF functions as a Rho-GAP in the Rho-dependent pathway to regulate constriction during cellularization

5.1 Introduction

RhoGEF2 (Rho-GTPase exchange factor2) is a well-studied molecule which activates Myosin II and is established as a crucial molecule in the Rho-dependent signalling pathway. DRhoGEF2 was identified in a genetic screen studying Rho signalling pathway components and maternal effects of zygotic lethal mutations (Barrett et al., 1997; Hacker & Perrimon, 1998; Padash Barmchi et al., 2005). RhoGEF2 is deposited maternally and is expressed ubiquitously throughout embryogenesis (Padash Barmchi et al., 2005). This molecule is localised to the actomyosin network at the furrow canal (Crest et al., 2012; Padash Barmchi et al., 2005) using its PDZ domain during cellularization (Wenzl, Yan, Laupsien, & Grosshans, 2010). RhoGEF2 depletion results in the inhibition of constriction of the actomyosin network. This leads to increased ring size and formation of multiple nucleated compartments during cellularization (Barrett et al., 1997; Hacker & Perrimon, 1998), DRhoGEF2 recruits apically and regulates cortical actin changes influencing epithelial cell shape changes during gastrulation (Barrett et al., 1997; Hacker & Perrimon, 1998). In summary, RhoGEF2 localises at the furrow tip and functions in regulating ring constriction in cellularization (Barmchi et al., 2005; Grosshans et al., 2005; Wenzl, Yan, Laupsien, & Grosshans, 2010).

DRhoGEF2 was established as a positive regulator of Rho1 by stimulating Myosin II via a Rho1 dependent pathway in *Drosophila* S2 cells. Overexpression of RhoGEF2 leads to a contracted S2 cell morphology similar to overexpression of constitutively active Rho1 mutant, Rho1V14 (Rogers et al., 2004). In contrast, injection of the dominant-negative form of Rho induced gross malformations in the actomyosin network which phenocopy RhoGEF2 depletion (Halsell et al., 2000). Perturbations in Rho1-GTP levels

modulate Rho-kinase (ROK) activation which in turn influences the actomyosin network. DROK depletion using RNAi or Y-27632 drug in the background of DRhoGEF2 overexpression leads to a reduction in contracted morphological defects (Rogers et al., 2004). Spatiotemporal activation of RhoGEF2 is sufficient to induce differential contractility in the actomyosin network during different stages of cellularization (Krueger et al., 2019). Optogenetic activation of RhoGEF2 during the priming phase and late stage leads to increased Myosin II levels which perturbs actomyosin network configurations and enhances constriction (Krueger et al., 2019). These studies provide evidence that RhoGEF2 is an upstream molecule that gives rise to Rho-GTP to activate the downstream effector, Rho-kinase. Rho-Kinase finally phosphorylates Myosin II which regulates the contraction process (Rogers et al., 2004).

RhoGEF2 leads to the formation of RhoA-GTP which in turn activates the Rho kinases Drok and Drak for Myosin II phosphorylation. Embryos injected with a ROCK inhibitor, Y-27632 inhibits Myosin II recruitment at the cellularization front compared to control (Krajcovic & Minden, 2012; Royou et al., 2004). Myosin II is unevenly distributed in clumps with dramatically reduced phosphorylation in Drak mutant during cellularization. In addition, Drak mutant impairs actomyosin contractility by showing lower circularity compared to control embryos (Chougule et al., 2016). Phospho-deficient mutants of the light chain of Myosin II, Squash (Sqh^{AA}) and Drok mutants show increased ring perimeter suggesting loss of constriction during cellularization (Xue & Sokac, 2016). In addition, the small subunit of Myosin II phosphatase, MBS, helps restrict Myosin II activity during cellularization. Thus, inhibition of Myosin II using pharmacological inhibitor Y-27632, Sqh^{AA}, Drak and Drok mutants lead to the loss of constriction during cellularization.

Previous studies established RhoGEF2 and Myosin II functions in modulating the constriction process, whereas a RhoGAP domain containing protein that inhibits contractility remains to be elucidated. The function of RhoGAPs during tissue morphogenesis has been generally less studied as compared to RhoGEFs. In contrast to RhoGEF2 function, RhoGAP domain containing proteins are likely to play a key role in inhibiting Myosin II activation. For example, depletion of RhoGAP containing proteins

RGA3 and RGA4 in the *C.elegans* embryo leads to enhanced contractility of the anterior cortex due to increased recruitment of Myosin II (Regev et al., 2017; Schmutz et al., 2007). CGAP, a RhoGAP protein identified to play a role in Rho-GTP hydrolysis in *Drosophila* embryos, is involved in inhibiting apical constriction in gastrulation. It is enriched at the furrow canal and C-GAP mutant embryos also show increased constriction of actomyosin rings in cellularization (Mason et al., 2016). Thus, C-GAP is necessary for restricting ring constriction in cellularization. However, analysis of RhoGAP function in a spatio-temporal manner in regulating actomyosin ring contractility has not been studied in cellularization.

Here we report the mechanism involving GRAF, another RhoGAP protein in regulating contractile ring formation and constriction in cellularization in *Drosophila* embryogenesis. This is the first demonstration that GRAF works along with RhoGEF2 in maintaining Rho-GTP levels. Loss of RhoGEF2 and Myosin II activation suppressed the hypercontractility phenotype of *Graf* mutants. Our studies show a crucial role for GRAF in inhibiting actomyosin contractility in cellularization. The appropriate level of GRAF at the furrow membrane is crucial for maintaining the balance between RhoGTP and RhoGDP which in turn regulates the temporal activity of Myosin II during contractile ring constriction in cellularization. Thus, GRAF is involved in the Rho-dependent pathway which regulates the constriction process.

5.2 Material and methods

5.2.1 *Drosophila* stocks

Fly stocks and crosses were maintained in regular cornmeal agar. The detailed genotypes, stock numbers and source of stocks Table 5.1.

Stock	Genotype	Source/Reference
1	Canton-S	Lab stock originally obtained Bloomington <i>Drosophila</i> Stock Center

2	<i>nanos</i> -Gal4	Lab stock
3	w; <i>mat67</i> -Gal4; <i>mat15</i> -Gal4	Girish Ratnaparkhi, IISER, Pune, India
4	y[1] v[1]; P{TRiP.HMC03427}attP40 (GRAF shRNA1, <i>Graf^f</i>)	BDSC, #51853
5	y[1] v[1]; P{TRiP.GL01207}attP40 (Myosin II binding subunit, MBS shRNA)	BDSC, #41625
6	y[1] sc[*] v[1] sev[21]; P{TRiP.HMS01118}attP2 (RhoGEF2 shRNA)	BDSC, #34643
7	y[1] w[*]; P{UASpT7.RhoGEF2}5 (RhoGEF2 overexpression)	BDSC, #9386
8	UASp-rok-shRNA (<i>rokⁱ</i>)	(Yixie Zhang et al., 2018)
9	y[1] w[67]c[23] P{EPgy2}Graf[EY09461] (GRAF overexpression)	BDSC, #17571
10	w; <i>mat67</i> Spider-GFP-Sqh-mcherry/TM3ser	(Martin et al., 2009)
11	y[1] w[67]c[23] P{EPgy2}Graf[EY09461]/FM7a; P{UASpT7.RhoGEF2}5/Tb (GRAF-OE;RhoGEF2-OE)	This study
12	y[1] sc[*] v[1] sev[21]; P{TRiP.HMC03427}attP40/cyo;P{TRiP.HMS01118}attP2/Tb (<i>Graf^f</i> ;RhoGEF2 ⁱ)	This study
13	y[1] sc[*] v[1] GRAF[CR57]/FM7a; P{TRiP.HMS01118}attP2/Tb (<i>Graf^{CR57}</i> ;RhoGEF2 ⁱ)	This study
14	y[1] sc[*] v[1] GRAF[CR57]/FM7a; UASp-rok-	This study

	shRNA/Tb (<i>Graf</i> ^{CR57} ;rok ⁱ)	
15	y[1] w[67]c[23] P{EPgy2}Graf[EY09461]/FM7a; P{TRiP.GL01207}attP40/cyo (GRAF-OE; <i>mbs</i> ⁱ)	This study
16	y[1] sc[*] v[1] GRAF[CR57]/FM7a;mat67Sqh- mCherry/cyo	This study

Table 5.1: *Drosophila* stocks and their source

5.2.2 Live imaging of *Drosophila* embryos

For live imaging, 2-2.5 hrs embryos were collected on sucrose agar plates and dechorionated with 100% bleach for 1 min and mounted on 2 well coverslip bottom Labtek chambers. Mounted embryos were filled with 1X PBS (Manos Mavrakis et al., 2008) and imaged using 40X/1.4NA oil objective on Zeiss or Leica SP8 microscope with a frame rate of 1.74s/frame and 2s/frame respectively.

5.2.3 Immunostaining

0-3.5 hrs embryos were collected on sucrose-agar plates, washed, dechorionated with 100% bleach and washed again. To visualize GRAF and Dlg immunostained embryos, dechorionated embryos were heat fixed with boiled 1X Triton salt solution (10x-0.5%Triton X-100 and 7%NaCl in water) for 1 min and instantly adding ice-cold 1X washing buffer. After cooling on ice, embryos were devitellinized in a 1:1 mix of MeOH and heptane followed by three washes in 1X PBST (1X PBS with 0.3% Triton X-100) for 5 min each. After washing, embryos were blocked in 2% BSA in 1X PBST for 1 hr and then incubated in primary antibody (Table 2.4) overnight at 4 °C. This was followed by three 1X PBST washes and incubated in fluorescently coupled secondary antibodies (Molecular probes) at 1:1000 dilution for 1 hr at room temperature. Embryos were washed three times in 1X PBST for 5 min each. DNA was labelled with Hoechst 33258 (1:1000, Molecular Probes) for 5 min in the second 1X PBST wash. Finally, embryos were mounted in Slow fade Gold antifade (Molecular Probes).

2.8 Analysis

2.8.1 Quantification of mean fluorescence intensity from immunostainings

The imaging of fixed control and mutant embryos immunostained with antibodies against GRAF along with Dlg and Zipper along with Dlg was carried out on the Leica SP8 confocal microscope at the same laser power and gain settings. To estimate the mean fluorescence intensity of GRAF and Zipper from immunostaining, a single optical section from the Z-stack containing the brightest intensity at the furrow tip was chosen. Fluorescence intensity was obtained in this section by drawing ROIs using the segmented line tool around the ring to get the average intensity using Fiji software (<http://fiji.sc/wiki/index.php/Fiji>) (Rueden et al., 2017). The ring intensity obtained was divided by the cytosol intensity obtained from a large square ROI in the apical most region above the nuclei from the same image. This membrane to cytosol ratio for GRAF antibody fluorescence in control embryos, *Graf*^{CR57}, GRAF-OE and Zipper antibody fluorescence in control and *Graf*^{CR57} was plotted for different stages of cellularization.

2.8.2 Quantification of mean fluorescence intensity from live-imaging

Live imaging of Sqh-mCherry expressing embryos in various genotypes was used to quantify fluorescence intensity change during the last five time points in late cellularization. To estimate these changes quantitatively across all genotypes, images were obtained with sum intensity per pixel across the Z-axis from a total of five stacks: two stacks above and two stacks below of the brightest section at the furrow tip covering a depth of 4 μm in late cellularization. The mean ring intensity per pixel was extracted by drawing a segmented ROI on the ring. The inter-ring intensity per pixel was extracted by drawing an ROI in between adjacent rings that had reduced Sqh-mCherry intensity. The ring intensity per pixel was expressed as a ratio to interring intensity per pixel. Finally, the normalized intensity of the ring was shown as a scatter plot.

2.8.3 Quantification of the contractile ring area

Live movies from embryos expressing Sqh-mCherry of different genotypes were used to quantify contractile ring area. Sqh-mCherry fluorescence images containing sum intensity were obtained across 5 optical sections at the base of the furrow with the brightest section in the middle. 5-10 rings were marked manually using a polygon tool in these images and the area was computed in ImageJ. The mean \pm s.d. for the area was computed and plotted with time using Graphpad Prism 5.0.

2.8.4 Quantification of furrow membrane length

Sqh-mCherry fluorescence was used to identify furrow tips during cellularization. Membrane length was measured using the ImageJ line tool every 2 mins in (5 furrow lengths per time point were recorded in each embryo). These lengths were plotted against time as a scatter plot using Graphpad Prism 5.0.

5.2 Results

5.2.1 GRAF overexpression driven loss of contractility is suppressed by an additional increase of RhoGEF2

The RhoGAP domain of GRAF is crucial for regulating ring constriction during cellularization. Delay in Myosin II recruitment and loss of contractility was seen in GRAF overexpression. This is likely due to decreased Rho-GTP levels resultant from increased RhoGTP hydrolysis via RhoGAP activity of GRAF. In contrast, hyper constriction phenotype on *Graf* depletion is likely to have occurred due to increased Rho-GTP. Previous reports show that the RhoGEF2 mutant causes the ring constriction inhibition during cellularization by lowering Rho-GTP levels (Barmchi et al., 2005; Grosshans et al., 2005; Wenzl, Yan, Laupsien, & Großhans, 2010). GRAF overexpression, therefore, phenocopies the loss of RhoGEF2. Optogenetic activation of RhoGEF2 leads to increased constriction in early cellularization (Krueger et al., 2019) and phenocopy *Graf*^{CR57} mutant. Overexpression of RhoGEF2 (RhoGEF2-OE) leads to increased constriction of apical caps in the syncytial division cycles (Dey & Rikhy, 2020). We

overexpressed RhoGEF2 maternally in embryos and imaged them live using Sqh-mCherry in cellularization. Sqh-mCherry was found in patches that were more spread in RhoGEF2-OE embryos as compared to controls and similar to *Graf*^{CR57} mutant embryos. Relative levels and activity of GAP and GEF are likely to regulate the rate of contractility (Mason et al., 2016). Since overexpression of RhoGEF2 and GRAF are going to have opposing effects on levels of Rho-GTP, we tested if the constriction phenotype of RhoGEF2 could be inhibited by GRAF overexpression. We found that similar to *Graf*^{CR57}, overexpression of RhoGEF2 also caused ring hyper constriction as compared to controls in cellularization (Figure 5.1A,C). One possible way to rescue GRAF overexpression is RhoGEF2 overexpression, which leads to increased Rho-GTP levels. We further tested if overexpression of RhoGEF2 could be inhibited by GRAF overexpression. We found that the ring constriction dynamics in GRAF-OE; RhoGEF2-OE was similar to controls (Figure 5.1A,C). The phenotypes of ring inhibition in GRAF-OE and hyper constriction in RhoGEF2-OE were suppressed in GRAF-OE; RhoGEF2-OE embryos (Figure 5.1A,C). This suppression was also seen in actin architecture in fixed GRAF-OE; RhoGEF2-OE embryos stained with phalloidin (Figure 5.1B). It is interesting to note that GRAF-OE embryos stained for phalloidin show a change from the polygonal F-actin organization at the furrow tip to the circular ring stage but do not show ring constriction. RhoGEF2-OE embryos showed an increase in Sqh-mCherry at the ring relative to the inter-ring in late cellularization as compared to controls. This increase was suppressed in the GRAF-OE; RhoGEF2-OE combination (Figure 5.1D). It is therefore likely that Rho-GTP levels were increased to an appropriate level in GRAF-OE; RhoGEF2-OE embryos to cause ring constriction at a level similar to controls, thereby restoring the rate of constriction similar to controls.

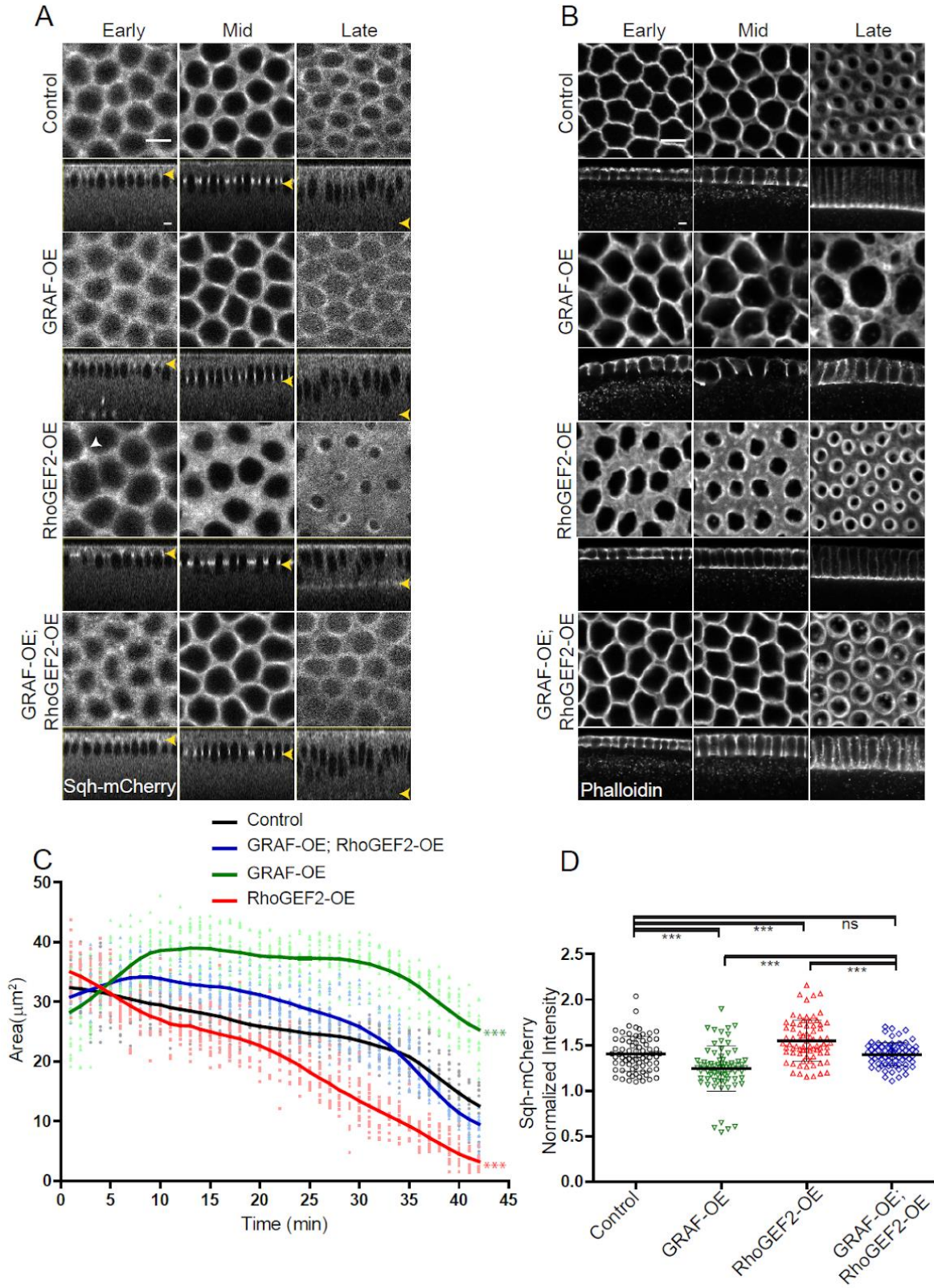


Figure 5.1: GRAF overexpression driven loss of ring constriction is suppressed by RhoGEF2 overexpression in cellularization.

(A) The increased constriction seen in RhoGEF2-OE embryos is suppressed in GRAF-OE similar to controls when imaged live with Sqh-mCherry (grey)(yellow arrowhead marks furrow tip in sagittal sections, white arrowhead marks Sqh-mCherry foci in RhoGEF2-OE) and **(B)** when stained with phalloidin (B, GRAF-OE 100% show loss of constriction n=50 embryos, RhoGEF2-OE 96.15% show enhanced constriction n=52 embryos, GRAF-OE; RhoGEF2-OE 57.69% show constriction comparable to controls n=52 embryos). **(C)** Quantification of contractile ring area from Sqh-mCherry shows a decreased area in RhoGEF2-OE, an increased area in GRAF-OE and normal area in GRAF-OE; RhoGEF2-OE as compared to controls (n=15 rings, 5 rings per embryo, 3 embryos) (control values were repeated from Figure 4.3 and GRAF-OE values were repeated from Figure 4.5 for comparison). Data is represented as mean±s.d. ***P<0.001, One-way ANOVA, Repeated measure with Dunnett's multiple comparison test, the GRAF-OE, RhoGEF2-OE is statistically different from controls and GRAF-OE; RhoGEF2-OE. **(D)** Quantification of Sqh-mCherry in late cellularization in RhoGEF2-OE shows increased intensity as compared to controls and GRAF-OE; RhoGEF2-OE shows Sqh-mCherry intensity a reduced intensity as compared to RhoGEF2-OE and is similar to controls (control and GRAF-OE values were repeated from Figure 4.7 for comparison) (n=75 rings, 5 rings per time point, 5 time points, 3 embryos each). Data is represented as mean±s.d. ns, non-significant ***P<0.001, two-tailed Mann-Whitney test. Scale bars: 5 µm

5.2.2 GRAF depletion induced hypercontractility in cellularization is suppressed by additional depletion of RhoGEF2

RhoGEF2 mutant leads to shortened furrow length and cap expansion in the syncytial division cycles. In contrast, overexpression of RhoGEF2 overexpression leads to constricted apical caps in the syncytial division cycles (Dey & Rikhy, 2020). RhoGEF2 depletion is known to inhibit ring constriction during cellularization by inhibiting the levels of Rho-GTP (Barmchi et al., 2005; Grosshans et al., 2005; Wenzl, Yan, Laupsien, & Großhans, 2010). We depleted RhoGEF2 by driving maternal expression of RNAi against RhoGEF2 (*RhoGEF2ⁱ*) to visualize furrow length and ring dynamics with Sqh-mCherry in cellularization. *RhoGEF2ⁱ* expressing embryos showed polygonal organization in mid cellularization and this phenotype was similar to GRAF overexpression. The previous report suggests that *RhoGEF2ⁱ* expressing embryos showed loss of constriction in cellularization (Figure 5.2A) (Barmchi et al., 2005; Wenzl, Yan, Laupsien, & Großhans, 2010). Sqh-mCherry fluorescence was present in a polygonal shape and appeared diffuse at the furrow tip in cellularization. In our previous study, quantification of Sqh-mCherry and Zipper in *RhoGEF2ⁱ* embryos shows a loss of membrane signal in syncytial

division cycles (Dey & Rikhy, 2020). Both *RhoGEF2ⁱ* and *Graf^{CR57}* show antagonistic constriction defects; this combination can be tested to check whether defects can be rescued. The *Graf^{CR57}; RhoGEF2ⁱ* combination showed ring constriction similar to control embryos in early and mid cellularization (Figure 5.2A,C). This combination showed better recruitment of Sqh-mCherry similar to control embryos in early and mid cellularization (Figure 5.2A,C). The *Graf^{CR57}; RhoGEF2ⁱ* was shown to suppress the hypercontractility defect of *Graf^{CR57}* in late cellularization (35-45 min, Figure 5.2C) even though this was not completely suppressed when compared to controls. *RhoGEF2ⁱ* embryos showed reduced Sqh-mCherry fluorescence in the ring relative to the inter-ring region as compared to controls in late cellularization. *Graf^{CR57}; RhoGEF2ⁱ* embryos showed a decrease in Sqh-mCherry levels as compared to *Graf^{CR57}* even though it remained higher than controls (Figure 5.2D). The suppression of hyper constriction and ring expansion seen in *Graf^{CR57}; RhoGEF2ⁱ* is also observed in fixed *Graf^f; RhoGEF2ⁱ* embryos stained with fluorescent phalloidin (Figure 5.2B). The suppression of ring constriction in the *Graf^{CR57}; RhoGEF2ⁱ* and *Graf^f; RhoGEF2ⁱ* combinations is likely due to restoration of Rho-GTP levels similar to control embryos. Finally, balanced Rho-GTP levels result in ring constriction regulation to the same extent as in control embryos.

This suggests that Rho-GTP was indeed present in *RhoGEF2* depleted embryos. It is also possible that RhoGEF2 inhibition was incomplete in *RhoGEF2ⁱ* embryos or another RhoGEF2 compensated Rho-GTP levels to balance the lack of RhoGTPase activity in *Graf^{CR57}* mutants.

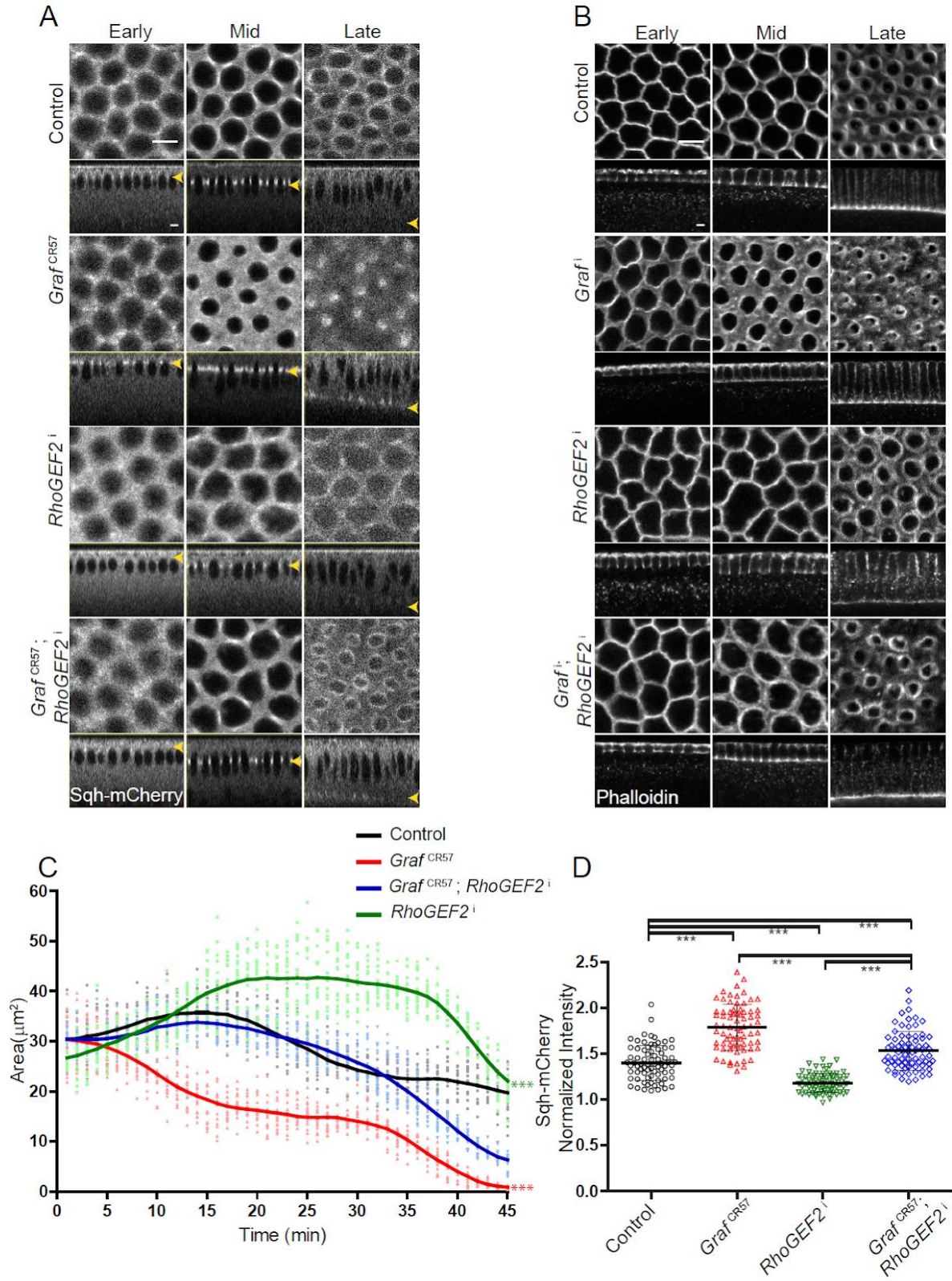


Figure 5.2: *Graf^{CR57}* hyper constriction phenotype is suppressed by RhoGEF2 depletion.

(A) *Graf^{CR57}* shows hyper constriction, *RhoGEF2ⁱ* shows loss of constriction and *Graf^{CR57}; RhoGEF2ⁱ* combinations shows ring sizes comparable to control embryos when imaged live with Sqh-mCherry (grey) (yellow arrowhead denotes furrow tip). **(B)** *Graf^f* shows hyper constriction, *RhoGEF2ⁱ* shows loss of constriction and *Graf^f; RhoGEF2ⁱ* combination shows ring sizes comparable to control embryos when stained with fluorescent phalloidin (B, *Graf^f* 95.71% show enhanced ring constriction n=70, *RhoGEF2ⁱ* 78.5% show loss of constriction n=14, *Graf^f; RhoGEF2ⁱ* 57.14%, rings comparable to controls n=21). **(C)** Quantification of contractile ring area from Sqh-mCherry expressing embryos shows decreased area in *Graf^{CR57}*, increased area in *RhoGEF2ⁱ* and rescued area in *Graf^{CR57}; RhoGEF2ⁱ* (n=15 rings, 5 rings per embryo, 3 embryos) (control values were repeated from Figure 4.3 and *Graf^{CR57}* values were repeated from Figure 4.3 for comparison). Data is represented as mean±s.d. ***P<0.001 One-way ANOVA, Repeated measure with Dunnett's Multiple comparison test, the *Graf^{CR57}* and *RhoGEF2ⁱ* statistically different from controls and *Graf^{CR57}; RhoGEF2ⁱ*. **(D)** Sqh-mCherry intensity in late cellularization in *RhoGEF2ⁱ* is decreased as compared to controls. *Graf^{CR57}; RhoGEF2ⁱ* shows a decrease in Sqh-mCherry intensity as compared to *Graf^{CR57}* and rescue in comparison with *RhoGEF2ⁱ* (control and *Graf^{CR57}* values were repeated from Figure 4.7 for comparison)(n=75 rings, 5 rings per time point, 5 time points, 3 embryos each). Data is represented as mean±s.d. ***P<0.001, two-tailed Mann-Whitney test. Scale bars: 5 µm

5.2.3 RhoGEF2 overexpressed and depleted embryos retain GRAF protein at the contractile ring during cellularization

RhoGEF2-OE embryos were stained with GRAF antibody along with Dlg, membrane marker. GRAF antibody staining in RhoGEF-OE embryos showed recruitment of GRAF at contractile rings in early and mid cellularization. GRAF immunostaining was seen at an increased level in late cellularization in RhoGEF2-OE embryos as compared to controls (Figure 5.3A). Immunostaining of *RhoGEF2ⁱ* with GRAF and Dlg antibodies showed that GRAF recruitment occurred at the furrow in early and mid stages of cellularization and was lost in the late stage similar to controls (Figure 5.3B). The furrow extension dynamics in RhoGEF2 depleted embryos with the slow and fast phase of cellularization were similar to control (Figure 5.3C). The rate of furrow extension of RhoGEF2-OE was decreased in the fast phase (Figure 5.3C). Although, RhoGEF2 perturbation effect the furrow dynamics but GRAF retains at the furrow tip during cellularization.

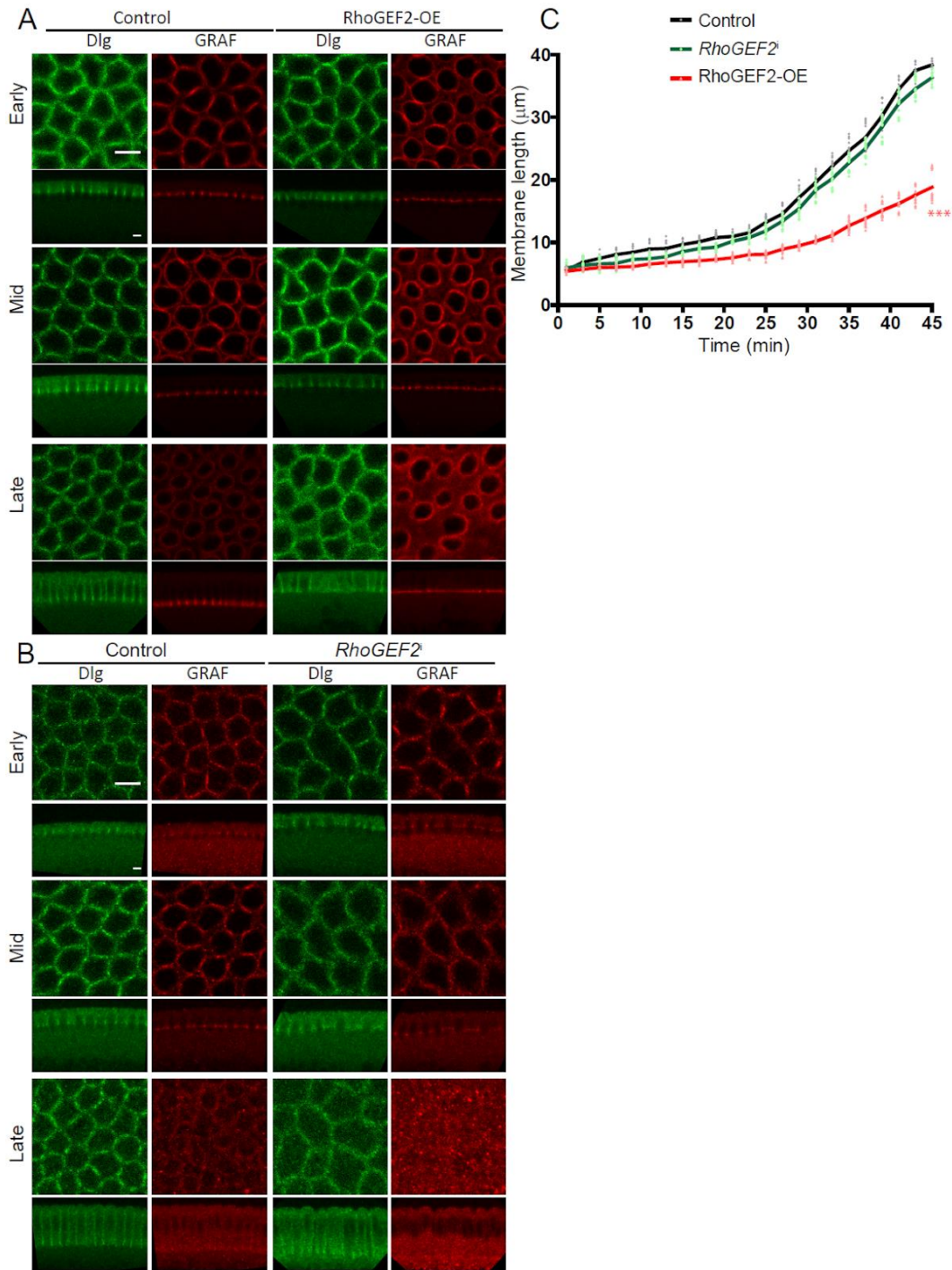


Figure 5.3: RhoGEF2 depletion and overexpression retain GRAF recruitment.

(A) Fixed embryos stained with GRAF and Dlg antibodies show increased staining of GRAF in *nanos*-Gal4; RhoGEF2 (RhoGEF2-OE) embryos in mid and late cellularization (100% embryos show increased GRAF staining as compared to controls, n=20 embryos). The furrow tip is organised as a ring in RhoGEF2-OE in early cellularization as compared to controls. **(B)** Fixed embryos stained with GRAF and Dlg antibodies show similar GRAF staining in *nanos*-Gal4; *RhoGEF2* RNAi expressing embryos knockdown as compared

to controls (100% embryos show GRAF staining comparable to controls, n=14 embryos). The furrow tip is organized as a polygon in *RhoGEF2ⁱ* in mid and late stages as compared to rings in controls. **(C)** Furrow length is quantified from live imaging of controls, *RhoGEF2ⁱ* and RhoGEF2-OE embryos. *RhoGEF2ⁱ* shows similar dynamics or furrow extension as compared to controls. RhoGEF2-OE shows a significantly shorter length compared to controls in the slow phase and the fast phase. The final furrow length at 45 min remains significantly shorter than controls. Data is represented as mean±s.d. ***P<0.001 One-way ANOVA, Repeated Measure with Dunnett's Multiple comparison test, Rho-GEF2-OE is statistically different from controls and *RhoGEF2ⁱ*. Scale bars: 5 μm

5.2.4 Hyper constriction defects in MBS depleted embryos are suppressed by GRAF overexpression

Rho-kinase is known to phosphorylate and deactivate Myosin II phosphatase (Amano et al., 2010; Kimura et al., 1996; T. Mizuno et al., 1999). Mutants of the Myosin II binding subunit (MBS) of Myosin II phosphatase were unable to execute Myosin II deactivation (Tomoaki Mizuno et al., 2002; Tan et al., 2003). We maternally expressed RNAi against MBS (*mbsⁱ*) and stained embryos with phalloidin to check ring architecture. We found that *mbsⁱ* expression is likely to increase Myosin II activation in cellularization. As expected, *mbsⁱ* expression leads to hyper constriction of the ring at the furrow throughout cellularization (Figure 5.4). The hyper constriction phenotype in *mbsⁱ* expressing embryos was suppressed by GRAF overexpression.

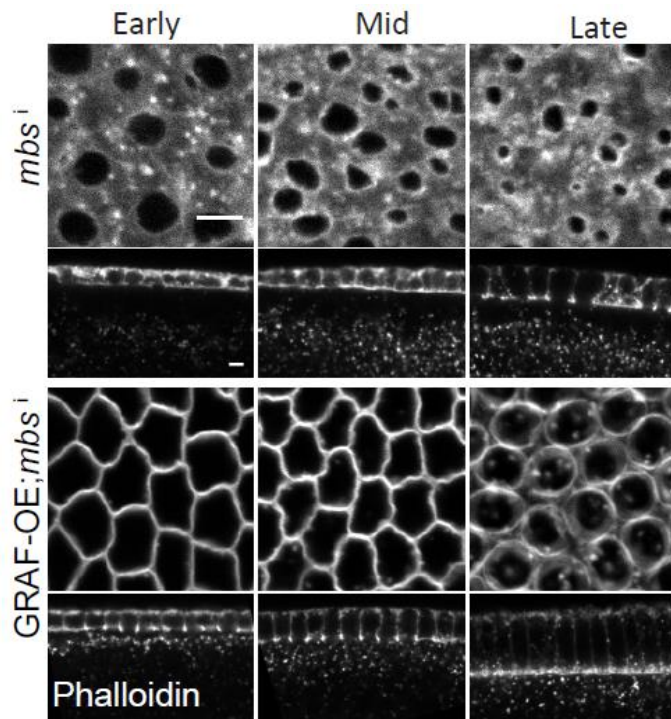


Figure 5.4: GRAF overexpression suppresses the hyper constriction phenotype in MBS depleted embryos.

Embryos stained with fluorescently coupled phalloidin show enhanced constriction in *nanos*-Gal4, MBS RNAi (*mbsⁱ*) embryos (100% show constriction, n=36 embryos). The *mbsⁱ*; GRAF-OE combination shows suppression (60% show constriction similar to controls, n=10 embryos) of the hyper constriction defects seen in *mbsⁱ* embryos. Scale bars: 5 μ m

5.2.5 GRAF depletion induced hypercontractility in cellularization is lost by additional depletion of ROK

Myosin II levels were sustained at the furrow in *Graf^{CR57}* mutant embryos. *Drosophila* Rho Kinase (Rok) activates Myosin II by phosphorylation in a Rho-GTP dependent manner (Chougule et al., 2016; Xue & Sokac, 2016). We depleted Rho-kinase in order to test if activated Myosin II was responsible for the hypercontractility phenotype in *Graf^{CR57}* embryos. Rho-kinase maternal depletion was achieved using RNAi against ROK (*rokⁱ*) along with Sqh-mCherry in the background of control and *Graf^{CR57}* embryos. As expected, *rokⁱ* expressing embryos showed a diffused signal of Sqh-mCherry with loss of ring constriction, having a larger ring area than control embryos in cellularization (Figure 5.5 A, B). The *rokⁱ* expression in the background of *Graf^{CR57}* shows a diffused

distribution of Sqh-mCherry similar to *rok*ⁱ embryos. The combination of *Graf*^{CR57}; *rok*ⁱ led to a loss of hyper-constriction phenotype seen in *Graf*^{CR57} embryos (Figure 5.5A,B). Rho-GTP was likely to be unaffected in *rok*ⁱ mutant embryos as ROK acts downstream of Rho-GTP. It is interesting to note that the ring area in the *Graf*^{CR57}; *rok*ⁱ combination mutant embryos were significantly higher as compared to controls due to the absence of active Myosin II.

The Sqh-mCherry intensity in the ring compared to the inter-ring in both *rok*ⁱ and *Graf*^{CR57}; *rok*ⁱ was decreased as compared to controls (Figure 5.5C). The suppression of the *Graf* mutant phenotype of hyper constriction with Rok depletion shows that Myosin II activation is a cause of the phenotype. Myosin II activation is a necessary step to execute ring constriction in cellularization.

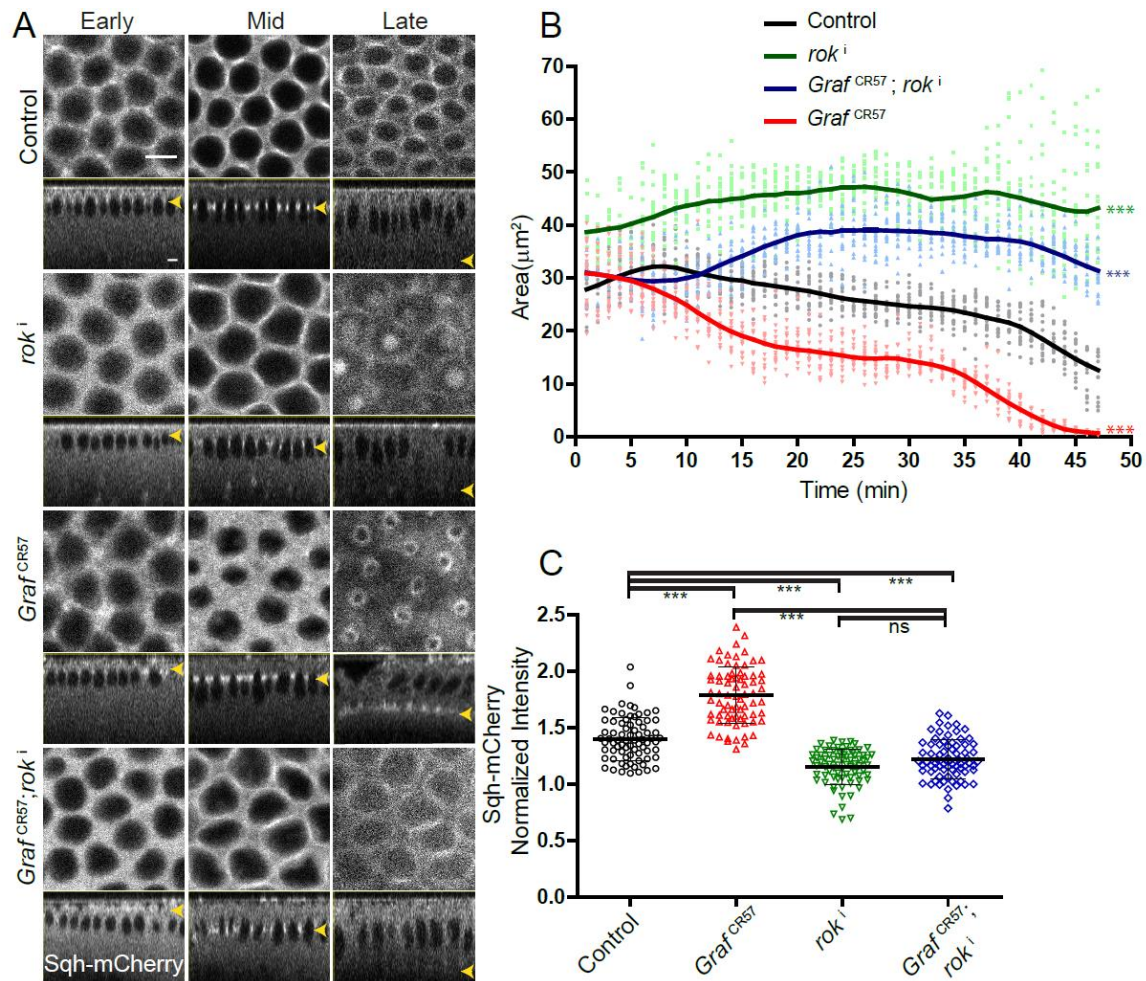


Figure 5.5: The hyper constriction phenotype of *Graf*^{CR57} embryos is suppressed by additional depletion of Rok

(A) *Graf*^{CR57} shows hyper constricted contractile rings, *rok*ⁱ shows loss of ring constriction and the *Graf*^{CR57};*rok*ⁱ combination shows suppression of the hyper constriction phenotype seen in *Graf*^{CR57} when imaged live with Sqh-mCherry (grey) (yellow arrowhead denotes furrow tip). **(B)** Quantification of contractile ring area from Sqh-mCherry embryos shows a decreased area in *Graf*^{CR57}, an increased area in *rok*ⁱ and increased area in *Graf*^{CR57};*rok*ⁱ compared to controls (n=15 rings, 5 per embryo, 3 embryos) (control values were repeated from Figure 3 and *Graf*^{CR57} values were repeated from Figure 4.3 for comparison). Data is represented as mean±s.d. ***P<0.001 One-way ANOVA, Repeated measure with Dunnett's multiple comparison test, the *Graf*^{CR57}, *rok*ⁱ and *Graf*^{CR57};*rok*ⁱ ring area are statistically different from controls. **(C)** Quantification of Sqh-mCherry intensity in late cellularization in *rok*ⁱ and *Graf*^{CR57};*rok*ⁱ shows decreased intensity in comparison to controls (control and *Graf*^{CR57} values were repeated from Figure 4.7 for comparison) (n=75 rings, 5 rings per time point, 5 time points, 3 embryos each). Data is represented as mean±s.d. ns, non-significant ***P<0.001, two-tailed Mann-Whitney test. Scale bars: 5 μm

5.2.6 GRAF is a bonafide Rho-GAP protein that acts as a negative regulator for constriction during cellularization

The spatial pattern of GRAF recruitment varies with the dynamics of the actomyosin network. GRAF localizes precisely to the furrow tip in early cellularization, increases in mid cellularization and finally becomes cytoplasmic at late stages (Figure 5.6). *Graf* depletion showing pre-mature and hyper constriction defects are caused by inhibition of Rho-GTPase hydrolysis resulting in increased Rho-GTP levels. This increased Rho-GTP levels, in turn, activate Myosin II which is essential for ring constriction. In contrast, ROK depletion, which inactivates Myosin II, in *Graf* depletion background shows expanded rings due to inhibition of constriction (Figure 5.6) (Sharma & Rikhy, 2021). This suggests that the constriction process is dependent on Myosin II activity. In summary, our findings show that the RhoGEF activity of RhoGEF2 and the RhoGAP activity of *Graf* is required to maintain appropriate levels of Rho-GTP for activation of Myosin II for ring constriction during cellularization.

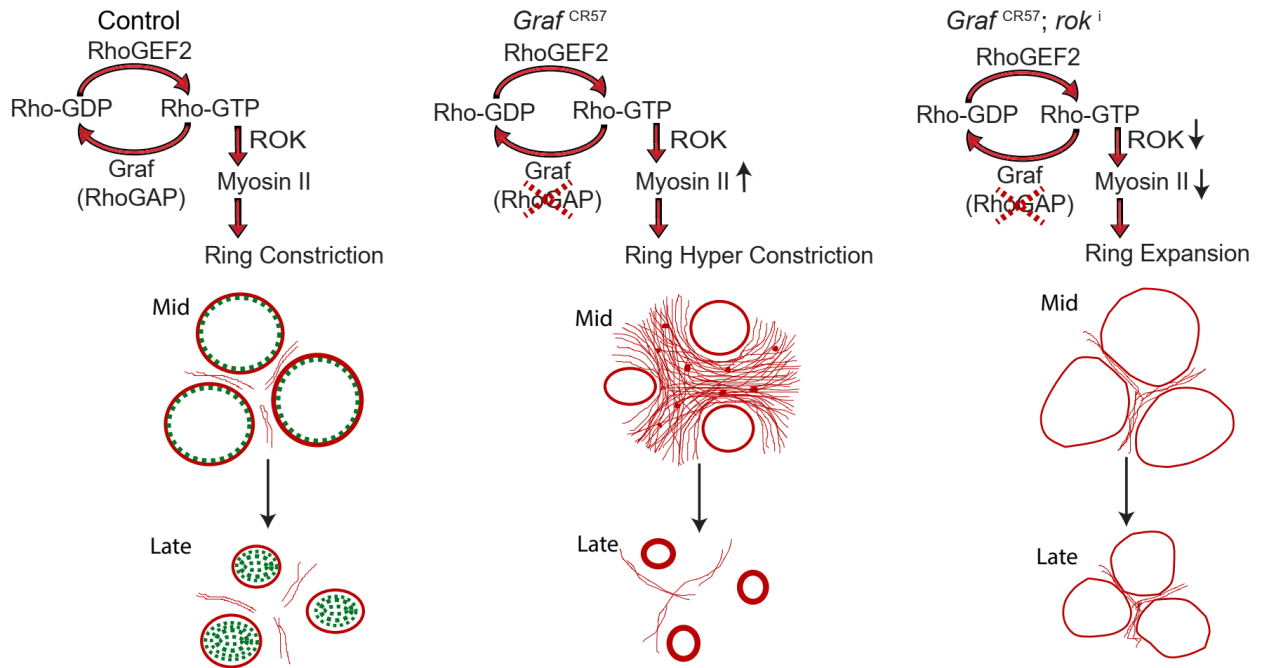


Figure 5.6: GRAF is a bonafide Rho-GAP protein that requires Myosin II activity for constriction during cellularization. Schematic shows that GRAF plays a role in regulating Rho-GTP levels as a RhoGAP. GRAF is uniformly present at the contractile ring during mid stage and becomes cytosolic in late stages to drive the contraction process. *Graf* depletion shows a hyper constriction phenotype and Rok depletion suppresses the hyper constriction phenotype seen in *Graf* mutant embryos. *Graf* mutant embryos show Myosin II accumulation at the ring in mid and late cellularization and in the inter ring region in mid cellularization.

5.3 Conclusion and discussion

In this study, we have shown that the GRAF inhibits ring constriction dependent on Myosin II activity at the furrow during cellularization. Myosin II activity is regulated by Rho-GTP generated in Rho GDP-GTP cycling. This Rho-GTP cycling is therefore regulated in a spatiotemporal manner by RhoGEF2 and RhoGAP domain of GRAF during cellularization. This further suggests that an increase in Rho-GTP levels leads to hyper constriction of the contractile ring. Moreover, RhoGEF2 overexpression does not affect the recruitment of GRAF on the furrow. This suggests that GRAF recruitment is independent of perturbation in RhoGEF2 levels. RhoGEF2 and Myosin II inactivation in Rok depletion suppresses the hypercontractility phenotype in *Graf* mutant embryos.

Taken together, our study shows that spatiotemporal recruitment of GRAF might be required for fine-tuning of RhoA activity which ensures regulated constriction events during various stages of cellularization.

GRAF functions in clathrin-independent endocytosis of the EGFR receptor in hematopoiesis in *Drosophila* (Kim et al., 2017). GRAF1 is associated with small G-protein Cdc42 to carry out clathrin independent endocytosis (Lundmark et al., 2008). The small GTPase Arf1 recruits the human homologue of GRAF, ArhGAP10 which is required in clathrin independent endocytosis of GPI anchored proteins (Kumari & Mayor, 2008). In *Drosophila*, Arf1 is activated by Steppke (ArfGEF). Steppke is enriched at the furrow tip during early cellularization and induces local endocytosis leading to restricted actomyosin activity. Interestingly, Steppke mediated endocytosis at the leading edge of the cellularization furrow plays a role in limiting Rho1 activity. Depletion of *Drosophila* ArfGEF, *steppke* shows decreased endocytosis driven tubule formation at the furrow and enhanced Rho1 induced hyper constriction in cellularization (D. M. Lee & Harris, 2013). The *steppke* mutant partially phenocopies *Graf* defect, giving rise to reduced endocytosis with enhanced actomyosin activity via Rho1 activation. Thus, it provides the clue that ArfGEF might be important in the recruitment of GRAF in *Drosophila* cellularization. Even though GRAF has been found to play a role in endocytosis in other systems, GRAF staining did not mark vesicles during cellularization. However, it is possible that GRAF and ArfGEF work either in the same or independent pathways to regulate endocytic processes at the furrow and in turn regulate Rho1 activity during constriction.

Surprisingly, homozygous *Graf*^{CR57} mutant flies are viable. The other homozygous *Graf*^{fl} mutant generated with an imprecise P-element excision strategy is also viable (Kim et al., 2017). Although in our study, the *Graf*^{CR57} mutant adults show sterility defects. This suggests that there could be other RhoGAP domain containing proteins that regulate RhoA-GTP levels in the absence of GRAF in cellularization. RhoGAP92B is another uncharacterised BAR, RhoGAP and SH3 domain containing protein expressed in early embryogenesis (Contrino et al., 2012). Whether it contributes to the regulation of RhoA-GTP levels remains to be ascertained. RhoGAP containing protein CGAP is required for

RhoA-GTP cycling to produce Myosin II pulses for apical constriction during gastrulation in *Drosophila*. CGAP mutant embryos also show hyper constriction during cellularization which phenocopies *Graf* defects (Mason et al., 2016). In addition, RhoGAP68F is also required for coordinated apical constriction during gastrulation (Sanny et al., 2006). It is likely that GRAF, RhoGAP92B, CGAP and RhoGAP68F together regulate ring constriction during cellularization and apical constriction during gastrulation. Therefore, even if one of the proteins is absent, cellularization is likely to continue normally due to the redundancy in the RhoGAP function. It is possible that C-GAP protein depletion in *Graf* mutant embryos may enhance the phenotype of hyper constriction seen in cellularization. This redundancy of function in the RhoGAP proteins appears as a general feature and is seen in many organisms. RGA3 and RGA4 are examples of two RhoGAP proteins which regulate RhoA activity in early embryogenesis in *C. elegans* (Schmutz et al., 2007). In order to dissect redundancy, screening could be performed with perturbed levels of RhoGEF2 and RhoGAP proteins in *Graf* depletion background, to check for enhancers or repressors contributing towards constriction defects.

CHAPTER 6

GRAF domain function in contractility and recruitment of protein at the contractile ring during cellularization

6.1 Introduction

GRAF is a multidomain protein containing N-terminal BAR, PH, RhoGAP and C-terminal SH3 domains (Lundmark et al., 2008). Originally this molecule was identified with RhoGAP domain which influences the GTPase activity of RhoA and the SH3 domain which binds to the C-terminal domain of FAK. The members of the GRAF protein family are ArhGAP42/GRAF3 (Bai et al., 2013), ArhGAP26/GRAF (Hildebrand et al., 1996), ArhGAP10/GRAF2/ PSGAP (X. R. Ren et al., 2001; Shibata et al., 2001), Oligophrenin-1 (Billuart et al., 1998) and others. All members of this protein family are RhoGAPs consisting of BAR-PH and C-terminal SH3 domains, with the exception of Oligophrenin-1 (OPHN1) protein related to X-linked mental retardation, in which the SH3 domain is absent (Billuart et al., 1998). GRAF gene in other organisms such as *Drosophila* (*Dm Graf*, CG8948) and *C. elegans* (T04C9.1) also share similar domains.

The BAR domain of GRAF1 functions in sculpting the membrane, as is evidenced by its labelling of tubular and punctate structures in NIH 3T3 and HeLa cells. Mutation of specific residues in the BAR domain (KK131/132EE) results in the loss of its affinity to bind membranes, becoming cytoplasmic in cells (Lundmark et al., 2008). Lipid bending is compromised in BAR domain deletion and mutation in specific residues within the BAR domain (K121E/K131E/K132E). Cells carrying this deletion or mutation show a dramatic reduction in the induction of multinucleated myotubes. Thus, membrane bending or sculpting depending on the BAR domain is specifically required for myoblast fusion (J. T. Doherty et al., 2011).

ArhGAP42 BAR domain shows an autoinhibitory role towards the GAP activity. As revealed by studies in which expression of BAR domain deletion resulting in decreased active RhoA levels and increased stress fibers, focal adhesion dynamics and cell migration (Luo et al., 2017). *In vitro* and *in vivo* studies show that BAR domain deletion leads to lowered Rho-GTP levels. This suggests that the BAR domain is inhibitory towards the Rho-GAP domain (Eberth et al., 2009; Luo et al., 2017). Similarly, the GAP domain also shows an autoinhibitory function to the BAR-PH domain. When the ArhGAP42 GAP domain is deleted, it results in enhanced tubulovesicular membrane formation *in vitro* and membrane tubulation in cells (Luo et al., 2017). OPHN1 and GRAF1 (GRAF subfamily) BAR domains show an intramolecular interaction towards the GAP domain, masking it to suppress the GAP activity. GRAF proteins in their inhibited state, are able to bind and generate lipid tubules *in vitro* and *in vivo*. Thus, the BAR domain plays a dual role in membrane binding and regulation of GAP activity (Eberth et al., 2009).

In vitro studies show that GRAF1 BAR and PH domains localize specifically to PI(4,5)P2-enriched, tubular lipid structures (Lundmark et al., 2008). Clathrin-independent endocytosis requires BAR and PH domains of GRAF1 that remodel membranes to generate or stabilize endocytic tubules *in vivo*. BAR and PH domains of GRAF1 are sufficient to mediate membrane binding resulting in a reduction of surface tension (G. J. Doherty & Lundmark, 2009; J. T. Doherty et al., 2011; Lundmark et al., 2008). The purified PH domain of GRAF1 shows weak interaction with PS or PI(4,5)P2-enriched liposomes, suggesting that BAR and PH domain both form a combined lipid interacting structural unit that facilitates efficient binding to the membrane. Positive ridge and hydrophobic amino acids in the GRAF1 PH domain contributes towards membrane binding, which was shown by mutating residues in the positive ridge (K277E/R278Q) and hydrophobic amino acids (F280 and F303 to alanines) in cells and *in vitro*. GRAF1 PH domain residue (K277E/R278Q) and GAP-domain (R412D) mutant show increased stress fibers. Thus, the dual activity of BAR and PH domain is required for membrane recruitment of GRAF1 protein which suppresses membrane blebbing to spatially regulate GAP activity (Holst et al., 2017).

GRAF overexpression phenocopies the microinjection of C3 exoenzyme (rho inhibitor) showing reduced Rho activity giving rise to filopodia-like extensions in growing cells (J. M. Taylor et al., 1998, 1999). *In vitro* assay of ArhGAP42 demonstrates GTPase activity towards RhoA and cdc42 but not Rac1, similar to other members of the GRAF RhoGAP family (Billuart et al., 1998; Hildebrand et al., 1996; X. R. Ren et al., 2001). *Graf* deficient mice show increased Rho-GTP levels and enhanced Myosin II foci in isolated blood vessels (Bai et al., 2013). RhoGAP domain specifically regulates the GTPase activity of RhoA. In addition, GRAF1 GAP activity which limits RhoA regulates induction of skeletal muscle differentiation (J. T. Doherty et al., 2011).

GRAF1 SH3 domain is shown to bind the Dynamin1 purified from brain cytosol and HeLa cell lysates. The SH3 C-terminally deleted GRAF1 gets recruited on long static tubules which shows that Dynamin and GRAF1 interact to regulate the scission and stability of these tubules (Lundmark et al., 2008). GRAF SH3 mediated protein interactions are needed for inducing skeletal muscle differentiation as shown by decreased tropomyosin expression in the SH3 domain (E719Q) mutant (Hildebrand et al., 1996). ArhGAP42 (human GRAF) acts as a regulator of cytoskeletal dynamics and cell adhesion where the SH3 domain was necessary for protein recruitment to actin stress fibers and focal adhesions (Luo et al., 2017). It is possible that the SH3 domain binds indirectly to actin filaments through bridging proteins, such as targeting of srGAP2 to actin via formin-like protein 1 (FMNL1) (Mason et al., 2011).

We assessed the role of GRAF domain deletions on contractile ring formation in *Drosophila* cellularization. We found that GRAF domain deletion affects GRAF protein recruitment and dissociation from the ring during cellularization.

6.2 Material and methods

6.2.1 *Drosophila* stocks

Fly stocks and crosses were maintained in regular cornmeal agar. The detailed genotypes, stock numbers and source of stocks are a part of Table 6.1.

Stock	Genotype	Source/Reference
1	y[1] sc[*] v[1] GRAF[CR57]/FM7a;mat67Sqh-mCherry/cyo	This study
2	y[1] sc[*] v[1] GRAF[CR57]/FM7a; p[pUASp GRAF EGFP G1] attp40/cyo	This study
3	y[1] sc[*] v[1] GRAF[CR57]/FM7a; p[pUASp GRAF ΔRhoGAP-EGFP] attp40/cyo	This study
4	y[1] sc[*] v[1] GRAF[CR57]/FM7a; p[UASp-GRAF ΔBAR- GFP] attp40/cyo	This study
5	y[1] sc[*] v[1] GRAF[CR57]/FM7a; p[UASp-GRAF ΔPH-GFP P1] attp40/cyo	This study
6	y[1] sc[*] v[1] GRAF[CR57]/FM7a; p[UASp-GRAF ΔSH3- GFP] attp40/cyo	This study

Table 6.1: *Drosophila* stocks and their source

6.2.2 Live imaging of *Drosophila* embryos

For live imaging, 2-2.5 hrs embryos were collected on sucrose agar plates and dechorionated with 100% bleach for 1 min and mounted on 2 well coverslip bottom Labtek chambers. Mounted embryos were filled with 1X PBS (Manos Mavrakis et al., 2008) and imaged using 40X/1.4NA oil objective on Zeiss or Leica SP8 microscope with a frame rate of 1.74s/frame and 2s/frame respectively.

6.2.3 Quantification of mean fluorescence intensity from live-imaging

Inter-ring Sqh-mCherry intensity during mid stages

Live imaging of embryos containing different genotypes ($Graf^{CR57}$, $Graf^{CR57};GRAF$ -GFP, $Graf^{CR57};GRAF\Delta BAR$ -GFP, $Graf^{CR57};GRAF\Delta PH$ -GFP, $Graf^{CR57};GRAF\Delta RhoGAP$ -GFP and $Graf^{CR57};GRAF\Delta SH3$ -GFP) were used to quantify the Sqh-mCherry intensity in

interring region during mid stages (13µm). To estimate these changes quantitatively across all genotypes, images were obtained with sum intensity per pixel across the Z-axis from a total of five stacks: two stacks above and two stacks below of the brightest section at the furrow tip covering a depth of 4 µm by taking five time points during the mid cellularization. The mean ring intensity per pixel was extracted by drawing a segmented ROI on the ring. The inter-ring intensity per pixel was extracted by drawing an ROI in between adjacent rings that had increased Sqh-mCherry intensity. The inter-ring intensity per pixel was expressed as a ratio to ring intensity per pixel (mean ring intensity subtracted cytosol intensity). Finally, the normalized intensity of the ring was shown as a scatter plot.

Ring Sqh-mCherry intensity during late stages

Live imaging of embryos containing different genotypes (*Graf*^{CR57}, *Graf*^{CR57}; GRAF-GFP, *Graf*^{CR57};GRAFΔBAR-GFP, *Graf*^{CR57};GRAFΔPH-GFP, *Graf*^{CR57};GRAF ΔRhoGAP-GFP and *Graf*^{CR57};GRAFΔSH3-GFP) were used to quantify the Sqh-mCherry intensity at rings during late stages (30µm). To estimate these changes quantitatively across all genotypes, images were obtained with sum intensity per pixel across the Z-axis from a total of five stacks: two stacks above and two stacks below of the brightest section at the furrow tip covering a depth of 4 µm in late cellularization. The mean ring intensity per pixel was extracted by drawing a segmented ROI on the ring. The inter-ring intensity per pixel was extracted by drawing an ROI in between adjacent rings that had reduced Sqh-mCherry intensity. The ring intensity per pixel was expressed as a ratio to interring intensity per pixel. Finally, the normalized intensity of the ring was shown as a scatter plot.

GRAF domain deletions intensity during mid and late stages

Live imaging of embryos containing different genotypes (*Graf*^{CR57};GRAF-GFP, *Graf*^{CR57};GRAFΔBAR-GFP, *Graf*^{CR57};GRAFΔPH-GFP, *Graf*^{CR57};GRAFΔRhoGAP-GFP and *Graf*^{CR57};GRAFΔSH3-GFP) were used to quantify the GFP fluorescence intensity change during mid (13µm) and late stages (30µm). Images with Z projection of sum intensity were obtained from two stacks above and two stacks below of the brightest

section at the furrow tip covering a depth of 4 μm . ROIs across the furrow tip from 5 or 10 rings were drawn in these images for each time point to obtain the mean signal intensity. The mean intensity obtained at each time point was represented as a ratio to the cytosolic mean fluorescence value obtained across cellularization within each embryo and finally plotted as a 'normalized intensity vs stages'.

6.3 Result

6.3.1 GRAF BAR, PH, RhoGAP and SH3 domains are necessary for regulation of ring constriction during cellularization.

In order to dissect the function of GRAF's domains in regulating actomyosin ring constriction, we generated fluorescently tagged GRAF transgenes lacking individual domains in the protein. These domains are expressed with UAS elements using maternal gal4 in the background of *Graf*^{CR57} mutant. In the mutant background, embryos expressing GFP tagged domain deletion protein are used for live imaging along with Sqh-mCherry, which marks the actomyosin ring during cellularization.

Graf^{CR57} shows hypercontractility defect during cellularization when compared to control, as shown earlier. We expressed GRAF-GFP full-length protein in *Graf*^{CR57} background, *Graf*^{CR57}; GRAF-GFP, which rescued the hypercontractility defect. In contrast, expressing *Graf*^{CR57}; GRAF Δ RhoGAP-GFP, lacking the RhoGAP domain, retains hypercontractility when compared to *Graf*^{CR57}; GRAF-GFP embryos in mid and late cellularization. Hence, we established that GRAF protein requires the RhoGAP domain to regulate contractility. We expressed the *Graf*^{CR57}; GRAF Δ BAR-GFP and *Graf*^{CR57}; GRAF Δ PH-GFP constructs with Sqh-mCherry lacking BAR and PH domains. These domain deletions show hyper constriction defects with 50% penetrance in the mid and late stages of cellularization (Figure 6.1A). We took these defective embryos for further ring area quantification. The quantification of mid and late cellularization stages were performed corresponding to the 13 μm and 30 μm membrane lengths. The ring area in *Graf*^{CR57}; GRAF Δ RhoGAP-GFP, *Graf*^{CR57}; GRAF Δ BAR-GFP and *Graf*^{CR57}; GRAF Δ PH-GFP are significantly reduced during mid and late stages when compared to control (Figure 6.1B,C).

We maternally expressed GRAF transgene lacking the SH3 domain in the background of *Graf*^{CR57} mutant, *Graf*^{CR57}; GRAF Δ SH3-GFP with Sqh-mCherry. Interestingly, *Graf*^{CR57}; GRAF Δ SH3-GFP qualitatively shows hyper constriction defect when compared to *Graf*^{CR57}; GRAF-GFP (Figure 6.1A). It results in significantly reduced ring area compared to *Graf*^{CR57}; GRAF-GFP during mid and late cellularization (Figure 6.1B,C). However, there is a decrease in hyper constriction defect as shown by the increased ring area when compared to *Graf*^{CR57}. Hence, the SH3 domain of GRAF plays a significant role in the regulation of ring area during cellularization.

Taken together, all domain deletions of GRAF protein show constriction defects. Hence, all domains are required in ring constriction during mid and late cellularization

6.3.2 GRAF BAR, PH, RhoGAP and SH3 domain deletions lead to altered distribution of Myosin II in cellularization.

Living embryos expressing GRAF lacking BAR, PH, RhoGAP and SH3 domain each in the *Graf*^{CR57} background along with Sqh-mCherry were used for assessing Myosin II recruitment analysis during mid and late stages. Qualitatively, these domain deletions exhibit an enriched distribution of Sqh-mCherry between neighbouring rings during mid stages compared to the control and *Graf*^{CR57}; GRAF-GFP (Figure 6.1A). The Sqh-mCherry intensity was quantified using the ratio of inter-ring intensity to the ring intensity during mid cellularization. All domain deletions as well as *Graf*^{CR57} mutant showed a significantly increased Myosin II intensity in between the rings as compared to *Graf*^{CR57}; GRAF-GFP during mid cellularization (Figure 6.1D). In addition to this, these domain deletions show retention of Sqh-mCherry signal at the rim of the ring during late cellularization to varying degrees (Figure 6.1A). The Sqh-mCherry intensity was quantified using the ratio of ring intensity to the inter-ring intensity during late cellularization. During late cellularization, all domain deletions as well as *Graf*^{CR57} show significantly higher Myosin II intensity at the rim of the rings when compared to *Graf*^{CR57}; GRAF-GFP (Figure 6.1E). In summary, all domain deletions result in a perturbation of Myosin II recruitment at the furrow tip during mid and late stages. Hence, all the domains of GRAF likely play a role in regulating Myosin II activity during cellularization.

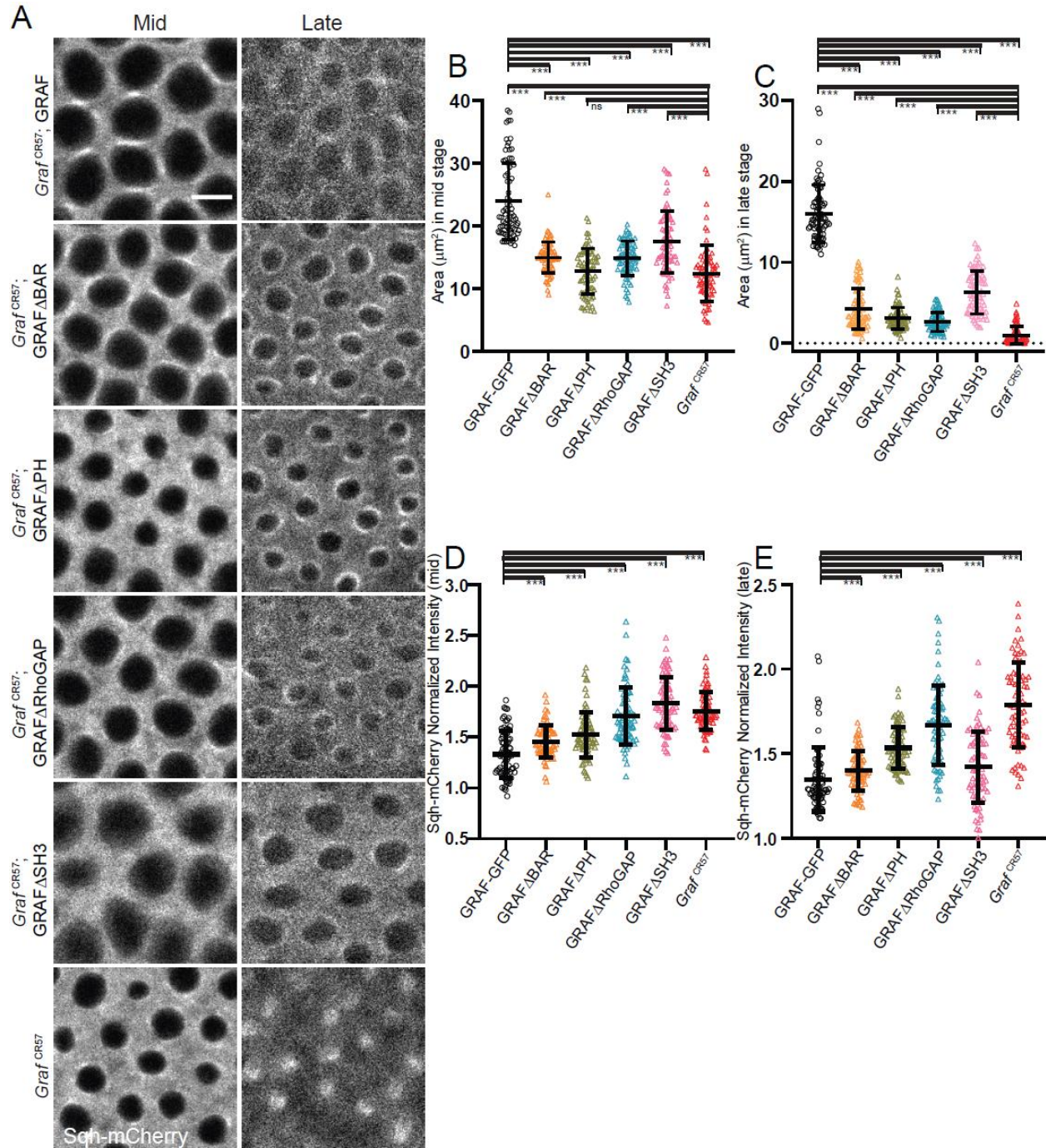


Figure 6.1: GRAF BAR, PH, RhoGAP and SH3 domains are necessary for ring constriction regulation via Myosin II recruitment during cellularization.

(A) Live embryos showing contractile ring visualized using Sqh-mCherry in *Graf^{CR57}*; GRAF-GFP, *Graf^{CR57}*; GRAF Δ BAR-GFP, *Graf^{CR57}*; GRAF Δ PH-GFP, *Graf^{CR57}*; GRAF Δ RhoGAP-GFP, *Graf^{CR57}*; GRAF Δ SH3-GFP and *Graf^{CR57}* during mid (furrow length 13 μm) and late (furrow length 30 μm) cellularization. **(B-C)** Area analysis in all genotypes at **(B)** mid and **(C)** late cellularization. All the domain deletion and *Graf^{CR57}* mutants

show significantly reduced area when compared to *Graf*^{CR57}; GRAF-GFP during mid and late stages. The spread-out signal in the inter ring region at mid stage and concentrated accumulation of Sqh-mCherry at the rings at a late stage. **(D-E)** Quantification of Sqh-mCherry intensity in all domain deletions show increased intensity during **(D)** mid and **(E)** late cellularization when compared to *Graf*^{CR57}; GRAF-GFP.

n=75 rings, 5 rings per time point, 5 time points per embryo, 3 embryos of all genotypes. Data represented as mean±s.d. ***P<0.001, two-tailed Mann Whitney test. Scale bars: 5 µm.

6.3.3 The BAR and SH3 domains are necessary for the enrichment of GRAF on the ring

In order to analyse the effect of the particular domain in recruiting GRAF protein to the furrow tip during cellularization, we used the maternally expressed GFP tagged domain deletion transgenes in the *Graf*^{CR57} background. The *Graf*^{CR57}; GRAF-GFP tagged protein gets specifically recruited at the furrow tip during cellularization. It has been observed previously that GRAF is enriched selectively during the transition from the polygonal network to the ring stage and is gradually lost from the furrow tip during late cellularization. In this experiment, we checked recruitment of the BAR and SH3 domain deletions specifically during mid and late cellularization. We observed that the GRAFΔBAR-GFP protein shows reduced localization to the furrow tip when compared to GRAF-GFP during mid cellularization. In contrast, GRAFΔBAR-GFP protein is reduced on the ring during late cellularization when compared to the GRAF-GFP (Figure 6.2A). GRAFΔBAR-GFP shows significantly reduced intensity during mid cellularization when compared to control (Figure 6.2B). In contrast, the intensity was not significantly different when compared to *Graf*^{CR57}; GRAF-GFP intensity during late cellularization (Figure 6.2C).

GRAFΔSH3-GFP protein also shows a severe reduction in localization to the furrow tip with much more cytosolic signal when compared to GRAF-GFP during mid cellularization. Qualitatively, there is no visible enrichment of the *Graf*^{CR57}; GRAFΔSH3-GFP protein on the ring relative to the cytosol and shows cytoplasmic distribution during mid cellularization compared to GRAF-GFP (Figure 6.2A). GRAFΔSH3-GFP shows significantly reduced intensity during mid and late cellularization when compared to control (Figure 6.2 B, C). Thus, GRAFΔSH3-GFP shows lower enrichment at the ring when compared to GRAFΔBAR-GFP throughout mid and late cellularization.

In summary, both BAR and SH3 domains of GRAF protein are crucial for the recruitment of the protein to the rings during mid cellularization.

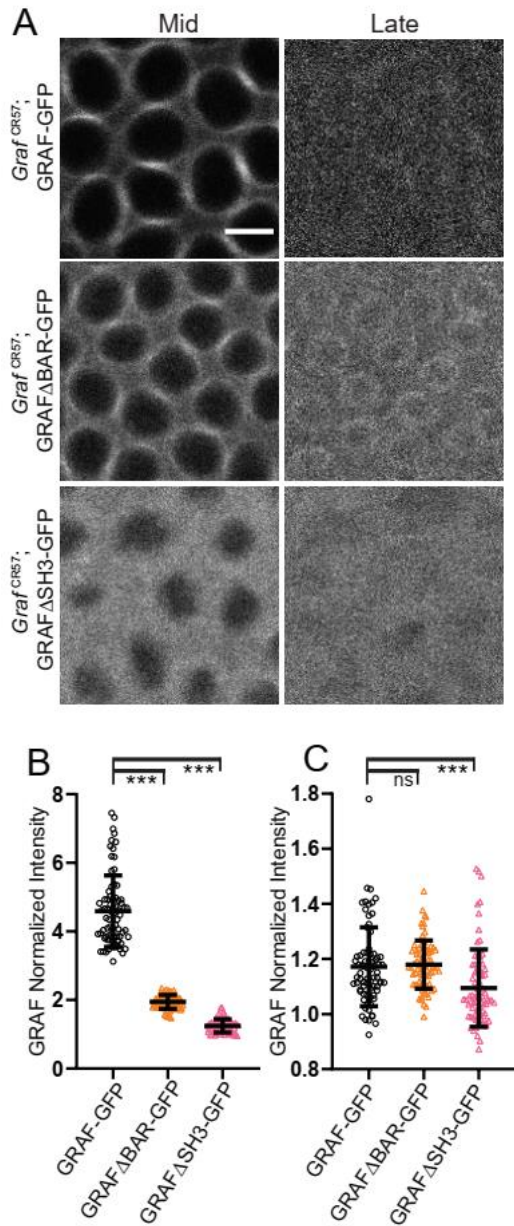


Figure 6.2: The BAR and SH3 domains are necessary for the GRAF on the ring.

(A) Distribution of the GFP tagged protein at the furrow tip in *Graf^{CR57}*; GRAF-GFP, *Graf^{CR57}*; GRAFΔBAR-GFP, *Graf^{CR57}*; GRAFΔSH3-GFP at mid and late cellularization. *Graf^{CR57}*; GRAFΔBAR-GFP, *Graf^{CR57}*; GRAFΔSH3-GFP show cytoplasmic signal during mid cellularization when compared to control. Scale bar: 5μm. **(B-C)** Quantification of enrichment of the GRP signal on the membrane relative to the cytosol at **(B)** mid and **(C)** late cellularization. *Graf^{CR57}*; GRAFΔBAR-GFP is significantly reduced during mid stages and

it becomes non-significant during late stages. *Graf*^{CR57}; GRAF Δ SH3-GFP show reduced signal at mid and late cellularization. n=75 rings, 5 rings per time point, 5 time points per embryo, 3 embryos of all genotypes. Data represented as mean \pm s.d. ns, non-significant, ***P<0.001, two-tailed Mann Whitney test.

6.3.4 The PH and RhoGAP domains are important for the dissociation of GRAF from the ring.

In order to dissect the effect of the particular domain in dissociating GRAF protein from the furrow tip during cellularization, we used the maternally expressed GFP tagged domain deletion transgenes in the *Graf*^{CR57} background. In *Graf*^{CR57}; GRAF-GFP the protein is enriched at the furrow tip during mid stage and then gradually dissociates during late cellularization. In this experiment, we checked PH and Rho-GAP domain deletion recruitment and its role in dissociation from the ring during mid and late cellularization. We observed GRAF Δ PH-GFP protein showing more spread signal at the contractile ring when compared to GRAF-GFP during mid cellularization. In contrast, GRAF Δ PH-GFP protein signal is retained at the ring during late cellularization when compared to the *Graf*^{CR57}; GRAF-GFP (Figure 6.3A). GRAF Δ PH-GFP shows significantly reduced intensity during mid cellularization when compared to control (Figure 6.3B). In contrast, the intensity was significantly higher when compared to GRAF-GFP intensity during late cellularization (Figure 6.3B).

Similar to GRAF Δ PH-GFP, we observed that GRAF Δ RhoGAP-GFP protein shows enriched signal with intense punctae at the furrow tip when compared to GRAF-GFP during mid cellularization. It retains signal with punctae during late cellularization when compared to the GRAF-GFP (Figure 6.3A). GRAF Δ RhoGAP-GFP shows significantly increased intensity during mid and late cellularization when compared to control (Figure 6.3 B,C). Thus, GRAF Δ RhoGAP-GFP shows higher enrichment consistently throughout mid and late cellularization relative to GRAF-GFP.

In summary, both PH and Rho-GAP domains of GRAF protein are required for the dissociation of the protein from the furrow tip during late cellularization.

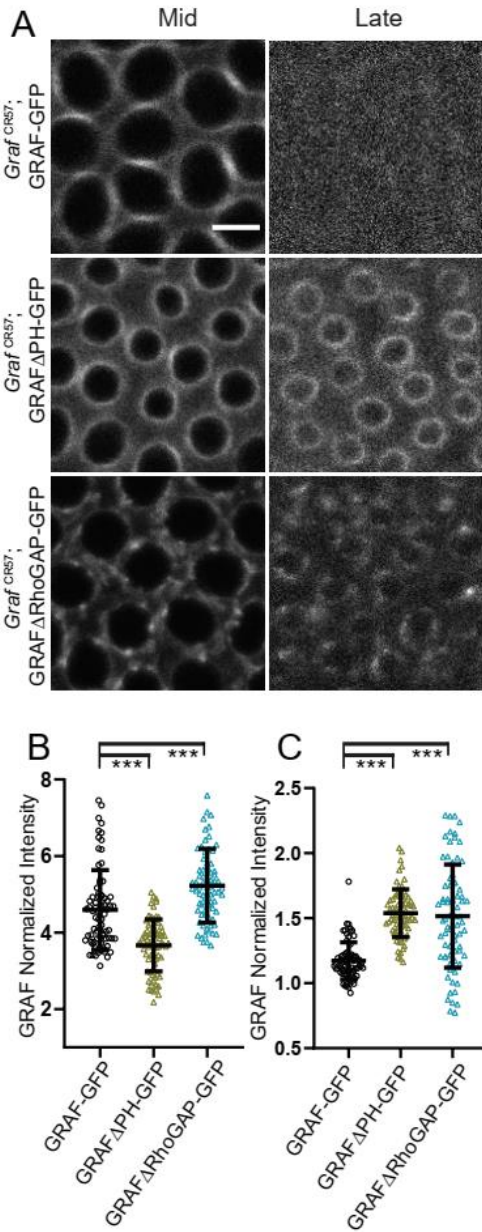


Figure 6.3: The PH and RhoGAP domains are important for the dissociation of GRAF from the ring.

(A) Distribution of the GFP tagged protein at the furrow tip in *Graf^{CR57}*; GRAF-GFP, *Graf^{CR57}*; GRAFΔPH-GFP, *Graf^{CR57}*; GRAFΔRhoGAP-GFP at mid and late cellularization. *Graf^{CR57}*; GRAFΔPH-GFP, *Graf^{CR57}*; GRAFΔRhoGAP-GFP show retained signal during late cellularization when compared to control. Scale bar: 5μm. **(B-C)** Quantification of enrichment of the GRP signal on the membrane relative to the cytosol at **(B)** mid and **(C)** late cellularization. *Graf^{CR57}*; GRAFΔPH-GFP show significantly reduced signal at mid cellularization and enhanced signal at late cellularization. *Graf^{CR57}*; GRAFΔRhoGAP-GFP shows significantly enhanced signal at mid and late cellularization. n=75 rings, 5 rings per time point, 5 time points

per embryo, 3 embryos of all genotypes. Data represented as mean±s.d. ***P<0.001, two-tailed Mann Whitney test.

6.4 Conclusion and discussion

The domains of GRAF are each required for restricting Myosin II dependent contractility. We find that the loss of each domain shows Myosin II dependent hypercontractility. SH3 and BAR domains of GRAF regulate its recruitment at the furrow tip during mid cellularization whereas RhoGAP and PH domains regulate the protein dissociation during late cellularization (Figure 6.4). The loss of BAR and SH3 domain may indirectly lead to decrease in RhoGAP activity which is required at the furrow tip thereby causing hyper contractility. In addition, the loss of PH and RhoGAP domains deletion results in increased localization at the furrow tip and hyper contractility, possibly due to increased RhoGAP activity. All domains rescue the hyper contractility defect as compared to the *Graf* mutant. This indicates that GRAF inhibits ring constriction through multiple mechanisms and not just by mechanism of the RhoGAP activity.

The RhoGAP domain activity is likely to be important in regulating constriction based on the hyper constriction defect being the most severe and closer to the *Graf* mutant. The SH3 domain also seems to play a crucial role in constriction and is needed for the recruitment of some unknown protein interactor(s) which in turn regulate constriction. The BAR and PH domains play important roles in regulating ring constriction might function at membrane curvature or binding regions of furrow tip. Thus, GRAF multi-domain architecture is likely to regulate its own RhoGAP activity, Myosin II activity, GRAF membrane recruitment and coordinate the recruitment of other contractile ring proteins during contractile ring formation and constriction.

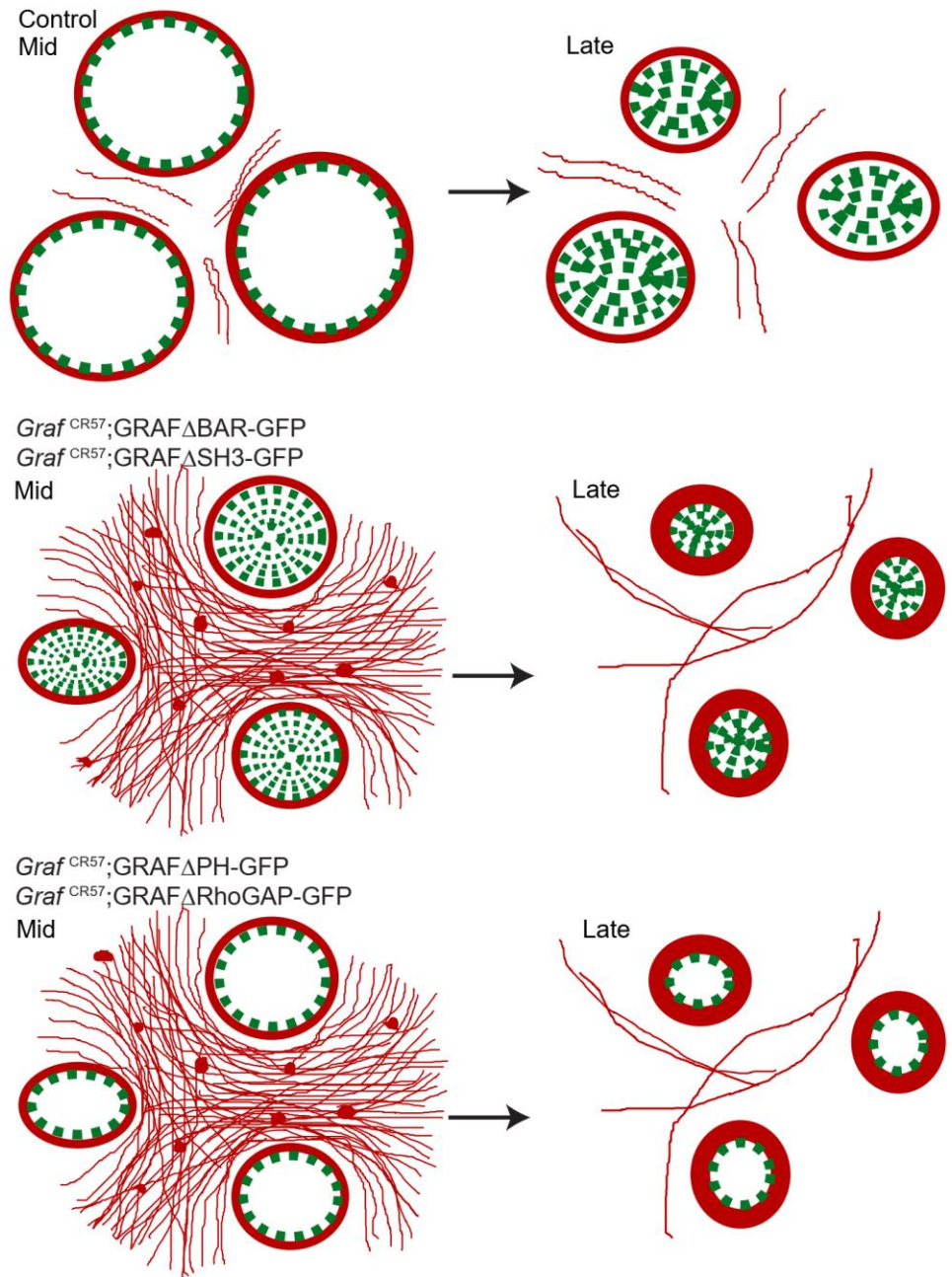


Figure 6.4: GRAF domains are necessary for Myosin II dependent ring constriction. GRAF recruitment regulates Myosin II levels needed for actomyosin assembly and constriction in control embryos. The BAR and SH3 domains of GRAF regulate its recruitment to the furrow tip during mid stage whereas PH and RhoGAP domain controls the dissociation of protein during late stage

Lipid co-sedimentation assay of GRAF1 BAR and PH shows the highest binding towards PI(4,5)P2-enriched liposomes. GRAF1 PH domain mutation (K277E/R278Q) significantly reduced binding to PI(4,5)P2 *in vitro* and impaired membrane recruitment in HeLa cells (Holst et al., 2017). These domains work together to generate and stabilize endocytic tubules *in vivo* (Lundmark et al., 2008). GRAF1 BAR domain containing point mutation (KK131/132EE) does not recruit to tubular membrane structures and is cytoplasmic. This suggests that the BAR domain is sensitive towards membrane curvature. The mislocalization of the protein seen in the BAR domain deletion might be indicative of a failure in curvature sensing at the furrow tip during cellularization.

The phospholipid, PI(3,4,5)P2 is enriched at the base of contractile rings in the slow phase and its presence is important for limiting actomyosin contractility and ring constriction (Reversi et al., 2014). Bottleneck protein is a key regulator of actin organization in cellularization (Schejter & Wieschaus, 1993b). *Bottleneck* mutants show hyper constriction and sustained Myosin II recruitment at the furrow in cellularization, similar to GRAF mutant embryos. An increase in PI(4,5)P2 leads to a phenotype of hyper constriction similar to Bottleneck and GRAF mutant embryos (Reversi et al., 2014). *In vitro* studies suggest that GRAF BAR and PH domains act as a structural unit to regulate membrane curvature and binding. The BAR and PH domains of GRAF show interaction with PI(4,5)P2 containing liposomes (G. J. Doherty & Lundmark, 2009; Holst et al., 2017; Lundmark et al., 2008). Thus, GRAF BAR and PH domain are likely to maintain PI(4,5)P2 levels to regulate constriction. The 50% penetrance defects shown by the hypercontractility phenotype in both *Graf*^{CR57}; GRAF Δ BAR-GFP and *Graf*^{CR57}; GRAF Δ PH-GFP provides clues related to some compensation in absence of either domain. Thus, GRAF BAR and PH domain might work synergistically as reported by other F-BAR domain proteins.

Interestingly SH3 domain deletion causes complete mislocalization of the protein throughout cellularization. The reason for this mislocalization is that GRAF SH3 domain is required for protein-protein interaction and hence contribute towards further hyper-constriction defects. Previous studies have shown using pulldown assay that GRAF C-terminal SH3 interacts with focal adhesion kinase which regulates cortical actin and stress

fibers in mammalian cells (Hildebrand et al., 1996; Luo et al., 2017). The GRAF SH3 domain may interact with key actin regulatory proteins and regulate its recruitment to the ring. Graf1 SH3 domain used as bait for rat brain cytosol is shown to interact with Dynamin, GIT1 and FAK (J. T. Doherty et al., 2011; Häsler et al., 2020; Lundmark et al., 2008). Thus, it is possible that Dynamin is required for the membrane recruitment of GRAF. Another binding partner of the SH3 domain could be actin-binding and cross-linker proteins which are crucial for regulating actin-dependent contractility. Depletion of one of the actin crosslinkers, Cheerio, causes hyper constriction defects (Krueger et al., 2019) which phenocopies *Graf* mutant. Hence, Cheerio could be a potential interactor that might function in GRAF recruitment. In addition, this domain shows interaction with Rab-binding proteins such as WDR44 and MICAL1 which allows GRAF mediated trafficking (Häsler et al., 2020). In summary, the recruitment defect seen in SH3 domain deletion is likely due to the perturbation in its interaction with a wide range of endocytic regulators, actin regulators and trafficking molecules. In contrast to recruitment defects, SH3 domain deletion provides less severe hyper constriction defects as compared to loss of the RhoGAP domain. This could be due to the better resistance towards hyper constriction contributed by the RhoGAP domain regulating Rho-GTP activity which partially rescues the hypercontractility defect even in the absence of the SH3 domain.

In vitro studies have shown an autoinhibitory interaction between the BAR-PH and RhoGAP domains (Eberth et al., 2009). It is possible that in the absence of the RhoGAP domain, the BAR domain is released from autoinhibition to promote more stable recruitment of GRAF protein. A similar effect on releasing autoinhibition of RhoGAP domain is likely to occur on the loss of BAR and PH domain respectively. RhoGAP domain deletion shows the maximum hyper constriction defect when compared to control and other domain deletions. So, this suggests that the function of the RhoGAP domain involved in regulating Rho-GTP levels, which in turn activates Myosin II, plays a predominant role in regulating the constriction process.

This analysis suggests that the GRAF multi-domain protein is likely to have intramolecular interactions and autoregulation which contribute towards regulation of

constriction through Myosin II activation. BAR and SH3 domains may act as one functional unit which regulates the initial recruitment to the furrow tip, acting in tandem with unknown interacting partners. PH and RhoGAP domains act as another functional unit which is necessary for the dissociation of protein from furrow tip.

CHAPTER 7

Thesis summary and future perspectives

GRAF protein recruitment is enriched from early to mid stages and becomes cytoplasmic during late stages of cellularization. GRAF protein function is involved in inhibiting ring constriction. *Graf* mutants give rise to hyper constriction defects that result in squeezing nuclei and thus are important in maintaining nuclear integrity (Figure 7.1A). Hyper-constriction is due to increased tension in the actomyosin network which is revealed by increased recoil velocity during laser ablations. GRAF-OE shows loss of constriction defects in all stages of cellularization. Taken altogether, *Graf* mutant and GRAF overexpression show antagonistic phenotypes leading to the conclusion that GRAF is a regulator of contractile machinery during the *Drosophila* cellularization.

GRAF also regulates Dia, Anillin, Peanut levels and recruitment at the contractile ring (Figure 7.1B). GRAF protein shows colocalization with Myosin II and Rho-GTP during the early and mid stages. Rho-GTP and Myosin II signal at the furrow canal persists during late cellularization whereas GRAF is lost from the furrow canal. *Graf* depletion shows sustained Rho-GTP levels which causes increased Myosin II which promotes hypercontractility defects. This is further checked by RhoGAP domain deletion which is likely to have increased Rho-GTP levels giving rise to hyper constriction defects. GRAF is a bonafide Rho-GAP molecule acting along with RhoGEF2 to regulate Rho-GTP levels. Furthermore, the evidence in regulating Rho GDP-GTP cycling is provided by the suppression of *Graf* depletion hyper constriction by RhoGEF2 depletion. GRAF depletion along with ROK depletion shows relaxed rings and suppresses the hypercontractility phenotype in *Graf* mutant embryos. GRAF mediated contractility is dependent on Myosin II activation by Rho-kinase. Taken together, our study dissects the mechanism of spatio-temporal recruitment of GRAF which is necessary to provide appropriate RhoA levels to execute regulated constriction during cellularization (Figure 7.1C).

GRAF domain analysis provides further insights into each domain's contribution towards hyper constriction defects during mid and late stages. These domain deletions show increased Myosin II, suggesting that each domain is either directly or indirectly involved in regulating the Myosin II dependent constriction process. BAR and SH3 domains are required to guide protein recruitment at the contractile ring during mid stage whereas PH and RhoGAP domains are crucial for the dissociation of the protein from the ring during the late stage (Figure 7.1D). Finally, GRAF acts as a negative regulator which is likely to mediate a systematic transition from contractile ring formation to ring constriction, regulating the precise timings of the actomyosin contraction process.

7.1 Recruitment of GRAF: association and dissociation dynamics at the contractile ring

RhoGEF (Pbl) is shown to bind Rho-GTPase-activating protein (RacGAP50C) of the centralspindlin complex and preferentially recruit at the contractile ring (Crest et al., 2012; Somers et al., 2003). Rho1 activation is initiated once RhoGEF2 gets recruited at the contractile ring. In contrast, how GRAF recruitment is temporally controlled is still unknown.

Multi domain proteins like GRAF containing membrane binding and RhoGAP domains are poised to regulate RhoA-GTP levels in a highly regulated manner — spatially and temporally— during an actomyosin contractility driven process. A study on dormant cells, demonstrated that the activation of PI3K pathway and attachment of integrin $\alpha 5\beta 1$ to fibronectin result in GRAF recruitment. In contrast, integrin $\alpha 5\beta 1$ and PI3K inhibition lead to reduced membrane recruitment of Graf (Barrois et al, Cancer Microenviron. 2009). PI3K and FAK mutants may be upstream molecules which lead to GRAF recruitment during cellularization. Another strategy which can be employed is to find the possible interactors of GRAF protein using a pull down assay, which could provide the potential upstream molecules regulating its recruitment dynamics.

GRAF BAR domain has been shown to play a role in clathrin independent endocytosis. The small GTPase Arf1 recruits the human homologue of GRAF, ArhGAP10

in clathrin independent endocytosis of GPI anchored proteins (Kumari & Mayor, 2008). Interestingly, endocytosis at the cellularization furrow plays a role in controlling Rho1 activity. Mutants of ArfGEF, *steppke* in *Drosophila* are deficient in endocytosis and shows enhanced Rho1 induced hyper constriction phenotype in cellularization. It is possible that in *steppke* mutants GRAF recruitment is perturbed which gives rise to similar hyper constriction defects through the Rho pathway. Thus, *Steppke* might act as an upstream molecule regulating GRAF recruitment dynamics.

Future studies will be focused on finding upstream proteins that are involved in GRAF recruitment at the contractile ring and its dissociation from the contractile ring. It would be interesting to check whether the same upstream molecules are sufficient to fine tune the association and dissociation of GRAF or whether it requires different molecules.

7.2 GRAF function in regulating actin network during cellularization

This study focuses on dissecting the pathway where GRAF protein is involved in activating Myosin II to regulate constriction. Future studies can focus on the function of actin regulators in orchestrating ring constriction in the *Graf* mutant background. The C-terminally deleted SH3 mutant of GRAF may interact with key actin regulatory proteins and regulate its recruitment to the ring. Previous studies have shown that GRAF colocalizes to cortical actin and stress fibers, with paxillin and FAK at focal adhesions in mammalian cells. GRAF recruitment leads to stabilized cortical actin and cell spreading (Barrios & Wieder, 2009). GRAF SH3 domain was shown to directly interact with FAK protein involved in regulating actin stress fibers in migrating cells (Hildebrand et al., 1996; Luo et al., 2017). In our study, we have shown that the SH3 domain of GRAF is necessary for its membrane recruitment. This recruitment is likely dependent on some interacting partners. Hence, biochemical assays involving pulldown followed by mass spectrometry can be aimed at finding interacting partners of the GRAF SH3 domain.

The ring constriction process involves the actomyosin network containing actin regulatory proteins comprising nucleators, crosslinkers, depolymerizing proteins, scaffold

proteins and phospholipid regulatory proteins (Adam et al., 2000; Afshar et al., 2000; Christine M. Field et al., 2005; Grosshans et al., 2005; Krueger et al., 2019; Manos Mavrakis et al., 2014). Similar to *Graf* mutants, ring hyper constriction has been seen in mutants of actin cross-linker proteins *Cheerio* and *Bottleneck*. On the other hand, *Fimbrin* mutant, also an actin cross-linker protein, phenocopies GRAF overexpression, showing a lack of constriction in cellularization (Krueger et al., 2019). Actin crosslinkers such as *Fimbrin* show retention of polygonal shape during late cellularization whereas *Bottleneck* and *Cheerio* mutants show hyper constriction defects during early stage (Krueger et al., 2019). Mutants in F-actin stabilising proteins *Anillin* and the septin *Peanut* show defects in a ring shape (Christine M. Field et al., 2005; Manos Mavrakis et al., 2014). Mutants of actin nucleators such as *Diaphanous* cause decreased constriction and ingression defects during cellularization (Afshar et al., 2000; Grosshans et al., 2005). The role of these actin crosslinkers and nucleator in influencing actin architecture can be checked in the background of *Graf* depletion in regulating constriction. Another aspect to be checked is F-actin organization and dynamics in defective hyper constricted rings at high resolution in *Graf*^{CR57} mutants.

7.3 GRAF interaction with cadherin and associated proteins involved in membrane trafficking regulation during cellularization

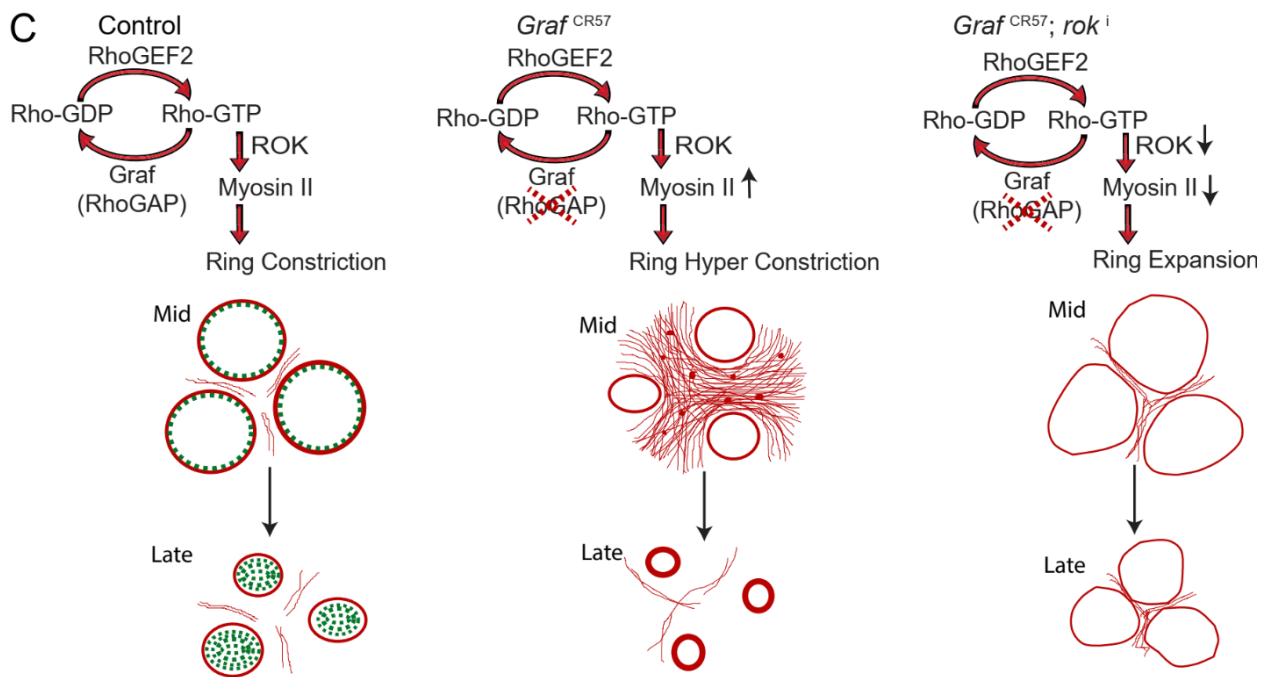
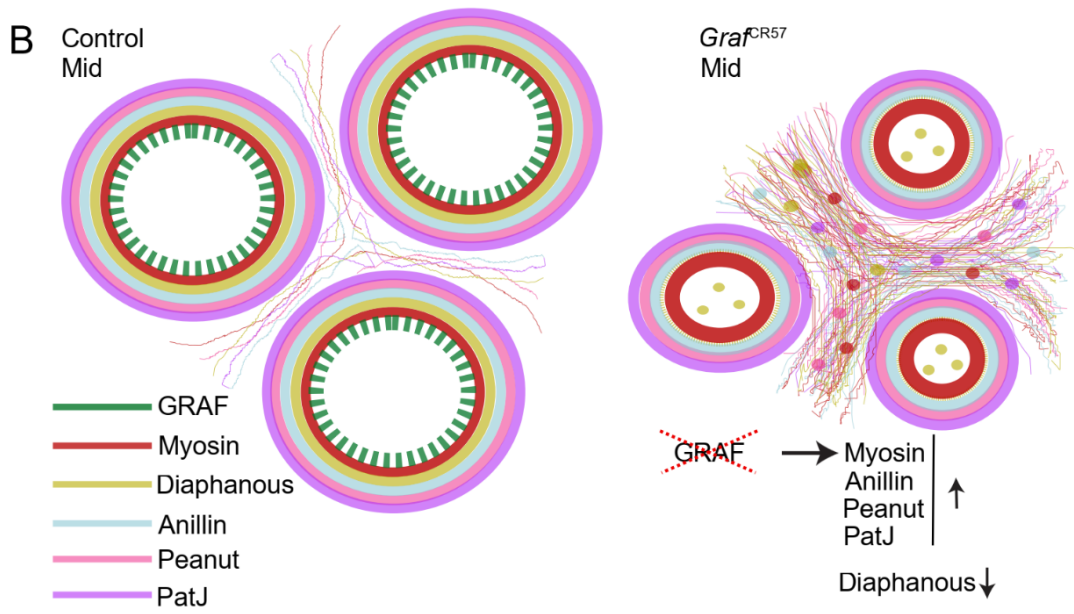
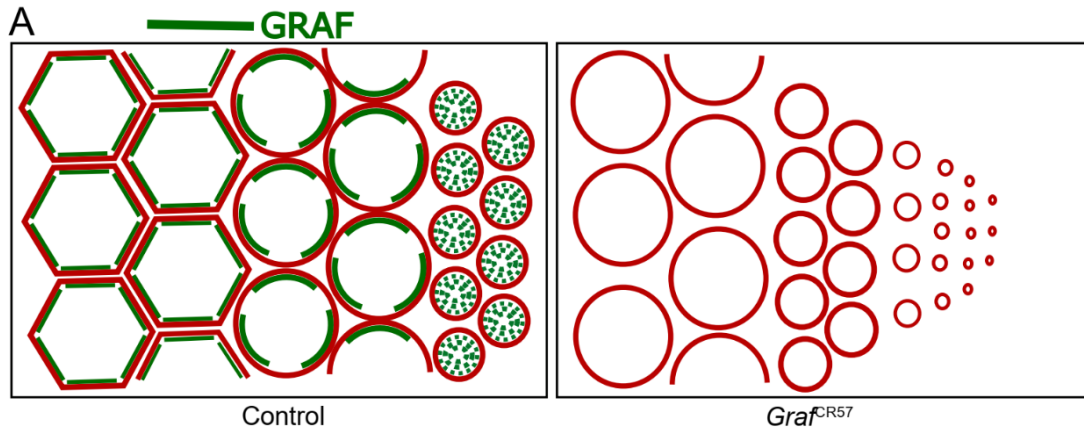
GRAF was shown to recruit to cell-cell junctions that overlap with E-cad. Its depletion results in attaining cell migrating ability with loss of epithelial integrity (Yao et al., 2015). In MCF10A cells, this epithelial E-cadherin is replaced by mesenchymal N-cadherin which is a hallmark of EMT transition (Regev et al., 2017). During cellularization, apicobasal polarity is being established in epithelial cells. Thus, it would be interesting to observe any disruption in epithelial integrity in *Graf* depletion background.

GRAF BAR-PH and GRAF2 knockdown show reduced export of neosynthesized E-cadherin. GRAF2 and Rab8 are colocalized with intracellular puncta of E-cadherin during vesicular trafficking (Häsler et al., 2020). C-GAP depletion disrupts E-cad localization which spreads across the apical surface compared to control (Mason et al., 2016). It is possible that *Graf* depletion causes E-cad localization defects during late

cellularization. The enriched apical E-cad can disrupt the actomyosin network required for constriction during ventral furrow invagination.

7.4 GRAF role in conventional cytokinesis

Modifications in human GRAF1 gene in the form of truncations, mutations, and deletions are associated with myeloid malignancies such as AML (acute myeloid leukaemia) and MDS (myelodysplastic syndrome) (Bojesen et al., 2006; Borkhardt et al., 2000; Panagopoulos et al., 2004; J. Qian et al., 2011; Z. Qian et al., 2010). In AML blood cells overproliferate whereas in MDS cells are not formed properly. *Drosophila Graf* mutant larvae show elevated plasmatocytes than control due to increased cellular proliferation (Kim et al., 2017). It could be possible that this increased cellular proliferation is due to cytokinetic defects. In cytokinesis, actomyosin is organized in a contractile ring and further gets contracted to form daughter cells. This study from specialized cellularization showing the spatio-temporal regulation of contractile rings can be further extended to cytokinetic cells. It will be necessary to elucidate how GRAF functions in cytokinesis—either by affecting Myosin II recruitment or activation. One can exploit the *Drosophila* mitotic domain, mitosis 14 stage which is found in the head region of the embryo to check for cytokinetic defects in *Graf* mutants.



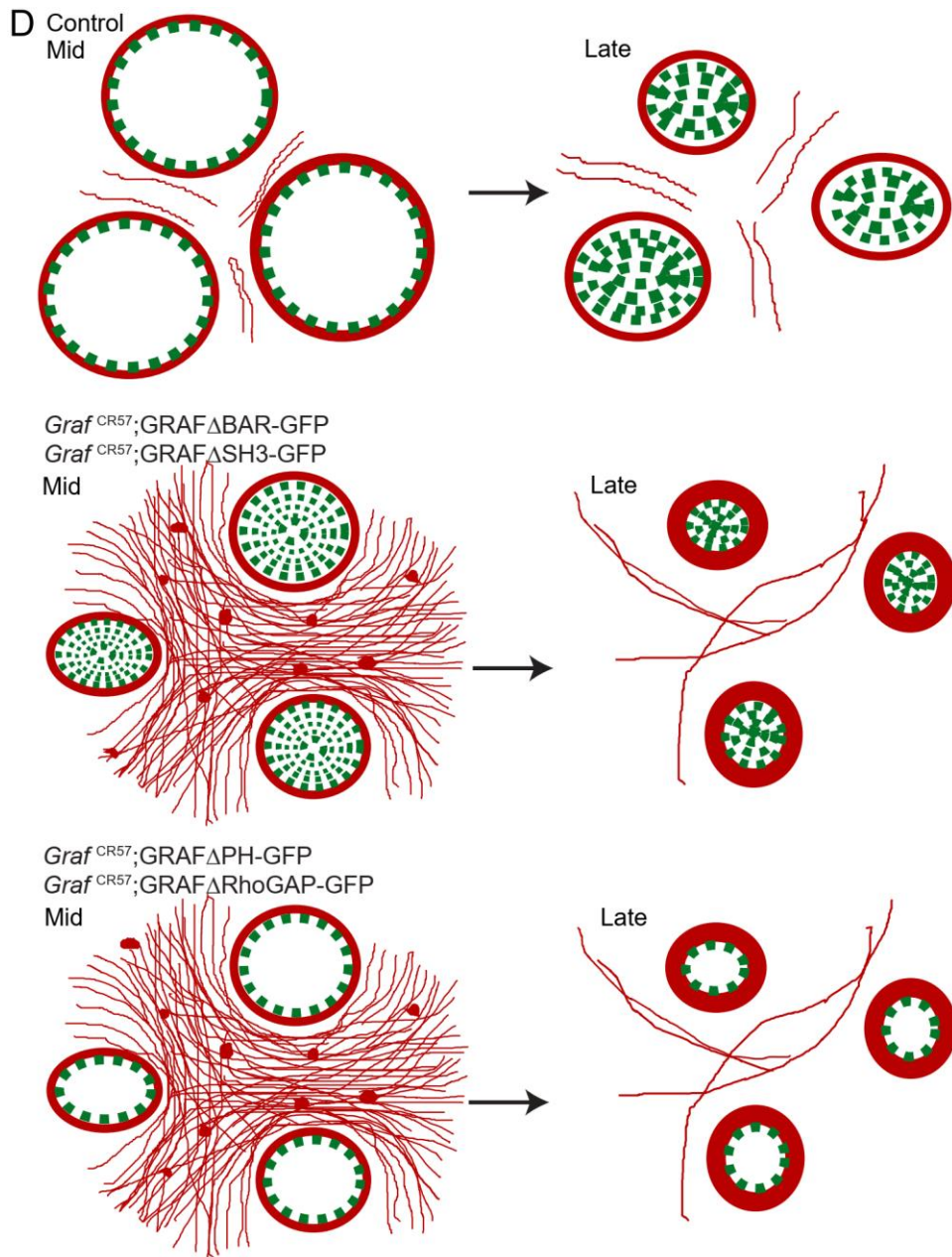


Figure 7.1: Summary models. (A) GRAF protein spatio-temporal recruitment transition from mid to late cellularization regulates contractility during the *Drosophila* cellularization. GRAF shows enrichment at the furrow tip till mid cellularization which could be directly involved in regulating the precise timings of actomyosin contraction process. (B) GRAF is required for recruitment of key contractile proteins during the *Drosophila* cellularization. *Graf* depletion shows sustained Myosin II, Anillin, Peanut and PatJ recruitment during late cellularization correlating with increased contraction in the ring. In contrast, Diaphanous get reduced in *Graf* mutants. (C) GRAF is a bona fide Rho-GAP protein that requires Myosin II activity for constriction during cellularization GRAF plays a role in regulating Rho-GTP levels as a RhoGAP to drive the contraction

process. *Graf* depletion shows a hyper constriction phenotype and Rok depletion suppresses the hyper constriction phenotype seen in *Graf* mutant embryos. *Graf* mutant embryos show Myosin II accumulation at the ring in mid and late cellularization and in the inter ring region in mid cellularization. **(D)** GRAF domains are necessary for Myosin II dependent ring constriction. GRAF recruitment regulates Myosin II levels needed for actomyosin assembly and constriction in control embryos. The BAR and SH3 domains of GRAF regulate its recruitment to the furrow tip during mid stage whereas PH and RhoGAP domain controls the dissociation of protein during late stage

Appendix

A.1 Screening based on RNAi mediated knockdown of BAR domain proteins and its assessment using embryonic lethality, phenotype and localization.

BAR domain proteins were selected based on embryonic developmental expression modENCODE data (modENCODE Consortium et al., 2010). The modENCODE development RNA-Seq data provides temporal mRNA expression data for specific genes during the development (modENCODE Consortium et al., 2010). Using 0-2 hr embryo expression profile, BAR domain proteins were selected on the basis of their expression profile in the early embryo. The shRNA of these BAR domain proteins were crossed with maternal nanosgal4 at 29°C to generate specific BAR domain protein knockdown during embryonic stages (Table A3). These BAR domain protein knockdown embryos were used to score for embryonic lethality after 48 hours at 29°C temperature. Among these BAR domain knockdown embryos, nostrin depleted embryos showed the highest lethality (98%) whereas MIM showed the lowest lethality (8.42%). In addition, specific BAR domain protein immunostaining shows localization in the syncytial and cellularization embryonic stages. Islet cell autoantigen-69 (ICA-69) staining shows puncta throughout cellularization and ASAP shows cytoplasmic puncta and membrane signal in syncytial stages. Centaurin beta1A (CenB1A) shows nuclear staining whereas RhoGAP92B shows membrane signal in cellularization (Table A). The phenotypes were assayed using phalloidin which mark F-actin in these BAR domain knockdown embryos. MIM knockdown embryos showed severe membrane ruffling along with punctate actin-rich structures. The pseudo cleavage membranes in these embryos were morphologically disorganized in the syncytial stages. Sorting nexin16 knockdown showed an increased cytoplasmic actin signal along with an absence of pseudocleavage furrows in the syncytial stages. RhoGAP92B shows shorter or defective furrows in syncytial stages (Figure 1). Further analysis is needed to check the efficient knockdown of these proteins using immunostaining and western blotting.

CenB1A CRISPR mutant embryos show apical actin aggregation defects during cellularization. During early cellularization, the apical most region is increased in size when compared to control. During mid cellularization, mutant embryos show huge actin aggregates that are present at the apical region when compared to control and are retained during late cellularization (Figure 2). Thus, Centaurin beta1A protein might be involved in the endocytosis which regulating membrane trafficking during cellularization.

BAR domain class	BAR domain protein	RNAi knockdown or CRISPR mutant		Localization
		Embryonic lethality [Control-7%(320)]	Phenotype	
F-BAR	Nostrin	98.86%(351)	Pre-blastoderm arrest	
PH/PX-BAR	Centaurin Beta1A	-	Apical actin clumps in cellularization	Nuclear signal
	ArfGAP with SH3 domain, ankyrin repeat and PH domain	-	-	Cytoplasm puncta and membrane signal in syncytial
	Sorting nexin 16	28.6% (300)	Cytoplasmic actin during syncytial	-
	Islet cell autoantigen 69	-	-	Puncta in cellularization
	GTPase regulator associated with focal adhesion kinase	80.45%(532)	Contractile ring defects	Membrane signal in cellularization
N-BAR	Endophilin B	24.6%(300)		
	RhoGAP92B	16%(325)	Membrane ruffling in syncytial	Membrane signal in cellularization
I-BAR	Missing in metastasis	8.42%(534)	Membrane ruffled with actin clumps	

Table A: BAR domain proteins screening based on embryonic lethality, phenotype and localization during *Drosophila* syncytial and cellularization stage. BAR domain proteins are classified based on the domain class such as F-BAR, PH/PX-BAR, N-BAR and I-BAR. The maternal knockdown embryos were used to carry out embryonic lethality. The defects were further checked using phalloidin staining and localization using antibody staining.

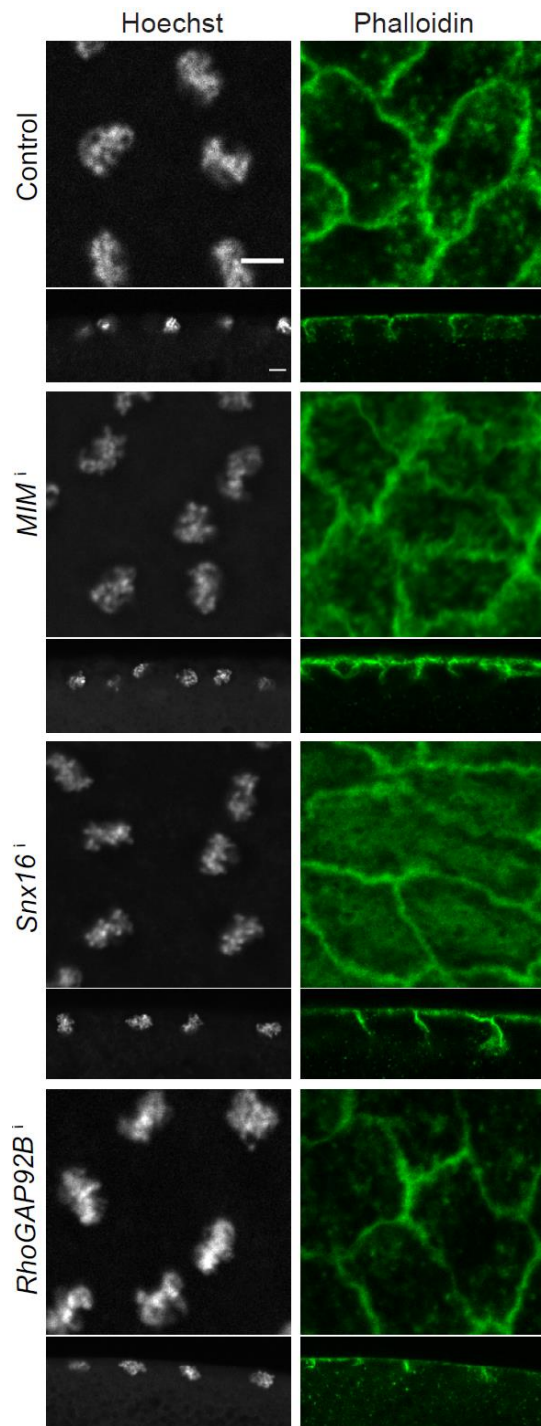


Figure 1: Knockdown of BAR domain proteins MIM, sorting nexin16 and RhoGAP92B show disorganized actin architecture. Phalloidin staining marks cortical F-actin in control embryos in cycle12 syncytial stages. In MIM knockdown embryos, loose cortical actin is observed with actin puncta in the cytoplasmic region (100%, n=9 embryos). In sorting nexin 16 depletion (100%, n=6 embryos), the diffuse cytoplasmic actin staining is observed whereas RhoGAP92B shows shorter furrows (37.5%, n=8 embryos)

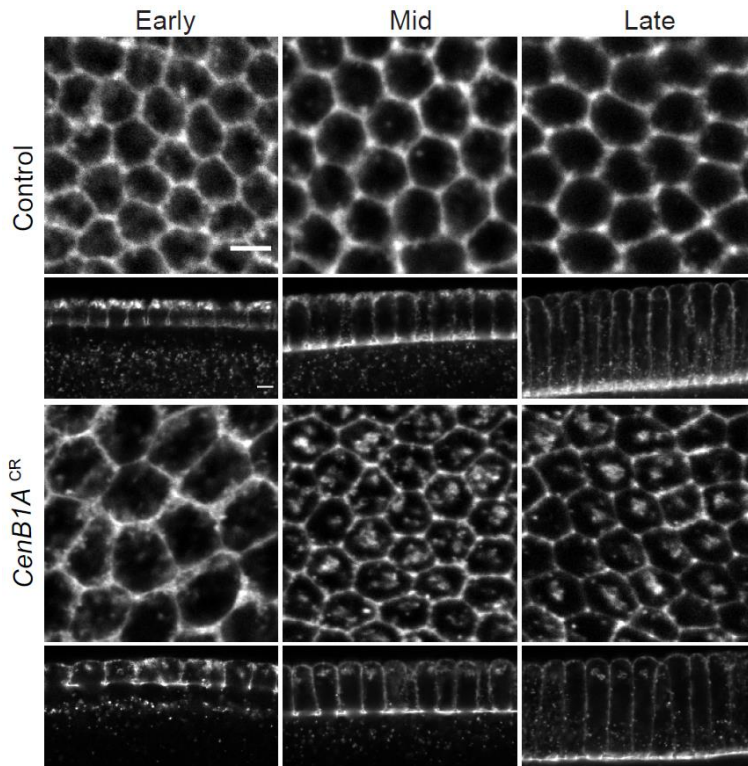


Figure 2: *CenB1A* mutant embryos shows actin clumps during mid and late cellularization. Control embryos show apical F-actin during cellularization. Apical actin aggregation with huge clumps are observed in centaurin beta 1a (77.41%, n=62 embryos) depletion during mid and late cellularization when compared to controls the apical most region is increased in size when compared to control.

A.2 RhoGAP domain proteins screening based on RNAi mediated knockdown to check for embryonic lethality.

The RhoGAP domain proteins screening were carried out using a maternal knockdown strategy where shRNA against RhoGAPs were crossed with *mat67;mat15 gal4* (Table C). The crosses were set up at 29°C temperature test for embryonic lethality at different time points-5 days old and 2 weeks old, at 29°C temperature. RhoGAP71E and RhoGAP19D provided the highest lethality when compared to others when 5 days old whereas RhoGAP1A and RhoGAP54D provided the highest lethality when compared to when 2 weeks old (Table B).

Female adults having tumbleweed knockdown did not lay any eggs whereas those with RhoGAP15B knockdown laid very few embryos. The F1 female flies of tumbleweed and RhoGAP15B were taken to check for ovary defects. The phalloidin staining reveals that cortical F-actin is collapsed and aggregated with ring canals in tumbleweed depletion (Figure 3). The compartments to form nurse cells were no longer present in tumbleweed depletion when compared to control. The actin aggregation in the form of huge clumps in the oocyte compartment is seen in RhoGAP15B knockdown when compared to control (Figure 3). Thus, ovary defects of tumbleweed and RhoGAP15B perturb oocyte development, thereby contributing towards defective egg-laying.

RhoGAP domain protein	Embryonic lethality(%)	
	5 days old	2 weeks old
RhoGAP5A	6.6 (330)	38.5 (200)
RhoGAP68F	5.8 (240)	13.0 (200)
OCRL	5.0 (216)	6.5 (200)
RhoGAP93B	3.3 (330)	31.6 (230)
RhoGAP54D	11.7 (230)	51.0 (200)
RhoGAP1A	18.0 (200)	69.0 (200)
RhoGAPp190	9.0 (200)	Did not lay sufficient eggs
RhoGAP18B	6.0 (200)	Did not lay sufficient eggs
RhoGAP71E	50.5 (105)	Did not lay sufficient eggs
RhoGAP19D	58.0 (200)	Did not lay sufficient eggs
RhoGAP15B	Not done	84.5 (238)
Tumble weed	Did not lay sufficient eggs	Did not lay sufficient eggs
Control	5.3(132)	20(192)

Table B: RhoGAP domain proteins screening based on embryonic lethality from 5 days and 2 weeks old flies at 29°C temperature. RhoGAP71E and RhoGAP19D provide the highest lethality when compared to others at 5 days old whereas RhoGAP1A and RhoGAP15B provide the highest lethality when compared to others at 2 weeks old.

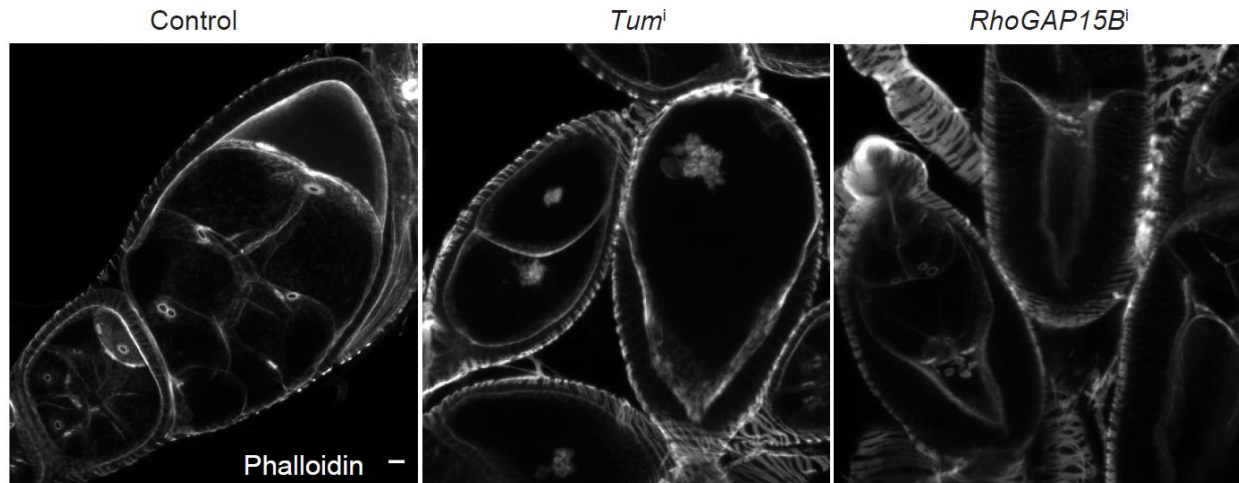


Figure 3: Tumbleweed knockdown in the ovary shows nurse membrane collapse and actin aggregation in developing oocyte in RhoGAP15B depletion. Control ovary shows F-actin marking the ring canal and membrane. Severe defects were observed affecting membrane and ring canal collapse in tumbleweed depletion (100%, n=56 ovarioles) when compared to control. Actin clumps are observed in developing oocytes in RhoGAP15B depletion (85.7%, n=28 ovarioles) when compared to control.

Stock	Genotype	Source/Reference
1	Canton-S	Lab stock originally obtained Bloomington <i>Drosophila</i> Stock Center
2	<i>nanos</i> -Gal4	Lab stock
3	w; <i>mat67</i> -Gal4; <i>mat15</i> -Gal4	Girish Ratnaparkhi, IISER, Pune, India
4	y[1] v[1]; P{y[+t7.7] v[+t1.8]=TRiP.GL01145}attP2/TM3, Sb[1] (Nostrin shRNA)	BDSC, #42776
5	y[1] sc[*] v[1] sev[21]; P{y[+t7.7]}	BDSC, #38992

	v[+t1.8]=TRiP.HMS019 08}attP40 (Sorting nexin16 shRNA)	
6	y[1] sc[*] v[1] sev[21]; P{y[+t7.7] v[+t1.8]=TRiP.HMS012 85}attP2 (EndophilinB shRNA)	BDSC, #34935
7	y[1] sc[*] v[1] sev[21]; P{y[+t7.7] v[+t1.8]=TRiP.HMS002 68}attP2 (RhoGAP92B shRNA)	BDSC, #33391
8	y[1] sc[*] v[1] sev[21]; P{y[+t7.7] v[+t1.8]=TRiP.GL015 68}attP40 (MIM shRNA)	BDSC, #43223
9	y1 v1; P{TRiP.HMJ23704}attP40/CyO (RhoGAP5A shRNA)	BDSC, #62349
10	y1 sc* v1; P{TRiP.GL00580}attP2 (RhoGAP68F shRNA)	BDSC, #36620
11	y1 sc* v1; P{TRiP.HMS01201}attP2/TM3, Sb1 (OCRL shRNA)	BDSC, #34722
12	y1 sc* v1; P{TRiP.HMS01440}attP2 (RhoGAP93B shRNA)	BDSC, #35027
13	y1 v1; P{TRiP.HMS03522}attP40 (RhoGAP54D shRNA)	BDSC, #54051
14	y[1] sc[*] v[1]; P{y[+t7.7] v[+t1.8]=TRiP.HMS00267} attP2/TM3, Sb[1] (RhoGAP1A shRNA)	BDSC, #33390
15	y1 v1; P{TRiP.HMJ02052}attP40 (RhoGAPp190 shRNA)	BDSC, #43987
16	y1 v1; P{TRiP.HMS02391}attP40/CyO (RhoGAP18B shRNA)	BDSC, #56856

17	y1 sc* v1; P{TRiP.HMS00412}attP2 (RhoGAP71E shRNA)	BDSC, #32417
18	y1 sc* v1; P{TRiP.HMS00352}attP2 (RhoGAP19D shRNA)	BDSC, #32361
19	y1 v1; P{TRiP.HMJ02093}attP40/CyO (RhoGAP15B shRNA)	BDSC, #42527
20	y1 sc* v1; P{TRiP.HMS01417}attP2 (Tumbleweed shRNA)	BDSC, #35007

Table C: *Drosophila* stocks used for BAR domain and RhoGAP proteins screening

Bibliography

- Abou-Kheir, W., Isaac, B., Yamaguchi, H., & Cox, D. (2008). Membrane targeting of WAVE2 is not sufficient for WAVE2-dependent actin polymerization: a role for IRSp53 in mediating the interaction between Rac and WAVE2. In *Journal of Cell Science* (Vol. 121, Issue 3, pp. 379–390). <https://doi.org/10.1242/jcs.010272>
- Adam, J. C., Pringle, J. R., & Peifer, M. (2000). Evidence for functional differentiation among *Drosophila* septins in cytokinesis and cellularization. *Molecular Biology of the Cell*, 11(9), 3123–3135.
- Adams, R. R., Tavares, A. A., Salzberg, A., Bellen, H. J., & Glover, D. M. (1998). pavarotti encodes a kinesin-like protein required to organize the central spindle and contractile ring for cytokinesis. *Genes & Development*, 12(10), 1483–1494.
- Afshar, K., Stuart, B., & Wasserman, S. A. (2000). Functional analysis of the *Drosophila* diaphanous FH protein in early embryonic development. *Development*, 127(9), 1887–1897.
- Agarwal, P., & Zaidel-Bar, R. (2019). Principles of Actomyosin Regulation In Vivo. *Trends in Cell Biology*, 29(2), 150–163.
- Ahmed, S., Bu, W., Lee, R. T. C., Maurer-Stroh, S., & Goh, W. I. (2010). F-BAR domain proteins: Families and function. *Communicative & Integrative Biology*, 3(2), 116–121.
- Alberts, A. S. (2001). Identification of a Carboxyl-terminal Diaphanous-related Formin Homology Protein Autoregulatory Domain. In *Journal of Biological Chemistry* (Vol. 276, Issue 4, pp. 2824–2830). <https://doi.org/10.1074/jbc.m006205200>
- Amano, M., Ito, M., Kimura, K., Fukata, Y., Chihara, K., Nakano, T., Matsuura, Y., & Kaibuchi, K. (1996). Phosphorylation and Activation of Myosin by Rho-associated Kinase (Rho-kinase). In *Journal of Biological Chemistry* (Vol. 271, Issue 34, pp. 20246–20249). <https://doi.org/10.1074/jbc.271.34.20246>
- Amano, M., Nakayama, M., & Kaibuchi, K. (2010). Rho-kinase/ROCK: A key regulator of the cytoskeleton and cell polarity. *Cytoskeleton*, 67(9), 545–554.

- Ambroggio, E., Sorre, B., Bassereau, P., Goud, B., Manneville, J.-B., & Antony, B. (2010). ArfGAP1 generates an Arf1 gradient on continuous lipid membranes displaying flat and curved regions. *The EMBO Journal*, *29*(2), 292–303.
- Andrianantoandro, E., & Pollard, T. D. (2006). Mechanism of actin filament turnover by severing and nucleation at different concentrations of ADF/cofilin. *Molecular Cell*, *24*(1), 13–23.
- Aspenström, P. (1997). A Cdc42 target protein with homology to the non-kinase domain of FER has a potential role in regulating the actin cytoskeleton. In *Current Biology* (Vol. 7, Issue 7, pp. 479–487). [https://doi.org/10.1016/s0960-9822\(06\)00219-3](https://doi.org/10.1016/s0960-9822(06)00219-3)
- Aspenström, P. (2009). Roles of F-BAR/PCH proteins in the regulation of membrane dynamics and actin reorganization. *International Review of Cell and Molecular Biology*, *272*, 1–31.
- Aspenström, P. (2019). BAR Domain Proteins Regulate Rho GTPase Signaling. *Advances in Experimental Medicine and Biology*, *1111*, 33–53.
- Bai, X., Lenhart, K. C., Bird, K. E., Suen, A. A., Rojas, M., Kakoki, M., Li, F., Smithies, O., Mack, C. P., & Taylor, J. M. (2013). The smooth muscle-selective RhoGAP GRAF3 is a critical regulator of vascular tone and hypertension. *Nature Communications*, *4*, 2910.
- Barmchi, M. P., Rogers, S., & Häcker, U. (2005). DRhoGEF2 regulates actin organization and contractility in the *Drosophila* blastoderm embryo. In *Journal of Cell Biology* (Vol. 168, Issue 4, pp. 575–585). <https://doi.org/10.1083/jcb.200407124>
- Barrett, K., Leptin, M., & Settleman, J. (1997). The Rho GTPase and a Putative RhoGEF Mediate a Signaling Pathway for the Cell Shape Changes in *Drosophila* Gastrulation. In *Cell* (Vol. 91, Issue 7, pp. 905–915). [https://doi.org/10.1016/s0092-8674\(00\)80482-1](https://doi.org/10.1016/s0092-8674(00)80482-1)
- Barr, F. A., & Gruneberg, U. (2007). Cytokinesis: Placing and Making the Final Cut. In *Cell* (Vol. 131, Issue 5, pp. 847–860). <https://doi.org/10.1016/j.cell.2007.11.011>
- Barrios, J., & Wieder, R. (2009). Dual FGF-2 and Intergrin $\alpha 5\beta 1$ Signaling Mediate GRAF-Induced RhoA Inactivation in a Model of Breast Cancer Dormancy. In *Cancer Microenvironment* (Vol. 2, Issue 1, pp. 33–47). <https://doi.org/10.1007/s12307-009-0019-6>
- Basant, A., & Glotzer, M. (2018). Spatiotemporal Regulation of RhoA during Cytokinesis. *Current Biology: CB*, *28*(9), R570–R580.

- Baumgart, T., Capraro, B. R., Zhu, C., & Das, S. L. (2011). Thermodynamics and mechanics of membrane curvature generation and sensing by proteins and lipids. *Annual Review of Physical Chemistry*, 62, 483–506.
- Bement, W. M., Benink, H. A., & von Dassow, G. (2005). A microtubule-dependent zone of active RhoA during cleavage plane specification. *The Journal of Cell Biology*, 170(1), 91–101.
- Bement, W. M., Leda, M., Moe, A. M., Kita, A. M., Larson, M. E., Golding, A. E., Pfeuti, C., Su, K.-C., Miller, A. L., Goryachev, A. B., & von Dassow, G. (2015). Activator–inhibitor coupling between Rho signalling and actin assembly makes the cell cortex an excitable medium. In *Nature Cell Biology* (Vol. 17, Issue 11, pp. 1471–1483). <https://doi.org/10.1038/ncb3251>
- Bement, W. M., Miller, A. L., & von Dassow, G. (2006). Rho GTPase activity zones and transient contractile arrays. *BioEssays: News and Reviews in Molecular, Cellular and Developmental Biology*, 28(10), 983–993.
- Bertin, A., McMurray, M. A., Thai, L., Garcia, G., 3rd, Votin, V., Grob, P., Allyn, T., Thorner, J., & Nogales, E. (2010). Phosphatidylinositol-4,5-bisphosphate promotes budding yeast septin filament assembly and organization. *Journal of Molecular Biology*, 404(4), 711–731.
- Bezanilla, M., Forsburg, S. L., & Pollard, T. D. (1997). Identification of a second myosin-II in *Schizosaccharomyces pombe*: Myp2p is conditionally required for cytokinesis. *Molecular Biology of the Cell*, 8(12), 2693–2705.
- Bickel, T., Jeppesen, C., & Marques, C. M. (2001). Local entropic effects of polymers grafted to soft interfaces. In *The European Physical Journal E* (Vol. 4, Issue 1, pp. 33–43). <https://doi.org/10.1007/s101890170140>
- Bieling, P., Telley, I. A., & Surrey, T. (2010). A minimal midzone protein module controls formation and length of antiparallel microtubule overlaps. *Cell*, 142(3), 420–432.
- Bi, E., Maddox, P., Lew, D. J., Salmon, E. D., McMillan, J. N., Yeh, E., & Pringle, J. R. (1998). Involvement of an actomyosin contractile ring in *Saccharomyces cerevisiae* cytokinesis. *The Journal of Cell Biology*, 142(5), 1301–1312.

- Billuart, P., Bienvenu, T., Ronce, N., des Portes, V., Vinet, M. C., Zemni, R., Carrié, A., Beldjord, C., Kahn, A., Moraine, C., & Chelly, J. (1998). Oligophrenin 1 encodes a rho-GAP protein involved in X-linked mental retardation. *Pathologie-Biologie*, *46*(9), 678.
- Blood, P. D., & Voth, G. A. (2006). Direct observation of Bin/amphiphysin/Rvs (BAR) domain-induced membrane curvature by means of molecular dynamics simulations. *Proceedings of the National Academy of Sciences of the United States of America*, *103*(41), 15068–15072.
- Bojesen, S. E., Ammerpohl, O., Weinhäusl, A., Haas, O. A., Mettal, H., Bohle, R. M., Borkhardt, A., & Fuchs, U. (2006). Characterisation of the GRAF gene promoter and its methylation in patients with acute myeloid leukaemia and myelodysplastic syndrome. *British Journal of Cancer*, *94*(2), 323–332.
- Bompard, G., Sharp, S. J., Freiss, G., & Machesky, L. M. (2005). Involvement of Rac in actin cytoskeleton rearrangements induced by MIM-B. *Journal of Cell Science*, *118*(Pt 22), 5393–5403.
- Borkhardt, A., Bojesen, S., Haas, O. A., Fuchs, U., Bartelheimer, D., Loncarevic, I. F., Bohle, R. M., Harbott, J., Repp, R., Jaeger, U., Viehmann, S., Henn, T., Korth, P., Scharr, D., & Lampert, F. (2000). The human GRAF gene is fused to MLL in a unique t(5;11)(q31;q23) and both alleles are disrupted in three cases of myelodysplastic syndrome/acute myeloid leukemia with a deletion 5q. In *Proceedings of the National Academy of Sciences* (Vol. 97, Issue 16, pp. 9168–9173). <https://doi.org/10.1073/pnas.150079597>
- Bos, J. L., Rehmann, H., & Wittinghofer, A. (2007). GEFs and GAPs: critical elements in the control of small G proteins. *Cell*, *129*(5), 865–877.
- Breidenich, M., Netz, R. R., & Lipowsky, R. (2000). The shape of polymer-decorated membranes. In *Europhysics Letters (EPL)* (Vol. 49, Issue 4, pp. 431–437). <https://doi.org/10.1209/epl/i2000-00167-2>
- Busch, D. J., Houser, J. R., Hayden, C. C., Sherman, M. B., Lafer, E. M., & Stachowiak, J. C. (2015). Intrinsically disordered proteins drive membrane curvature. *Nature Communications*, *6*, 7875.
- Bu, W., Lim, K. B., Yu, Y. H., Chou, A. M., Sudhakaran, T., & Ahmed, S. (2010). Cdc42 interaction with N-WASP and Toca-1 regulates membrane tubulation, vesicle formation and vesicle motility: implications for endocytosis. *PLoS One*, *5*(8), e12153.

- Campelo, F., McMahon, H. T., & Kozlov, M. M. (2008). The hydrophobic insertion mechanism of membrane curvature generation by proteins. *Biophysical Journal*, *95*(5), 2325–2339.
- Cao, J., Albertson, R., Riggs, B., Field, C. M., & Sullivan, W. (2008). Nuf, a Rab11 effector, maintains cytokinetic furrow integrity by promoting local actin polymerization. *The Journal of Cell Biology*, *182*(2), 301–313.
- Cao, J., Crest, J., Fasulo, B., & Sullivan, W. (2010). Cortical actin dynamics facilitate early-stage centrosome separation. *Current Biology: CB*, *20*(8), 770–776.
- Carnahan, R. H., & Gould, K. L. (2003). The PCH family protein, Cdc15p, recruits two F-actin nucleation pathways to coordinate cytokinetic actin ring formation in *Schizosaccharomyces pombe*. *The Journal of Cell Biology*, *162*(5), 851–862.
- Casal, E., Federici, L., Zhang, W., Fernandez-Recio, J., Priego, E.-M., Miguel, R. N., DuHadaway, J. B., Prendergast, G. C., Luisi, B. F., & Laue, E. D. (2006). The crystal structure of the BAR domain from human Bin1/amphiphysin II and its implications for molecular recognition. *Biochemistry*, *45*(43), 12917–12928.
- Chircop, M. (2014). Rho GTPases as regulators of mitosis and cytokinesis in mammalian cells. *Small GTPases*, *5*. <https://doi.org/10.4161/sgtp.29770>
- Chougule, A. B., Hastert, M. C., & Thomas, J. H. (2016). Drak Is Required for Actomyosin Organization During *Drosophila* Cellularization. *G3*, *6*(4), 819–828.
- Chou, T., Kim, K. S., & Oster, G. (2001). Statistical thermodynamics of membrane bending-mediated protein-protein attractions. *Biophysical Journal*, *80*(3), 1075–1087.
- Conrad, G. W., & Rappaport, R. (1981). Mechanisms of Cytokinesis in Animal Cells. In *Mitosis/Cytokinesis* (pp. 365–396). <https://doi.org/10.1016/b978-0-12-781240-3.50020-2>
- Contrino, S., Smith, R. N., Butano, D., Carr, A., Hu, F., Lyne, R., Rutherford, K., Kalderimis, A., Sullivan, J., Carbon, S., Kephart, E. T., Lloyd, P., Stinson, E. O., Washington, N. L., Perry, M. D., Ruzanov, P., Zha, Z., Lewis, S. E., Stein, L. D., & Micklem, G. (2012). modMine: flexible access to modENCODE data. *Nucleic Acids Research*, *40*(Database issue), D1082–D1088.
- Crawford, J. M., Harden, N., Leung, T., Lim, L., & Kiehart, D. P. (1998). Cellularization in *Drosophila melanogaster* Is Disrupted by the Inhibition of Rho Activity and the Activation of Cdc42 Function. *Developmental Biology*, *204*(1), 151–164.

- Crest, J., Concha-Moore, K., & Sullivan, W. (2012). RhoGEF and positioning of rappaport-like furrows in the early *Drosophila* embryo. *Current Biology: CB*, 22(21), 2037–2041.
- Cunto, F. D., Di Cunto, F., Calautti, E., Hsiao, J., Ong, L., Topley, G., Turco, E., & Paolo Dotto, G. (1998). Citron Rho-interacting Kinase, a Novel Tissue-specific Ser/Thr Kinase Encompassing the Rho-Rac-binding Protein Citron. In *Journal of Biological Chemistry* (Vol. 273, Issue 45, pp. 29706–29711). <https://doi.org/10.1074/jbc.273.45.29706>
- Daum, B., Auerswald, A., Gruber, T., Hause, G., Balbach, J., Kühlbrandt, W., & Meister, A. (2016). Supramolecular organization of the human N-BAR domain in shaping the sarcolemma membrane. In *Journal of Structural Biology* (Vol. 194, Issue 3, pp. 375–382). <https://doi.org/10.1016/j.jsb.2016.03.017>
- David, C., Solimena, M., & De Camilli, P. (1994). Autoimmunity in stiff-Man syndrome with breast cancer is targeted to the C-terminal region of human amphiphysin, a protein similar to the yeast proteins, Rvs167 and Rvs161. *FEBS Letters*, 351(1), 73–79.
- D'Avino, P. P., Giansanti, M. G., & Petronczki, M. (2015). Cytokinesis in Animal Cells. In *Cold Spring Harbor Perspectives in Biology* (Vol. 7, Issue 4, p. a015834). <https://doi.org/10.1101/cshperspect.a015834>
- D'Avino, P. P., Savoian, M. S., & Glover, D. M. (2005). Cleavage furrow formation and ingression during animal cytokinesis: a microtubule legacy. *Journal of Cell Science*, 118(Pt 8), 1549–1558.
- Dawson, J. C., Legg, J. A., & Machesky, L. M. (2006). Bar domain proteins: a role in tubulation, scission and actin assembly in clathrin-mediated endocytosis. *Trends in Cell Biology*, 16(10), 493–498.
- Dean, S. O., Rogers, S. L., Stuurman, N., Vale, R. D., & Spudich, J. A. (2005). Distinct pathways control recruitment and maintenance of myosin II at the cleavage furrow during cytokinesis. In *Proceedings of the National Academy of Sciences* (Vol. 102, Issue 38, pp. 13473–13478). <https://doi.org/10.1073/pnas.0506810102>
- DeBiasio, R. L., LaRocca, G. M., Post, P. L., & Taylor, D. L. (1996). Myosin II transport, organization, and phosphorylation: evidence for cortical flow/solation-contraction coupling during cytokinesis and cell locomotion. In *Molecular Biology of the Cell* (Vol. 7, Issue 8, pp. 1259–1282). <https://doi.org/10.1091/mbc.7.8.1259>

- Dechant, R., & Glotzer, M. (2003). Centrosome separation and central spindle assembly act in redundant pathways that regulate microtubule density and trigger cleavage furrow formation. *Developmental Cell*, 4(3), 333–344.
- de Kreuk, B.-J., & Hordijk, P. L. (2012). Control of Rho GTPase function by BAR-domains [Review of *Control of Rho GTPase function by BAR-domains*]. *Small GTPases*, 3(1), 45–52.
- de Kreuk, B.-J., Nethe, M., Fernandez-Borja, M., Anthony, E. C., Hensbergen, P. J., Deelder, A. M., Plomann, M., & Hordijk, P. L. (2011). The F-BAR domain protein PACSIN2 associates with Rac1 and regulates cell spreading and migration. *Journal of Cell Science*, 124(Pt 14), 2375–2388.
- De Lozanne, A., & Spudich, J. A. (1987). Disruption of the Dictyostelium myosin heavy chain gene by homologous recombination. *Science*, 236(4805), 1086–1091.
- Dey, B., & Rikhy, R. (2020). DE-cadherin and Myosin II balance regulates furrow length for onset of polygon shape in syncytial Drosophila embryos. *Journal of Cell Science*. <https://doi.org/10.1242/jcs.240168>
- Disanza, A., Bisi, S., Winterhoff, M., Milanesi, F., Ushakov, D. S., Kast, D., Marighetti, P., Romet-Lemonne, G., Müller, H.-M., Nickel, W., Linkner, J., Waterschoot, D., Ampère, C., Cortellino, S., Palamidessi, A., Dominguez, R., Carlier, M.-F., Faix, J., & Scita, G. (2013). CDC42 switches IRSp53 from inhibition of actin growth to elongation by clustering of VASP. *The EMBO Journal*, 32(20), 2735–2750.
- Doherty, G. J., & Lundmark, R. (2009). GRAF1-dependent endocytosis. *Biochemical Society Transactions*, 37(Pt 5), 1061–1065.
- Doherty, J. T., Lenhart, K. C., Cameron, M. V., Mack, C. P., Conlon, F. L., & Taylor, J. M. (2011). Skeletal muscle differentiation and fusion are regulated by the BAR-containing Rho-GTPase-activating protein (Rho-GAP), GRAF1. *The Journal of Biological Chemistry*, 286(29), 25903–25921.
- Dommersnes, P. G., & Fournier, J.-B. (1999). N-body study of anisotropic membrane inclusions: Membrane mediated interactions and ordered aggregation. In *The European Physical Journal B* (Vol. 12, Issue 1, pp. 9–12). <https://doi.org/10.1007/s100510050968>

- Douglas, M. E., Davies, T., Joseph, N., & Mishima, M. (2010). Aurora B and 14-3-3 coordinately regulate clustering of centralspindlin during cytokinesis. *Current Biology: CB*, 20(10), 927–933.
- Drummond, M. L., Li, M., Tarapore, E., Nguyen, T. T. L., Barouni, B. J., Cruz, S., Tan, K. C., Oro, A. E., & Atwood, S. X. (2018). Actin polymerization controls cilia-mediated signaling. *The Journal of Cell Biology*, 217(9), 3255–3266.
- D'Souza-Schorey, C., Boshans, R. L., McDonough, M., Stahl, P. D., & Van Aelst, L. (1997). A role for POR1, a Rac1-interacting protein, in ARF6-mediated cytoskeletal rearrangements. *The EMBO Journal*, 16(17), 5445–5454.
- Dyer, N., Rebollo, E., Domínguez, P., Elkhatib, N., Chavrier, P., Daviet, L., González, C., & González-Gaitán, M. (2007). Spermatocyte cytokinesis requires rapid membrane addition mediated by ARF6 on central spindle recycling endosomes. *Development*, 134(24), 4437–4447.
- Eberth, A., Lundmark, R., Gremer, L., Dvorsky, R., Koessmeier, K. T., McMahon, H. T., & Ahmadian, M. R. (2009). A BAR domain-mediated autoinhibitory mechanism for RhoGAPs of the GRAF family. *Biochemical Journal*, 417(1), 371–377.
- Echard, A., Hickson, G. R. X., Foley, E., & O'Farrell, P. H. (2004). Terminal Cytokinesis Events Uncovered after an RNAi Screen. In *Current Biology* (Vol. 14, Issue 18, pp. 1685–1693). <https://doi.org/10.1016/j.cub.2004.08.063>
- Echard, A., & O'Farrell, P. H. (2003). The degradation of two mitotic cyclins contributes to the timing of cytokinesis. *Current Biology: CB*, 13(5), 373–383.
- Eda, M., Yonemura, S., Kato, T., Watanabe, N., Ishizaki, T., Madaule, P., & Narumiya, S. (2001). Rho-dependent transfer of Citron-kinase to the cleavage furrow of dividing cells. *Journal of Cell Science*, 114(Pt 18), 3273–3284.
- Eggert, U. S., Kiger, A. A., Richter, C., Perlman, Z. E., Perrimon, N., Mitchison, T. J., & Field, C. M. (2004). Parallel chemical genetic and genome-wide RNAi screens identify cytokinesis inhibitors and targets. *PLoS Biology*, 2(12), e379.
- Eggert, U. S., Mitchison, T. J., & Field, C. M. (2006). Animal cytokinesis: from parts list to mechanisms. *Annual Review of Biochemistry*, 75, 543–566.

- Ennomani, H., Letort, G., Guérin, C., Martiel, J.-L., Cao, W., Nédélec, F., De La Cruz, E. M., Théry, M., & Blanchoin, L. (2016). Architecture and Connectivity Govern Actin Network Contractility. *Current Biology: CB*, 26(5), 616–626.
- Fares, H., Peifer, M., & Pringle, J. R. (1995). Localization and possible functions of Drosophila septins. *Molecular Biology of the Cell*, 6(12), 1843–1859.
- Farsad, K., Ringstad, N., Takei, K., Floyd, S. R., Rose, K., & De Camilli, P. (2001). Generation of high curvature membranes mediated by direct endophilin bilayer interactions. *The Journal of Cell Biology*, 155(2), 193–200.
- Fededa, J. P., & Gerlich, D. W. (2012). Molecular control of animal cell cytokinesis. In *Nature Cell Biology* (Vol. 14, Issue 5, pp. 440–447). <https://doi.org/10.1038/ncb2482>
- Field, C. M., al-Awar, O., Rosenblatt, J., Wong, M. L., Alberts, B., & Mitchison, T. J. (1996). A purified Drosophila septin complex forms filaments and exhibits GTPase activity. *The Journal of Cell Biology*, 133(3), 605–616.
- Field, C. M., & Alberts, B. M. (1995). Anillin, a contractile ring protein that cycles from the nucleus to the cell cortex. In *Journal of Cell Biology* (Vol. 131, Issue 1, pp. 165–178). <https://doi.org/10.1083/jcb.131.1.165>
- Field, C. M., Coughlin, M., Doberstein, S., Marty, T., & Sullivan, W. (2005). Characterization of anillin mutants reveals essential roles in septin localization and plasma membrane integrity. *Development*, 132(12), 2849–2860.
- Fielding, A. B., Schonteich, E., Matheson, J., Wilson, G., Yu, X., Hickson, G. R. X., Srivastava, S., Baldwin, S. A., Prekeris, R., & Gould, G. W. (2005). Rab11-FIP3 and FIP4 interact with Arf6 and the exocyst to control membrane traffic in cytokinesis. *The EMBO Journal*, 24(19), 3389–3399.
- Figard, L., & Sokac, A. M. (2014). A membrane reservoir at the cell surface. In *BioArchitecture* (Vol. 4, Issue 2, pp. 39–46). <https://doi.org/10.4161/bioa.29069>
- Figard, L., Xu, H., Garcia, H. G., Golding, I., & Sokac, A. M. (2013). The Plasma Membrane Flattens Out to Fuel Cell-Surface Growth during Drosophila Cellularization. In *Developmental Cell* (Vol. 27, Issue 6, pp. 648–655). <https://doi.org/10.1016/j.devcel.2013.11.006>

- Fishkind, D. J., & Wang, Y. L. (1993). Orientation and three-dimensional organization of actin filaments in dividing cultured cells. In *Journal of Cell Biology* (Vol. 123, Issue 4, pp. 837–848). <https://doi.org/10.1083/jcb.123.4.837>
- Foe, V. E., & Alberts, B. M. (1983). Studies of nuclear and cytoplasmic behaviour during the five mitotic cycles that precede gastrulation in *Drosophila* embryogenesis. *Journal of Cell Science*, *61*, 31–70.
- Foe, V. E., Field, C. M., & Odell, G. M. (2000). Microtubules and mitotic cycle phase modulate spatiotemporal distributions of F-actin and myosin II in *Drosophila* syncytial blastoderm embryos. In *Development* (Vol. 127, Issue 9, pp. 1767–1787). <https://doi.org/10.1242/dev.127.9.1767>
- Frescas, D., Mavrakis, M., Lorenz, H., Delotto, R., & Lippincott-Schwartz, J. (2006). The secretory membrane system in the *Drosophila* syncytial blastoderm embryo exists as functionally compartmentalized units around individual nuclei. *The Journal of Cell Biology*, *173*(2), 219–230.
- Frost, A., De Camilli, P., & Unger, V. M. (2007). F-BAR proteins join the BAR family fold [Review of *F-BAR proteins join the BAR family fold*]. *Structure*, *15*(7), 751–753.
- Frost, A., Perera, R., Roux, A., Spasov, K., Destaing, O., Egelman, E. H., De Camilli, P., & Unger, V. M. (2008). Structural basis of membrane invagination by F-BAR domains. *Cell*, *132*(5), 807–817.
- Funato, Y., Terabayashi, T., Suenaga, N., Seiki, M., Takenawa, T., & Miki, H. (2004). IRSp53/Eps8 complex is important for positive regulation of Rac and cancer cell motility/invasiveness. *Cancer Research*, *64*(15), 5237–5244.
- Gaillard, J., Neumann, E., Van Damme, D., Stoppin-Mellet, V., Ebel, C., Barbier, E., Geelen, D., & Vantard, M. (2008). Two microtubule-associated proteins of *Arabidopsis* MAP65s promote antiparallel microtubule bundling. *Molecular Biology of the Cell*, *19*(10), 4534–4544.
- Gallop, J. L., Jao, C. C., Kent, H. M., Butler, P. J. G., Evans, P. R., Langen, R., & McMahon, H. T. (2006). Mechanism of endophilin N-BAR domain-mediated membrane curvature. *The EMBO Journal*, *25*(12), 2898–2910.

- Gerald, N. J., Damer, C. K., O'Halloran, T. J., & De Lozanne, A. (2001). Cytokinesis failure in clathrin-minus cells is caused by cleavage furrow instability. *Cell Motility and the Cytoskeleton*, 48(3), 213–223.
- Gerisch, G., & Weber, I. (2000). Cytokinesis without myosin II. In *Current Opinion in Cell Biology* (Vol. 12, Issue 1, pp. 126–132). [https://doi.org/10.1016/s0955-0674\(99\)00066-6](https://doi.org/10.1016/s0955-0674(99)00066-6)
- Ge, W., & Balasubramanian, M. K. (2008). Pxl1p, a paxillin-related protein, stabilizes the actomyosin ring during cytokinesis in fission yeast. *Molecular Biology of the Cell*, 19(4), 1680–1692.
- Giansanti, M. G., Belloni, G., & Gatti, M. (2007). Rab11 is required for membrane trafficking and actomyosin ring constriction in meiotic cytokinesis of *Drosophila* males. *Molecular Biology of the Cell*, 18(12), 5034–5047.
- Giansanti, M. G., Bonaccorsi, S., & Gatti, M. (1999). The role of anillin in meiotic cytokinesis of *Drosophila* males. *Journal of Cell Science*, 112 (Pt 14), 2323–2334.
- Giansanti, M. G., Bonaccorsi, S., Williams, B., Williams, E. V., Santolamazza, C., Goldberg, M. L., & Gatti, M. (1998). Cooperative interactions between the central spindle and the contractile ring during *Drosophila* cytokinesis. *Genes & Development*, 12(3), 396–410.
- Giansanti, M. G., Farkas, R. M., Bonaccorsi, S., Lindsley, D. L., Wakimoto, B. T., Fuller, M. T., & Gatti, M. (2004). Genetic dissection of meiotic cytokinesis in *Drosophila* males. *Molecular Biology of the Cell*, 15(5), 2509–2522.
- Giet, R., & Glover, D. M. (2001). *Drosophila* Aurora B Kinase Is Required for Histone H3 Phosphorylation and Condensin Recruitment during Chromosome Condensation and to Organize the Central Spindle during Cytokinesis. In *Journal of Cell Biology* (Vol. 152, Issue 4, pp. 669–682). <https://doi.org/10.1083/jcb.152.4.669>
- Gillingham, A. K., & Munro, S. (2007). The Small G Proteins of the Arf Family and Their Regulators. In *Annual Review of Cell and Developmental Biology* (Vol. 23, Issue 1, pp. 579–611). <https://doi.org/10.1146/annurev.cellbio.23.090506.123209>
- Glotzer, M. (2001). Animal Cell Cytokinesis. In *Annual Review of Cell and Developmental Biology* (Vol. 17, Issue 1, pp. 351–386). <https://doi.org/10.1146/annurev.cellbio.17.1.351>
- Glotzer, M. (2005). The Molecular Requirements for Cytokinesis. In *Science* (Vol. 307, Issue 5716, pp. 1735–1739). <https://doi.org/10.1126/science.1096896>

- Glotzer, M. (2009). The 3Ms of central spindle assembly: microtubules, motors and MAPs. *Nature Reviews. Molecular Cell Biology*, 10(1), 9–20.
- Goff, X. L., Le Goff, X., Motegi, F., Salimova, E., Mabuchi, I., & Simanis, V. (2000). The *S. pombe* *rlc1* gene encodes a putative myosin regulatory light chain that binds the type II myosins *myo3p* and *myo2p*. In *Journal of Cell Science* (Vol. 113, Issue 23, pp. 4157–4163). <https://doi.org/10.1242/jcs.113.23.4157>
- Goldbach, P., Wong, R., Beise, N., Sarpal, R., Trimble, W. S., & Brill, J. A. (2010). Stabilization of the actomyosin ring enables spermatocyte cytokinesis in *Drosophila*. *Molecular Biology of the Cell*, 21(9), 1482–1493.
- Gómez-Cavazos, J. S., Lee, K.-Y., Lara-González, P., Li, Y., Desai, A., Shiau, A. K., & Oegema, K. (2020). A Non-canonical BRCT-Phosphopeptide Recognition Mechanism Underlies RhoA Activation in Cytokinesis. *Current Biology: CB*, 30(16), 3101–3115.e11.
- Gönczy, P., Echeverri, C., Oegema, K., Coulson, A., Jones, S. J. M., Copley, R. R., Duperon, J., Oegema, J., Brehm, M., Cassin, E., Hannak, E., Kirkham, M., Pichler, S., Flohrs, K., Goessen, A., Leidel, S., Alleaume, A.-M., Martin, C., Özlü, N., ... Hyman, A. A. (2000). Functional genomic analysis of cell division in *C. elegans* using RNAi of genes on chromosome III. In *Nature* (Vol. 408, Issue 6810, pp. 331–336). <https://doi.org/10.1038/35042526>
- Goode, B. L., & Eck, M. J. (2007). Mechanism and function of formins in the control of actin assembly. *Annual Review of Biochemistry*, 76, 593–627.
- Graziano, B. R., Yu, H.-Y. E., Alioto, S. L., Eskin, J. A., Ydenberg, C. A., Waterman, D. P., Garabedian, M., & Goode, B. L. (2014). The F-BAR protein Hof1 tunes formin activity to sculpt actin cables during polarized growth. *Molecular Biology of the Cell*, 25(11), 1730–1743.
- Green, R. A., Paluch, E., & Oegema, K. (2012). Cytokinesis in Animal Cells. In *Annual Review of Cell and Developmental Biology* (Vol. 28, Issue 1, pp. 29–58). <https://doi.org/10.1146/annurev-cellbio-101011-155718>
- Grevengoed, E. E., Fox, D. T., Gates, J., & Peifer, M. (2003). Balancing different types of actin polymerization at distinct sites: roles for Abelson kinase and Enabled. *The Journal of Cell Biology*, 163(6), 1267–1279.

- Grosshans, J., Wenzl, C., Herz, H.-M., Bartoszewski, S., Schnorrer, F., Vogt, N., Schwarz, H., & Müller, H.-A. (2005). RhoGEF2 and the formin Dia control the formation of the furrow canal by directed actin assembly during *Drosophila* cellularisation. *Development*, *132*(5), 1009–1020.
- Guertin, D. A., Trautmann, S., & McCollum, D. (2002). Cytokinesis in eukaryotes. *Microbiology and Molecular Biology Reviews: MMBR*, *66*(2), 155–178.
- Guha, M., Zhou, M., & Wang, Y.-L. (2005). Cortical actin turnover during cytokinesis requires myosin II. *Current Biology: CB*, *15*(8), 732–736.
- Guigas, G., & Weiss, M. (2016). Effects of protein crowding on membrane systems. *Biochimica et Biophysica Acta*, *1858*(10), 2441–2450.
- Gunsalus, K. C., Bonaccorsi, S., Williams, E., Verni, F., Gatti, M., & Goldberg, M. L. (1995). Mutations in twinstar, a *Drosophila* gene encoding a cofilin/ADF homologue, result in defects in centrosome migration and cytokinesis. In *Journal of Cell Biology* (Vol. 131, Issue 5, pp. 1243–1259). <https://doi.org/10.1083/jcb.131.5.1243>
- Guo, S., & Kemphues, K. J. (1996). A non-muscle myosin required for embryonic polarity in *Caenorhabditis elegans*. In *Nature* (Vol. 382, Issue 6590, pp. 455–458). <https://doi.org/10.1038/382455a0>
- Guse, A., Mishima, M., & Glotzer, M. (2005). Phosphorylation of ZEN-4/MKLP1 by aurora B regulates completion of cytokinesis. *Current Biology: CB*, *15*(8), 778–786.
- Gwatkin, R. (1995). Developmental biology by Scott F. Gilbert, Sinauer Associates, Inc., Sunderland, MA, 4th ed., 1994, 894 pp, \$57.95. In *Molecular Reproduction and Development* (Vol. 41, Issue 3, pp. 398–398). <https://doi.org/10.1002/mrd.1080410316>
- Haarer, B. K., & Pringle, J. R. (1987). Immunofluorescence localization of the *Saccharomyces cerevisiae* CDC12 gene product to the vicinity of the 10-nm filaments in the mother-bud neck. *Molecular and Cellular Biology*, *7*(10), 3678–3687.
- Hacker, U., & Perrimon, N. (1998). DRhoGEF2 encodes a member of the Dbl family of oncogenes and controls cell shape changes during gastrulation in *Drosophila*. In *Genes & Development* (Vol. 12, Issue 2, pp. 274–284). <https://doi.org/10.1101/gad.12.2.274>
- Hall, A. (2012). Rho family GTPases. *Biochemical Society Transactions*, *40*(6), 1378–1382.

- Halsell, S. R., Chu, B. I., & Kiehart, D. P. (2000). Genetic analysis demonstrates a direct link between rho signaling and nonmuscle myosin function during drosophila morphogenesis. *Genetics*, *156*(1), 469.
- Häsler, S. L.-A., Vallis, Y., Pasche, M., & McMahon, H. T. (2020). GRAF2, WDR44, and MICAL1 mediate Rab8/10/11–dependent export of E-cadherin, MMP14, and CFTR Δ F508. In *Journal of Cell Biology* (Vol. 219, Issue 5). <https://doi.org/10.1083/jcb.201811014>
- Hauf, S., Cole, R. W., LaTerra, S., Zimmer, C., Schnapp, G., Walter, R., Heckel, A., van Meel, J., Rieder, C. L., & Peters, J.-M. (2003). The small molecule Hesperadin reveals a role for Aurora B in correcting kinetochore-microtubule attachment and in maintaining the spindle assembly checkpoint. *The Journal of Cell Biology*, *161*(2), 281–294.
- Haviv, L., Gillo, D., Backouche, F., & Bernheim-Groswasser, A. (2008). A cytoskeletal demolition worker: myosin II acts as an actin depolymerization agent. *Journal of Molecular Biology*, *375*(2), 325–330.
- Heath, R. J. W., & Insall, R. H. (2008). F-BAR domains: multifunctional regulators of membrane curvature. *Journal of Cell Science*, *121*(Pt 12), 1951–1954.
- He, B., Martin, A., & Wieschaus, E. (2016). Flow-dependent myosin recruitment during Drosophila cellularization requires zygotic dunk activity. *Development*, *143*(13), 2417–2430.
- Heer, N. C., & Martin, A. C. (2017). Tension, contraction and tissue morphogenesis. *Development*, *144*(23), 4249–4260.
- Heinrich, M. C., Capraro, B. R., Tian, A., Isas, J. M., Langen, R., & Baumgart, T. (2010). Quantifying Membrane Curvature Generation of Drosophila Amphiphysin N-BAR Domains. In *The Journal of Physical Chemistry Letters* (Vol. 1, Issue 23, pp. 3401–3406). <https://doi.org/10.1021/jz101403q>
- Heisenberg, C.-P., & Bellaïche, Y. (2013). Forces in Tissue Morphogenesis and Patterning. In *Cell* (Vol. 153, Issue 5, pp. 948–962). <https://doi.org/10.1016/j.cell.2013.05.008>
- Henne, W. M., Kent, H. M., Ford, M. G. J., Hegde, B. G., Daumke, O., Butler, P. J. G., Mittal, R., Langen, R., Evans, P. R., & McMahon, H. T. (2007). Structure and analysis of FCHo2 F-BAR domain: a dimerizing and membrane recruitment module that effects membrane curvature. *Structure*, *15*(7), 839–852.

- Henson, J. H., Ditzler, C. E., Germain, A., Irwin, P. M., Vogt, E. T., Yang, S., Wu, X., & Shuster, C. B. (2017). The ultrastructural organization of actin and myosin II filaments in the contractile ring: new support for an old model of cytokinesis. *Molecular Biology of the Cell*, 28(5), 613–623.
- Hickson, G. R. X., Echard, A., & O'Farrell, P. H. (2006). Rho-kinase Controls Cell Shape Changes during Cytokinesis. In *Current Biology* (Vol. 16, Issue 4, pp. 359–370). <https://doi.org/10.1016/j.cub.2005.12.043>
- Hickson, G. R. X., Matheson, J., Riggs, B., Maier, V. H., Fielding, A. B., Prekeris, R., Sullivan, W., Barr, F. A., & Gould, G. W. (2003). Arfophilins are dual Arf/Rab 11 binding proteins that regulate recycling endosome distribution and are related to Drosophila nuclear fallout. *Molecular Biology of the Cell*, 14(7), 2908–2920.
- Hickson, G. R. X., & O'Farrell, P. H. (2008). Rho-dependent control of anillin behavior during cytokinesis. *The Journal of Cell Biology*, 180(2), 285–294.
- Hildebrand, J. D., Taylor, J. M., & Parsons, J. T. (1996). An SH3 domain-containing GTPase-activating protein for Rho and Cdc42 associates with focal adhesion kinase. *Molecular and Cellular Biology*, 16(6), 3169–3178.
- Hime, G. R., Brill, J. A., & Fuller, M. T. (1996). Assembly of ring canals in the male germ line from structural components of the contractile ring. *Journal of Cell Science*, 109 (Pt 12), 2779–2788.
- Hime, G., & Saint, R. (1992). Zygotic expression of the pebble locus is required for cytokinesis during the postblastoderm mitoses of Drosophila. *Development*, 114(1), 165–171.
- Hiramoto, Y. (1975). FORCE EXERTED BY THE CLEAVAGE FURROW OF SEA URCHIN EGGS. In *Development, Growth and Differentiation* (Vol. 17, Issue 1, pp. 27–38). <https://doi.org/10.1111/j.1440-169x.1975.00027.x>
- Hirose, K., Kawashima, T., Iwamoto, I., Nosaka, T., & Kitamura, T. (2001). MgcRacGAP Is Involved in Cytokinesis through Associating with Mitotic Spindle and Midbody. In *Journal of Biological Chemistry* (Vol. 276, Issue 8, pp. 5821–5828). <https://doi.org/10.1074/jbc.m007252200>
- Ho, H.-Y. H., Rohatgi, R., Lebensohn, A. M., Le Ma, Li, J., Gygi, S. P., & Kirschner, M. W. (2004). Toca-1 mediates Cdc42-dependent actin nucleation by activating the N-WASP-WIP complex. *Cell*, 118(2), 203–216.

- Holly, R. M., Mavor, L. M., Zuo, Z., & Blankenship, J. T. (2015). A rapid, membrane-dependent pathway directs furrow formation through RalA in the early *Drosophila* embryo. *Development*, *142*(13), 2316–2328.
- Holst, M. R., Vidal-Quadras, M., Larsson, E., Song, J., Hubert, M., Blomberg, J., Lundborg, M., Landström, M., & Lundmark, R. (2017). Clathrin-Independent Endocytosis Suppresses Cancer Cell Blebbing and Invasion. *Cell Reports*, *20*(8), 1893–1905.
- Hu, C.-K., Coughlin, M., Field, C. M., & Mitchison, T. J. (2008). Cell polarization during monopolar cytokinesis. *The Journal of Cell Biology*, *181*(2), 195–202.
- Hu, C.-K., Coughlin, M., Field, C. M., & Mitchison, T. J. (2011). KIF4 regulates midzone length during cytokinesis. *Current Biology: CB*, *21*(10), 815–824.
- Icking, A., Matt, S., Opitz, N., Wiesenthal, A., Müller-Esterl, W., & Schilling, K. (2005). NOSTRIN functions as a homotrimeric adaptor protein facilitating internalization of eNOS. *Journal of Cell Science*, *118*(Pt 21), 5059–5069.
- Icking, A., Schilling, K., Wiesenthal, A., Opitz, N., & Müller-Esterl, W. (2006). FCH/Cdc15 domain determines distinct subcellular localization of NOSTRIN. *FEBS Letters*, *580*(1), 223–228.
- Ishizaki, T., Maekawa, M., Fujisawa, K., Okawa, K., Iwamatsu, A., Fujita, A., Watanabe, N., Saito, Y., Kakizuka, A., Morii, N., & Narumiya, S. (1996). The small GTP-binding protein Rho binds to and activates a 160 kDa Ser/Thr protein kinase homologous to myotonic dystrophy kinase. *The EMBO Journal*, *15*(8), 1885–1893.
- Itoh, T., Erdmann, K. S., Roux, A., Habermann, B., Werner, H., & De Camilli, P. (2005). Dynamin and the actin cytoskeleton cooperatively regulate plasma membrane invagination by BAR and F-BAR proteins. *Developmental Cell*, *9*(6), 791–804.
- Jacobs, T., & Hall, C. (2005). Rho GAPs — Regulators of Rho GTPases and More. In *Proteins and Cell Regulation* (pp. 93–112). https://doi.org/10.1007/1-4020-3462-8_5
- Janson, M. E., Loughlin, R., Loiodice, I., Fu, C., Brunner, D., Nédélec, F. J., & Tran, P. T. (2007). Crosslinkers and motors organize dynamic microtubules to form stable bipolar arrays in fission yeast. *Cell*, *128*(2), 357–368.
- Jantsch-Plunger, V., Gönczy, P., Romano, A., Schnabel, H., Hamill, D., Schnabel, R., Hyman, A. A., & Glotzer, M. (2000). CYK-4: A Rho family gtpase activating protein (GAP) required

- for central spindle formation and cytokinesis. *The Journal of Cell Biology*, 149(7), 1391–1404.
- Jodoin, J. N., Coravos, J. S., Chanet, S., Vasquez, C. G., Tworoger, M., Kingston, E. R., Perkins, L. A., Perrimon, N., & Martin, A. C. (2015). Stable Force Balance between Epithelial Cells Arises from F-Actin Turnover. *Developmental Cell*, 35(6), 685–697.
- Jordan, P., & Karess, R. (1997). Myosin Light Chain-activating Phosphorylation Sites Are Required for Oogenesis in *Drosophila*. In *Journal of Cell Biology* (Vol. 139, Issue 7, pp. 1805–1819). <https://doi.org/10.1083/jcb.139.7.1805>
- Kaitna, S., Mendoza, M., Jantsch-Plunger, V., & Glotzer, M. (2000). Incenp and an Aurora-like kinase form a complex essential for chromosome segregation and efficient completion of cytokinesis. In *Current Biology* (Vol. 10, Issue 19, pp. 1172–1181). [https://doi.org/10.1016/s0960-9822\(00\)00721-1](https://doi.org/10.1016/s0960-9822(00)00721-1)
- Kanada, M., Nagasaki, A., & Uyeda, T. Q. P. (2005). Adhesion-dependent and Contractile Ring-independent Equatorial Furrowing during Cytokinesis in Mammalian Cells. In *Molecular Biology of the Cell* (Vol. 16, Issue 8, pp. 3865–3872). <https://doi.org/10.1091/mbc.e05-03-0233>
- Kao, L.-R., & Megraw, T. L. (2009). Centrocortin cooperates with centrosomin to organize *Drosophila* embryonic cleavage furrows. *Current Biology: CB*, 19(11), 937–942.
- Karess, R. E., Chang, X. J., Edwards, K. A., Kulkarni, S., Aguilera, I., & Kiehart, D. P. (1991). The regulatory light chain of nonmuscle myosin is encoded by spaghetti-squash, a gene required for cytokinesis in *Drosophila*. *Cell*, 65(7), 1177–1189.
- Karr, T. L., & Alberts, B. M. (1986). Organization of the cytoskeleton in early *Drosophila* embryos. *The Journal of Cell Biology*, 102(4), 1494–1509.
- Kast, D. J., Yang, C., Disanza, A., Boczkowska, M., Madasu, Y., Scita, G., Svitkina, T., & Dominguez, R. (2014). Mechanism of IRSp53 inhibition and combinatorial activation by Cdc42 and downstream effectors. *Nature Structural & Molecular Biology*, 21(4), 413–422.
- Kasza, K. E., Farrell, D. L., & Zallen, J. A. (2014). Spatiotemporal control of epithelial remodeling by regulated myosin phosphorylation. In *Proceedings of the National Academy of Sciences* (Vol. 111, Issue 32, pp. 11732–11737). <https://doi.org/10.1073/pnas.1400520111>

- Keaton, M. A. (2007). Review of “The Cell Cycle: Principles of Control” by David O. Morgan. In *Cell Division* (Vol. 2, Issue 1, p. 27). <https://doi.org/10.1186/1747-1028-2-27>
- Kessels, M. M., & Qualmann, B. (2004). The syndapin protein family: linking membrane trafficking with the cytoskeleton. *Journal of Cell Science*, *117*(Pt 15), 3077–3086.
- Kiehart, D. P. (1990). The actin membrane skeleton in Drosophila development. *Seminars in Cell Biology*, *1*(5), 325–339.
- Kim, S., Nahm, M., Kim, N., Kwon, Y., Kim, J., Choi, S., Choi, E. Y., Shim, J., Lee, C., & Lee, S. (2017). Graf regulates hematopoiesis through GEEC endocytosis of EGFR. *Development*, *144*(22), 4159–4172.
- Kimura, K., Ito, M., Amano, M., Chihara, K., Fukata, Y., Nakafuku, M., Yamamori, B., Feng, J., Nakano, T., Okawa, K., Iwamatsu, A., & Kaibuchi, K. (1996). Regulation of Myosin Phosphatase by Rho and Rho-Associated Kinase (Rho-Kinase). In *Science* (Vol. 273, Issue 5272, pp. 245–248). <https://doi.org/10.1126/science.273.5272.245>
- Kinoshita, M., Field, C. M., Coughlin, M. L., Straight, A. F., & Mitchison, T. J. (2002). Self- and Actin-Templated Assembly of Mammalian Septins. In *Developmental Cell* (Vol. 3, Issue 6, pp. 791–802). [https://doi.org/10.1016/s1534-5807\(02\)00366-0](https://doi.org/10.1016/s1534-5807(02)00366-0)
- Kinoshita, M., Kumar, S., Mizoguchi, A., Ide, C., Kinoshita, A., Haraguchi, T., Hiraoka, Y., & Noda, M. (1997). Nedd5, a mammalian septin, is a novel cytoskeletal component interacting with actin-based structures. *Genes & Development*, *11*(12), 1535–1547.
- Kitayama, C., Sugimoto, A., & Yamamoto, M. (1997). Type II myosin heavy chain encoded by the myo2 gene composes the contractile ring during cytokinesis in *Schizosaccharomyces pombe*. *The Journal of Cell Biology*, *137*(6), 1309–1319.
- Knecht, D. A., & Loomis, W. F. (1987). Antisense RNA inactivation of myosin heavy chain gene expression in *Dictyostelium discoideum*. *Science*, *236*(4805), 1081–1086.
- Kondo, T., Hamao, K., Kamijo, K., Kimura, H., Morita, M., Takahashi, M., & Hosoya, H. (2011). Enhancement of myosin II/actin turnover at the contractile ring induces slower furrowing in dividing HeLa cells. In *Biochemical Journal* (Vol. 435, Issue 3, pp. 569–576). <https://doi.org/10.1042/bj20100837>
- Kosako, H., Goto, H., Yanagida, M., Matsuzawa, K., Fujita, M., Tomono, Y., Okigaki, T., Odai, H., Kaibuchi, K., & Inagaki, M. (1999). Specific accumulation of Rho-associated kinase at the cleavage furrow during cytokinesis: cleavage furrow-specific phosphorylation of

- intermediate filaments. In *Oncogene* (Vol. 18, Issue 17, pp. 2783–2788). <https://doi.org/10.1038/sj.onc.1202633>
- Kotadia, S., Crest, J., Tram, U., Riggs, B., & Sullivan, W. (2010). Blastoderm Formation and Cellularisation in *Drosophila melanogaster*. In *Encyclopedia of Life Sciences*. <https://doi.org/10.1002/9780470015902.a0001071.pub2>
- Kouranti, I., Sachse, M., Arouche, N., Goud, B., & Echard, A. (2006). Rab35 regulates an endocytic recycling pathway essential for the terminal steps of cytokinesis. *Current Biology: CB*, 16(17), 1719–1725.
- Kovacs, E. M., Makar, R. S., & Gertler, F. B. (2006). Tuba stimulates intracellular N-WASP-dependent actin assembly. *Journal of Cell Science*, 119(Pt 13), 2715–2726.
- Kovar, D. R., Kuhn, J. R., Tichy, A. L., & Pollard, T. D. (2003). The fission yeast cytokinesis formin Cdc12p is a barbed end actin filament capping protein gated by profilin. In *Journal of Cell Biology* (Vol. 161, Issue 5, pp. 875–887). <https://doi.org/10.1083/jcb.200211078>
- Krajcovic, M. M., & Minden, J. S. (2012). Assessing the critical period for Rho kinase activity during *Drosophila* ventral furrow formation. *Developmental Dynamics: An Official Publication of the American Association of Anatomists*, 241(11), 1729–1743.
- Krueger, D., Quinkler, T., Mortensen, S. A., Sachse, C., & De Renzis, S. (2019). Cross-linker-mediated regulation of actin network organization controls tissue morphogenesis. *The Journal of Cell Biology*, 218(8), 2743–2761.
- Krugmann, S., Jordens, I., Gevaert, K., Driessens, M., Vandekerckhove, J., & Hall, A. (2001). Cdc42 induces filopodia by promoting the formation of an IRSp53:Mena complex. *Current Biology: CB*, 11(21), 1645–1655.
- Kumari, S., & Mayor, S. (2008). ARF1 is directly involved in dynamin-independent endocytosis. *Nature Cell Biology*, 10(1), 30–41.
- Kumar, M., Pushpa, K., & Mylavarapu, S. V. S. (2015). Splitting the cell, building the organism: Mechanisms of cell division in metazoan embryos. *IUBMB Life*, 67(7), 575–587.
- Kunda, P., & Baum, B. (2009). The actin cytoskeleton in spindle assembly and positioning. In *Trends in Cell Biology* (Vol. 19, Issue 4, pp. 174–179). <https://doi.org/10.1016/j.tcb.2009.01.006>

- Kurasawa, Y., Earnshaw, W. C., Mochizuki, Y., Dohmae, N., & Todokoro, K. (2004). Essential roles of KIF4 and its binding partner PRC1 in organized central spindle midzone formation. *The EMBO Journal*, *23*(16), 3237–3248.
- Laporte, D., Coffman, V. C., Lee, I.-J., & Wu, J.-Q. (2011). Assembly and architecture of precursor nodes during fission yeast cytokinesis. *The Journal of Cell Biology*, *192*(6), 1005–1021.
- Lecuit, T., & Wieschaus, E. (2000). Polarized insertion of new membrane from a cytoplasmic reservoir during cleavage of the *Drosophila* embryo. *The Journal of Cell Biology*, *150*(4), 849–860.
- Lee, D. M., & Harris, T. J. C. (2013). An Arf-GEF regulates antagonism between endocytosis and the cytoskeleton for *Drosophila* blastoderm development. *Current Biology: CB*, *23*(21), 2110–2120.
- Lee, D. M., & Harris, T. J. C. (2014). Coordinating the cytoskeleton and endocytosis for regulated plasma membrane growth in the early *Drosophila* embryo [Review of *Coordinating the cytoskeleton and endocytosis for regulated plasma membrane growth in the early Drosophila embryo*]. *Bioarchitecture*, *4*(2), 68–74.
- Lee, S. H., Kerff, F., Chereau, D., Ferron, F., Klug, A., & Dominguez, R. (2007). Structural basis for the actin-binding function of missing-in-metastasis. *Structure*, *15*(2), 145–155.
- Lehner, C. F. (1992). The pebble gene is required for cytokinesis in *Drosophila*. In *Journal of Cell Science* (Vol. 103, Issue 4, pp. 1021–1030). <https://doi.org/10.1242/jcs.103.4.1021>
- Lemmon, M. A. (2008). Membrane recognition by phospholipid-binding domains. *Nature Reviews. Molecular Cell Biology*, *9*(2), 99–111.
- Levayer, R., & Lecuit, T. (2012). Biomechanical regulation of contractility: spatial control and dynamics. *Trends in Cell Biology*, *22*(2), 61–81.
- Lichte, B., Veh, R. W., Meyer, H. E., & Kilimann, M. W. (1992). Amphiphysin, a novel protein associated with synaptic vesicles. *The EMBO Journal*, *11*(7), 2521–2530.
- Lim, K. B., Bu, W., Goh, W. I., Koh, E., Ong, S. H., Pawson, T., Sudhakaran, T., & Ahmed, S. (2008). The Cdc42 effector IRSp53 generates filopodia by coupling membrane protrusion with actin dynamics. *The Journal of Biological Chemistry*, *283*(29), 20454–20472.

- Lin, J., Liu, J., Wang, Y., Zhu, J., Zhou, K., Smith, N., & Zhan, X. (2005). Differential regulation of cortactin and N-WASP-mediated actin polymerization by missing in metastasis (MIM) protein. *Oncogene*, *24*(12), 2059–2066.
- Lipowsky, R. (2013). Spontaneous tubulation of membranes and vesicles reveals membrane tension generated by spontaneous curvature. *Faraday Discussions*, *161*, 305–331; discussion 419–459.
- Lippincott, J., & Li, R. (1998). Sequential assembly of myosin II, an IQGAP-like protein, and filamentous actin to a ring structure involved in budding yeast cytokinesis. *The Journal of Cell Biology*, *140*(2), 355–366.
- Li, R. (2007). Cytokinesis in development and disease: variations on a common theme. *Cellular and Molecular Life Sciences: CMLS*, *64*(23), 3044–3058.
- Liu, J., Lee, D. M., Yu, C. G., Angers, S., & Harris, T. J. C. (2015). Stepping stone: a cytohesin adaptor for membrane cytoskeleton restraint in the syncytial *Drosophila* embryo. In *Molecular Biology of the Cell* (Vol. 26, Issue 4, pp. 711–725). <https://doi.org/10.1091/mbc.e14-11-1554>
- Liu, S., Xiong, X., Zhao, X., Yang, X., & Wang, H. (2015). F-BAR family proteins, emerging regulators for cell membrane dynamic changes-from structure to human diseases. *Journal of Hematology & Oncology*, *8*, 47.
- Loïodice, I., Staub, J., Setty, T. G., Nguyen, N.-P. T., Paoletti, A., & Tran, P. T. (2005). Ase1p organizes antiparallel microtubule arrays during interphase and mitosis in fission yeast. *Molecular Biology of the Cell*, *16*(4), 1756–1768.
- Longtine, M. S., DeMarini, D. J., Valencik, M. L., Al-Awar, O. S., Fares, H., De Virgilio, C., & Pringle, J. R. (1996). The septins: roles in cytokinesis and other processes. In *Current Opinion in Cell Biology* (Vol. 8, Issue 1, pp. 106–119). [https://doi.org/10.1016/s0955-0674\(96\)80054-8](https://doi.org/10.1016/s0955-0674(96)80054-8)
- Low, S. H., Li, X., Miura, M., Kudo, N., Quiñones, B., & Weimbs, T. (2003). Syntaxin 2 and Endobrevin Are Required for the Terminal Step of Cytokinesis in Mammalian Cells. In *Developmental Cell* (Vol. 4, Issue 5, pp. 753–759). [https://doi.org/10.1016/s1534-5807\(03\)00122-9](https://doi.org/10.1016/s1534-5807(03)00122-9)

- Lundmark, R., Doherty, G. J., Howes, M. T., Cortese, K., Vallis, Y., Parton, R. G., & McMahon, H. T. (2008). The GTPase-activating protein GRAF1 regulates the CLIC/GEEC endocytic pathway. *Current Biology: CB*, *18*(22), 1802–1808.
- Luo, W., Janoštiak, R., Tolde, O., Ryzhova, L. M., Koudelková, L., Dibus, M., Brábek, J., Hanks, S. K., & Rosel, D. (2017). ARHGAP42 is activated by Src-mediated tyrosine phosphorylation to promote cell motility. *Journal of Cell Science*, *130*(14), 2382–2393.
- Mabuchi, I., Hamaguchi, Y., Fujimoto, H., Morii, N., Mishima, M., & Narumiya, S. (1993). A rho-like protein is involved in the organisation of the contractile ring in dividing sand dollar eggs. In *Zygote* (Vol. 1, Issue 4, pp. 325–331). <https://doi.org/10.1017/s0967199400001659>
- Mabuchi, I., & Okuno, M. (1977). The effect of myosin antibody on the division of starfish blastomeres. In *Journal of Cell Biology* (Vol. 74, Issue 1, pp. 251–263). <https://doi.org/10.1083/jcb.74.1.251>
- Mabuchi, I., Tsukita, S., Tsukita, S., & Sawai, T. (1988). Cleavage furrow isolated from newt eggs: contraction, organization of the actin filaments, and protein components of the furrow. In *Proceedings of the National Academy of Sciences* (Vol. 85, Issue 16, pp. 5966–5970). <https://doi.org/10.1073/pnas.85.16.5966>
- Madaule, P., Eda, M., Watanabe, N., Fujisawa, K., Matsuoka, T., Bito, H., Ishizaki, T., & Narumiya, S. (1998). Role of citron kinase as a target of the small GTPase Rho in cytokinesis. In *Nature* (Vol. 394, Issue 6692, pp. 491–494). <https://doi.org/10.1038/28873>
- Maddox, A. S., Habermann, B., Desai, A., & Oegema, K. (2005). Distinct roles for two *C. elegans* anillins in the gonad and early embryo. In *Development* (Vol. 132, Issue 12, pp. 2837–2848). <https://doi.org/10.1242/dev.01828>
- Maddox, A. S., Lewellyn, L., Desai, A., & Oegema, K. (2007). Anillin and the septins promote asymmetric ingression of the cytokinetic furrow. *Developmental Cell*, *12*(5), 827–835.
- Mangione, M. C., & Gould, K. L. (2019). Molecular form and function of the cytokinetic ring. *Journal of Cell Science*, *132*(12). <https://doi.org/10.1242/jcs.226928>
- Martin, A. C., Kaschube, M., & Wieschaus, E. F. (2009). Pulsed contractions of an actin-myosin network drive apical constriction. *Nature*, *457*(7228), 495–499.
- Mason, F. M., Heimsath, E. G., Higgs, H. N., & Soderling, S. H. (2011). Bi-modal regulation of a formin by srGAP2. *The Journal of Biological Chemistry*, *286*(8), 6577–6586.

- Mason, F. M., Tworoger, M., & Martin, A. C. (2013). Apical domain polarization localizes actin-myosin activity to drive ratchet-like apical constriction. *Nature Cell Biology*, *15*(8), 926–936.
- Mason, F. M., Xie, S., Vasquez, C. G., Tworoger, M., & Martin, A. C. (2016). RhoA GTPase inhibition organizes contraction during epithelial morphogenesis. *The Journal of Cell Biology*, *214*(5), 603–617.
- Mastrorarde, D. N., McDonald, K. L., Ding, R., & McIntosh, J. R. (1993). Interpolar spindle microtubules in PTK cells. *The Journal of Cell Biology*, *123*(6 Pt 1), 1475–1489.
- Masuda, M., Takeda, S., Sone, M., Ohki, T., Mori, H., Kamioka, Y., & Mochizuki, N. (2006). Endophilin BAR domain drives membrane curvature by two newly identified structure-based mechanisms. *The EMBO Journal*, *25*(12), 2889–2897.
- Matsumura, F. (2005). Regulation of myosin II during cytokinesis in higher eukaryotes. *Trends in Cell Biology*, *15*(7), 371–377.
- Matsumura, F., Ono, S., Yamakita, Y., Totsukawa, G., & Yamashiro, S. (1998). Specific Localization of Serine 19 Phosphorylated Myosin II during Cell Locomotion and Mitosis of Cultured Cells. In *Journal of Cell Biology* (Vol. 140, Issue 1, pp. 119–129). <https://doi.org/10.1083/jcb.140.1.119>
- Matsumura, F., Yamakita, Y., & Yamashiro, S. (2011). Myosin light chain kinases and phosphatase in mitosis and cytokinesis. *Archives of Biochemistry and Biophysics*, *510*(2), 76–82.
- Mattila, P. K., Pykäläinen, A., Saarikangas, J., Paavilainen, V. O., Vihinen, H., Jokitalo, E., & Lappalainen, P. (2007). Missing-in-metastasis and IRSp53 deform PI(4,5)P₂-rich membranes by an inverse BAR domain-like mechanism. *The Journal of Cell Biology*, *176*(7), 953–964.
- Maupin, P., & Pollard, T. D. (1986). Arrangement of actin filaments and myosin-like filaments in the contractile ring and of actin-like filaments in the mitotic spindle of dividing HeLa cells. *Journal of Ultrastructure and Molecular Structure Research*, *94*(1), 92–103.
- Mavrakis, M. (2016). Visualizing septins in early *Drosophila* embryos. *Methods in Cell Biology*, *136*, 183–198.

- Mavrakakis, M., Azou-Gros, Y., Tsai, F.-C., Alvarado, J., Bertin, A., Iv, F., Kress, A., Brasselet, S., Koenderink, G. H., & Lecuit, T. (2014). Septins promote F-actin ring formation by crosslinking actin filaments into curved bundles. *Nature Cell Biology*, *16*(4), 322–334.
- Mavrakakis, M., Rikhy, R., Lilly, M., & Lippincott-Schwartz, J. (2008). Fluorescence imaging techniques for studying Drosophila embryo development. *Current Protocols in Cell Biology / Editorial Board, Juan S. Bonifacino ... [et Al.]*, Chapter 4, Unit 4.18.
- Mavrakakis, M., Rikhy, R., & Lippincott-Schwartz, J. (2009). Plasma membrane polarity and compartmentalization are established before cellularization in the fly embryo. *Developmental Cell*, *16*(1), 93–104.
- May, K. M., Watts, F. Z., Jones, N., & Hyams, J. S. (1997). Type II myosin involved in cytokinesis in the fission yeast, *Schizosaccharomyces pombe*. *Cell Motility and the Cytoskeleton*, *38*(4), 385–396.
- Mazumdar, A., & Mazumdar, M. (2002). How one becomes many: blastoderm cellularization in *Drosophila melanogaster*. *BioEssays: News and Reviews in Molecular, Cellular and Developmental Biology*, *24*(11), 1012–1022.
- McCullough, B. R., Blanchoin, L., Martiel, J.-L., & De la Cruz, E. M. (2008). Cofilin increases the bending flexibility of actin filaments: implications for severing and cell mechanics. *Journal of Molecular Biology*, *381*(3), 550–558.
- McKay, H. F., & Burgess, D. R. (2011). “Life is a highway”: membrane trafficking during cytokinesis. *Traffic*, *12*(3), 247–251.
- Meitinger, F., Richter, H., Heisel, S., Hub, B., Seufert, W., & Pereira, G. (2013). A safeguard mechanism regulates Rho GTPases to coordinate cytokinesis with the establishment of cell polarity. *PLoS Biology*, *11*(2), e1001495.
- Mendes Pinto, I., Rubinstein, B., Kucharavy, A., Unruh, J. R., & Li, R. (2012). Actin depolymerization drives actomyosin ring contraction during budding yeast cytokinesis. *Developmental Cell*, *22*(6), 1247–1260.
- Mendes Pinto, I., Rubinstein, B., & Li, R. (2013). Force to divide: structural and mechanical requirements for actomyosin ring contraction. *Biophysical Journal*, *105*(3), 547–554.
- Merrill, P. T., Sweeton, D., & Wieschaus, E. (1988). Requirements for autosomal gene activity during precellular stages of *Drosophila melanogaster*. *Development*, *104*(3), 495–509.

- Miki, H., Yamaguchi, H., Suetsugu, S., & Takenawa, T. (2000). IRSp53 is an essential intermediate between Rac and WAVE in the regulation of membrane ruffling. *Nature*, *408*(6813), 732–735.
- Millard, T. H., Bompard, G., Heung, M. Y., Dafforn, T. R., Scott, D. J., Machesky, L. M., & Fütterer, K. (2005). Structural basis of filopodia formation induced by the IRSp53/MIM homology domain of human IRSp53. *The EMBO Journal*, *24*(2), 240–250.
- Miller, K. G., & Kiehart, D. P. (1995). Fly division. *The Journal of Cell Biology*, *131*(1), 1–5.
- Mim, C., Cui, H., Gawronski-Salerno, J. A., Frost, A., Lyman, E., Voth, G. A., & Unger, V. M. (2012). Structural basis of membrane bending by the N-BAR protein endophilin. *Cell*, *149*(1), 137–145.
- Mishima, M., Kaitna, S., & Glotzer, M. (2002). Central spindle assembly and cytokinesis require a kinesin-like protein/RhoGAP complex with microtubule bundling activity. *Developmental Cell*, *2*(1), 41–54.
- Mishima, M., Pavicic, V., Grüneberg, U., Nigg, E. A., & Glotzer, M. (2004). Cell cycle regulation of central spindle assembly. In *Nature* (Vol. 430, Issue 7002, pp. 908–913). <https://doi.org/10.1038/nature02767>
- Mizuno, T., Amano, M., Kaibuchi, K., & Nishida, Y. (1999). Identification and characterization of Drosophila homolog of Rho-kinase. *Gene*, *238*(2), 437–444.
- Mizuno, T., Tsutsui, K., & Nishida, Y. (2002). Drosophila myosin phosphatase and its role in dorsal closure. *Development*, *129*(5), 1215–1223.
- modENCODE Consortium, Roy, S., Ernst, J., Kharchenko, P. V., Kheradpour, P., Negre, N., Eaton, M. L., Landolin, J. M., Bristow, C. A., Ma, L., Lin, M. F., Washietl, S., Arshinoff, B. I., Ay, F., Meyer, P. E., Robine, N., Washington, N. L., Di Stefano, L., Berezhikov, E., ... Kellis, M. (2010). Identification of functional elements and regulatory circuits by Drosophila modENCODE. *Science*, *330*(6012), 1787–1797.
- Mollinari, C., Kleman, J.-P., Jiang, W., Schoehn, G., Hunter, T., & Margolis, R. L. (2002). PRC1 is a microtubule binding and bundling protein essential to maintain the mitotic spindle midzone. In *Journal of Cell Biology* (Vol. 157, Issue 7, pp. 1175–1186). <https://doi.org/10.1083/jcb.200111052>
- Montagnac, G., Echard, A., & Chavrier, P. (2008). Endocytic traffic in animal cell cytokinesis. *Current Opinion in Cell Biology*, *20*(4), 454–461.

- Moskalenko, S., Henry, D. O., Rosse, C., Mirey, G., Camonis, J. H., & White, M. A. (2002). The exocyst is a Ral effector complex. In *Nature Cell Biology* (Vol. 4, Issue 1, pp. 66–72). <https://doi.org/10.1038/ncb728>
- Motegi, F., Nakano, K., Kitayama, C., Yamamoto, M., & Mabuchi, I. (1997). Identification of Myo3, a second type-II myosin heavy chain in the fission yeast *Schizosaccharomyces pombe*. *FEBS Letters*, 420(2-3), 161–166.
- Mulinari, S., & Häcker, U. (2010). Rho-guanine nucleotide exchange factors during development: Force is nothing without control. *Small GTPases*, 1(1), 28–43.
- Munjal, A., Philippe, J.-M., Munro, E., & Lecuit, T. (2015). A self-organized biomechanical network drives shape changes during tissue morphogenesis. *Nature*, 524(7565), 351–355.
- Murrell, M., Oakes, P. W., Lenz, M., & Gardel, M. L. (2015). Forcing cells into shape: the mechanics of actomyosin contractility. *Nature Reviews. Molecular Cell Biology*, 16(8), 486–498.
- Murthy, K., & Wadsworth, P. (2005). Myosin-II-Dependent Localization and Dynamics of F-Actin during Cytokinesis. In *Current Biology* (Vol. 15, Issue 8, pp. 724–731). <https://doi.org/10.1016/j.cub.2005.02.055>
- Murthy, M., & Schwarz, T. L. (2004). The exocyst component Sec5 is required for membrane traffic and polarity in the *Drosophila* ovary. In *Development* (Vol. 131, Issue 2, pp. 377–388). <https://doi.org/10.1242/dev.00931>
- Naim, V., Imarisio, S., Di Cunto, F., Gatti, M., & Bonaccorsi, S. (2004). *Drosophila* Citron Kinase Is Required for the Final Steps of Cytokinesis. In *Molecular Biology of the Cell* (Vol. 15, Issue 11, pp. 5053–5063). <https://doi.org/10.1091/mbc.e04-06-0536>
- Nakagawa, O., Fujisawa, K., Ishizaki, T., Saito, Y., Nakao, K., & Narumiya, S. (1996). ROCK-I and ROCK-II, two isoforms of Rho-associated coiled-coil forming protein serine/threonine kinase in mice. In *FEBS Letters* (Vol. 392, Issue 2, pp. 189–193). [https://doi.org/10.1016/0014-5793\(96\)00811-3](https://doi.org/10.1016/0014-5793(96)00811-3)
- Naqvi, N. I., Wong, K. C., Tang, X., & Balasubramanian, M. K. (2000). Type II myosin regulatory light chain relieves auto-inhibition of myosin-heavy-chain function. *Nature Cell Biology*, 2(11), 855–858.

- Neto, H., Collins, L. L., & Gould, G. W. (2011). Vesicle trafficking and membrane remodelling in cytokinesis. In *Biochemical Journal* (Vol. 437, Issue 1, pp. 13–24). <https://doi.org/10.1042/bj20110153>
- Neto, H., & Gould, G. W. (2011). The regulation of abscission by multi-protein complexes. *Journal of Cell Science*, 124(Pt 19), 3199–3207.
- Neufeld, T. P., & Rubin, G. M. (1994). The *Drosophila* peanut gene is required for cytokinesis and encodes a protein similar to yeast putative bud neck filament proteins. *Cell*, 77(3), 371–379.
- Neujahr, R., Heizer, C., & Gerisch, G. (1997). Myosin II-independent processes in mitotic cells of *Dictyostelium discoideum*: redistribution of the nuclei, re-arrangement of the actin system and formation of the cleavage furrow. In *Journal of Cell Science* (Vol. 110, Issue 2, pp. 123–137). <https://doi.org/10.1242/jcs.110.2.123>
- Nislow, C., Sellitto, C., Kuriyama, R., & McIntosh, J. R. (1990). A monoclonal antibody to a mitotic microtubule-associated protein blocks mitotic progression. *The Journal of Cell Biology*, 111(2), 511–522.
- Niswonger, M. L., & O'Halloran, T. J. (1997). A novel role for clathrin in cytokinesis. *Proceedings of the National Academy of Sciences of the United States of America*, 94(16), 8575–8578.
- Noguchi, T., & Mabuchi, I. (2001). Reorganization of actin cytoskeleton at the growing end of the cleavage furrow of *Xenopus* egg during cytokinesis. In *Journal of Cell Science* (Vol. 114, Issue 2, pp. 401–412). <https://doi.org/10.1242/jcs.114.2.401>
- Normand, G., & King, R. W. (2010). Understanding Cytokinesis Failure. In *Advances in Experimental Medicine and Biology* (pp. 27–55). https://doi.org/10.1007/978-1-4419-6199-0_3
- O'Connell, C. B., Warner, A. K., & Wang, Y.-L. (2001). Distinct roles of the equatorial and polar cortices in the cleavage of adherent cells. In *Current Biology* (Vol. 11, Issue 9, pp. 702–707). [https://doi.org/10.1016/s0960-9822\(01\)00181-6](https://doi.org/10.1016/s0960-9822(01)00181-6)
- Oegema, K., Savoian, M. S., Mitchison, T. J., & Field, C. M. (2000). Functional Analysis of a Human Homologue of the *Drosophila* Actin Binding Protein Anillin Suggests a Role in Cytokinesis. In *Journal of Cell Biology* (Vol. 150, Issue 3, pp. 539–552). <https://doi.org/10.1083/jcb.150.3.539>

- Oh, Y., Schreiter, J., Nishihama, R., Wloka, C., & Bi, E. (2013). Targeting and functional mechanisms of the cytokinesis-related F-BAR protein Hof1 during the cell cycle. In *Molecular Biology of the Cell* (Vol. 24, Issue 9, pp. 1305–1320). <https://doi.org/10.1091/mbc.e12-11-0804>
- Ono, K., Parast, M., Alberico, C., Benian, G. M., & Ono, S. (2003). Specific requirement for two ADF/cofilin isoforms in distinct actin-dependent processes in *Caenorhabditis elegans*. In *Journal of Cell Science* (Vol. 116, Issue 10, pp. 2073–2085). <https://doi.org/10.1242/jcs.00421>
- Padash Barmchi, M., Rogers, S., & Häcker, U. (2005). DRhoGEF2 regulates actin organization and contractility in the *Drosophila* blastoderm embryo. *The Journal of Cell Biology*, 168(4), 575–585.
- Panagopoulos, I., Kitagawa, A., Isaksson, M., Mörse, H., Mitelman, F., & Johansson, B. (2004). MLL/GRAF fusion in an infant acute monocytic leukemia (AML M5b) with a cytogenetically cryptic ins(5;11)(q31;q23q23). In *Genes, Chromosomes and Cancer* (Vol. 41, Issue 4, pp. 400–404). <https://doi.org/10.1002/gcc.20097>
- Pang, X., Fan, J., Zhang, Y., Zhang, K., Gao, B., Ma, J., Li, J., Deng, Y., Zhou, Q., Egelman, E. H., Hsu, V. W., & Sun, F. (2014). A PH Domain in ACAP1 Possesses Key Features of the BAR Domain in Promoting Membrane Curvature. In *Developmental Cell* (Vol. 31, Issue 1, pp. 73–86). <https://doi.org/10.1016/j.devcel.2014.08.020>
- Park, J.-M., & Lubensky, T. C. (1996). Interactions between membrane Inclusions on Fluctuating Membranes. In *Journal de Physique I* (Vol. 6, Issue 9, pp. 1217–1235). <https://doi.org/10.1051/jp1:1996125>
- Pavicic-Kaltenbrunner, V., Mishima, M., & Glotzer, M. (2007). Cooperative assembly of CYK-4/MgcRacGAP and ZEN-4/MKLP1 to form the centralspindlin complex. *Molecular Biology of the Cell*, 18(12), 4992–5003.
- Pelissier, A., Chauvin, J.-P., & Lecuit, T. (2003). Trafficking through Rab11 endosomes is required for cellularization during *Drosophila* embryogenesis. *Current Biology: CB*, 13(21), 1848–1857.
- Peter, B. J., Kent, H. M., Mills, I. G., Vallis, Y., Butler, P. J. G., Evans, P. R., & McMahon, H. T. (2004). BAR domains as sensors of membrane curvature: the amphiphysin BAR structure. *Science*, 303(5657), 495–499.

- Pichot, C. S., Arvanitis, C., Hartig, S. M., Jensen, S. A., Bechill, J., Marzouk, S., Yu, J., Frost, J. A., & Corey, S. J. (2010). Cdc42-interacting protein 4 promotes breast cancer cell invasion and formation of invadopodia through activation of N-WASp. *Cancer Research*, *70*(21), 8347–8356.
- Piekny, A. J., & Maddox, A. S. (2010). The myriad roles of Anillin during cytokinesis. *Seminars in Cell & Developmental Biology*, *21*(9), 881–891.
- Piekny, A. J., & Mains, P. E. (2002). Rho-binding kinase (LET-502) and myosin phosphatase (MEL-11) regulate cytokinesis in the early *Caenorhabditis elegans* embryo. In *Journal of Cell Science* (Vol. 115, Issue 11, pp. 2271–2282). <https://doi.org/10.1242/jcs.115.11.2271>
- Piekny, A., Werner, M., & Glotzer, M. (2005). Cytokinesis: welcome to the Rho zone. *Trends in Cell Biology*, *15*(12), 651–658.
- Pinar, M., Coll, P. M., Rincón, S. A., & Pérez, P. (2008). *Schizosaccharomyces pombe* Pxl1 is a paxillin homologue that modulates Rho1 activity and participates in cytokinesis. *Molecular Biology of the Cell*, *19*(4), 1727–1738.
- Pollard, T. D., & O’Shaughnessy, B. (2019). Molecular Mechanism of Cytokinesis. In *Annual Review of Biochemistry* (Vol. 88, Issue 1, pp. 661–689). <https://doi.org/10.1146/annurev-biochem-062917-012530>
- Pollard, T. D., & Wu, J.-Q. (2010). Understanding cytokinesis: lessons from fission yeast. *Nature Reviews. Molecular Cell Biology*, *11*(2), 149–155.
- Powers, J., Bossinger, O., Rose, D., Strome, S., & Saxton, W. (1998). A nematode kinesin required for cleavage furrow advancement. *Current Biology: CB*, *8*(20), 1133–1136.
- Prekeris, R., & Gould, G. W. (2008). Breaking up is hard to do – membrane traffic in cytokinesis. In *Journal of Cell Science* (Vol. 121, Issue 10, pp. 1569–1576). <https://doi.org/10.1242/jcs.018770>
- Prévost, C., Zhao, H., Manzi, J., Lemichez, E., Lappalainen, P., Callan-Jones, A., & Bassereau, P. (2015). IRSp53 senses negative membrane curvature and phase separates along membrane tubules. *Nature Communications*, *6*, 8529.
- Prigent, M., Dubois, T., Raposo, G., Derrien, V., Tenza, D., Rossé, C., Camonis, J., & Chavrier, P. (2003). ARF6 controls post-endocytic recycling through its downstream exocyst complex effector. *The Journal of Cell Biology*, *163*(5), 1111–1121.

- Pring, M., Evangelista, M., Boone, C., Yang, C., & Zigmond, S. H. (2003). Mechanism of formin-induced nucleation of actin filaments. *Biochemistry*, *42*(2), 486–496.
- Prokopenko, S. N., Brumby, A., O'Keefe, L., Prior, L., He, Y., Saint, R., & Bellen, H. J. (1999). A putative exchange factor for Rho1 GTPase is required for initiation of cytokinesis in *Drosophila*. In *Genes & Development* (Vol. 13, Issue 17, pp. 2301–2314). <https://doi.org/10.1101/gad.13.17.2301>
- Prudnikova, T. Y., Rawat, S. J., & Chernoff, J. (2015). Molecular pathways: targeting the kinase effectors of RHO-family GTPases. *Clinical Cancer Research: An Official Journal of the American Association for Cancer Research*, *21*(1), 24–29.
- Pruyne, D. (2002). Role of Formins in Actin Assembly: Nucleation and Barbed-End Association. In *Science* (Vol. 297, Issue 5581, pp. 612–615). <https://doi.org/10.1126/science.1072309>
- Pykäläinen, A., Boczkowska, M., Zhao, H., Saarikangas, J., Rebowski, G., Jansen, M., Hakanen, J., Koskela, E. V., Peränen, J., Vihinen, H., Jokitalo, E., Salminen, M., Ikonen, E., Dominguez, R., & Lappalainen, P. (2011). Pinkbar is an epithelial-specific BAR domain protein that generates planar membrane structures. *Nature Structural & Molecular Biology*, *18*(8), 902–907.
- Qian, J., Qian, Z., Lin, J., Yao, D.-M., Chen, Q., Li, Y., Ji, R.-B., Yang, J., Xiao, G.-F., & Wang, Y.-L. (2011). Abnormal methylation of GRAF promoter Chinese patients with acute myeloid leukemia. *Leukemia Research*, *35*(6), 783–786.
- Qian, Z., Qian, J., Lin, J., Yao, D.-M., Chen, Q., Ji, R.-B., Li, Y., Xiao, G.-F., & Li, J.-Y. (2010). GTPase regulator associated with the focal adhesion kinase (GRAF) transcript was down-regulated in patients with myeloid malignancies. *Journal of Experimental & Clinical Cancer Research: CR*, *29*, 111.
- Qualmann, B., Koch, D., & Kessels, M. M. (2011). Let's go bananas: revisiting the endocytic BAR code. In *The EMBO Journal* (Vol. 30, Issue 17, pp. 3501–3515). <https://doi.org/10.1038/emboj.2011.266>
- Raich, W. B., Moran, A. N., Rothman, J. H., & Hardin, J. (1998). Cytokinesis and midzone microtubule organization in *Caenorhabditis elegans* require the kinesin-like protein ZEN-4. *Molecular Biology of the Cell*, *9*(8), 2037–2049.

- Ramesh, P., Baroji, Y. F., Reihani, S. N. S., Stamou, D., Oddershede, L. B., & Bendix, P. M. (2013). FBAR Syndapin 1 recognizes and stabilizes highly curved tubular membranes in a concentration dependent manner. In *Scientific Reports* (Vol. 3, Issue 1). <https://doi.org/10.1038/srep01565>
- Rao, Y., & Haucke, V. (2011). Membrane shaping by the Bin/amphiphysin/Rvs (BAR) domain protein superfamily. In *Cellular and Molecular Life Sciences* (Vol. 68, Issue 24, pp. 3983–3993). <https://doi.org/10.1007/s00018-011-0768-5>
- Rao, Y., Ma, Q., Vahedi-Faridi, A., Sundborger, A., Pechstein, A., Puchkov, D., Luo, L., Shupliakov, O., Saenger, W., & Haucke, V. (2010). Molecular basis for SH3 domain regulation of F-BAR-mediated membrane deformation. *Proceedings of the National Academy of Sciences of the United States of America*, *107*(18), 8213–8218.
- Rappaport, R. (1985). Repeated furrow formation from a single mitotic apparatus in cylindrical sand dollar eggs. *The Journal of Experimental Zoology*, *234*(1), 167–171.
- Rauzi, M., Lenne, P.-F., & Lecuit, T. (2010). Planar polarized actomyosin contractile flows control epithelial junction remodelling. *Nature*, *468*(7327), 1110–1114.
- Regev, M., Sabanay, H., Kartvelishvily, E., Kam, Z., & Bershadsky, A. D. (2017). Involvement of Rho GAP GRAF1 in maintenance of epithelial phenotype. *Cell Adhesion & Migration*, *11*(4), 367–383.
- Renard, H.-F., Simunovic, M., Lemièrre, J., Boucrot, E., Garcia-Castillo, M. D., Arumugam, S., Chambon, V., Lamaze, C., Wunder, C., Kenworthy, A. K., Schmidt, A. A., McMahon, H. T., Sykes, C., Bassereau, P., & Johannes, L. (2015). Endophilin-A2 functions in membrane scission in clathrin-independent endocytosis. *Nature*, *517*(7535), 493–496.
- Ren, X. R., Du, Q. S., Huang, Y. Z., Ao, S. Z., Mei, L., & Xiong, W. C. (2001). Regulation of CDC42 GTPase by proline-rich tyrosine kinase 2 interacting with PSGAP, a novel pleckstrin homology and Src homology 3 domain containing rhoGAP protein. *The Journal of Cell Biology*, *152*(5), 971–984.
- Ren, X., Sun, J., Housden, B. E., Hu, Y., Roesel, C., Lin, S., Liu, L.-P., Yang, Z., Mao, D., Sun, L., Wu, Q., Ji, J.-Y., Xi, J., Mohr, S. E., Xu, J., Perrimon, N., & Ni, J.-Q. (2013). Optimized gene editing technology for *Drosophila melanogaster* using germ line-specific Cas9. *Proceedings of the National Academy of Sciences of the United States of America*, *110*(47), 19012–19017.

- Reversi, A., Loeser, E., Subramanian, D., Schultz, C., & De Renzis, S. (2014). Plasma membrane phosphoinositide balance regulates cell shape during *Drosophila* embryo morphogenesis. *The Journal of Cell Biology*, *205*(3), 395–408.
- Reymann, A.-C., Staniscia, F., Erzberger, A., Salbreux, G., & Grill, S. W. (2016). Cortical flow aligns actin filaments to form a furrow. In *eLife* (Vol. 5). <https://doi.org/10.7554/elife.17807>
- Ridley, A. J. (2015). Rho GTPase signalling in cell migration. *Current Opinion in Cell Biology*, *36*, 103–112.
- Riggs, B., Rothwell, W., Mische, S., Hickson, G. R. X., Matheson, J., Hays, T. S., Gould, G. W., & Sullivan, W. (2003). Actin cytoskeleton remodeling during early *Drosophila* furrow formation requires recycling endosomal components Nuclear-fallout and Rab11. *The Journal of Cell Biology*, *163*(1), 143–154.
- Rikhy, R., Mavrakis, M., & Lippincott-Schwartz, J. (2015). Dynamin regulates metaphase furrow formation and plasma membrane compartmentalization in the syncytial *Drosophila* embryo. *Biology Open*, *4*(3), 301–311.
- Roberts-Galbraith, R. H., Chen, J.-S., Wang, J., & Gould, K. L. (2009). The SH3 domains of two PCH family members cooperate in assembly of the *Schizosaccharomyces pombe* contractile ring. *The Journal of Cell Biology*, *184*(1), 113–127.
- Roberts-Galbraith, R. H., & Gould, K. L. (2010). Setting the F-BAR: functions and regulation of the F-BAR protein family. *Cell Cycle*, *9*(20), 4091–4097.
- Roberts-Galbraith, R. H., Ohi, M. D., Ballif, B. A., Chen, J.-S., McLeod, I., Hayes McDonald, W., Gygi, S. P., Yates, J. R., & Gould, K. L. (2010). Dephosphorylation of F-BAR Protein Cdc15 Modulates Its Conformation and Stimulates Its Scaffolding Activity at the Cell Division Site. In *Molecular Cell* (Vol. 39, Issue 1, pp. 86–99). <https://doi.org/10.1016/j.molcel.2010.06.012>
- Robinson, D. N., & Cooley, L. (1996). Stable intercellular bridges in development: the cytoskeleton lining the tunnel. In *Trends in Cell Biology* (Vol. 6, Issue 12, pp. 474–479). [https://doi.org/10.1016/0962-8924\(96\)84945-2](https://doi.org/10.1016/0962-8924(96)84945-2)
- Rogers, S. L., Wiedemann, U., Häcker, U., Turck, C., & Vale, R. D. (2004). *Drosophila* RhoGEF2 Associates with Microtubule Plus Ends in an EB1-Dependent Manner. In *Current Biology* (Vol. 14, Issue 20, pp. 1827–1833). <https://doi.org/10.1016/j.cub.2004.09.078>

- Romero, S., Le Clainche, C., Didry, D., Egile, C., Pantaloni, D., & Carlier, M.-F. (2004). Formin is a processive motor that requires profilin to accelerate actin assembly and associated ATP hydrolysis. *Cell*, *119*(3), 419–429.
- Royou, A., Field, C., Sisson, J. C., Sullivan, W., & Karess, R. (2004). Reassessing the role and dynamics of nonmuscle myosin II during furrow formation in early *Drosophila* embryos. *Molecular Biology of the Cell*, *15*(2), 838–850.
- Rueden, C. T., Schindelin, J., Hiner, M. C., DeZonia, B. E., Walter, A. E., Arena, E. T., & Eliceiri, K. W. (2017). ImageJ2: ImageJ for the next generation of scientific image data. *BMC Bioinformatics*, *18*(1), 529.
- Saarikangas, J., & Barral, Y. (2011). The emerging functions of septins in metazoans. *EMBO Reports*, *12*(11), 1118–1126.
- Saarikangas, J., Hakanen, J., Mattila, P. K., Grumet, M., Salminen, M., & Lappalainen, P. (2008). ABBA regulates plasma-membrane and actin dynamics to promote radial glia extension. *Journal of Cell Science*, *121*(Pt 9), 1444–1454.
- Saarikangas, J., Zhao, H., Pykäläinen, A., Laurinmäki, P., Mattila, P. K., Kinnunen, P. K. J., Butcher, S. J., & Lappalainen, P. (2009). Molecular mechanisms of membrane deformation by I-BAR domain proteins. *Current Biology: CB*, *19*(2), 95–107.
- Sagot, I., Rodal, A. A., Moseley, J., Goode, B. L., & Pellman, D. (2002). An actin nucleation mechanism mediated by Bni1 and Profilin. In *Nature Cell Biology* (Vol. 4, Issue 8, pp. 626–631). <https://doi.org/10.1038/ncb834>
- Sakamuro, D., Elliott, K. J., Wechsler-Reya, R., & Prendergast, G. C. (1996). BIN1 is a novel MYC-interacting protein with features of a tumour suppressor. *Nature Genetics*, *14*(1), 69–77.
- Salazar, M. A., Kwiatkowski, A. V., Pellegrini, L., Cestra, G., Butler, M. H., Rossman, K. L., Serna, D. M., Sondek, J., Gertler, F. B., & De Camilli, P. (2003). Tuba, a Novel Protein Containing Bin/Amphiphysin/Rvs and Dbl Homology Domains, Links Dynamin to Regulation of the Actin Cytoskeleton. In *Journal of Biological Chemistry* (Vol. 278, Issue 49, pp. 49031–49043). <https://doi.org/10.1074/jbc.m308104200>
- Sanny, J., Chui, V., Langmann, C., Pereira, C., Zahedi, B., & Harden, N. (2006). *Drosophila* RhoGAP68F is a putative GTPase activating protein for RhoA participating in gastrulation. *Development Genes and Evolution*, *216*(9), 543–550.

- Schejter, E. D., Rose, L. S., Postner, M. A., & Wieschaus, E. (1992). Role of the Zygotic Genome in the Restructuring of the Actin Cytoskeleton at the Cycle-14 Transition during *Drosophila* Embryogenesis. In *Cold Spring Harbor Symposia on Quantitative Biology* (Vol. 57, Issue 0, pp. 653–659). <https://doi.org/10.1101/sqb.1992.057.01.071>
- Schejter, E. D., & Wieschaus, E. (1993a). Functional elements of the cytoskeleton in the early *Drosophila* embryo. *Annual Review of Cell Biology*, 9, 67–99.
- Schejter, E. D., & Wieschaus, E. (1993b). bottleneck acts as a regulator of the microfilament network governing cellularization of the *Drosophila* embryo. *Cell*, 75(2), 373–385.
- Schiel, J. A., & Prekeris, R. (2013). Membrane dynamics during cytokinesis. In *Current Opinion in Cell Biology* (Vol. 25, Issue 1, pp. 92–98). <https://doi.org/10.1016/j.ceb.2012.10.012>
- Schmutz, C., Stevens, J., & Spang, A. (2007). Functions of the novel RhoGAP proteins RGA-3 and RGA-4 in the germ line and in the early embryo of *C. elegans*. *Development*. <https://dev.biologists.org/content/134/19/3495.short>
- Schroeder, T. E. (1972). THE CONTRACTILE RING. In *Journal of Cell Biology* (Vol. 53, Issue 2, pp. 419–434). <https://doi.org/10.1083/jcb.53.2.419>
- Schwayer, C., Sikora, M., Slováková, J., Kardos, R., & Heisenberg, C.-P. (2016). Actin Rings of Power. In *Developmental Cell* (Vol. 37, Issue 6, pp. 493–506). <https://doi.org/10.1016/j.devcel.2016.05.024>
- Schweisguth, F., Lepesant, J. A., & Vincent, A. (1990). The serendipity alpha gene encodes a membrane-associated protein required for the cellularization of the *Drosophila* embryo. *Genes & Development*, 4(6), 922–931.
- Schweisguth, F., Vincent, A., & Lepesant, J. A. (1991). Genetic analysis of the cellularization of the *Drosophila* embryo. *Biology of the Cell / under the Auspices of the European Cell Biology Organization*, 72(1-2), 15–23.
- Schweitzer, J. K., Burke, E. E., Goodson, H. V., & D'Souza-Schorey, C. (2005). Endocytosis resumes during late mitosis and is required for cytokinesis. *The Journal of Biological Chemistry*, 280(50), 41628–41635.
- Schweitzer, Y., & Kozlov, M. M. (2015). Membrane-mediated interaction between strongly anisotropic protein scaffolds. *PLoS Computational Biology*, 11(2), e1004054.

- Scita, G., Confalonieri, S., Lappalainen, P., & Suetsugu, S. (2008). IRSp53: crossing the road of membrane and actin dynamics in the formation of membrane protrusions. *Trends in Cell Biology*, 18(2), 52–60.
- Sen, A., Nagy-Zsvér-Vadas, Z., & Krahn, M. P. (2012). Drosophila PATJ supports adherens junction stability by modulating Myosin light chain activity. *The Journal of Cell Biology*, 199(4), 685–698.
- Severson, A. F., Baillie, D. L., & Bowerman, B. (2002). A Formin Homology Protein and a Profilin Are Required for Cytokinesis and Arp2/3-Independent Assembly of Cortical Microfilaments in *C. elegans*. In *Current Biology* (Vol. 12, Issue 24, pp. 2066–2075). [https://doi.org/10.1016/s0960-9822\(02\)01355-6](https://doi.org/10.1016/s0960-9822(02)01355-6)
- Severson, A. F., Hamill, D. R., Clayton Carter, J., Schumacher, J., & Bowerman, B. (2000). The Aurora-related kinase AIR-2 recruits ZEN-4/CeMKLP1 to the mitotic spindle at metaphase and is required for cytokinesis. In *Current Biology* (Vol. 10, Issue 19, pp. 1162–1171). [https://doi.org/10.1016/s0960-9822\(00\)00715-6](https://doi.org/10.1016/s0960-9822(00)00715-6)
- Shandala, T., Gregory, S. L., Dalton, H. E., Smallhorn, M., & Saint, R. (2004). Citron Kinase is an essential effector of the Pbl-activated Rho signalling pathway in *Drosophila melanogaster*. In *Development* (Vol. 131, Issue 20, pp. 5053–5063). <https://doi.org/10.1242/dev.01382>
- Sharma, S., & Rikhy, R. (2021). Spatiotemporal recruitment of RhoGTPase protein GRAF inhibits actomyosin ring constriction in *Drosophila* cellularization. *eLife*, 10. <https://doi.org/10.7554/eLife.63535>
- Shelton, C. A., Carter, J. C., Ellis, G. C., & Bowerman, B. (1999). The nonmuscle myosin regulatory light chain gene *mlc-4* is required for cytokinesis, anterior-posterior polarity, and body morphology during *Caenorhabditis elegans* embryogenesis. *The Journal of Cell Biology*, 146(2), 439–451.
- Sherlekar, A., & Rikhy, R. (2016). Syndapin promotes pseudocleavage furrow formation by actin organization in the syncytial *Drosophila* embryo. *Molecular Biology of the Cell*, 27(13), 2064–2079.
- Shibata, H., Oishi, K., Yamagiwa, A., Matsumoto, M., Mukai, H., & Ono, Y. (2001). PKN interacts with the SH3 Domains of Graf and a Novel Graf Related Protein, Graf 2, Which

- Are GTPase Activating Proteins for Rho Family. In *Journal of Biochemistry* (Vol. 130, Issue 1, pp. 23–31). <https://doi.org/10.1093/oxfordjournals.jbchem.a002958>
- Shimada, A., Niwa, H., Tsujita, K., Suetsugu, S., Nitta, K., Hanawa-Suetsugu, K., Akasaka, R., Nishino, Y., Toyama, M., Chen, L., Liu, Z.-J., Wang, B.-C., Yamamoto, M., Terada, T., Miyazawa, A., Tanaka, A., Sugano, S., Shirouzu, M., Nagayama, K., ... Yokoyama, S. (2007). Curved EFC/F-BAR-domain dimers are joined end to end into a filament for membrane invagination in endocytosis. *Cell*, *129*(4), 761–772.
- Shi, Z., & Baumgart, T. (2015). Membrane tension and peripheral protein density mediate membrane shape transitions. *Nature Communications*, *6*, 5974.
- Simunovic, M., Evergren, E., Golushko, I., Prévost, C., Renard, H.-F., Johannes, L., McMahon, H. T., Lorman, V., Voth, G. A., & Bassereau, P. (2016). How curvature-generating proteins build scaffolds on membrane nanotubes. *Proceedings of the National Academy of Sciences of the United States of America*, *113*(40), 11226–11231.
- Simunovic, M., Voth, G. A., Callan-Jones, A., & Bassereau, P. (2015). When Physics Takes Over: BAR Proteins and Membrane Curvature. *Trends in Cell Biology*, *25*(12), 780–792.
- Sisson, J. C., Field, C., Ventura, R., Royou, A., & Sullivan, W. (2000). Lava Lamp, a Novel Peripheral Golgi Protein, Is Required for *Drosophila melanogaster* Cellularization. In *Journal of Cell Biology* (Vol. 151, Issue 4, pp. 905–918). <https://doi.org/10.1083/jcb.151.4.905>
- Sivadon, P., Crouzet, M., & Aigle, M. (1997). Functional assessment of the yeast Rvs161 and Rvs167 protein domains. *FEBS Letters*, *417*(1), 21–27.
- Skop, A. R. (2004). Dissection of the Mammalian Midbody Proteome Reveals Conserved Cytokinesis Mechanisms. In *Science* (Vol. 305, Issue 5680, pp. 61–66). <https://doi.org/10.1126/science.1097931>
- Skop, A. R., Bergmann, D., Mohler, W. A., & White, J. G. (2001). Completion of cytokinesis in *C. elegans* requires a brefeldin A-sensitive membrane accumulation at the cleavage furrow apex. In *Current Biology* (Vol. 11, Issue 10, pp. 735–746). [https://doi.org/10.1016/s0960-9822\(01\)00231-7](https://doi.org/10.1016/s0960-9822(01)00231-7)
- Sokac, A. M., & Wieschaus, E. (2008a). Local actin-dependent endocytosis is zygotically controlled to initiate *Drosophila* cellularization. *Developmental Cell*, *14*(5), 775–786.

- Sokac, A. M., & Wieschaus, E. (2008b). Zygoticly controlled F-actin establishes cortical compartments to stabilize furrows during *Drosophila* cellularization. *Journal of Cell Science*, *121*(11), 1815–1824.
- Somers, W. G., Gregory Somers, W., & Saint, R. (2003). A RhoGEF and Rho Family GTPase-Activating Protein Complex Links the Contractile Ring to Cortical Microtubules at the Onset of Cytokinesis. In *Developmental Cell* (Vol. 4, Issue 1, pp. 29–39). [https://doi.org/10.1016/s1534-5807\(02\)00402-1](https://doi.org/10.1016/s1534-5807(02)00402-1)
- Somma, M. P., Fasulo, B., Cenci, G., Cundari, E., & Gatti, M. (2002). Molecular Dissection of Cytokinesis by RNA Interference in *Drosophila* Cultured Cells. In *Molecular Biology of the Cell* (Vol. 13, Issue 7, pp. 2448–2460). <https://doi.org/10.1091/mbc.01-12-0589>
- Sönnichsen, B., Koski, L. B., Walsh, A., Marschall, P., Neumann, B., Brehm, M., Alleaume, A.-M., Artelt, J., Bettencourt, P., Cassin, E., Hewitson, M., Holz, C., Khan, M., Lazik, S., Martin, C., Nitzsche, B., Ruer, M., Stamford, J., Winzi, M., ... Echeverri, C. J. (2005). Full-genome RNAi profiling of early embryogenesis in *Caenorhabditis elegans*. *Nature*, *434*(7032), 462–469.
- Sorre, B., Callan-Jones, A., Manzi, J., Goud, B., Prost, J., Bassereau, P., & Roux, A. (2012). Nature of curvature coupling of amphiphysin with membranes depends on its bound density. *Proceedings of the National Academy of Sciences of the United States of America*, *109*(1), 173–178.
- Stachowiak, M. R., Laplante, C., Chin, H. F., Guirao, B., Karatekin, E., Pollard, T. D., & O’Shaughnessy, B. (2014). Mechanism of cytokinetic contractile ring constriction in fission yeast. *Developmental Cell*, *29*(5), 547–561.
- Stevenson, V., Hudson, A., Cooley, L., & Theurkauf, W. E. (2002). Arp2/3-dependent pseudocleavage [correction of psuedocleavage] furrow assembly in syncytial *Drosophila* embryos. *Current Biology: CB*, *12*(9), 705–711.
- Storchova, Z., & Pellman, D. (2004). From polyploidy to aneuploidy, genome instability and cancer. In *Nature Reviews Molecular Cell Biology* (Vol. 5, Issue 1, pp. 45–54). <https://doi.org/10.1038/nrm1276>
- Straight, A. F., Cheung, A., Limouze, J., Chen, I., Westwood, N. J., Sellers, J. R., & Mitchison, T. J. (2003). Dissecting temporal and spatial control of cytokinesis with a myosin II Inhibitor. *Science*, *299*(5613), 1743–1747.

- Straight, A. F., Field, C. M., & Mitchison, T. J. (2005). Anillin Binds Nonmuscle Myosin II and Regulates the Contractile Ring. In *Molecular Biology of the Cell* (Vol. 16, Issue 1, pp. 193–201). <https://doi.org/10.1091/mbc.e04-08-0758>
- Strickland, L. (2004). Pathways for membrane trafficking during cytokinesis. In *Trends in Cell Biology* (Vol. 14, Issue 3, pp. 115–118). <https://doi.org/10.1016/j.tcb.2004.01.006>
- Sudhaharan, T., Sem, K. P., Liew, H. F., Yu, Y. H., Goh, W. I., Chou, A. M., & Ahmed, S. (2016). The Rho GTPase RhoA signals through IRTKS, Eps8 and WAVE2 to generate dorsal membrane ruffles and filopodia. *Journal of Cell Science*, 129(14), 2829–2840.
- Suetsugu, S., Murayama, K., Sakamoto, A., Hanawa-Suetsugu, K., Seto, A., Oikawa, T., Mishima, C., Shirouzu, M., Takenawa, T., & Yokoyama, S. (2006). The RAC binding domain/IRSp53-MIM homology domain of IRSp53 induces RAC-dependent membrane deformation. *The Journal of Biological Chemistry*, 281(46), 35347–35358.
- Suetsugu, S., Toyooka, K., & Senju, Y. (2010). Subcellular membrane curvature mediated by the BAR domain superfamily proteins. *Seminars in Cell & Developmental Biology*, 21(4), 340–349.
- Su, J., Chow, B., Boulianne, G. L., & Wilde, A. (2013). The BAR domain of amphiphysin is required for cleavage furrow tip–tubule formation during cellularization in *Drosophila* embryos. In *Molecular Biology of the Cell* (Vol. 24, Issue 9, pp. 1444–1453). <https://doi.org/10.1091/mbc.e12-12-0878>
- Su, K.-C., Takaki, T., & Petronczki, M. (2011). Targeting of the RhoGEF Ect2 to the equatorial membrane controls cleavage furrow formation during cytokinesis. *Developmental Cell*, 21(6), 1104–1115.
- Sullivan, W., Fogarty, P., & Theurkauf, W. (1993). Mutations affecting the cytoskeletal organization of syncytial *Drosophila* embryos. *Development*, 118(4), 1245–1254.
- Sullivan, W., & Theurkauf, W. E. (1995). The cytoskeleton and morphogenesis of the early *Drosophila* embryo. In *Current Opinion in Cell Biology* (Vol. 7, Issue 1, pp. 18–22). [https://doi.org/10.1016/0955-0674\(95\)80040-9](https://doi.org/10.1016/0955-0674(95)80040-9)
- Svitkina, T. M., & Borisy, G. G. (1999). Arp2/3 complex and actin depolymerizing factor/cofilin in dendritic organization and treadmilling of actin filament array in lamellipodia. *The Journal of Cell Biology*, 145(5), 1009–1026.

- Swanson, M. M., & Poodry, C. A. (1980). Pole cell formation in *Drosophila melanogaster*. In *Developmental Biology* (Vol. 75, Issue 2, pp. 419–430). [https://doi.org/10.1016/0012-1606\(80\)90173-6](https://doi.org/10.1016/0012-1606(80)90173-6)
- Takeda, T., Robinson, I. M., Savoian, M. M., Griffiths, J. R., Whetton, A. D., McMahon, H. T., & Glover, D. M. (2013). *Drosophila* F-BAR protein Syndapin contributes to coupling the plasma membrane and contractile ring in cytokinesis. *Open Biology*, 3(8), 130081.
- Takei, K., Slepnev, V. I., Haucke, V., & De Camilli, P. (1999). Functional partnership between amphiphysin and dynamin in clathrin-mediated endocytosis. *Nature Cell Biology*, 1(1), 33–39.
- Takenawa, T. (2010). Phosphoinositide-binding interface proteins involved in shaping cell membranes. *Proceedings of the Japan Academy. Series B, Physical and Biological Sciences*, 86(5), 509–523.
- Takeya, R., Taniguchi, K., Narumiya, S., & Sumimoto, H. (2008). The mammalian formin FHOD1 is activated through phosphorylation by ROCK and mediates thrombin-induced stress fibre formation in endothelial cells. *The EMBO Journal*, 27(4), 618–628.
- Tan, C., Stronach, B., & Perrimon, N. (2003). Roles of myosin phosphatase during *Drosophila* development. *Development*, 130(4), 671–681.
- Tang, B. L. (2012). Membrane Trafficking Components in Cytokinesis. In *Cellular Physiology and Biochemistry* (Vol. 30, Issue 5, pp. 1097–1108). <https://doi.org/10.1159/000343301>
- Tarricone, C., Xiao, B., Justin, N., Walker, P. A., Rittinger, K., Gamblin, S. J., & Smerdon, S. J. (2001). The structural basis of Arfaptin-mediated cross-talk between Rac and Arf signalling pathways. *Nature*, 411(6834), 215–219.
- Tatsumoto, T., Xie, X., Blumenthal, R., Okamoto, I., & Miki, T. (1999). Human Ect2 Is an Exchange Factor for Rho Gtpases, Phosphorylated in G2/M Phases, and Involved in Cytokinesis. In *Journal of Cell Biology* (Vol. 147, Issue 5, pp. 921–928). <https://doi.org/10.1083/jcb.147.5.921>
- Taylor, J. M., Hildebrand, J. D., Mack, C. P., Cox, M. E., & Parsons, J. T. (1998). Characterization of graf, the GTPase-activating protein for rho associated with focal adhesion kinase. Phosphorylation and possible regulation by mitogen-activated protein kinase. *The Journal of Biological Chemistry*, 273(14), 8063–8070.

- Taylor, J. M., Macklem, M. M., & Parsons, J. T. (1999). Cytoskeletal changes induced by GRAF, the GTPase regulator associated with focal adhesion kinase, are mediated by Rho. In *Journal of Cell Science* (Vol. 112, Issue 2, pp. 231–242). <https://doi.org/10.1242/jcs.112.2.231>
- Taylor, M. J., Perrais, D., & Merrifield, C. J. (2011). A high precision survey of the molecular dynamics of mammalian clathrin-mediated endocytosis. *PLoS Biology*, 9(3), e1000604.
- Thomas, J. H., & Wieschaus, E. (2004). src64 and tec29 are required for microfilament contraction during Drosophila cellularization. *Development*, 131(4), 863–871.
- Thompson, H. M., Skop, A. R., Euteneuer, U., Meyer, B. J., & McNiven, M. A. (2002). The large GTPase dynamin associates with the spindle midzone and is required for cytokinesis. *Current Biology: CB*, 12(24), 2111–2117.
- Totsukawa, G., Yamakita, Y., Yamashiro, S., Hartshorne, D. J., Sasaki, Y., & Matsumura, F. (2000). Distinct Roles of Rock (Rho-Kinase) and Mlck in Spatial Regulation of Mlc Phosphorylation for Assembly of Stress Fibers and Focal Adhesions in 3t3 Fibroblasts. In *Journal of Cell Biology* (Vol. 150, Issue 4, pp. 797–806). <https://doi.org/10.1083/jcb.150.4.797>
- Tsujita, K., Suetsugu, S., Sasaki, N., Furutani, M., Oikawa, T., & Takenawa, T. (2006). Coordination between the actin cytoskeleton and membrane deformation by a novel membrane tubulation domain of PCH proteins is involved in endocytosis. *The Journal of Cell Biology*, 172(2), 269–279.
- Turner, F. R., Rudolf Turner, F., & Mahowald, A. P. (1977). Scanning electron microscopy of Drosophila melanogaster embryogenesis. In *Developmental Biology* (Vol. 57, Issue 2, pp. 403–416). [https://doi.org/10.1016/0012-1606\(77\)90225-1](https://doi.org/10.1016/0012-1606(77)90225-1)
- Van Aelst, L., & D'Souza-Schorey, C. (1997). Rho GTPases and signaling networks. In *Genes & Development* (Vol. 11, Issue 18, pp. 2295–2322). <https://doi.org/10.1101/gad.11.18.2295>
- Van Aelst, L., Joneson, T., & Bar-Sagi, D. (1996). Identification of a novel Rac1-interacting protein involved in membrane ruffling. *The EMBO Journal*, 15(15), 3778–3786.
- Vasquez, C. G., Tworoger, M., & Martin, A. C. (2014). Dynamic myosin phosphorylation regulates contractile pulses and tissue integrity during epithelial morphogenesis. In

Journal of Cell Biology (Vol. 206, Issue 3, pp. 435–450).
<https://doi.org/10.1083/jcb.201402004>

- Vavylonis, D., Wu, J.-Q., Hao, S., O'Shaughnessy, B., & Pollard, T. D. (2008). Assembly Mechanism of the Contractile Ring for Cytokinesis by Fission Yeast. In *Science* (Vol. 319, Issue 5859, pp. 97–100). <https://doi.org/10.1126/science.1151086>
- Verbrugghe, K. J. C., & White, J. G. (2004). SPD-1 is required for the formation of the spindle midzone but is not essential for the completion of cytokinesis in *C. elegans* embryos. *Current Biology: CB*, 14(19), 1755–1760.
- von Dassow, G. (2009). Concurrent cues for cytokinetic furrow induction in animal cells. *Trends in Cell Biology*, 19(4), 165–173.
- Wachtler, V., Huang, Y., Karagiannis, J., & Balasubramanian, M. K. (2006). Cell cycle-dependent roles for the FCH-domain protein Cdc15p in formation of the actomyosin ring in *Schizosaccharomyces pombe*. *Molecular Biology of the Cell*, 17(7), 3254–3266.
- Wadsworth, P. (2005). Cytokinesis: Rho Marks the Spot. In *Current Biology* (Vol. 15, Issue 21, pp. R871–R874). <https://doi.org/10.1016/j.cub.2005.10.021>
- Wagner, E., & Glotzer, M. (2016). Local RhoA activation induces cytokinetic furrows independent of spindle position and cell cycle stage. *The Journal of Cell Biology*, 213(6), 641–649.
- Warn, R. M., Bullard, B., & Magrath, R. (1980). Changes in the distribution of cortical myosin during the cellularization of the *Drosophila* embryo. *Journal of Embryology and Experimental Morphology*, 57, 167–176.
- Warn, R. M., & Magrath, R. (1983). F-actin distribution during the cellularization of the *Drosophila* embryo visualized with FL-phalloidin. *Experimental Cell Research*, 143(1), 103–114.
- Warn, R. M., Magrath, R., & Webb, S. (1984). Distribution of F-actin during cleavage of the *Drosophila* syncytial blastoderm. *The Journal of Cell Biology*, 98(1), 156–162.
- Watanabe, N., Madaule, P., Reid, T., Ishizaki, T., Watanabe, G., Kakizuka, A., Saito, Y., Nakao, K., Jockusch, B. M., & Narumiya, S. (1997). p140mDia, a mammalian homolog of *Drosophila* diaphanous, is a target protein for Rho small GTPase and is a ligand for profilin. *The EMBO Journal*, 16(11), 3044–3056.

- Watson, J. R., Fox, H. M., Nietlispach, D., Gallop, J. L., Owen, D., & Mott, H. R. (2016). Investigation of the Interaction between Cdc42 and Its Effector TOCA1: HANDOVER OF Cdc42 TO THE ACTIN REGULATOR N-WASP IS FACILITATED BY DIFFERENTIAL BINDING AFFINITIES. *The Journal of Biological Chemistry*, 291(26), 13875–13890.
- Weissenhorn, W. (2005). Crystal structure of the endophilin-A1 BAR domain. *Journal of Molecular Biology*, 351(3), 653–661.
- Wenzl, C., Yan, S., Laupsien, P., & Großhans, J. (2010). Localization of RhoGEF2 during Drosophila cellularization is developmentally controlled by slam. In *Mechanisms of Development* (Vol. 127, Issues 7-8, pp. 371–384). <https://doi.org/10.1016/j.mod.2010.01.001>
- Wenzl, C., Yan, S., Laupsien, P., & Grosshans, J. (2010). Localization of RhoGEF2 during Drosophila cellularization is developmentally controlled by Slam. *Mechanisms of Development*, 127(7-8), 371–384.
- Wienke, D. C., Knetsch, M. L., Neuhaus, E. M., Reedy, M. C., & Manstein, D. J. (1999). Disruption of a dynamin homologue affects endocytosis, organelle morphology, and cytokinesis in Dictyostelium discoideum. *Molecular Biology of the Cell*, 10(1), 225–243.
- Willet, A. H., McDonald, N. A., Bohnert, K. A., Baird, M. A., Allen, J. R., Davidson, M. W., & Gould, K. L. (2015). The F-BAR Cdc15 promotes contractile ring formation through the direct recruitment of the formin Cdc12. *The Journal of Cell Biology*, 208(4), 391–399.
- Wilson, G. M., Fielding, A. B., Simon, G. C., Yu, X., Andrews, P. D., Hames, R. S., Frey, A. M., Peden, A. A., Gould, G. W., & Prekeris, R. (2005). The FIP3-Rab11 protein complex regulates recycling endosome targeting to the cleavage furrow during late cytokinesis. *Molecular Biology of the Cell*, 16(2), 849–860.
- Winter, C. G., Wang, B., Ballew, A., Royou, A., Karess, R., Axelrod, J. D., & Luo, L. (2001). Drosophila Rho-Associated Kinase (Drok) Links Frizzled-Mediated Planar Cell Polarity Signaling to the Actin Cytoskeleton. In *Cell* (Vol. 105, Issue 1, pp. 81–91). [https://doi.org/10.1016/s0092-8674\(01\)00298-7](https://doi.org/10.1016/s0092-8674(01)00298-7)
- Withee, J., Galligan, B., Hawkins, N., & Garriga, G. (2004). Caenorhabditis elegans WASP and Ena/VASP Proteins Play Compensatory Roles in Morphogenesis and Neuronal Cell Migration. In *Genetics* (Vol. 167, Issue 3, pp. 1165–1176). <https://doi.org/10.1534/genetics.103.025676>

- Wu, J.-Q., Kuhn, J. R., Kovar, D. R., & Pollard, T. D. (2003). Spatial and temporal pathway for assembly and constriction of the contractile ring in fission yeast cytokinesis. *Developmental Cell*, 5(5), 723–734.
- Wu, S. K., & Priya, R. (2019). Spatio-Temporal Regulation of RhoGTPases Signaling by Myosin II. *Frontiers in Cell and Developmental Biology*, 7, 90.
- Wu, T., Shi, Z., & Baumgart, T. (2014). Mutations in BIN1 associated with centronuclear myopathy disrupt membrane remodeling by affecting protein density and oligomerization. *PloS One*, 9(4), e93060.
- Xie, H., Surka, M., Howard, J., & Trimble, W. S. (1999). Characterization of the mammalian septin H5: distinct patterns of cytoskeletal and membrane association from other septin proteins. *Cell Motility and the Cytoskeleton*, 43(1), 52–62.
- Xue, Z. (2017). *Back-to-back Mechanisms Drive Actomyosin Ring Closure During Drosophila Embryo Cleavage*.
- Xue, Z., & Sokac, A. M. (2016). -Back-to-back mechanisms drive actomyosin ring closure during Drosophila embryo cleavage. *The Journal of Cell Biology*, 215(3), 335–344.
- Xu, Y., Moseley, J. B., Sagot, I., Poy, F., Pellman, D., Goode, B. L., & Eck, M. J. (2004). Crystal structures of a Formin Homology-2 domain reveal a tethered dimer architecture. *Cell*, 116(5), 711–723.
- Yamagishi, A., Masuda, M., Ohki, T., Onishi, H., & Mochizuki, N. (2004). A novel actin bundling/filopodium-forming domain conserved in insulin receptor tyrosine kinase substrate p53 and missing in metastasis protein. *The Journal of Biological Chemistry*, 279(15), 14929–14936.
- Yamashiro, S., Totsukawa, G., Yamakita, Y., Sasaki, Y., Madaule, P., Ishizaki, T., Narumiya, S., & Matsumura, F. (2003). Citron kinase, a Rho-dependent kinase, induces di-phosphorylation of regulatory light chain of myosin II. *Molecular Biology of the Cell*, 14(5), 1745–1756.
- Yan, S., Lv, Z., Winterhoff, M., Wenzl, C., Zobel, T., Faix, J., Bogdan, S., & Grosshans, J. (2013). The F-BAR protein Cip4/Toca-1 antagonizes the formin Diaphanous in membrane stabilization and compartmentalization. *Journal of Cell Science*, 126(Pt 8), 1796–1805.
- Yao, F., Kausalya, J. P., Sia, Y. Y., Teo, A. S. M., Lee, W. H., Ong, A. G. M., Zhang, Z., Tan, J. H. J., Li, G., Bertrand, D., Liu, X., Poh, H. M., Guan, P., Zhu, F., Pathiraja, T. N.,

- Ariyaratne, P. N., Rao, J., Woo, X. Y., Cai, S., ... Hillmer, A. M. (2015). Recurrent Fusion Genes in Gastric Cancer: CLDN18-ARHGAP26 Induces Loss of Epithelial Integrity. *Cell Reports*, 12(2), 272–285.
- Yoneda, M., & Dan, K. (1972). Tension at the Surface of the Dividing Sea-Urchin Egg. In *Journal of Experimental Biology* (Vol. 57, Issue 3, pp. 575–587). <https://doi.org/10.1242/jeb.57.3.575>
- Yoon, Y., Zhang, X., & Cho, W. (2012). Phosphatidylinositol 4,5-bisphosphate (PtdIns(4,5)P₂) specifically induces membrane penetration and deformation by Bin/amphiphysin/Rvs (BAR) domains. *The Journal of Biological Chemistry*, 287(41), 34078–34090.
- Young, P. E., Pesacreta, T. C., & Kiehart, D. P. (1991). Dynamic changes in the distribution of cytoplasmic myosin during *Drosophila* embryogenesis. *Development*, 111(1), 1–14.
- Young, P. E., Richman, A. M., Ketchum, A. S., & Kiehart, D. P. (1993). Morphogenesis in *Drosophila* requires nonmuscle myosin heavy chain function. *Genes & Development*, 7(1), 29–41.
- Yüce, Ö., Piekny, A., & Glotzer, M. (2005). An ECT2–centralspindlin complex regulates the localization and function of RhoA. In *Journal of Cell Biology* (Vol. 170, Issue 4, pp. 571–582). <https://doi.org/10.1083/jcb.200501097>
- Yumura, S. (2001). Myosin II dynamics and cortical flow during contractile ring formation in *Dictyostelium* cells. In *Journal of Cell Biology* (Vol. 154, Issue 1, pp. 137–146). <https://doi.org/10.1083/jcb.200011013>
- Zemel, A., Ben-Shaul, A., & May, S. (2008). Modulation of the spontaneous curvature and bending rigidity of lipid membranes by interfacially adsorbed amphipathic peptides. *The Journal of Physical Chemistry. B*, 112(23), 6988–6996.
- Zeng, X.-C., Luo, X., Wang, S.-X., & Zhan, X. (2013). Fibronectin-mediated cell spreading requires ABBA-Rac1 signaling. *Journal of Cellular Biochemistry*, 114(4), 773–781.
- Zhang, D., & Glotzer, M. (2015). The RhoGAP activity of CYK-4/MgcRacGAP functions non-canonically by promoting RhoA activation during cytokinesis. *eLife*, 4. <https://doi.org/10.7554/eLife.08898>
- Zhang, J., Kong, C., Xie, H., McPherson, P. S., Grinstein, S., & Trimble, W. S. (1999). Phosphatidylinositol polyphosphate binding to the mammalian septin H5 is modulated by GTP. *Current Biology: CB*, 9(24), 1458–1467.

- Zhang, Y., Werling, U., & Edelmann, W. (2012). SLiCE: a novel bacterial cell extract-based DNA cloning method. *Nucleic Acids Research*, *40*(8), e55.
- Zhang, Y., Werling, U., & Edelmann, W. (2014). Seamless Ligation Cloning Extract (SLiCE) cloning method. *Methods in Molecular Biology*, *1116*, 235–244.
- Zhang, Y., Yu, J. C., Jiang, T., Fernandez-Gonzalez, R., & Harris, T. J. C. (2018). Collision of Expanding Actin Caps with Actomyosin Borders for Cortical Bending and Mitotic Rounding in a Syncytium. In *Developmental Cell* (Vol. 45, Issue 5, pp. 551–564.e4). <https://doi.org/10.1016/j.devcel.2018.04.024>
- Zheng, D., Niu, S., Yu, D., Zhan, X. H., Zeng, X., Cui, B., Chen, Y., Yoon, J., Martin, S. S., Lu, X., & Zhan, X. (2010). Abba promotes PDGF-mediated membrane ruffling through activation of the small GTPase Rac1. In *Biochemical and Biophysical Research Communications* (Vol. 401, Issue 4, pp. 527–532). <https://doi.org/10.1016/j.bbrc.2010.09.087>
- Zhou, M., & Wang, Y.-L. (2008). Distinct pathways for the early recruitment of myosin II and actin to the cytokinetic furrow. *Molecular Biology of the Cell*, *19*(1), 318–326.
- Zhu, C., Bossy-Wetzel, E., & Jiang, W. (2005). Recruitment of MKLP1 to the spindle midzone/midbody by INCENP is essential for midbody formation and completion of cytokinesis in human cells. *Biochemical Journal*, *389*(Pt 2), 373–381.
- Zhu, C., Das, S. L., & Baumgart, T. (2012). Nonlinear sorting, curvature generation, and crowding of endophilin N-BAR on tubular membranes. *Biophysical Journal*, *102*(8), 1837–1845.
- Zhu, C., & Jiang, W. (2005). Cell cycle-dependent translocation of PRC1 on the spindle by Kif4 is essential for midzone formation and cytokinesis. *Proceedings of the National Academy of Sciences of the United States of America*, *102*(2), 343–348.
- Zigmond, S. H. (2004). Formin-induced nucleation of actin filaments. *Current Opinion in Cell Biology*, *16*(1), 99–105.
- Zirin, J., Hu, Y., Liu, L., Yang-Zhou, D., Colbeth, R., Yan, D., Ewen-Campen, B., Tao, R., Vogt, E., VanNest, S., Cavers, C., Villalta, C., Comjean, A., Sun, J., Wang, X., Jia, Y., Zhu, R., Peng, P., Yu, J., ... Perrimon, N. (2020). Large-Scale Transgenic Drosophila Resource Collections for Loss- and Gain-of-Function Studies. *Genetics*, *214*(4), 755–767.

